A STUDY OF ION CONCENTRATION FLUCTUATIONS IN TURBULENT DIFFUSION FLAMES USING CORRELATION TECHNIQUES

by

William Gordon Roberts B.Sc.

THESIS
541.361
ROB

15NW73 167022

A Thesis submitted for the Degree of Doctor of Philosophy in the University of Aston in Birmingham

August 1973

PREFACE

This thesis, which is being submitted for the Degree of Doctor of Philosophy in the University of Aston in Birmingham, is an account of the work conducted under the joint supervision of Professor F.M. Page in the Department of Chemistry, and Mr. H. Williams, Visiting Reader of Chemical Physics at the University of Aston in Birmingham from October 1969 to October 1972. Except where references have been given in the text, the work described herein is original and has not been submitted for a degree at any other University.

W. G. Roberts.

SUMMARY

An investigation of the interaction between chemistry and turbulence has been made by studying the effects of non equilibrium ion chemical kinetics in a turbulent diffusion flame. In such a system the charged species undergo a chemical reaction concurrently with turbulent mixing. Where the chemical reaction rate is greater than the appropriate mixing rate it has been theoretically predicted that a measurable difference should exist between the statistical functions used to describe the fluctuating species concentration field and that of a chemically inert constituent.

Experimental evidence for this phenomenon has been established by sampling the local ion concentration fluctuations in a turbulent diffusion flame, of nozzle Reynolds number 1.0×10^4 using a stationary electrostatic probe. The random positive ion saturation current collected by the probe was analysed to determine its auto correlation function. The ionisation field was generated by seeding the flame with acetylene and other metal salt solutions preselected on the basis of their Damkohler number values in the flame.

Studies have also been conducted to map the flame determining both autocorrelation and cross correlation functions to obtain further information for the interaction phenomenon and of the structure of the ion concentration field throughout the flame.

C O N T E N T S

Errata

Page

Throughout text. For metres per sec given as M sec^{-1} read m sec^{-1}

21. Equations 3.3

Equation for laminar flow read,

$$\rho\left(\frac{\partial U_i}{\partial t} + \frac{U_j \partial U_i}{\partial x_j}\right) = -\frac{\partial P}{\partial x_i} + \frac{\partial}{\partial x_j}\left(\mu \frac{\partial U_i}{\partial x_j}\right)$$

Equation for turbulent flow read,

$$\rho\left(\frac{\partial \bar{U}_i}{\partial t} + \frac{\bar{U}_j \partial \bar{U}_i}{\partial x_j}\right) = -\frac{\partial \bar{P}}{\partial x_i} + \frac{\partial}{\partial x_j}\left(\mu \frac{\partial \bar{U}_i}{\partial x_j} - \rho \overline{u_i u_j}\right)$$

57. Top of page read; ...where n, $\bar{V}$, T and m are number density, mean velocity, temperature and mass of the charged species respectively.

86. Equations 7.1 to 7.3 for equilibrium constant k read K.

86. - 88. Equations 7.4 to 7.11 for $[A]_o$ read $[A_o]$

142. Bottom line, for radioactive read radiative.

143. First sentence, for radioactive read radiative.

CHAPTER 1

INTRODUCTION

Turbulent combustion is of immense importance to modern technology. Examples of its application include industrial furnaces, internal combustion engines and turbojet and rocket engines. Despite this importance the nature of the physical processes occurring within a turbulent flame and the mechanism of propagation remain poorly understood. This unsatisfactory situation is largely due to the complexity of turbulent fluid motion and the additional complications which arise upon the presence of a chemical reaction in the flow.

An important feature of turbulence is its irregular motion. This condition renders the flow particularly resistant to a mathematical treatment. It is, however, possible to describe the motion by statistical analysis to determine such properties as scale and intensity of turbulence. Turbulence may be characterised in terms of various flow properties, for example, velocity, pressure or concentration of constituents. In order to provide insight into the physical processes occurring in turbulent motion it is necessary to investigate not only the mean values of such properties but also their fluctuations. During the early studies of turbulent flow, greater emphasis was directed at the measurement of the mean characteristics resulting from the action of turbulence rather than on the turbulent motions themselves. The limited experimental techniques available at the time contributed to this situation however, following the great improvements in electronic

instrumentation the study of turbulent motions is now more reliable and less tedious. One such instrument, the hot wire anemometer has become a well established tool for the sensing of velocity fluctations and has contributed greatly to the elucidation of the structure of the isothermal jet.

It has long been recognised that the presence of turbulence enhances the rate of mixing of initially separated components. The irregular motion has the ability to distribute fluid elements of different species over large distances, compared to those traversed during molecular motion. This, with the aid of molecular diffusion, leads to a reduction in concentration gradients with the eventual formation of a uniform mixture.

This process is of importance in turbulent diffusion flames where the rate of combustion is controlled by turbulent mixing of the initially unmixed fuel and air. Research on such flames has been largely centred upon the measurement of bulk properties such as flame height, shape and blow off characteristics. Progress on the determination of local turbulent parameters within flames has been somewhat slow, experimental difficulties in the hostile environment of the flame being a contributing factor. As a result little information regarding the physical processes taking place in turbulent flames is available. Knowledge of this nature would for example enable the determination of mass, momentum and heat transfer rates. This information would be of value in the design of efficient combustion appliances such as engine combustion chambers. To date, the lack of such data has limited the design of such equipment to the methods of trial and error.

A further interesting problem in turbulent combustion is the interaction between chemistry and turbulence. The phenomenon may be described by considering the presence of a chemically active but dynamically passive species in a turbulent environment. In such a system the species undergo a chemical reaction while concurrently under the influence of turbulent mixing. Chemistry may lead to either the production or removal of the reactant species. Turbulent mixing, however is a dissipative process and therefore only leads to the decay of the species concentration field. One aspect of the interaction namely the effect of turbulence upon a chemical reaction has been studied both experimentally and theoretically[1]. These investigations have shown that turbulence can enhance the rate of the reaction over the rate for the corresponding process in a laminar flow. This has been attributed to the fluctuations in the reactant concentration produced by the turbulent motion.

The other aspect of the interaction phenomenon is the effect chemistry has upon the internal physical structure of the species concentration field in the turbulent flow. When the reaction rate is in excess of the appropriate turbulent mixing rate chemistry will produce a greater change in the reactant concentration field compared to that due to the mixing action. Under these conditions therefore, chemistry will predominantly control the turbulent characteristics of the fluctuating concentration field. When the species undergoes a slow reaction it may be considered to be chemically inert and the changes in the concentration field will be controlled by turbulent mixing. Therefore, a measurable difference should exist between the statistical functions used to describe the reactant concentration field and those functions characteristic of the chemically

passive constituent. This phenomenon has been the subject of several theoretical treatments [2-4] however it appears to have been neglected experimentally.

It was this situation that initiated the work described in this thesis where experimental evidence for the interaction phenomenon has been sought by studying non-equilibrium ion chemical kinetics in a turbulent hydrogen diffusion flame. The flame was seeded with various metal additives preselected on the basis of their Damkohler number values. The Damkohler number is expressed as;

$$\text{Damkohler number } D_o = \frac{\text{Chemical reaction rate}}{\text{Turbulent mixing rate}}$$

This parameter enables the behaviour of the charged species in the flame to be predicted. For D_o values greater than unity the turbulent characteristics of the reactant concentration field will be governed by chemistry whereas values less than or equal to unity turbulent mixing controls. It has been observed that the required difference in the statistical functions was achieved using additives with the greatest difference in D_o values.

Ionisation in flame gases has received much attention over the past decade due primarily to the following of two lines of research. In one case attempts to enhance the ionisation levels was made for the possible use of flames for the generation of electricity. The other, a reduction in concentration levels was desired for the high electron concentration levels in rocket exhaust plumes impede and distort radio guidance signals. These studies have contributed greatly to the understanding of ion chemical reactions such that the mechanisms for metal ion formation and decay are

now generally known. This wealth of ion chemical kinetic data available together with the charged species being dynamically passive renders the turbulent flame a suitable system to study the interaction phenomenon.

The techniques employed for the measurement of ionisation levels in flame gases include; microwave attenuation, mass spectrometry and the electrostatic probe. Of the three the electrostatic probe probably provides the highest temporal and spacial resolution essential for the measurement of local turbulent parameters. Further advantages include its simplicity in construction and use. The instrument employed in these studies was a watercooled electrostatic probe suitably biased to collect the fluctuating positive ion saturation current. The signal was analysed by determining the correlation, power spectral density, probability density and cumulative distribution functions to measure the turbulent parameters which describe the local ion concentration field.

The statistical functions employed throughout these studies have been fully described in the following chapter. The basic concepts of turbulence and the manner in which the functions are employed to analyse the motion has been discussed in Chapter 3. An introduction to turbulent diffusion flames is treated in Chapter 4 together with a detailed discussion of the chemistry turbulence interaction phenomenon. Chapter 5 contains a review of electrostatic probe theory and includes the development of the Su and Lam[5] theory due to Clements and Smy[6] which considers a flowing plasma, being of particular relevance to this work. The apparatus employed in the project has been described

in Chapter 6, also given as an account of the basic mode of operation of the computer programs used in the determination of the statistical functions. Chapter 7 discusses the procedure employed for the preselection of the flame additives and describes the determination of the Damkohler number values for the charged species. The preliminary studies that provided experimental evidence for the interaction phenomenon have been described in Chapter 8. The experiments described in Chapters 9 and 10 provide an account of the autocorrelation and cross correlation studies which provided further evidence for the phenomenon and information of the structure of the ion concentration field throughout the flame. The measurement of mean gas velocity in both turbulent flame and isothermal jet provided information of the effects of combustion on mean velocity has been treated in Chapter 11. The observed greater mean velocities in the flame compared to those in the jet have been explained by conservation of momentum arguments. Chapter 12 describes the use of an inverted electrostatic probe. This is a new development of the probe technique and has been shown to be a valuable method for the measurement of convective velocities in flame plasmas. Further experimental evidence for the chemistry-turbulence interaction was obtained from measurements of normalised mean square values of the random probe signal for different flame additives. This study is described in Chapter 13. An agreement contained in the C.A.P.S. scheme between the Science Research Council and the Royal Dutch Shell Company required the author to spend a period of time at the Thornton Research Laboratories of the above company. The work conducted at these laboratories involved determination of a suitable technique

for the measurement of turbulent intensity of velocity fluctuations in flames. An account of these studies is given in Chapter 14. The main conclusions of the work described in the thesis are given in Chapter 15. The Appendix contains the computer programs employed during the study.

CHAPTER 2

STATISTICAL METHODS FOR THE ANALYSIS OF RANDOM DATA

The data representing a random physical phenomenon cannot be described by an explicit mathematical relationship since each observation of the phenomenon will be unique. A single observation of such processes over some short time interval is called a sample record and the collection of all sample records produced by this phenomenon is called a random process. The fluctuating positive ion current collected by an electrostatic probe immersed in a turbulent plasma constitutes a random process. In order to describe the properties of such processes various statistical functions are used.

2.1 Stationary Random Processes

A stationary random process is one where the mean value remains invarient with time. The mean value may be evaluated by determining the instantaneous value of each sample record at some time t, summing these values and dividing by the total number of sample records. This procedure is known as ensemble averaging. A more convenient method for the measurement of mean values may be possible by computing time averages where a single sample record is required. The time averaged mean value for a sample record over the observation time T is given by:

$$\text{Mean value } \mu = \lim_{T\to\infty} \frac{1}{T} \int_0^T x(t)\,dt. \qquad 2.1$$

If the mean value does not differ when computed using other sample records the random process is classified as ergodic. Ergodic random processes form an important class of random processes since they may be analysed using a single sample record employing the time averaging procedure. It is commonly found in practice that random data representing stationary physical processes are ergodic. The turbulent flame is no exception to this, being a stationary system; the random probe signals studied in this project have been considered to be ergodic processes. The statistical functions employed for their analysis will now be discussed.

2.2 Correlation Analysis

Correlation functions provide a measure of the similarity between random physical processes. This analytical technique is a method of extracting information from such phenomena in the time domain. It is theoretically possible to determine the correlation between any number of random processes;however only two waveforms will be considered here, being of particular relevance to this work. Two correlation functions have been employed, namely the cross correlation function and its special case, the auto-correlation function. Both these functions have been widely used in experimental studies of turbulent phenomena.

2.2.1 Auto-correlation Function

The auto-correlation function provides a measure of the similarity between a waveform and a time-delayed version of itself. This may be illustrated by considering the following sample record for a random process.

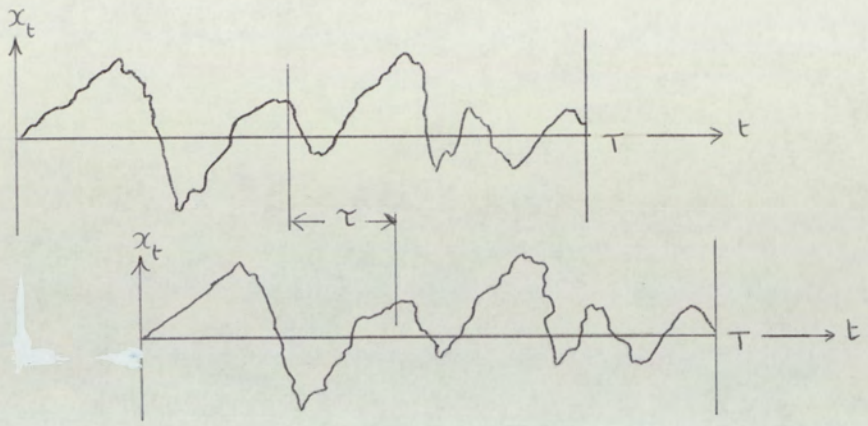

Fig 2.1

A measure of the auto-correlation between the values for the waveform x(t) at times t and t+τ may be obtained by determining the product of these values and time averaging over the observation time T. The complete auto-correlation function $R_x(\tau)$ may be obtained by repeating this procedure for varying delay times. A plot of $R_x(\tau)$ as a function of delay time τ will indicate a maximum value at τ=0 decreasing to zero as the waveforms become more dissimilar with increased delay time. The auto-correlation function is given by:

$$R_x(\tau) = \lim_{T\to\infty} \frac{1}{T} \int_0^T x(t)\, x(t+\tau)\, dt \qquad 2.2$$

The function $R_x(\tau)$ is a real valued even function and may have positive and negative values. The maximum value at τ=0 corresponds to the mean square value of the signal.

2.2.2 Cross Correlation Function

The cross correlation function describes the similarity between two non-identical waveforms obtained by time averaging the product of the value at a time t for one signal x(t) with the value of another signal y(t) at time t+τ over the

observation time T. This may be expressed by:

$$R_{xy}(\tau) = \lim_{T\to\infty} \frac{1}{T} \int_0^T x(t)\, y(t+\tau)\, dt \qquad 2.3$$

The cross correlation function is not even valued and its maximum value does not necessarily occur at $\tau=0$.

Both the auto and cross correlation function may be normalised by dividing the product terms by the root mean squares of the random processes. In the case of the auto correlation function where one signal is studied this is equivalent to dividing by the mean square value. The normalised functions are known as the correlation coefficients $\rho(\tau)$ which may take the values between ± 1.

$$\text{Auto correlation Coeff } \rho_x(\tau) = \lim_{T\to\infty} \frac{1}{T} \int_0^T \frac{x(t)x(t+\tau)}{\overline{(x^2)}}\, dt \qquad 2.4$$

$$\text{Cross correlation Coeff } \rho_{xy}(\tau) = \lim_{T\to\infty} \frac{1}{T} \int_0^T \frac{x(t)y(t+\tau)}{\overline{(x^2)}^{\frac{1}{2}}\, \overline{(y^2)}^{\frac{1}{2}}}\, dt \qquad 2.5$$

Correlation coefficients have been used throughout this work.

2.3 Spectral Analysis

The power spectral density function is an analytical technique which describes the properties of a random process in terms of its frequency content. This function is extensively used in the study of turbulence providing a description of the kinetic energy distribution within the flow field. This important aspect of turbulence will be discussed at length in the following chapter. The spectral function and the auto-correlation function, as shown below, are closely related such

that the two techniques provide the same information expressed in different forms, namely, in the frequency domain or the time domain. It is commonly found experimentally that a clearer description of the phenomenon in question may be furnished by either one of these functions.

2.3.1 Power Spectral Density Function

The power spectral density function describes the frequency content of a random signal in terms of the spectral density of its mean square value. This requires the computation of the mean square values of the data within a narrow bandwidth between the frequencies f and f+Δf over the entire frequency range. The mean square value Ψ^2 within the bandwidth Δf may be expressed as:

$$\Psi^2_x\ (f,f+\Delta f) = \lim_{T\to\infty} \frac{1}{T} \int_0^T x^2(t,f,f+\Delta f)\ dt \qquad 2.6$$

where x(t,f,f+Δf) is the portion of the waveform contained within the frequency range f to f+Δf.

The power spectral density function Gx(f) is defined as:

$$G_x(f) = \lim_{\Delta f\to o} \frac{\Psi^2(f,f+\Delta f)}{\Delta f} = \lim_{\Delta f\to o} \lim_{T\to\infty} \frac{1}{\Delta f T} \int_0^T x^2(t,f,f+\Delta f)\ dt \qquad 2.7$$

The quantity Gx(f) is a real valued non-negative function. It is related to the mean square value for the complete random process x(t) by:

$$\Psi^2_x = \int_0^\infty G_x(f)\ df \qquad 2.8$$

An important property of the power spectral density function lies in its relationship to the autocorrelation function. For stationary random processes the two functions

are related by a Fourier transform :

$$G_x(f) = 4 \int_0^\infty R_x(\tau) \cos 2\pi f\tau d\tau \qquad 2.9$$

$$R_x(\tau) = \int_0^\infty G_x(f) \cos 2\pi f\tau df \qquad 2.10$$

It is theoretically possible that a knowledge of the autocorrelation function enables the power spectral density function to be determined and vice versa employing one of the above transform equations. In practice to perform this procedure satisfactorily a very detailed knowledge of the random process is required which is commonly not available, such that the transform may be of limited value to the experimentalist. This prob lem was encountered with the electrostatic probe signals studied in this work. This difficulty may be overcome by expressing the random process as a Fourier integral and determining the mean square values at the various frequencies from the magnitude of the Fourier coefficients. This procedure will be treated in greater detail in the discussion of computer programs in Chapter 6.

2.4 Probability Analysis

Information regarding the amplitude characteristics of a random process may be obtained by determining the probability density function and the cumulative distribution function.

2.4.1 Probability Density Function

The probability density function describes the probability that the data will assume a value within some defined amplitude range at any instant in time. This may be illustrated by considering the following sample record of a random process.

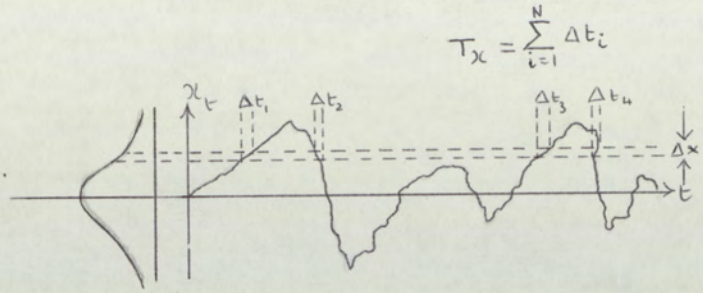

Fig. 2.2.

The probability of finding the function x(t) within the amplitude range x and x+Δx may be expressed by the ratio T_x/T where T_x is the total time spent by the function within the range (x,x+Δx) during the observation time T.

$$\text{Probability}\left[x>x(t)>x+\Delta x\right] = \frac{\sum_{i=1}^{N} \Delta t_i}{T} = \frac{T_x}{T} \qquad 2.11$$

The probability density function p_x may be expressed as:

$$p_x = \lim_{\Delta x \to o} \text{Prob}\left[\frac{x<x(t)<x+\Delta x}{\Delta x}\right] = \lim_{\Delta x \to o} \lim_{T \to \infty} \frac{1}{T}\left(\frac{T_x}{\Delta x}\right) \qquad 2.12$$

The most commonly encountered probability density function for random phenomena is the normal or Gaussian function which exhibits a symmetrical bell-shaped curve about the mean. This is illustrated in Fig. 2.2. The probability density functions determined in these studies were not Gaussian showing a distinct degree of asymmetry about the mean signal level. This phenomenon is known as skewness. Where the function has a longer tail to the right of the peak the function is said to be positively skewed and for the reverse case, negatively skewed. Examples of these two curve shapes are illustrated below:

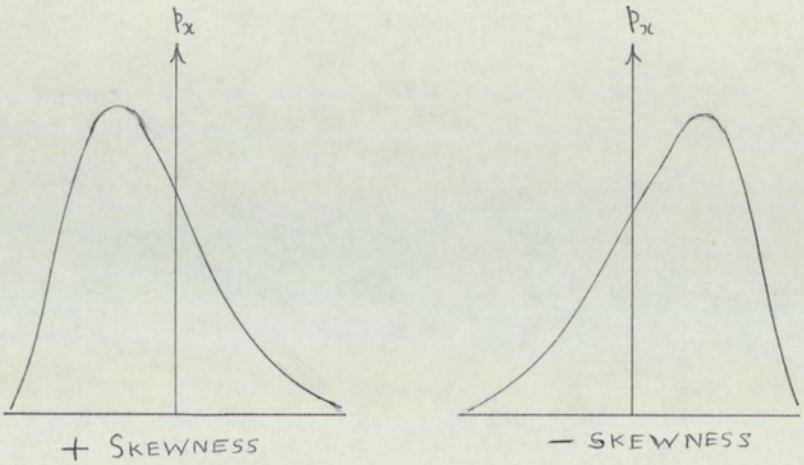

Fig. 2.3

A measure of the extent of asymmetry is given by the skewness factor expressed by the following empirical formula:

$$\text{Skewness Factor} \quad S = \frac{(\text{Mean} - \text{Mode})}{\text{Standard Deviation}} \qquad 2.13$$

The mode corresponds to the position on the abscissa where the maximum value of the function occurs. The skewness factor for the Gaussian function is zero.

2.4.2 Cumulative Distribution Function

The cumulative distribution function P_x describes the probability, or the portion of time some value of the random process x(t) may be found at or below a given amplitude. This function is equal to the integral of the probability density function between the limits $-\infty$ and some value x. i.e.

$$P_x = \text{Prob} \quad x(t) < x = \int_{-\infty}^{x} p_x \, dx \qquad 2.14$$

This function may sometimes provide a clearer description of the amplitude characteristics of a random process than those

supplied by the probability density function.

In the analysis of any random physical phenomena there is no predetermined method of telling which of the above statistical functions will extract the most useful information. Each must be applied and the resulting data carefully analysed. The computer programs used for their determination are discussed in Chapter 6; the programs are presented in the Appendix.

CHAPTER 3

TURBULENCE

3.1 Introduction:- Basic Concepts and Definition

Turbulence in contrast to laminar flow is characterised by its irregular motion. It may be generated by fluid flow past solid boundaries or by fluid layers of different velocities flowing over one another. The former condition is commonly referred to as wall turbulence, the latter as free turbulence. Free turbulence has been studied in this work.

The laminar flow of layers of fluid of slightly varying velocity over one another lead to the formation of a shear stress the result of the transfer of momentum from a faster moving layer to a slower moving layer. Viscosity of the fluid opposes the motion and sets up a velocity gradient across the layers and it is this gradient that provides the driving force for the momentum transport process. The viscous shear stress σ_v is directly proportional to the velocity gradient, the coefficient of viscosity η forming the proportionality constant. The momentum flows in the direction of the negative velocity gradient and for this reason σ_v is commonly expressed as a negative quantity.

$$\sigma_v = -\mu \frac{dv}{dx} \qquad 3.1$$

The momentum transport process is due to the random thermal motion of the molecules travelling across the layers carrying with them the properties of the layer they leave. By a similar

mechanism heat and mass transfer takes place when temperature and concentration gradients are present in the fluid.

These characteristics are common to laminar flows where the motion is steady with no acceleration of the layers and viscosity damping out any instabilities that may occur.

Increased flow rates produce greater velocity gradients and consequently enhanced momentum transfer rate leads to greater shear stresses. A critical velocity exists when the shear stresses become so great as to cause the breakdown of the steady laminar flow with the onset of turbulent motion. In addition to random thermal molecular motion "lumps" of fluid of various sizes move about the flow field in an irregular manner. The fluid "lumps", commonly termed eddies, may be considered to be conglomerations of molecules, their disordered motion producing fluctuations in the momentum, energy and concentration fields. An important feature of turbulence is its ability to enhance the transfer rates for momentum, energy and matter, being several orders of magnitude greater than the corresponding rates in laminar flow. This is attributed to the complex eddy motion able to convect these properties about the flow field more rapidly. The motion of the eddies, unlike gaseous molecular motion, does not occur independently of each other in that their motion at one region can influence the movement at some distant region.

Turbulence may thus be pictured as a complex eddy pattern composed of eddies of a wide range of sizes superimposed upon each other and upon the mean flow. The larger eddies possess most energy this being transferred to smaller eddies, with the smallest eddies being destroyed by viscous forces and their energy converted to heat. Turbulence is therefore a dissipative

process and requires a continuous supply of energy to be maintained otherwise the motion gradually decays.

Turbulence has proved a difficult phenomenon to define, probably the best definition available at present is given by Hinze[7]

"Turbulent fluid motion is an irregular condition of flow in which the various quantities show a random variation in both time and space co-ordinates so that statistically distinct values can be discerned."

This requires the "lumps" of fluid must not only move irregularly in time but also with respect to each other i.e. spacially. Fluid motion random in either time or space alone is, by definition, not turbulent.

An important dimensionless parameter used to distinguish between laminar and turbulent flows is the Reynolds number. It is expressed as the ratio of the inertial forces which impart an acceleration to the fluid particles to the viscous forces which oppose the fluid motion.

$$\text{Reynolds Number, } R_e = \frac{\text{Inertial Forces}}{\text{Viscous Forces}} = \frac{\rho \frac{U^2}{d}}{\mu \frac{U}{d^2}} = \frac{Ud}{\nu} \qquad 3.2$$

where U = flow velocity

d = characteristic length or diameter

ν = kinematic viscosity = $\frac{\text{viscosity}}{\text{density}} = \mu/\rho$

For Re < 2300 the flow is considered to be laminar. Between the range 2300-3200, commonly referred to as the transition region, the presence of small random flow fluctuations tend to be damped out by viscous forces but the flow

is unstable to larger fluctuations. Above Re 3200 the flow is considered to be turbulent.

3.2 Homogeneous and Isotropic Turbulence

The theoretical analysis of turbulent flow is often limited to the idealised and less complex cases of statistically homogeneous and isotropic turbulence. The former condition implies that the statistically determined mean values of fluctuations are independent of position in the flow field. Isotropic turbulence is a further restriction in that the mean values are independent of both position and direction.

The difference between the two kinds of turbulent flows may be illustrated by considering the root mean square (R.M.S.) value of the fluctuations in some flow property of interest, such as velocity, which provides a measure of the violence of the turbulent motion. For homogeneous turbulence to exist the R.M.S. values of the components along Cartesian co-ordinate axes, although each value may be different, will carry the same values throughout the flow field. The turbulence structure is therefore the same throughout the field. In the case of isotropic turbulence the R.M.S. values will be everywhere equal to each other irrespective of position or direction such that a perfectly disordered system reigns. Under these conditions no mean velocity gradients exist in the flow and therefore no shear stresses are present.

3.3 Reynolds Stresses

The first theoretical attempts to analyse turbulent fluid motion was by Osborne Reynolds. He used the Navier Stokes equations which describe laminar fluid motion and substituted

the instantaneous velocity terms for turbulent velocities expressed as the sum of a mean velocity and a fluctuating component, i.e.

$$U = \overline{U} + u$$

where U = instantaneous turbulent velocity

$\overline{U}$ = mean turbulent velocity

u = fluctuating velocity component

$\overline{u}$ = 0 by definition

The expressions for laminar fluid motion and that derived by Reynolds for turbulent motion are given below.

Laminar flow :

$$\rho\left(\frac{\partial U_i}{\partial t} + U_j \frac{\partial U_i}{\partial x_j}\right) = -\frac{\partial \rho}{\partial x_j} \quad \frac{\partial U}{\partial x_j} \qquad 3.3$$

Turbulent flow :

$$\rho\left(\frac{\partial \overline{U}_i}{\partial t} + \overline{U}_j \frac{\partial \overline{U}_i}{\partial x_j}\right) = -\frac{\partial \overline{P}}{\partial x_i} + \frac{\partial}{\partial x_j}\left(\frac{\mu \partial \overline{U}_i}{\partial x_j} - \rho \overline{u_i u_j}\right)$$

P = pressure, $\overline{U}$ = velocity, subscripts i, j = cartesian co-ordinates, the overbar denotes the time averaged quantity.

The equations shown are applicable to incompressible flows only. It is considered that compressibility effects are negligible when the square of the Mach number $U^2/c^2 \ll 1$, where U is the instantaneous velocityand c the velocity of sound. The incompressibility condition is considered valid for the

turbulent flames studied in this work where the nozzle flow velocity of 7.6×10^{1} $Msec^{-1}$, employed throughout the project, yielded a flame Mach number of 0.02.

It may be observed that the equation for turbulent motion differs from the laminar case only by the presence of the additional stress terms $\sigma_{ij} = -\rho\overline{u_i u_j}$. These stresses are commonly referred to as turbulent or Reynolds stresses and are present in turbulent flows in addition to the viscous stresses discussed in section 3.1. The physical significance of the Reynolds stresses is that they represent the mean rate of momentum transfer produced by the velocity fluctuations. The stresses are generally expressed as a negative quantity since the momentum flows in the direction of the negative velocity gradient in accordance with the nomenclature mentioned earlier. The symbol σ_{ij} refers to the stress acting on the fluid particles perpendicular to i in the direction of j.

The Reynold stresses σ_{ij} have both normal and tangential components. The normal stresses occur when i = j and may be illustrated by considering the stress σ_{11}. If a surface element of fluid of area dS is positioned perpendicular to the x_1 axis of a cartessian co-ordinate system and only turbulent motion is considered to pass through the element, such that no mean velocity $\bar{U}$ exists, the mean rate of momentum flow through dS is $\rho\overline{u_1^2}\, ds$. This flow represents a momentum flux directed along the x_1 axis. The momentum flux is equivalent to a force acting on the x_1 direction which produces a reaction upon the surface element dS and this in turn is equivalent to a pressure. The normal components of the Reynolds stress therefore represent a pressure acting upon the fluid particles in the flow field.

Since the flows in the turbulent flames employed in these studies are incompressible the influence of the normal components of the Reynolds stress may be considered to be negligible.

The tangential or shear stress components occur with $i \neq j$. These may be illustrated by considering the stress $\sigma_{2,} = -\rho \overline{u_1 u_2}$. The surface element dS is now positioned perpendicular to the x_2 axis. The fluid particles passing this plane have both u_1 and u_2 velocity components. On the average for a positive u_1 value the particles will also have a positive u_2 value and vice versa such that the term $\overline{u_1 u_2}$ is positive. In this case a force in the positive x_1 direction is exerted on the positive x_2 side of dS and an equal and opposite force acts on the negative x_2 side of dS in the negative x_1 direction. The forces represent a shear stress acting to distort the fluid element. It is the Reynolds shear stress therefore which are responsible for the deformation of the fluid elements in a turbulent flow field. A further important feature of the Reynolds shear stresses is they do work against the mean velocity gradients and this provides the energy necessary for the preservation of the turbulent motion.

The above illustrates how fluctuations in velocity generate the Reynolds stresses and lead to a transfer of momentum. This transfer rate is far in excess of that due only to viscous stresses and accounts for the enhanced momentum transfer rates for turbulent flows over the corresponding rates for laminar flows. This may be demonstrated by the following numerical illustration. Consider a flow field where the velocity fluctuations are ±10% of the mean velocity.

i.e. $\frac{u}{\overline{U}} = 0.1$ in a flow of nozzle Reynolds No = 10,000.

Reynolds stress = $\rho\overline{u^2} \equiv \rho \frac{\overline{u^2}}{(\overline{U})^2} (\overline{U})^2 = 0.01\ \rho(\overline{U})^2$

If the mean velocity gradient in the flow is given by $(\overline{U})/_d$. The viscous stress σ_v may be expressed as $\sigma_v = -\mu\overline{U}/_d$. The ratio of the mean transfer rates of momentum by Reynolds to viscous stresses is 100. This example clearly indicates how the presence of relatively low level of velocity fluctuations can lead to a pronounced increase in the momentum transfer rates in turbulent flows.

Fluctuations in other flow properties such as temperature or concentration produce a similar result where the transport rates for these quantities also become greater than the corresponding rates in laminar flows.

3.4 Turbulent Diffusion

It may be recalled that the fluctuations in the turbulent flow properties are the result of the irregular eddy motion. As a consequence of this motion the eddies are able to distribute such quantities as momentum, heat and matter over large distances about the flow field such that this eddy diffusive action produces high transport rates for these properties compared to those in non-turbulent flows, as discussed in the previous section.

The first attempts to characterise this feature of turbulence was by Boussinesq, who considered momentum transport and introduced the concept of an eddy viscosity e_m. This was based upon the assumption that the Reynolds stresses, like the viscous stresses, were directly proportional to the velocity

gradient, i.e.

$$\sigma_{ij} = -\rho\overline{u_i u_j} = e_m\left(\frac{\partial \bar{U}i}{\partial xj} + \frac{\partial \bar{U}j}{\partial xi}\right) \qquad 3.4$$

The eddy viscosity was considered to be a parameter characteristic of the local turbulent motion at the region of interest. It was not a true property of the fluid, unlike viscosity produced by thermal molecular motion, nor did it possess a constant value as given by equation 3.4 but varied over the entire flow field. The above equation did however have moderate success in predicting the mean velocity profiles in free jet flows where a pronounced velocity gradient and hence a shear stress in one direction i.e. normal to the mean flow enabled the constant eddy viscosity assumption to be made.

A further treatment, due to Prandtl, was the mixing length theory used to predict both the mean velocity and mass distribution profiles in a flow field. This theory was based upon the analogy between the irregular eddy motion and the random molecular motion in gases. The distance travelled by an eddy without undergoing distortion was referred to as the mixing length analogous to the mean free path for gas molecules. The theory included the concept of an eddy viscosity and in addition an eddy diffusion coefficient. The momentum transfer expression determined by Prandtl was given as follows:

$$\sigma_{ij} = -\rho\overline{u_i u_j} = \rho L^2 \left|\frac{d\bar{U}_1}{dx_2}\right| \frac{d\bar{U}}{dx_2} \qquad 3.5$$

$$e_m = L^2 \left|\frac{d\bar{U}_1}{dx_2}\right|$$

where σ_{ij} = the momentum transfer rate, ρ = fluid density, L = mixing length and $\frac{d\bar{U}_1}{dx_2}$ mean velocity gradient.

A similar expression was derived for the rate of mass transfer employing the eddy diffusion coefficient.

As with the Boussinesq treatment the Prandtl mixing length theory was only successful when applied to free turbulent flows.

The above theories were in principle unsound since they were based upon molecular transport processes. Turbulent eddies, unlike discrete gas molecules, form a continuum and adjacent eddies are continually in contact with each other such that the local turbulent behaviour at one region in the flow field is strongly dependent upon the turbulent motion at distant regions. Due to this condition the turbulent transport processes are not solely the result of local mean gradients but also to a complex interaction between the fluctuating and mean flow properties, the details of which remain largely unknown.

Of great practical importance is the process of turbulent mass transport which greatly increases the rate of mixing between initially separated fluid components in comparison with molecular mixing rates. The turbulent shear stresses break the components up into fluid "lumps" which become distributed about the flow field by eddy diffusion. In addition the stresses distort and stretch the "lumps" into fine threads. This combined action leads to an increase in the local concentration gradients rendering a greater area of contact between regions of differing concentration thereby enhancing the overall mixing rate. It is important to note that turbulence can only break the components up into particles comparable in size to the smallest eddies. The final stage of mixing leading to the formation of a uniform mixture must be completed by molecular diffusion

across the boundaries of adjacent eddies of varying composition.

Turbulent mixing is of importance in the mixing of unmixed fuel and air in turbulent diffusion flames since it is this process that controls the rate of combustion. This will be discussed at length in the following chapter.

3.5 Statistical Theories of Turbulence

The modern theories for characterising turbulence are based upon the statistical analysis of the random eddy behaviour developed by G.I. Taylor using the concepts of correlation and power spectral analysis discussed in the previous chapter. Their application to turbulent fluid motion will now be discussed.

Correlation Analysis

Taylor applied the following correlation analysis to velocity fluctuations in a turbulent flow field. It may also, however, be applied to the fluctuations in any flow property. The correlation between velocity fluctuations at two points A and B in the flow separated by a distance r in the x_1 direction is given as :

$$\text{Cross correlation function } R_{AB}(r) = \lim_{T\to\infty} \frac{1}{T}\int_0^T u_1(x)u_1(x+r)dt \qquad 3.6$$

or in terms of the correlation coefficients as :

$$\text{Cross correlation coefficient } \rho_{AB}(r) = \lim_{T\to\infty} \frac{1}{T}\int_0^T \frac{U_1(x)u_1(x+r)dt}{(u_1(x)^2)^{\frac{1}{2}}(u_1(x+r^2)^{\frac{1}{2}}}$$

where $u_1(x)$ represents the velocity fluctuations at A and $u_1(x+r)$ the velocity fluctuations at B. along the x axis.

For small values of r the fluctuations produced by the eddy motion will be "seen" simultaneously as they flow past both points giving a high correlation value. As r is increased the correlation value will fall since the fluctuations due to the small eddies will not be observed at both points at the same instant in time, thus only the fluctuations due to the larger eddies common to both A and B will be correlated. Upon further increases in r the correlation will tend to zero when the separation distance extends beyond the largest eddy diameter.

This distance introduces a further important parameter for characterising turbulence, namely the scale of turbulence which may be considered to be a statistical measure of the diameter of the largest eddies present at the region of interest in the flow. The distance required for the correlation to reach zero is not taken instead the area under the correlogram is measured giving the integral space scale of turbulence L_{x_1} in the x direction.

$$L_{x_1} = \int_0^\infty \rho_{AB} \, dr \qquad 3.7$$

An extension of the above spacial correlation treatment has been given by von Karman and Howarth [8] relating longitudinal and transverse cross correlation coefficients in homogeneous and isotropic turbulence. The longitudinal function f(r) is measured with the test points lying in the direction of the mean flow and the transverse function g(r); the points are located normal to this direction. These positions are illustrated below.

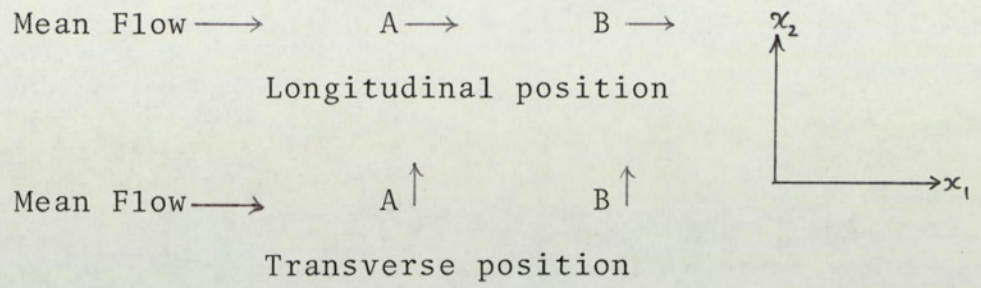

Fig. 3.1

The two correlation coefficients are expressed and related by the following :

Longitudinal cross correlation coefficient

$$f(r) = \lim_{T\to\infty} \frac{1}{T} \int_0^T \frac{u_1(x)\,u_1(x+r)}{(u_1(x)^2)^{\frac{1}{2}}\,(u_1(x+r)^2)^{\frac{1}{2}}}$$

Transverse cross correlation coefficient

$$g(r) = \lim_{T\to\infty} \frac{1}{T} \int_0^T \frac{u_2(x_1)\,u_2(x_1+r)}{(u_2(x_1)^2)^{1/2}\,(u_2(x_1+r)^2)^{1/2}}$$

The von Karman-Howarth relation:

$$g(r) = f(r) + \frac{r}{2}\frac{\partial f(r)}{\partial r} \qquad 3.8$$

The proof for this equation is given by Hinze [8]. If a knowledge of one of the above functions is known equation 3.8 enables the other function to be calculated. Alternatively if both have been experimentally determined, one function may be calculated which may be compared with the experimental profile to provide a rough indication as to the isotropy of the turbulent flow field.

The turbulent structure may be elucidated further by observing how the correlation function varies with time. Fluctuations at a single point in the flow may be auto-correlated for varying delay times. At zero time delay

maximum correlation must exist. After some short delay time the correlation will decrease slightly since the small eddies contributing to fluctuations at zero delay (τ) will have moved after a time ($t+\tau$) and only the fluctuations due to the larger eddies will be common at both times and they only will be correlated. Eventually, with the application of increased τ, the correlation will tend to zero since the eddies of all sizes present at time t will have sufficient time to flow from the point becoming replaced by a new eddy pattern from upstream in the flow. Analogous, to the space scale, discussed above, the area under the autocorrelogram provides a measure of the integral time scale of the turbulent flow field. This parameter may be considered to be an approximate measure of the time required for the largest eddies to pass the point of study in the flow field. The time scale is therefore defined as :

$$L_\tau = \int_0^\infty \rho(\tau)\,dt \qquad 3.9$$

An alternative method for the estimation of both space and time scales which is commonly used experimentally is to determine that scale where the correlation function has fallen to a value of 1/e of its initial value. This is particularly useful in the case of correlation coefficient profiles since it corresponds to the scale at $\rho = \frac{1}{e} \Xi 0.37$ for all cases.

Taylor's Hypothesis

Taylor considered a hypothetical turbulent flow field wherein no shear stresses exist and the eddy pattern does not therefore change shape appreciably. The eddies are considered to travel at the mean gas velocity $\overline{U}$ such that after a time τ

they will have travelled a distance $\bar{U}\tau = r$. This hypothesis may be applied to flows of low turbulent intensity where the frozen eddy pattern may be considered to exist. For such flow fields a knowledge of the autocorrelation function and mean gas velocity $\bar{U}$ will enable the spacial cross correlation function to be evaluated by using the above equation to transform the time delay axial values into values having the dimensions of length and vice versa.

Space-Time Correlation

The space-time cross correlation function is determined by cross correlating two non-identical signals from two spacially separated points lying parallel to the direction of mean flow and applying a time delay to the signal from the upstream position. This important extension of the correlation technique was developed byFavre and may be used to determine the local convective velocity of the turbulence pattern and the rate of distortion it undergoes during the travel period between the measuring points. The space-time cross correlation function is defined as:

$$\rho_{AB}(r,\tau) = \lim_{T\to\infty} \frac{1}{T} \int_0^T \frac{u(x;t)u(x+r;t+\tau)}{(u(x+t)^2)^{\frac{1}{2}} (u(x+r;t+\tau)^2)^{\frac{1}{2}}} \, dt \qquad 3.10$$

For a separation distance r in space the eddies at an upstream point A will arrive at a downstream point B after a time equal to $r/\bar{U}_c$ where $\bar{U}_c$ is the mean convective velocity of the eddy pattern. Upon the application of a time delay to the signal at A the correlation coefficient will be observed to

gradually increase producing a peak when the delay corresponds to the value $r/\overline{U}_c$ followed by a gradual decrease.

Consideration of Taylor's hypothesis where no eddy distortion occurs in the flow the cross correlation coefficient will exhibit peak values of unity for all values of the separation distance r. Under such conditions the various sized eddies travel at the same velocity given by r/τ_{max} where τ_{max} corresponds to the delay time at $\rho_{AB} = 1$ and this convective velocity is identical to the local mean gas velocity at the region of interest.

In practice the presence of the Reynolds shear stresses causes the eddy structure to undergo distortion during travel downstream. This results in the correlation peak values to decrease with increased r since the distortion of the eddies will be greater the larger the travel distance thus lowering the extent of correlation. A typical series of space-timecorrelograms for varying r values is shown in Fig. 3.2. The curve drawn such that it is at a tangent to each correlogram is known as the moving axis autocorrelation function. This may be considered to be the autocorrelogram obtained by an observer moving with the turbulent flow at the convective velocity. A plot of the various separation distances between A and B against the delay times where the moving axis autocorrelogram touches the relevant space-time correlogram will yield a straight line graph whose slope equals the convective velocity. In the practical case the convective velocity of the turbulent pattern and the mean velocity are not equal. The convective velocity is generally defined as the velocity of the main energy bearing eddies whereas the mean velocity is the time averaged velocity of the bulk gas flow. The different velocity terms will be examined

more fully in a later chapter.

The parameter defined as the time required for the moving axis autocorrelogram to fall to $^1/_e$ of its initial value is known as the moving axis time scale. This provides a measure of the rate of eddy distortion which takes place between the interest points A and B. Both convective and mean velocities together with moving axis time scales have been measured in the turbulent diffusion flame studied in this project.

3.6 Distribution of Energy in Turbulent Flows.

Information concerning the turbulent kinetic energy content in a flow field and how this energy is distributed among the eddies with respect to their size is provided by the power spectral density function. It may be recalled power spectral analysis provides the same information as correlation analysis but is presented in a different manner; spectral analysis provides information in the frequency domain and correlation analysis in the time domain.

The frequency of an eddy may be pictured as the inverse size of an eddy diameter. Hence as eddies flow passed a stationary observation point in the flow the larger eddies will contribute low frequency fluctuations whereas the smaller eddies are responcible for the high frequency components of the random signal.

The power spectrum most commonly used experimentally, as with this work, is the one dimensional spectrum determined by considering the fluctuations at one point in the flow and along one axis of a Cartesian coordinate system. The determination of the mean square value of the eddy fluctuations between the frequencies f and $f + \Delta f$ yields a measure of the energy content within the band width Δf. If this procedure is repeated over the entire frequency range of the random signal it enables an energy spectrum to be determined by plotting the mean square values within the

Fig. 3.2 Typical Space-Time Correlograms for Velocity Fluctuations in a Turbulent Flow Field

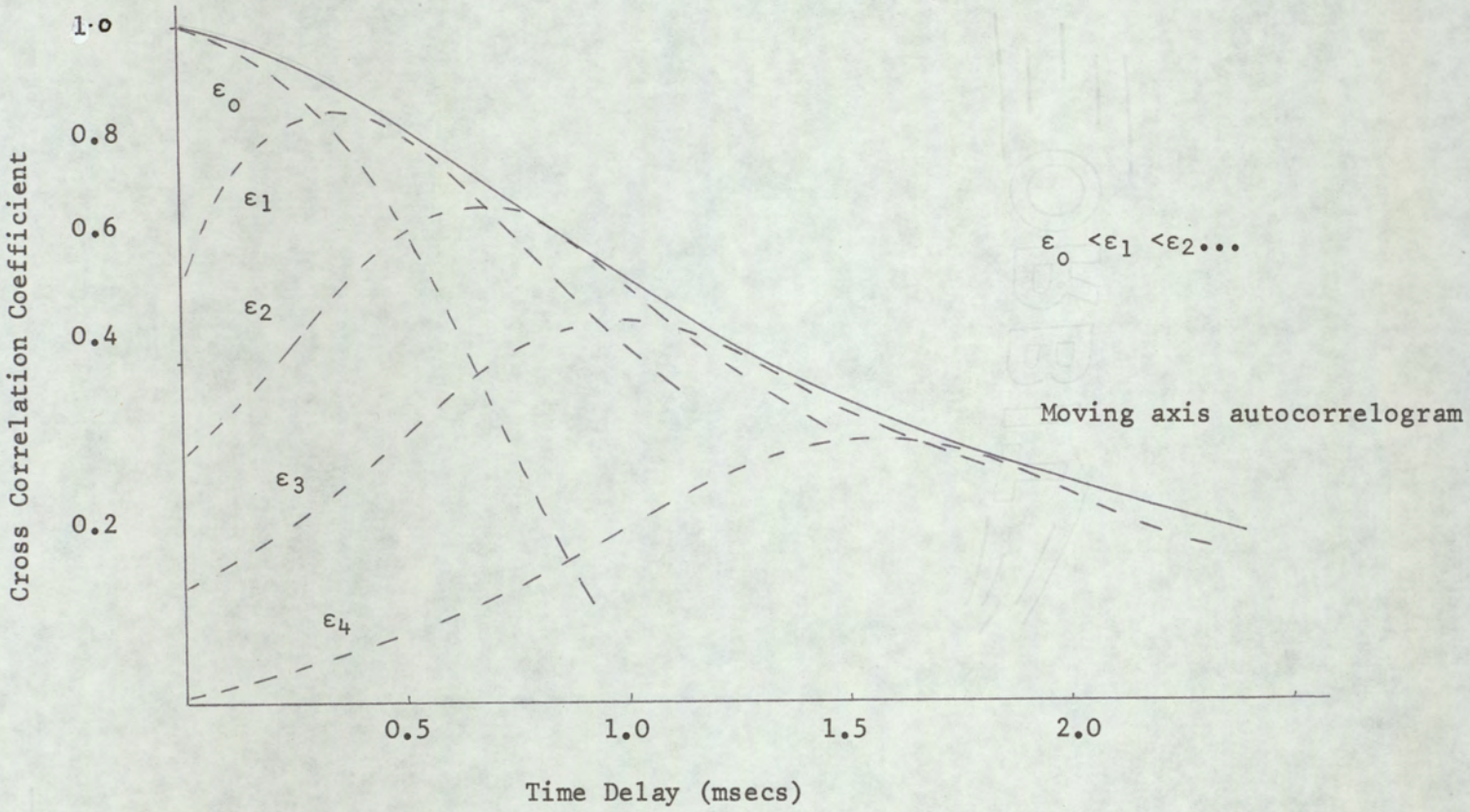

bandwidth Δf against frequency. Fig. 3.3 illustrates a typical one dimensional energy spectrum. The area enclosed by the curve is equal to the kinetic energy present in the signal such that:

$$\text{kinetic Energy} = \frac{1}{2}\rho\overline{U^2} = \int_0^\infty G(f)df$$

A more accurate analysis is provided by the three-dimensional power spectrum which includes the fluctuations along the three cartesian coordinate axes. This enables the total kinetic energy content at the measurement point to be evaluated:

$$\text{Total kinetic Energy} = \frac{1}{2}(\overline{u^2} + \overline{v^2} + \overline{w^2})\rho = \int_0^\infty E(f)df$$

It is generally not used experimentally owing to the complexity of the function.

A typical three dimensional power spectrum is shown in Fig. 3.4. As indicated the largest eddies which have an almost permanent character undergoing a slow decay do not possess the maximum energy. The region of the spectrum where the eddies make the largest contribution to the total energy content is known as the energy containing range with the maximum marked at f_e. In this region the Reynolds number will be high such that the inertial forces cause the eddies to undergo collision at interactions so as to produce smaller eddies, transferring some of their energy to product eddies. These eddies in turn produce yet smaller eddies and in this manner energy is transferred from the larger energy containing range to the smaller ones, the smallest eddies being destroyed by viscous effects as mentioned previously.

Fig. 3.3 Typical Power Spectrum for Velocity Fluctuations in a Turbulent Flow Field.

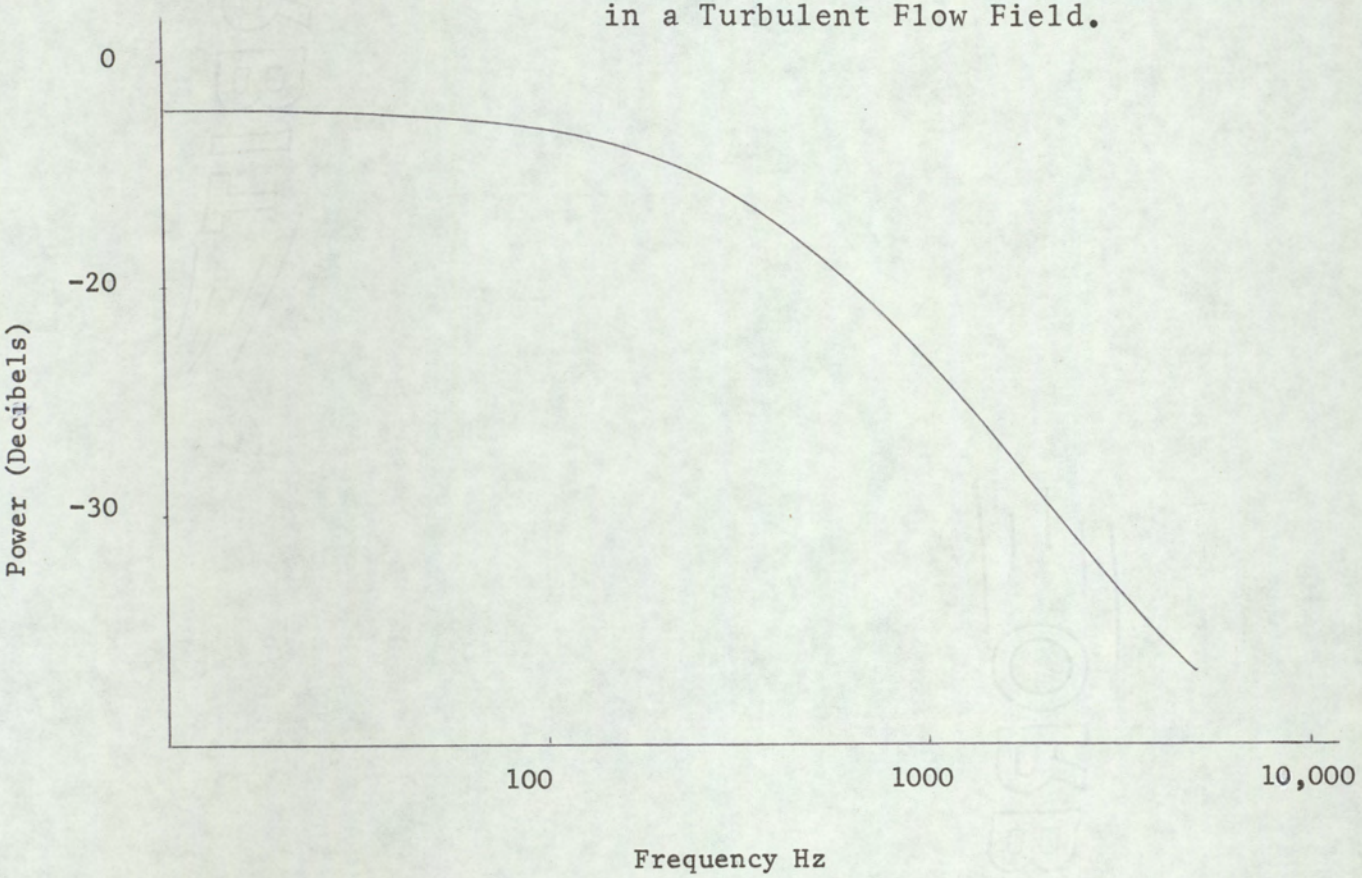

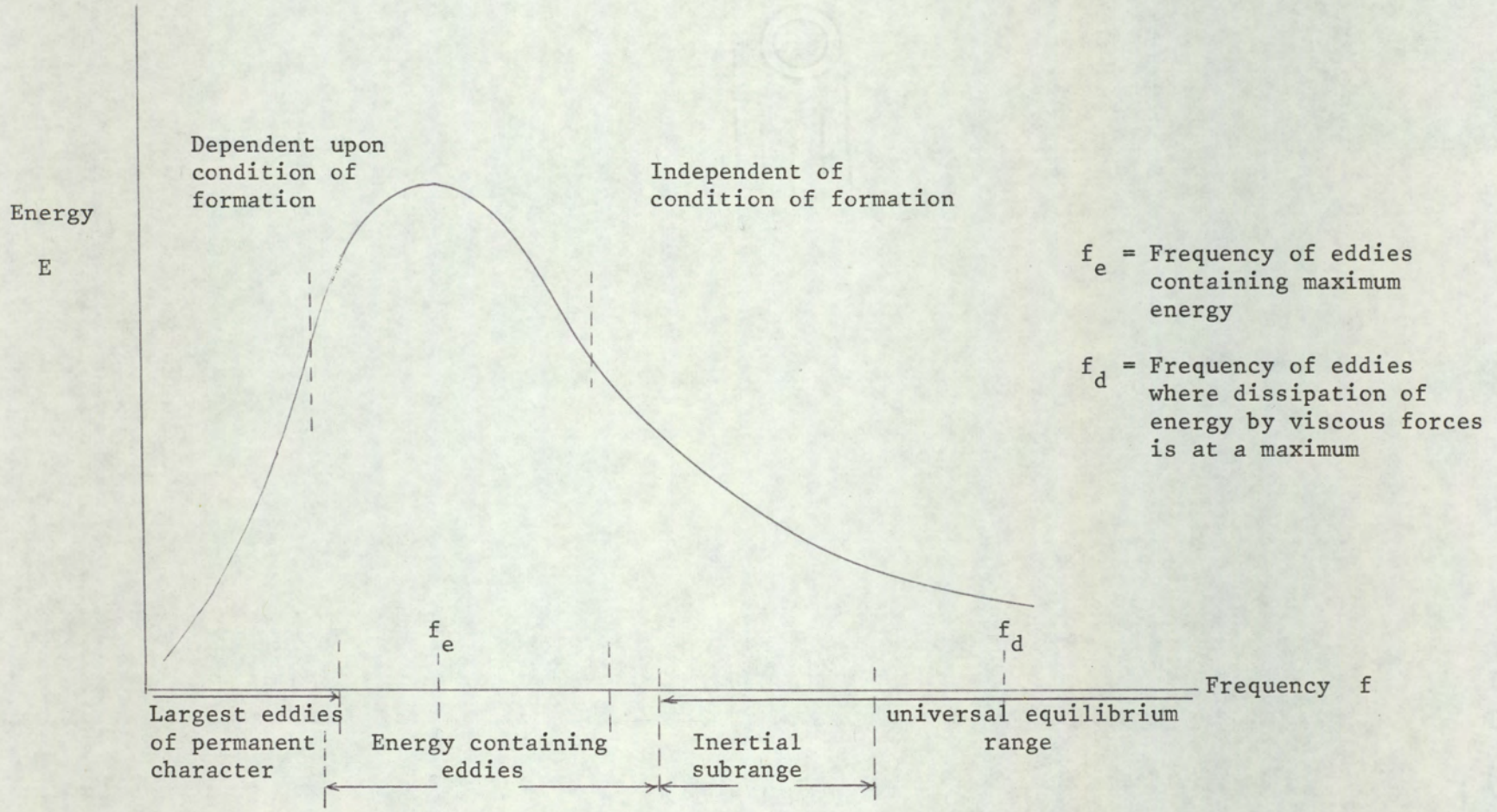

Fig. 3.4 Three Dimensional Power Spectrum Showing the Distribution of Energy in the Various Frequency Ranges

The rate of loss of turbulent energy may be related to the frequency of the eddy fluctuations in the flow. The frequency of the large eddies is less than the decay rate whilst the frequency of the smallest dissipating eddies will be greater. Between these frequencies it may therefore be concluded that a range of eddies exists with a frequency of the same order as the rate of energy loss. In this range the turbulence is considered to be statistically invarient in that the mean square values of the fluctuations is constant. The eddies in this high frequency range are therefore isotropic even if the rest of the turbulence field is anistropic. These eddies are considered to be in statistical equilibrium with each other being independent of the condition of formation and dependent only on the rate of energy loss and viscosity effects. Energy dissipation takes place over much of the region becoming more pronounced at the higher frequencies. This region where statistical equilibrium exists is known as the universal equilibrium range, where the turbulence is governed only by the rate of energy supplied to the system E and viscosity ν. This is the basis of Kolmogoroff's law. From dimensional analysis he deduced a length scale corresponding to the size of the smallest dissipating eddies and a velocity scale which may be influenced only by E and ν.

$$\text{Length scale} = \left(\frac{\nu^3}{E}\right)^{\frac{1}{4}}$$

$$\text{Velocity scale} = (\nu E)^{\frac{1}{4}}$$

At the lower frequency part of this region where higher Reynolds numbers exist the viscosity effects are negligible and the turbulence is characterised only by E. This portion of the universal equilibrium range is known as the inertial subrange. The rate of energy change in this subrange E is related to the power spectral density function G by

$$G = \text{constant} \times \bar{E}^{2/3} k^{-5/3}$$

where k = wave number related to frequency by:

$$k = \frac{2\pi f}{\bar{U}}$$

CHAPTER 4

TURBULENT FLAMES

4.1 Introduction

Research studies on turbulent flames have, in the main been directed at investigating the properties of premixed flames. Turbulent diffusion flames have been somewhat neglected although they are used more frequently in industry. Examples include the burning of producer gas with air in the manufacture of steel and the combustion of fuel droplets in Diesel and gas turbine engines. Studies of turbulent diffusion flames have, as a result, been confined to the measurement of such bulk properties as flame height and shape. In this chapter the properties of both premixed and diffusion turbulent flames will be discussed together with a review of existing flame propagation mechanisms. Also included is an account of the chemistry turbulence interaction phenomenon. Prior to this, however, a brief discussion of the chemical processes occurring in hydrogen and hydrocarbon flames will be presented.

4.2 Chemistry of Hydrogen and Hydrocarbon Flames

The oxidation of hydrogen in a flame takes place by the following reversible processes;

$$H + O_2 \rightleftharpoons OH + O \qquad (i)$$

$$O + H_2 \rightleftharpoons OH + H \qquad (ii)$$

$$OH + H_2 \rightleftharpoons H\,O + H \qquad (iii)$$

They result in the concentration of the free radicals H, O and OH being several orders of magnitude greater than the permitted

Saha equilibrium levels. The species recombined by the following ternary reactions,

$$H + H + X \rightarrow H_2 + X \qquad \text{(iv)}$$

$$OH + H + X \rightarrow H_2O + X \qquad \text{(v)}$$

which tend to reduce the disequilibrium downstream of the reaction zone. It has been shown however, these radicals may maintain equilibrium proportions with respect to each other by the more rapid bimolecular exchange process;

$$H_2O + H \rightleftharpoons H_2 + OH$$

$$H_2 + O \rightleftharpoons OH + H$$

The radical species H, O and OH do not produce any appreciable amounts of natural ionisation such that the burnt gas region of hydrogen flames have been extensively used for the study of nonequilibrium ion chemical kinetics of metal additives.

In contrast the hydrocarbon flame or hydrogen flames containing a trace of hydrocarbon produce high levels of natural ionisation. Knewstubb and Sugden[9] established the principal positive ions generated in the reaction zone to be H_3O^+ and $C_3H_3^+$. The former of these being longer lived persists further downstream in the flame.

The mechanism for the formation of H_3O^+ ion is given by the following chemionisation process

$$CH + O \rightarrow CHO^+ + e^- \qquad \text{(vi)}$$

$$CHO^+ + H_2O \rightarrow H_3O^+ + CO \qquad \text{(vii)}$$

$$H_3O^+ + e^- \rightarrow H_2O + H \qquad \text{(viii)}$$

High H_3O^+ concentration levels produced in the reaction zone which rapidly decays by the recombination reaction (viii)

The ionisation of alkali metals in hydrogen flames proceeds by the thermal ionisation process;

$$M + X \rightarrow M^+ + e^- + X \qquad \text{(ix)}$$

where X is a third body.

When metal additives are introduced into flames containing H_3O^+ species the charge exchange reaction

$$H_3O^+ + M \rightarrow M^+ + H_2O + H \qquad \text{(x)}$$

has been shown to occur[10]. This enables metals with high ionisation potentials such as lead which would not ionise by the thermal process to do so. It also enables elements such as sodium or potassium to attain their respective thermodynamic equilibrium levels more rapidly than is achieved by process (ix). The charge exchange reaction allows elements with ionisation potentials up to 8.3 eV to ionise whereas only those with ionisation potentials less than 6.3 eV may ionise by the thermal process.

4.3 Turbulent Premixed Flames

Free turbulent flames may readily be distinguished from laminar flames by the thickening of the flame front, the rounding and shortening of the tip of the flame and by the accoustical noise generated. The early investigations of turbulent premixed flames concentrated upon studies of direct and instantaneous schlieren photographs of such flames. This approach was used extensively by Karlovitz et al.[11] Under the conditions of laminar flow the familiar conical combustion wave is formed

which constitutes a sharp boundary between the unburnt and combusted gas. In direct photographs the wave profile is clearly visible as a line of luminosity from the reaction zone. Instantaneous schlieren photographs show a smooth profile produced by the sharp density gradient which exists between the unburnt and burnt gas.

When the gas flow rate is increased beyond the critical Reynolds number the onset of turbulence leads to the luminous core becoming shorter and more diffuse with the boundary between the unburnt and combusted gas becoming irregularly wrinkled. This effect becomes more pronounced with increased flame height and is due to the presence of large scale turbulent eddies. Schlieren photographs clearly illustrate the distorted flame front which presents sharp protruding edges towards the combusted gas and smooth curved surfaces towards the unburnt gas. The formation of this structure may be explained by consideration of Fig. 4.1. due to Karlovitz.[11] The large scale eddies may be considered to perturb the thin flame front such that it has a sinusoidal wave form. Then if each element of the flame surface proceeds at the laminar burning velocity then the flame envelope subsequently takes on the profiles (b), (c) and (d) as shown in Fig. 4.1, thereby assuming the structure described above.

Photographic techniques have proved useful for illustrating the effects of turbulence on a flame, however they cannot be interpreted to provide information regarding the local turbulent characteristics within a flame. Few measurements of local turbulent parameters in free turbulent premixed flames have been made. Of these Westenburg[12] determined turbulent intensity

Fig. 4.1 Karlovitz model illustrating the effect of turbulent fluctuations on the flame front, initially at position (a), proceeding at the laminar burning velocity to subsequent positions (b), (c) and (d)

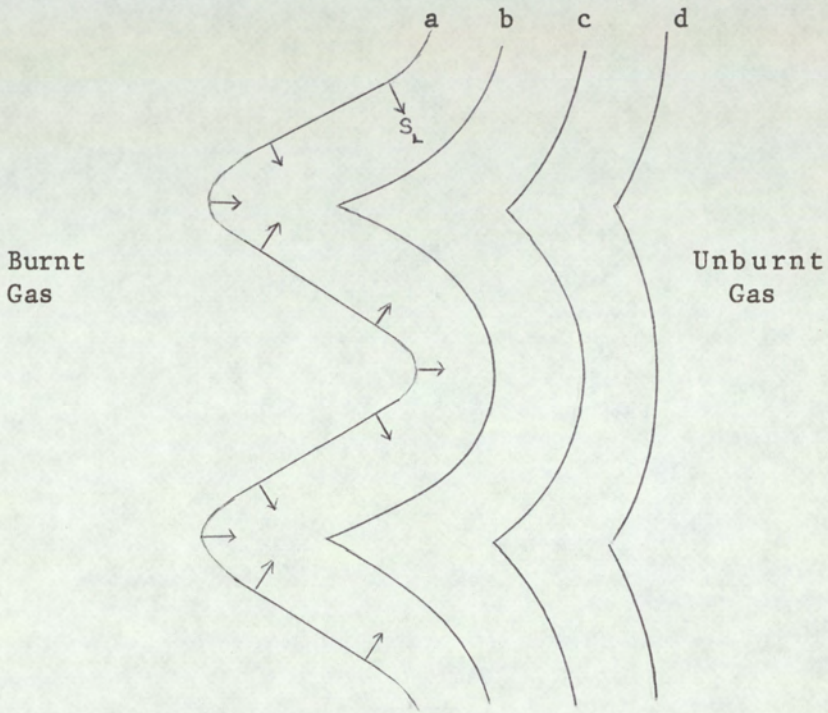

measurements in flames and jets using a helium diffusion technique. The aim of this work was to obtain evidence for the concept of flame generated turbulence. This and other mechanisms for turbulent flame propagation will be discussed in a later section.

4.4 Turbulent Diffusion Flames.

Flames produced by the flow of fuel into the atmosphere where the combustion process is controlled by the mixing of the initially unmixed fuel and air are classified as diffusion flames. When the gas flow is laminar burning is controlled by the molecular diffusion of atmospheric oxygen into the outer fuel regions such that the flame boundary is essentially defined as the region where the fuel and oxidant form a stoichiometric mixture. With increased flame height the boundary gradually moves towards the flame axis as fuel is consumed. When at the axis no further combustion occurs but the mixing of combustion products and air continues. The candle flame is an example of a laminar diffusion flame.

When the flow of fuel is increased turbulence is created when the frictional forces between the fast moving fuel stream and the stagnant atmosphere are sufficiently great. Much of our understanding of the structure of the turbulent diffusion flame has been derived from extensive studies conducted on the analogous isothermal jet.[13;14] The structure of a turbulent diffusion flame is shown in Fig. 4.2. In the centre of the flame is a conical shaped diffusion core which extends a short distance above the nozzle. No mixing occurs within the

Fig. 4.2 The Regions of a Turbulent Diffusion Flame

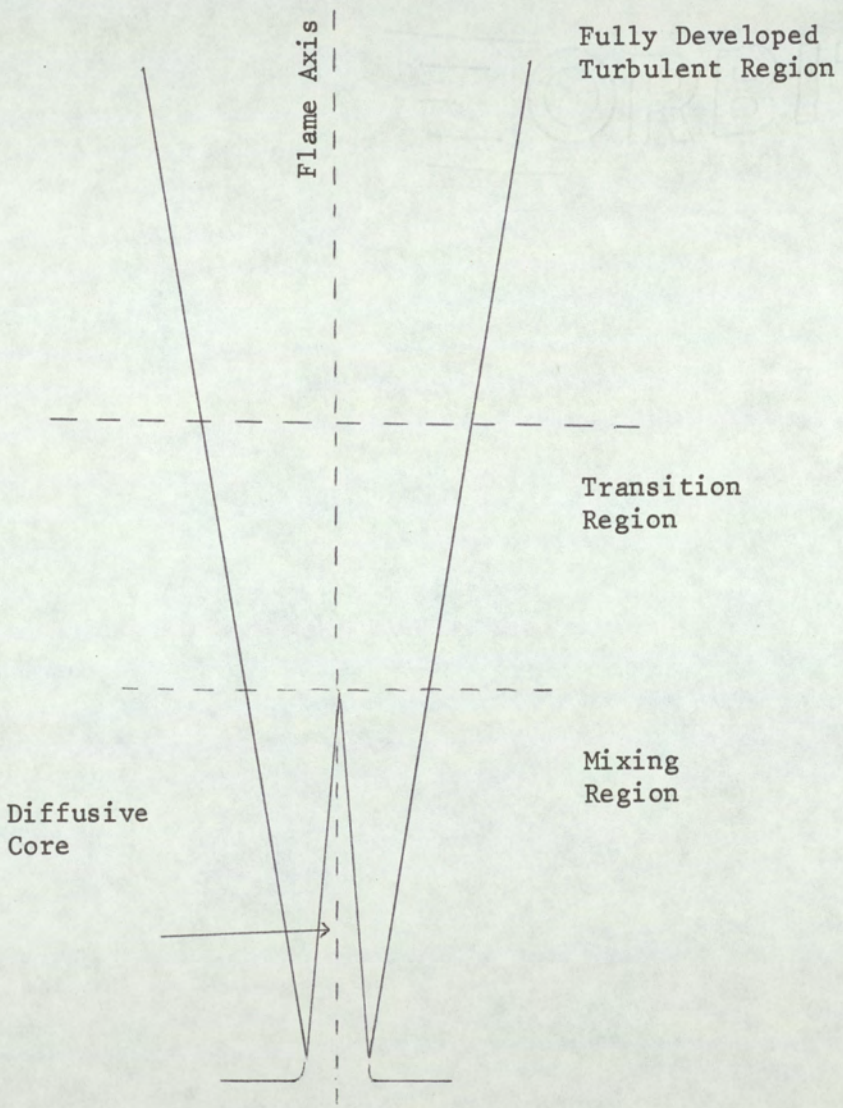

core and the flow in this region is considered to be laminar. Surrounding the core is a region of high velocity gradients normal to the direction of mean flow such that high turbulent shear stresses exist. This region is commonly referred to as the mixing zone since it is a region of intense turbulent mixing between the fuel stream and the stagnant atmosphere. It is here that most of the turbulence in the flame is generated. Extending beyond the diffusive core is the transition region and further downstream the fully developed turbulent region exists. Here the flame atmosphere boundary is highly distorted indicating the presence of large scale eddies. The work of Lawrence[13] with subsonic jets has shown from cross correlation measurements of velocity fluctuations the dimensions of the large scale eddies is controlled by the dimensions of the jet. It is considered this also applies to turbulent flames such that the characteristic spreading action of the flame with increased height results in the large eddies gradually increasing in size as they flow downstream. The spreading of the flame is due to the entrainment of air. The large scale eddies drawn in lumps of air into the flame. The turbulent shear stresses break the lumps into progressively smaller elements so increasing the area of contact between the fuel and air. This, it may be recalled, results in an increase in the local concentration gradients between eddies of varying composition thereby enhancing the mixing rate compared to the molecular mixing rate. Combustion, since it is a chemical reaction, is a molecular process thus fuel and oxygen must molecularly diffuse across adjacent eddy boundaries before burning can commence. The turbulent mixing action, by increasing the contact area between the fuel and air results in the greater volumetric burning rate in comparison to the laminar flame. The rate of molecular diffusion at

elevated flame temperatures may be several orders of magnitude greater than at room temperature such that the rate determining step in the combustion process is considered to be the rate of turbulent mixing. Mixing also occurs within the flame where the combusted gases and unburnt fuel gradually become diluted with excess entrained air, the process becoming more pronounced at larger downstream distances.

A further feature of turbulence present at the outer flame boundary regions is that of turbulent intermittency. This phenomenon occurs where turbulent and non-turbulent fluid elements become adjacent such as occurs during air entrainment where the large scale turbulent eddies are adjacent to elements of initially non-turbulent air. Intermittency was encountered during this project and its characteristics will be described later in the text. The phenonenon is a highly complex motion and has received little experimental study such that its properties remain largely unknown.

As has been mentioned previously, research on turbulent diffusion flames has been mainly concerned with bulk property measurements. Hottel et al[15] made extensive studies with both laminar and turbulent diffusion flames. Amongst these they observed that increasing the fuel gas flow rates, with the flow remaining laminar, produced an almost linear increase in the height of the diffusion flames. Further increases in the flow rate produce instabilities in the flame such that a slight decrease in height was observed. With additional increases the flames became turbulent and thereafter remained at almost a constant height, becoming independent of further

increases in gas flow. Further studies by Hawthorne[16] showed that the rate of mixing in hydrogen diffusion flames by measuring the mean rate of H_2 decay is smaller than in non-burning hydrogen jets. This was explained by considering the reaction zone to form an envelope round a core of cold gas emerging from the nozzle. Under these conditions the flame may be considered to be a cold high density jet entraining hot, low density products. This will result in little entrainment and therefore a lower mixing rate in the case of the flame.

Measurements of local turbulent parameters in turbulent diffusion flames, as was noted for premixed flames, are few in number. Eickhoff[17] and independently Becker and Brown[18] have determined turbulent intensity measurements in diffusion flames and jets, from static pressure measurements. They each found a decrease in intensity in the flame compared to that in the jet. The reasons for this are not clear, however, Eickhoff has suggested that this is due to a density effect. Gunter and Simon[19] have made measurements of turbulent intensity and turbulent scales using an optical probe to observed fluctuations in CH and C_2 radical emissions from small volumes within the reaction zone. Their turbulent intensity measurements across the flame at various flame heights showed two off axis peaks at the upstream flame regions. The peak positions gradually shifted to ward the axis with increased height eventually reaching the axis, producing a single on axis peak. This behaviour was attributed to the following of the reaction zone which, as in the laminar diffusion flame tends towards the flame axis as fuel is consumed. Measurements of the scale of turbulence on the flame axis show the values to gradually increase with increased distance from the burner, analogous to the findings of Lawrence[13] described above.

Burning Velocity

The burning velocity is the velocity with which a plane flame front moves normal to its surface through the unburnt gas mixture. It is a fundamental constant of a gas mixture and has been used extensively in theories on turbulent flame propagation. Difficulties arise in its measurement since a plane flame front is only observed under special conditions and in most cases the front is either curved or is not normal to the gas stream.

The general method employed for the measurement of burning velocity is that of Gouy. It involves the use of a stationary flame on a burner of circular cross section. It is assumed that the burning velocity is constant over the whole surface of the flame front. The front under these conditions is not normal to the direction of gas flow,however a component of the gas flow normal to the front is equal to the burning velocity Su. This is illustrated below

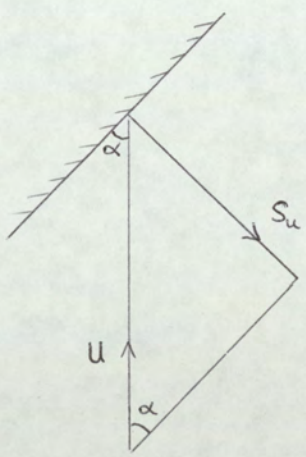

Fig. 4.3

If the area of the burner cross section A_o and the mean gas flow is U then the total volume of gas flow is given as A_oU. The total flame area A_f moves with velocity S_u, therefore since the flame is stationary,

$$S_u = \frac{UA_o}{A_f}$$

The flame area may be estimated from photographs of the flame using a planimeter. This method yields burning velocities within ±20%.

4.5 Turbulent Flame Propagation Mechanisms

Turbulent flame propagation theories have largely been determined from studies of turbulent premixed flames. The first attempt to measure and interpret the effect of turbulence on flame propagation was by Damkohler[20]. He visualised the flame in a turbulent flow to be identical in structure to the laminar flame, the front being wrinkled by eddies larger than the thickness of the front thereby being capable of greater consumption of gas mixture due to its increased surface area. The Damkohler model is illustrated in Fig. 4.4.

Diagram (a) illustrates a plane flame front in a laminar flow of uniform velocity profile. The front remains stationary if the gas velocity U is equal to the laminar burning velocity S_L. In the turbulent gas flow some fluid elements move at greater or lower velocity than the mean velocity and a simplified instantaneous velocity profile is illustrated in diagram (b). The greater velocity at the segment "x" will cause the flame front to bulge out as shown. Similarly the lower gas velocity at segment "y" will result in

Fig. 4.4 Damkohler's Wrinkled Flame Front Model in a Turbulent Flow

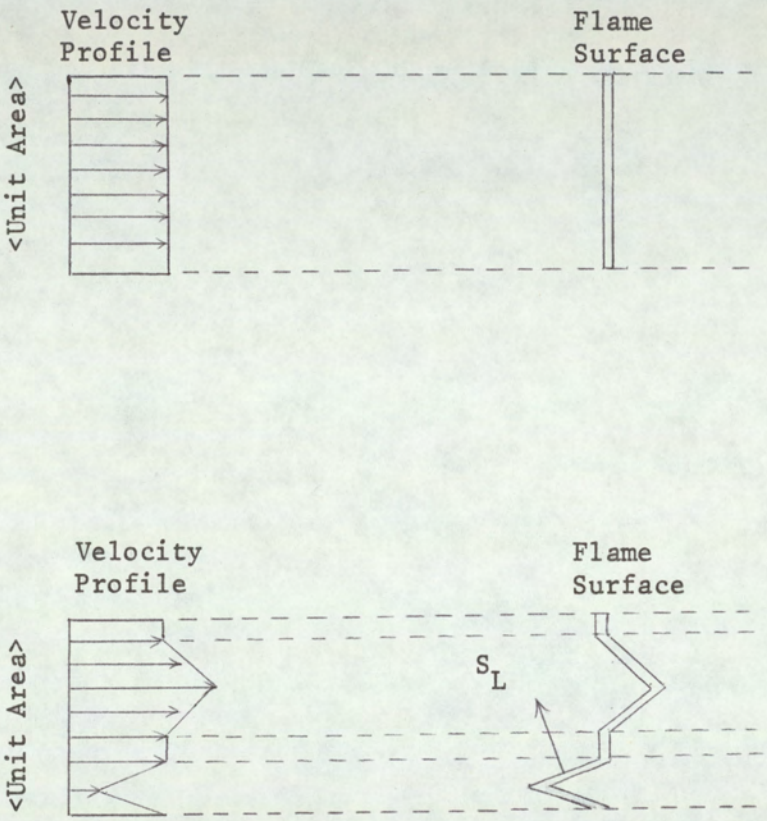

the formation of an inverted cone. Thus the smooth flame front produced under laminar flow conditions becomes distorted by the large scale turbulent eddies. In this way the surface area of flame front per unit area of the stream cross section becomes greater in comparison to the laminar case. Therefore in order for the turbulent flame to remain stationary the average gas velocity must be increased to some value S_T. For any element of the distorted flame front the rate of propagation normal to the wave remains equal to the laminar burning velocity S_L as shown in Fig. 4.4(b).

Damkohler therefore predicted the combustion wave does not disintegrate under turbulent conditions but retains its continuous structure.

Damkohler further considered the areas of the positive and negative cones produced by the fluctuations in the gas flow to be proportional to the root mean square of the velocity fluctuations and obtained the following expression for the turbulent burning velocity

$$S_T = S_L + u^1 \qquad 4.1$$

where u^1 = R.M.S. of velocity fluctuations.

Damkohler's experimental studies included the use of small flames where the scale of the turbulent eddies was much smaller than the thickness of the reaction zone. Under these conditions the turbulence would not appreciably wrinkle the flame front but would increase the rate of heat and mass transfer within the reaction zone thereby contributing to the enhanced burning velocity. He expressed the turbulent burning velocity for such flames as;

$$S_T = S_L \frac{\varepsilon_D}{k} \qquad 4.2$$

where $\frac{\varepsilon_D}{k}$ = $\frac{\text{Eddy Diffusivity}}{\text{Molecular Diffusivity}}$

Of major importance, however, was the wrinkled laminar flame model and following this concept several other theories emerged using the Damkohler model but differing in the methods employed to relate the turbulence properties to the increased burning velocity. Schelkin[21] expressed the turbulent burning velocity as;

$$S_T = S_L \left[1 + B \left(\frac{u^1}{S_L} \right)^2 \right]^{\frac{1}{2}} \qquad 4.3$$

Therefore for flames of high Reynolds number both the Damkohler and Schelkin models predict that the turbulent burning velocity becomes proportional to the intensity of the velocity fluctuations u^1

i.e. $S_T \propto u^1$

and therefore independent of the laminar burning velocity and of the nature of the fuel gas.

The experimental observations of Bollinger and Williams[22] using premixed, propane, ethylene and acetylene flames showed the turbulent burning velocity was not independent of the fuel gas and S_T was shown to have a clear dependence upon S_L. From their experimental measurements they determined the following empirical relationship.

$$S_T = 0.18\ S_L (d)^{0.26}\ (Re)^{0.24} \qquad 4.4$$

where d = diameter of burner nozzle.

The theoretically determined turbulent burning velocities were found to be appreciably lower than experimental values. To resolve this discrepancy several workers[11 ; 22] considered turbulence was generated in the flame itself thereby giving a higher u^1. The work of Westenberg [12] later established the concept to be unacceptable on the basis of lower turbulent intensity values in flames than in jets. Similar findings have been shown in this work employing the helium diffusion technique, as was used by Westenburg, and will be discussed in Chapter 14.

The wrinkled flame front concept has, despite the disagreement between theory and experiment found widespread support. Richmond et al[23] established that the flame front remains continuous by focussing light from a small section of the flame onto a photomultiplier tube. By observing various frequency components the level of light never tended to zero as would occur if the flame front became disrupted into separate flamelets.

For turbulent flames of high turbulent intensity Summerfield et al[24] considered the Damkohler model was not applicable and postulated that for a flame under these conditions the reaction zone becomes very wide such that it incorporates both large and small scale eddies and consists of isolated pockets of reacting gas.

Neither the wrinkled flame front nor the distributed reaction zone model are considered satisfactory propagation mechanisms when tested over a wider range of flow velocities. The Damkohler model appears to be the more suitable for flames of low Reynolds numbers and the Summerfield model for high

Reynolds number flows. This has since led to the mixed model concept[25] where upon increased flow rates the Damkohler model gradually gives way to the distributed reaction zone model, such that a transition region exists where both modes operate.

A possible mechanism for turbulent diffusion flame propagation has received little attention. Upon considering the turbulent mixing process the entrainment of large lumps of air to support combustion where burning occurs on the common surfaces between fuel and air it is difficult to conceive the wrinkled flame front model applies. The author is thus of the opinion that a mechanism similar to the distributed reaction zone model is therefore the more acceptable.

4.6 Chemistry Turbulence Interaction

It may be recalled that the interaction between chemistry and turbulence arising from the presence of a chemically active species in a turbulent flow was briefly described in Chapter 1. The two aspects of the phenomenon will now be discussed at greater length in terms of ion chemical kinetics in a turbulent flame, this being of relevance to this work.

Effects of Turbulence upon Chemistry

The fluctuations in the concentration field of a chemically active species has been noted previously to be due to the irregular turbulent motion. Since the reaction rate is dependent upon the concentration of the species, fluctuations in their concentration may also be expected to influence the

rate. The influence of turbulence upon a chemical reaction may be demonstrated by considering the recombination reaction between H_3O^+ ions and free electrons, a reaction that has been extensively used throughout this work.

The instantaneous species concentration may be expressed in a manner used previously, as the sum of a non zero time averaged value and a fluctuating component. For the reaction

$$H_3O^+ + e^- \xrightarrow{k_{H_3O^+}} H_2O + H$$

$$N_{H_3O^+} = \overline{N}_{H_3O^+} + n_{H_3O^+} \qquad 4.6$$

where $\overline{n}_{H_3O^+} = 0$

The recombination rate equation is given as;

$$- \frac{dN_{H_3O^+}}{dt} = k_{H_3O^+} \; N_{H_3O^+} \; N_{e^-} \qquad 4.7$$

where N_{e^-} = instantaneous electron concentration.

Since $N_{H_3O^+} = N_{e^-}$

$$- \frac{d\, N_{H_3O^+}}{dt} = k_{H_3O^+} \; N_{H_3O^+}{}^2 \qquad 4.8$$

This is equivalent to the rate expression for the reaction occurring in a laminar flame.

Substituting equation 4.6 in 4.8

$$- \frac{d\, N_{H_3O^+}}{dt} = k_{H_3O^+} \left[\overline{N}_{H_3O^+} + n_{H_3O^+} \right]^2$$

Time Averaging;

$$- \frac{\overline{dN}_{H_3O^+}}{dt} = k_{H_3O^+} \left[\overline{N}^2_{H_3O^+} + 2\overline{N}_{H_3O^+} \, \overline{n}_{H_3O^+} + \overline{n^2}_{H_3O^+} \right]$$

$$= k_{H_3O^+} \left[\overline{N}^2_{H_3O^+} + \overline{n^2}_{H_3O^+} \right]$$

$$= k_{H_3O^+} \overline{N}^2_{H_3O^+} \left[1 + \phi^2 \right]$$

where $\phi = \dfrac{(\overline{n^2}_{H_3O})^{\frac{1}{2}}}{\overline{N}_{H_3O}}$ = turbulent intensity

Hence in the case of a chemi-ion recombination reaction the mean reaction rate in a turbulent flame is enhanced by a value to the square of the turbulent intensity over the rate for the corresponding reaction in a turbulent flame.

Effect of Chemistry upon Turbulence

It may be recalled that experimental evidence for this aspect of the interaction phenomenon has been sought by studying ion chemical kinetics in a turbulent hydrogen diffusion flame. The phenonemon may be described by first considering the presence in the flame of a chemically inert species where the charged species number density is controlled by turbulent mixing. The high ion density levels produced in the reaction zone will become distributed throughout the flame by eddy transport. As mentioned previously, the stretching and distorting behaviour of the turbulent shear stresses result in an increase in the local concentration gradients such that with the aid of molecular diffusion the mixing action leads to a reduction in the ion density levels. Turbulent mixing is thus a dissipative process since the initially high ion density levels gradually decay during transport.

The local ion density pattern resulting from the irregular

eddy motion may be studied with the use of a suitably biased electrostatic probe. As regions of varying ion density are convected past the probe the instrument "follows" the fluctuations in the collected ion current. Analysis of the random signal will enable determination of parameters such as scale and intensity of turbulence which will be representative of the irregular turbulent motion at the region of interest.

Consider now the case where the charged species are chemically active. During eddy transport the species will concurrently undergo a chemical reaction. Providing the reaction rate is greater than the appropriate mixing rate, chemistry will result in the formation of a different ion density pattern compared to that produced by turbulent mixing independent of the reaction being either an ion production or an ion decay process. Under these conditions therefore, a measurable difference between the turbulence parameters representative of the chemically active and chemically passive ion concentration fields is to be expected.

Mention was made in Chapter 1 of the Damkohler number, given as the ratio of the chemical reaction rate to the turbulent mixing rate. Its value will therefore give an indication as to which process, whether chemistry or turbulent mixing, will predominantly control the ion density pattern.

Therefore in order to observe the required difference in the local turbulent parameters, charged species having a large difference in Damkohler number values should be employed. The selection of the metal additives used for the study of the interaction phenomenon will be described later in the text.

CHAPTER 5

ELECTROSTATIC PROBES

5.1 Introduction

The electrostatic probe has become a well established instrument for the experimental investigation of plasma properties. Probes have been used extensively in the determination of such properties as local ion concentrations enabling ion recombination rates to be evaluated essential for a study of ion chemical kinetics in flame plasmas. In comparison to other available techniques, namely, the microwave cavity and mass spectrometer, the electrostatic probe provides higher spacial resolution in addition to its greater simplicity and low expense.

The electrostatic probe consists basically of a small sphere or wire, usually of platinum, connected to an external circuit such that when immersed in a region of interest in a plasma it may be biased either positive or negative with respect to the plasma potential. The current drawn in the external circuit is a function of the charged species number density, the applied potential, and local conditions round the probe surface. In this work with atmospheric pressure flames the probe was biased highly negative with respect to the plasma such that a positive ion sheath or space charge surrounded the probe and the current drawn is termed the positive ion saturation current. Prior to a discussion of probes in high pressure plasmas a brief resume of the operation of single probes in low pressure plasmas would be relevant.

Langmuir and Mott-Smith[26] investigated such systems to determine electron concentrations and electron temperatures. The graph of current drawn by a probe in a low pressure plasma with varying potential, known as the probe characteristic, is shown in Fig. 5.1. The region AB is obtained at high positive bias where a negative sheath of electrons surrounds the probe, the current drawn corresponds to the electron saturation current. Increased positive bias leads to gradual increase in current owing to increase in sheath dimensions.

The formation of the space charge around the probe limits the amount of current drawn, it is thus space-charge limited. The point V_s corresponds to the plasma potential where no sheath exists. The current collected is determined by the number of electrons and ions reaching the probe surface. Since electrons have a greater random velocity than positive ions due to their small size, a net electron current is drawn. The transition region BC the probe becomes less positive than the plasma potential thus retarding the electron flow and attracting more positive ions. The point V_f is the floating or wall potential where no net current is drawn, the flux of electrons equals the flux of positive ion reaching the probe. This is the potential an isolated body immersed in a plasma would attain. The region BD corresponds to the positive ion saturation region where all electrons are repelled and a positive ion sheath surrounds the probe.

In practice the sheath formed does not completely shield the plasma from the probe potential and increased probe potential in both electron and positive ion saturation regions will lead to small increases in sheath diameter producing a gradual increase in saturation currents.

Fig. 5.1 Electrostatic Probe
Current Voltage Characteristic

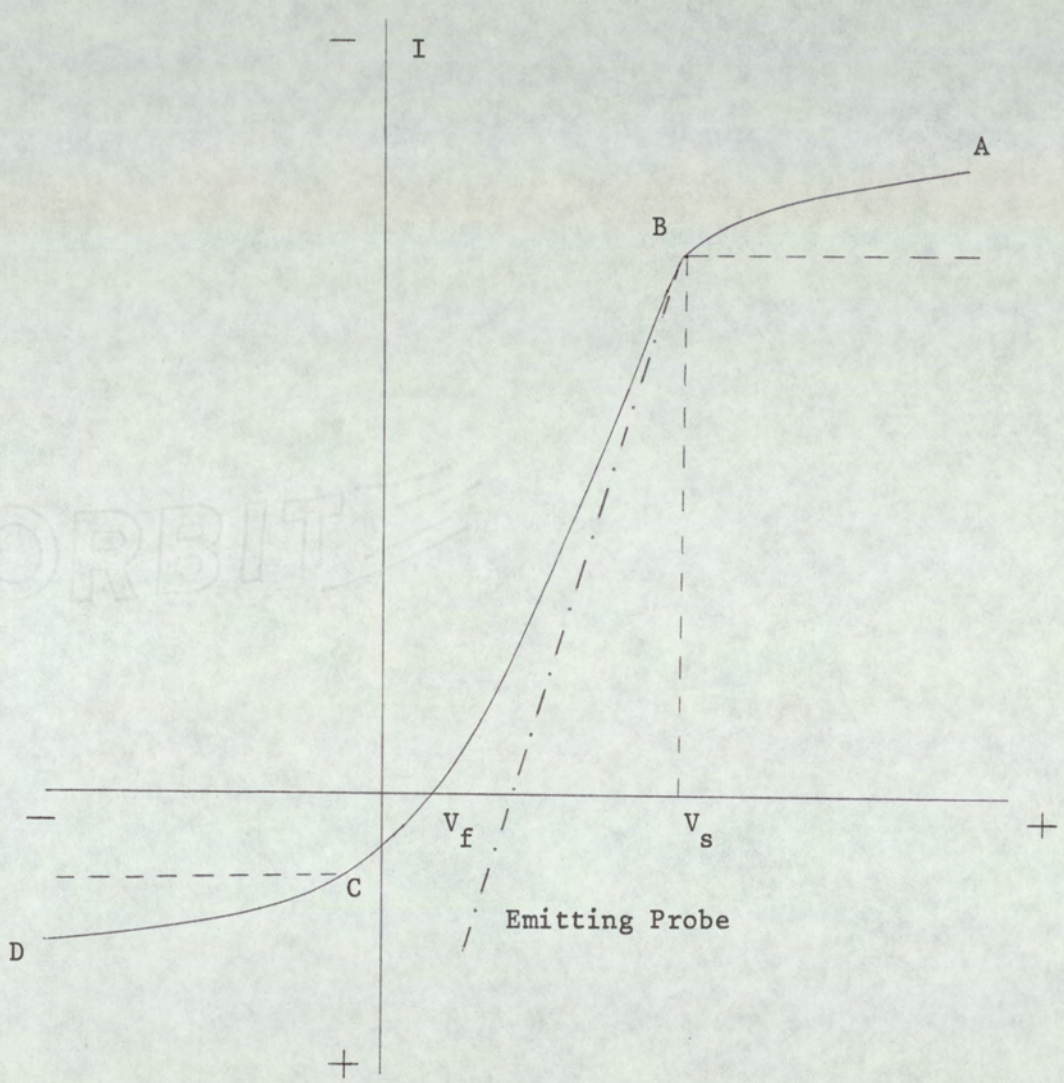

An important characteristic of the bulk plasma is the Debye length. The individual charged species are screened by an "atmosphere" of carriers of opposite charge. The effective thickness of such an atmosphere corresponds to the Debye length. It is an important parameter since the carriers mutually screen their microscopic electric fields rendering the bulk plasma macroscopically neutral. The Debye length is given by:

$$\lambda_D = \left(\frac{k\, T_e}{4\pi n_o e^2} \right)^{1/2} \qquad 5.1A$$

where n_o is the charge density, T_e the electron temperature and k is the Boltzmann constant.

The space charge sheath thickness is of the order of a Debye Length thus in low pressure plasmas where the mean free path of both ions and electrons is greater than λ_D no account need be taken of collisions between ions and neutral or other charged particles while crossing the sheath for the calculation of collected space charge limited currents.

5.2 Positive Ion and Electron Density Determination

When the sheath radius S is small in comparison to the probe radius a, the probe may be considered to be perfectly absorbing and any orbital motion the carriers may undergo can be neglected the probe current I may be expressed as

$$I = jr\, As \qquad 5.1$$

where jr is the random current density and As the surface area of the sheath.

The velocity distribution may be assumed to be Maxwellian such that

$$jr = \frac{1}{4} \Lambda \overline{V} = \frac{1}{2} n \left(\frac{2kT}{\pi\, m} \right)^{\frac{1}{2}} \qquad 5.2$$

where n, $\bar{V}$ T and m are number density the mean velocity and temperature of the charged species. For the thin sheath condition with a >>(S-a) the Langmuir-Child expression for space charged limited flow is

$$j = \frac{1}{9\pi}\left(\frac{2}{em}\right)^{\frac{1}{2}}\left(\frac{Vp - V_s}{(S-a)^2}\right)^{3/2}(1 + \frac{2.66}{\sqrt{\eta}}) \qquad 5.3$$

where $\eta = e(Vp-Us)/kT$

This enables the surface area As to be evaluated from the obtained value for S, which in turn permits the charge species number density to be evaluated using equations 5.1 and 5.2.

When the thin sheath condition does not apply the Langmuir-Child law must be modified to account for the orbital motion of the carriers and of probe geometry. The above relationships are equally valid for both positive ions and electrons. The electron temperature may be estimated as described below. In the case of positive ions they lose much of their kinetic energy upon collisions with neutral molecules thus equilibrating their temperature with these species such that the ion temperature may be taken to be equivalent to the neutral gas temperature.

5.3 Evaluation of Electron Temperature

In the transition region the electrons that reach the probe overcome its retarding electrostatic field by virtue of their random thermal energy. Assuming the velocity distribution is Maxwellian the electron density may be given by the following Boltzman law:

$$\eta = \eta_o\, e^{\frac{-eV}{kT_e}} \qquad 5.4$$

where η_o is the number density beyond the sheath and T_e the electron temperature. From equation 5.1 and 5.2

$$I = \frac{A s \eta}{2} \left(\frac{2k\ T_e}{\pi\ m} \right)^{\frac{1}{2}} = \left(\frac{k\ T_e}{2\pi m} \right)^{\frac{1}{2}} A s \eta_o e^{\frac{-eV}{kT_e}} \qquad 5.5$$

A plot of Ln I against V will yield a straight line graph of slope $-e/kT_e$ enabling T_e to be evaluate.

It is important to note the Boltzman law is only valid for a perfectly reflecting probe where species are returned maintaining the Maxwellian velocity distribution. However the conditions of large electron mean free path with respect to probe diameter have negligible adverse effect upon the distribution.

5.4 Double Probes

An important contribution to the use of probes was made by Johnson and Malter[27] concerning the double probe technique. In decaying plasmas the use of the Langmuir probe results in too large an electron current drawn thus disturbing the plasma producing erroneous measurements of plasma properties. This difficulty was overcome by the use of two probes connected via an external voltage source and when immersed in a plasma the whole system floats and the probes find their own potential with respect to the plasma potential. The operation of the double probe method is governed by the following

(i) Kirchhoffs law must be obeyed such that the net total current drawn by the probes is zero i.e. the total number of electrons flowing to the probes must equal the total number of ions.

(ii) The electron current to each probe is governed by the Boltzman Law.

As a consequence of the first requirement the electron current to the probes is governed by the total positive ion current to both probes. This is several orders of magnitude lower than that collected by a single probe, thus disturbance to the plasma is minimised.

The application of the double probe technique to high pressure flames was made by Travers and Williams[28]. They explained for single probe behaviour a condition of asymmetry is required where the saturation electron current be smaller than the saturation positive ion current otherwise the collected electron current to the probe is controlled by the flow of ions to the reference electrode and this ceases to define a reference of potential. This condition was shown to produce errors in electron concentration and temperature measurements. The required asymmetry has never been achieved in high pressure combustion systems. They concluded that determination of electron densities in high pressure flames by means of probes is unreliable.

5.5 Emitting Probes

In high temperature plasmas thermionic emission by the probe may occur if it becomes too hot a condition which will significantly affect the appearance of the probe characteristic . In the electron saturation region the electrons are drawn back but the electron current is little affected. As the probe becomes negatively biased with respect to plasma potential the electrons will be emitted producing an apparent positive ion current causing the characteristic to diverge as shown in Fig. 5.1. Under such conditions measurement of positive ion concentrations is not possible. In this work the electrostatic probe was water-cooled to prevent this condition from occurring.

5.6 Electrostatic Probes in Collision Dominated High Pressure Plasmas

The conditions set by Langmuir no longer apply to plasma pressures greater than 1mm Hg. Under these conditions the mean free paths for the charged species are smaller than either the Debye length or probe diameter. The carriers undergo many collisions en route to the probe and their motion may be described by diffusive and mobility laws. Such conditions exist in high pressure flames.

One of the more successful early theories relating probe current to plasma properties was by Shultz and Brown[29]. They used a cylindrical probe, negatively biased, in low pressure flames and considered the influence of varying number of collisions the positive ions underwent with neutral molecules in the sheath region. Their theory and experimental results agreed for flames up to 10mm Hg pressure.

The theoretical treatment of Su and Lam[5] has probably had widest application to electrostatic probe theory in high pressure collision dominated plasmas. They determined the charge distribution about a spherical probe using the continuity equations together with Poisson's equation making no assumption regarding presence of/boundary layer sheath. The application of appropriate boundary conditions and consideration of a wide range of probe potentials i.e. from highly negative to plasma potential enabled a theoretical probe characteristic to be determined. The characteristic is shown in Fig. 5.2. Their solutions gave rise to four distinct regions around a negatively biased probe, viz. the quasi neutral transition, ion sheath and ion diffusion region. The quasi neutral region, furthest from the probe, where the

Fig. 5.2 Variation in Ion Density **n** and electron density n_e in the vicinity of the Electrostatic Probe.

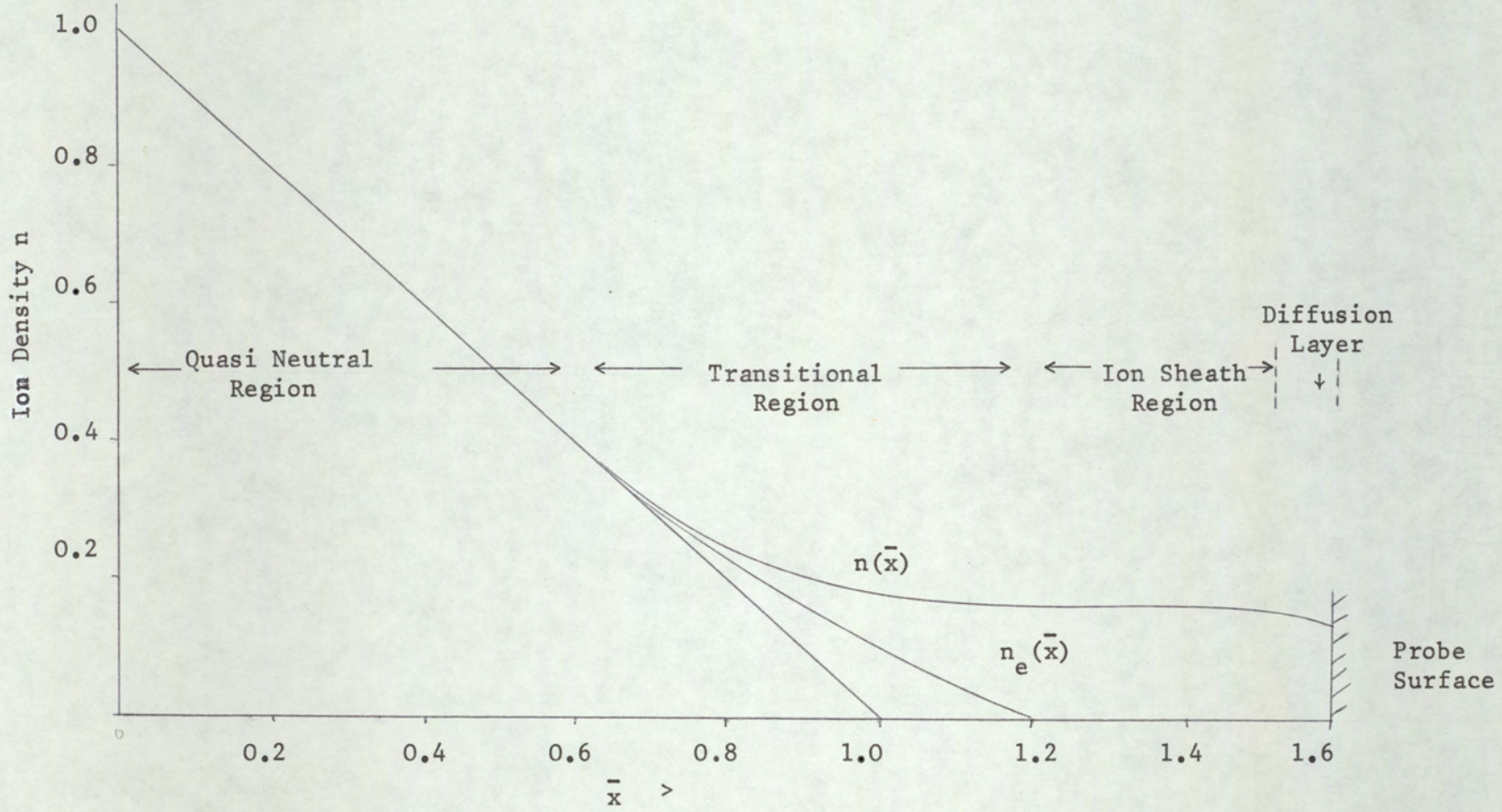

electrostatic potential is very small such that approximately equal concentrations of ions and electrons exist. The transition region with a decreased electron concentration and the ion concentration is slightly lower than in the bulk plasma. The ion sheath region where high electrostatic field exists with no electrons present followed by the ion-diffusion region adjacent to the probe surface. In this treatment the probe potential falls away asymptotically setting up different regions of field strength as apposed to earlier models considered a sheath existed and beyond this boundary layer normal plasma conditions existed.

A similar theory was deduced by Cohen[30] however this does not consider the highly negative potentials, thus the above theory of Su and Lam is more applicable to experimentalists working with flame plasmas.

The first experimental investigation using the Su and Lam theory was by Soundy and Williams[38] who transformed their equation into practical units:

$$No = \frac{1}{4\pi kT_i} \quad x\left(\frac{1}{4r_p\mu_i}\right)^{2/3} \quad \left(\frac{I^2}{\phi}\right)^{2/3} \qquad 5.6$$

where No, r_p, μ_i, and ϕ are the positive ion number density, probe radius, ionic mobility and probe biasing potential. The following assumptions were made in the derivation of this equation:

(i) Only singly charged species are present

(ii) The electron and positive ion temperatures are equal

(iii) The Debye Number i.e. the ratio of probe radius to Debye length is large

(iv) The probe is negatively biased such that the current collected is in the saturation region.

These conditions are easily met in atmospheric flames. It was verified that the above equation was of the right form but despite possible errors in the estimation of the ionic mobility the experimentally determined positive ion current was two orders of magnitude greater than the theoretically predicted value. To determine absolute ionisation levels the above workers calibrated the probe in an atmospheric pressure flame seeded with Cs using the technique described by Padley and Sugden[31]. Correct ion concentrations were obtainable using the following calibration relationship:

$$N_o = \text{constant} \times \left[\frac{1 + {}^{M_g}/_{M_{Cs^+}}}{1 + {}^{M_g}/_{M_i}} \right]^{2/3} \times \left(I\right)^{4/3} \qquad 5.7.$$

5.7 Influence of Probe Temperature upon Current Collection

Generally electrostatic probes immersed in plasmas such as flame gases are maintained cooler than their surroundings by either rotating the probe through the flame or by water cooling. This is contrary to the continuum theory conditions where it is assumed the probe and surrounding gases are maintained at the same temperature. Presence of a probe at a temperature lower than the flame gases produces a temperature gradient. Since charged particle number density and ion and electron diffusion coefficients are temperature dependent Thomas[32] considered this to be a possible explanation for the discrepancy between plasma densities determined experimentally and by the Su and Lam expression.

The ion diffusion-mobility equations where modified to include the effects of a temperature gradient and were solved in a similar manner to that used by Su and Lam. It was concluded that the cooled boundary layer around the probe behaved as a series resistor lowering the probe current by only a negligible amount.

5.8 Effects of Flow Velocity upon Ion Current in Collision Dominated Plasmas

A result of importance to the experimentalist working with electrostatic probes in high pressure collision dominated plasmas has been obtained by Clements and Smy[6]. They developed a theory due to Lam[33] who showed that the ion current collected by a probe operating under the above conditions becomes a function of the plasma flow velocity when the plasma flow rate exceeds $1 M sec^{-1}$. Clements and Smy[6] have deduced expressions for the collected positive ion current in terms of the plasma properties for negatively biased probes in both thick and thin sheath conditions.

Lam's theory considered the following conditions apply:

(a) $\alpha = \lambda_D / L \ll 1$ where λ_D is the Debye length and L is a characteristic length of the probe e.g. 2a, the L is the probe diameter V.

(b) $x = \dfrac{eV_p}{kT_e} \gg 1$ where $T_e = T_i$

(c) The electra Reynolds number R is given by

$$R = \frac{v_f L}{\mu_\infty \left(\frac{kT_e}{e}\right)}$$

where v_f = plasma flow velocity

μ_i = ion mobility

e = electronic charge

Clements and Smy have shown that for spherical probes at high negative bias and for both thick and thin sheath conditions the condition

$$R\alpha^2 x >> 1$$

applies such that the probe current arises predominantly from the convective flow of ions to the sheath as opposed to the normal ambipolar diffusion mechanism for quiescent plasmas.

The positive ion saturation current I_i for a probe operating under thick sheath conditions is related to the charge number density n_e by;

$$I_i = \frac{2(\pi\mu_i E_o)^{1/3} \ (n_e \ e \ v_f V_p)^{2/3}}{\log(I_i/2n_e \ e \ v_f \ a)} \qquad 5.8 \qquad \text{(M.K.S)}$$

where E_o = permittivity of free space, Vp = negative probe potential.

The equation derived for the thin sheath condition is given by;

$$I_i = 12.13.(\mu_i E_o)^{\frac{1}{4}}(n_e \ e \ v_f)^{\frac{3}{4}} \ Vp^{\frac{1}{2}} \ a^{5/4} \qquad 5.9. \qquad \text{(M.K.S)}$$

Using these relationships good agreement was obtained between theoretical and experimentally determined ion current values. In the case of the thick sheath expressed they estimated an accuracy of approximately 30%. For the thin sheath condition excellent agreement between theory and experiment for I; measured as a function of the various plasma properties was achieved. This work therefore, indicated the importance of including the effects of plasma motion in high pressure electrostatic probe theory.

5.9 Electrostatic Probes in Turbulent Media

A fluctuating ion current will be collected by a suitably biased probe when regions of varying charged particle number density are swept passed the probe wire. In order to obtain useful information of the charged species concentration field the probe must be able to respond sufficiently rapidly to the fluctuations in plasma density.

The operating frequency range for a probe in such an environment is governed by the dynamics of the sheath. As differing ion density regions pass the probe a redistribution of ions and electrons about the probe wire results producing a variation in sheath thickness. The electrons respond to the changes almost instantly however the heavier ions move sluggishly and require a finite time to adjust to each new situation.

The approach of a fluid element containing a high plasma density towards the probe causes the electrons to be repelled, the ions being attracted. The high ion density produces a more efficient shielding for the electrons from the probes electrostatic field. This enables the electrons to move closer to the probe wire thus the sheath contracts in size. The excess ions when collected produce a sharp pulse in ion current. The probe's electrostatic field now penetrates further into the bulk plasma. The electrons recede immediately but the ions require a specific time to sense the attracting field and are therefore initially present at too high a density and when collected produce a small overshoot current.The sheath then expands. For a probe present in transient conditions where the sheath thickness fluctuates the system may be considered to exist in a quasi steady state where the sheath never relaxes.

A theory for probe response in a turbulent flow[52] may be constructed by perturbing the steady state ion current equation

above the mean plasma properties . Taking the probe current to be a function of plasma density N and flow velocity V such that I= f(N V). Expanding in a Taylor series;

$$I = I_o(\bar{N}\ \bar{V}) + I_N\Delta N + I_V\Delta V + \tfrac{1}{2}(I_{NN}(\Delta N)^2 + I_{VV}(\Delta V)^2) + I_{NV}(\Delta N)(\Delta V) + \ldots \quad 5.10$$

where the subscripts refer to partial derivatives evaluated at N and V. The fluctuations may be considered to be small such that expansion to the 2nd order is sufficient.

Time averaging the above equation gives;

$$\bar{I} = I_o(\bar{N},\bar{V}) + \tfrac{1}{2}\left[I_N\overline{(\Delta N)^2} + I_V\overline{(\Delta V)^2}\right] + I_{NV}\overline{(\Delta N)(\Delta V)} + \cdots \quad 5.11$$

where $\bar{I}$ represents the mean probe current and I_o the calculated current from the mean plasma properties N and V.

It may be recalled the Clements and Smy[6] equation 5.9 relating the probe current to plasma properties in a non-turbulent flow may be expressed as;

$$I = \text{constant}\ N^{\frac{3}{4}}\ V^{\frac{3}{4}}$$

Differentiating the above equation and substituting for the derivatives in the Taylor series expansion gives;

$$\bar{I} = I_o + \frac{9}{16}\frac{I_o}{\bar{N}\bar{V}}\overline{(\Delta N)(\Delta V)} - \frac{3}{32}E_N^2 - \frac{3}{32}E_V^2 \quad 5.12$$

where E_N and E_V represent turbulent intensities in plasma density and flow velocity eg;

$$E_N = \frac{\left[\overline{(\Delta N)^2}\right]^{\frac{1}{2}}}{\bar{N}}$$

Equation 5. 2 may be expressed alternatively as;

$$\bar{I} = I_o + \frac{9}{16}E_N\,E_V\,R_{NV} - \frac{3}{32}\left[E_N^2 + E_V^2\right] \quad 5.13$$

where,

$$R_{NV} = \frac{\overline{\Delta N\ \Delta V}}{\left(\overline{\Delta N^2}\right)^{1/2}\left(\overline{\Delta V^2}\right)^{1/2}}$$

Equation 5. 3 may be simplified by making the following assumptions ,

(i) The low intensity in flow velocity encountered in this work makes the inequality $E_N > E_V$ probable.

(ii)It is unlikely that changes in flow velocity will produce

changes in plasma density so it may be assumed that $R_{NV}=0$ Hence equation 5.13 reduces to;

$$\bar{I} = I_o \left(1 - \frac{3}{32} E_N^2 \right) \qquad 5.14$$

Therefore if the fluctuations in E_N are of the order of 10% i.e. greater than those encountered in these studies the measured mean current is approximately equal to I_o The fluctuations in N and V thus have a negligible effect upon $\bar{I}$ when at low intensity.

An expression for the fluctuations in probe current i may be determined using the same procedure to the above where,

$$\overline{i^2} = \overline{(I - \bar{I})^2} \equiv \overline{I^2} - \bar{I}^2$$

Using equations 5.10 and 5.11 and the above assumptions it may be shown that;

$$\overline{i^2} = I_o \left(\frac{9}{16} I_o E_N^2 + \frac{9}{16} I_o E_V^2 + \frac{9}{8} E_N E_V R_{NV} \right) \qquad 5.15$$

which reduces to;

$$\frac{\left(\overline{i^2} \right)}{\bar{I}_o^2} = \frac{9}{16} E_N^2 \qquad 5.16$$

This equation illustrates that the random probe current is predominantly controlled by fluctuations in plasma density only; the fluctuations in other plasma properties having a negligible influence. This is an important result since it shows that the statistical analysis of the random probe current is directly related to the changes in ion density. It may be recalled this situation is of importance to this work where the changes in ion density due to chemical effects have been studied from measurements of $(\overline{i^2})$

CHAPTER 6

Apparatus

6.1 Meker Burner Design

The Meker burner used in the experiments with laminar flames was constructed by E.R. Miller[34]. The burner design is shown in Fig. 6.1. The upper chamber allows cooling water to circulate around the assembly of stainless steel hypodermic tubes, necessary since the tubes are soldered together. The centre chamber allows mixing of the supply gases to the outer shield flame and the lower chamber mixing of the supply gases and additives to the inner flame. The stainless steel tubes of internal diameter 8.13×10^{-4}M were individually located in pre-drilled brass discs and soldered together. An important feature of their arrangement was in their spacing to allow for lateral expansion of the burnt gases, by a factor of $(7)^{2/3}$ a development of Miller's. The brass discs provide the separation of the three chambers when inserted into the brass burner barrel. The upper disc forms the burner top held in position by small bolts, the other two are held by "O" rings. The base of the burner is similarly held by an "O" ring as a safety measure in case of flame flash back.

The burner produced a laminar flame, the outer flame protecting the inner flame from air entrainment for a distance of 10^{-2}M from the burner top. Small combustion zones were maintained above each tube of 1×10^{-3}M length providing an overall flat reaction zone important in the temporal studies of flame reactions.

Fig. 6.1 Meker Burner used for Generation of Laminar Flames

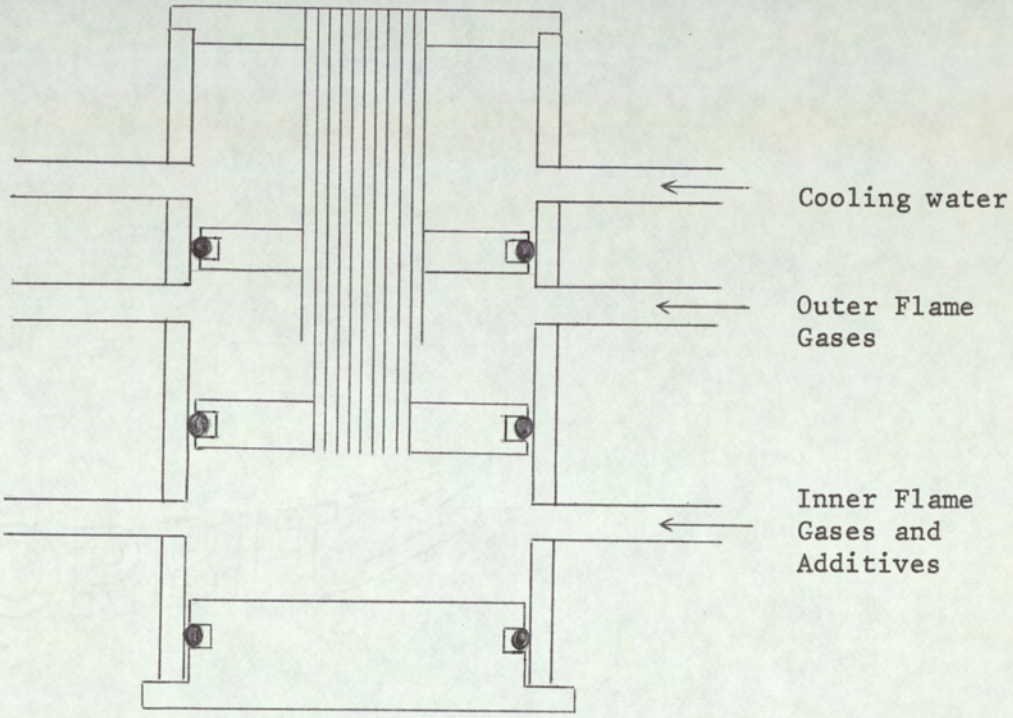

6.2 The Gas Delivery System

The unburnt gases were obtained from commercial hydrogen, oxygen and "white spot" nitrogen cylinders. The flow rates were regulated using Clockhouse needle valves and each gas was separately monitored using calibrated Rotameters. The flow rates for the gas supplies to the inner and outer flame were arranged such that both had the same convective velocity. All metal salt solutions used were introduced as fine sprays generated by a scent spray atomiser driven by part of the nitrogen supply to the inner flame. A settling chamber ensures that only the finest droplets enter the flame. This type of atomiser has been shown to be linear in operation, the partial pressure of metal atoms in the flame being proportional to the concentration of metal salt solution in the atomiser for all concentrations up to approximately 0.25 molar. Above this value salt deposition in the atomiser nozzle occurs, preventing its operation. The pressure drop across the nozzle was monitored using a mercury manometer.

6.3 Determination of Flame Temperature

Flame temperatures have been determined using the sodium D-line reversal technique. This method gives the value for the electronic excitation temperature for sodium which may be considered to provide the true thermodynamic temperature since the sodium atoms are in thermal equilibrium with those in the first excited state. This equilibrium condition was shown to exist by Griffiths and Awbrey[35] who showed temperatures determined by the reversal method agreed well with those values measured

using other techniques. The theory of the reversal method has been described in detail by several authors;[36 ; 37] the basic principles will now be described.

Light from a tungsten strip filament lamp was focussed, using a lens, to give an image of the lamp in the flame. A second lens focussed light from the image and a coincidence point in the flame onto an aperture slit of a Hilger constant deviation spectrometer. An aperture stop was placed close to this second lens to ensure that light reaching the spectrometer from both flame and lamp was confined within the same solid angle. A spray of 0.2M sodium chloride was introduced into the flame and with a small current flowing through the lamp, the D lines at 5890°A and 5896°A were viewed in emission through the spectrometer over the background continuum radiation from the lamp.

With increased current through the lamp the reversal point was eventually reached where the D lines are neither in absorption or emission but merge in with the background continuum. At this point the amount of radiation absorbed by the sodium atoms from the lamp is exactly compensated by their emission such that by Kirchhoff's law the brightness temperature of the lamp is equal to the flame temperature. The current flowing through the lamp was recorded and the procedure was repeated several times, approaching the reversal point from both absorption and emission directions.

The brightness temperature for various current values was obtained by calibration of the lamp at 6550 Å using a Leeds Northrop optical pyrometer, itself having been calibrated against a black body radiator. As the brightness temperature

of the lamp at 5890°A is required, the calibrated temperature values require correction using Wien's law and a knowledge of the emissivity of tungsten at the wavelengths 5890 Å and 6550 Å i.e.

$$\frac{1}{T_{\lambda^1}} - \frac{1}{T\lambda} = \frac{2.303}{C_2} (\lambda \log e_\lambda - \lambda^1 \log e_{\lambda^1})$$

where T_{λ^1}, T_λ are the brightness temperature at 6550 Å and 5890 Å with e_{λ^1} and e_λ the emissivity of tungsten at these wavelengths. C_2 is a second radiation constant equal to 1.438 cm.deg.

In the case of all the laminar flames studies by Miller[34] their temperatures were observed to rise rapidly to a constant value maintained between 1.5×10^{-2}M to 7.0×10^{-2}M above the burner. The determination of turbulent flame temperatures proved slightly more difficult since the D-lines were observed to flicker, producing greater error in the measurement of the reversal point.

6.4 Rotating Probe Assembly

The rotating probe apparatus as used in experiments with laminar flames is shown in Fig. 6.2. The cylindrical probe was constructed of platinum wire of 2.5×10^{-4} M diamter and 1×10^{-2}M in length supported in a boron nitride rod 9.6×10^{-3}M diameter, a material capable of retaining excellent electrical insultating properties at high temperatures. The probe was swept through the flame at approximately 1m sec^{-1}, this ensured the probe wire did not reach a temperature where the ionic emission would occur, residence time in the flame being approximately 20 m sec. Further, the rotation speed of the probe was

Fig. 6.2 Rotating Probe Assembly

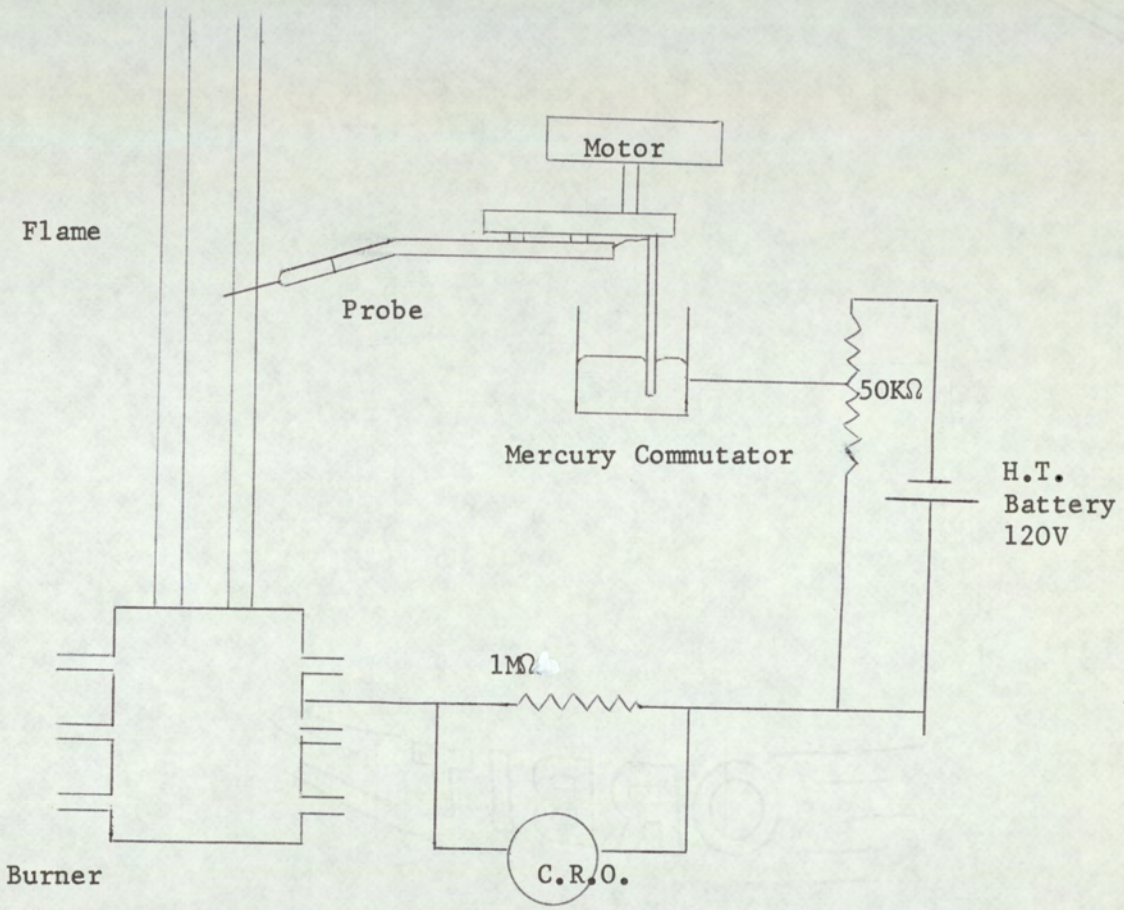

sufficiently slow such that it did not sweep its own atmosphere into the flame. Precautions were taken to ensure only the probe wire entered the inner flame, reducing disturbance effects caused by the boron nitride rod. These were further reduced by maintaining the probe wire at 30^0 to the horizontal such that any possible disturbance was created downstream of the probe wire.

The probe was biased 100 volts negative with respect to the burner top, this being maintained at ground potential. The current collected by the probe was metered on Cossor CD 110 oscilloscope externally triggered using a small magnet on the probe armature arranged such that it operated a reed switch as the probe entered the flame. The pulse displayed on the oscilloscope screen was measured by eye against the graticule.

Mains AC pick-up presented a problem when operating the C.R.O. at maximum sensitivity. This was largely eliminated by shielding the motor and mercury commutator with nickel foil. Further with continual use the probe surface became contaminated, producing a lowering of probe current. This necessitated the cleaning of the probe wire with concentrated hydrochloric acid and heating to dull red before each run.

6.5 Burner for Generation of Turbulent Flames

The burner assembly used for the study of turbulent flames as shown in Fig. 6.3 was manufactured entirely of stainless steel. The gas supplies were introduced via two pipes welded tangentially to the burner barrel near its base. They enter the burner swirl chamber where they are mixed by their swirling motion. The gas flow passes to an Amal flame trap consisting

Fig. 6.3 Burner used for Generation of Turbulent Flames

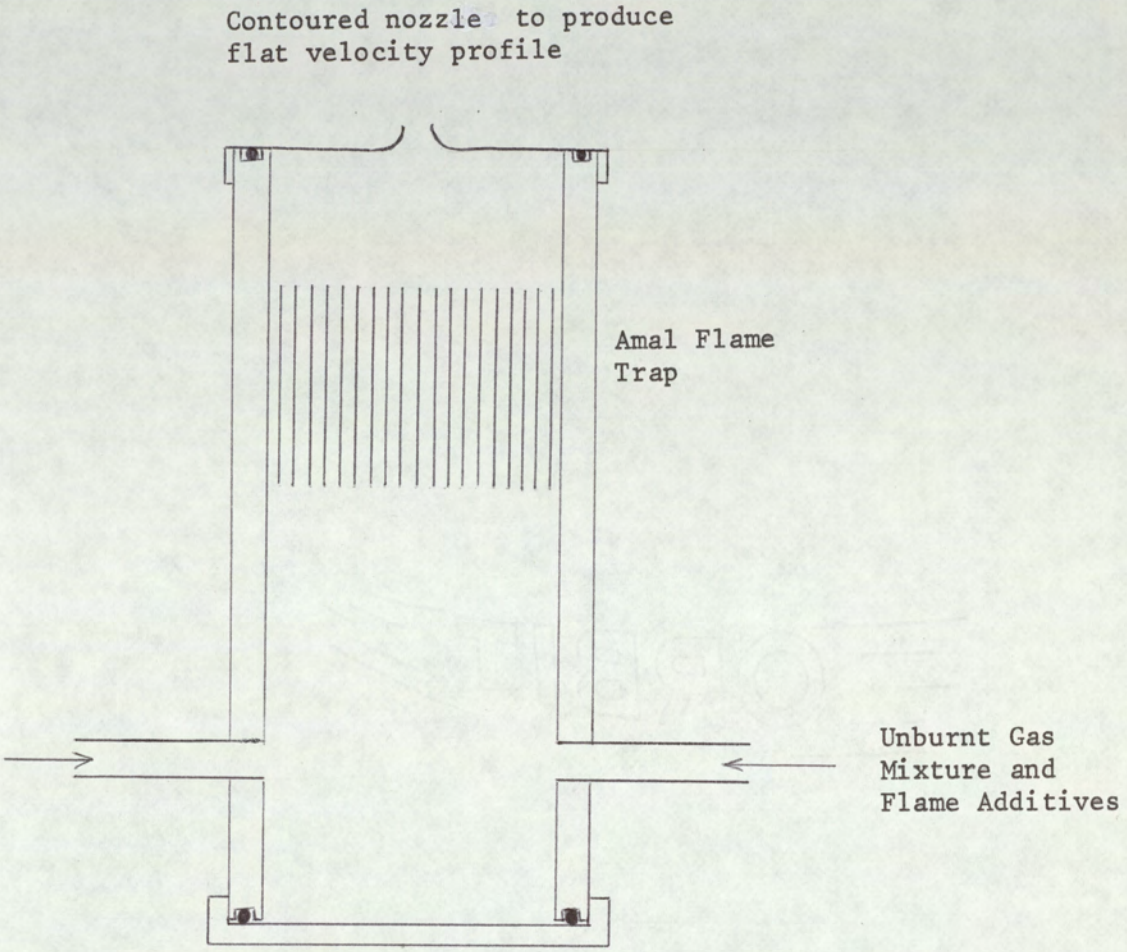

of sheets of corrugated and plain stainless steel foil rolled together, situated midway up the burner barrel, having a length of 7.6×10^{-2}m. As the gases enter this matrix the flow becomes laminarised, removing all swirling and surging motion, they attain in the mixing chamber. The gases are finally vented into the laboratory atmosphere through a specially designed contoured nozzle of 5.0×10^{-3}m throat diameter, conforming to the A.S.M.E. Standard for Fluid Meters suitable for producing a flat velocity profile at the nozzle for gas flows with a Reynolds Number of 1.0×10^{4}. The burner top containing the nozzle, screws onto the barrel; an 'O' ring contained in a groove in the barrel ensures a gastight seal. The burner base is similarly attached to the opposite end of the barrel.

The burner assembly was mounted within a frame such that if removed for the purposes of cleaning it could be replaced in its original position with respect to the probe mountings. All gas supplies to the burner were delivered in the manner discussed previously.

6.6 Water-cooled Electrostatic Probes

Experiments with turbulent flames involved a study of localised regions within the flame which required a stationary probe made as small as possible to reduce disturbance effects to the gas flow. Initial studies with fixed probes similar in construction to the rotating probe described earlier using a fine platinum wire supported in a boron nitride rod proved fruitless. The boron nitride rod became too hot when inserted into the flame, losing its electrical insulating property.

Fig. 6.4 Watercooled Electrostatic Probe

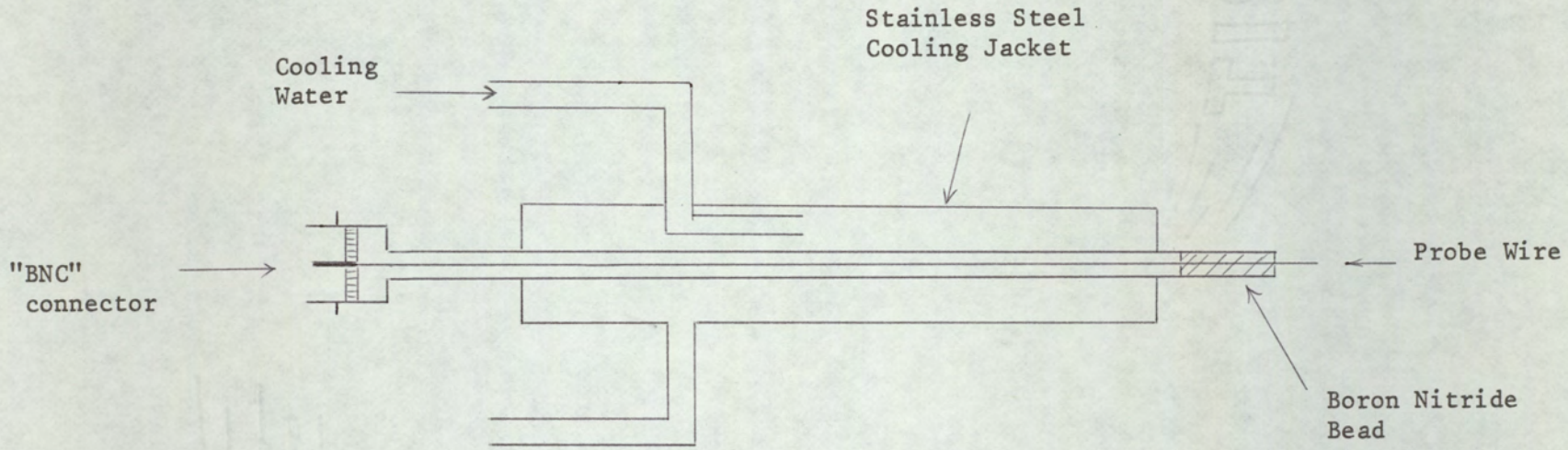

This problem was overcome by use of the water-cooled electrostatic probe of design shown in Fig. 6.4. The platinum probe wire was contained in a stainless steel tube of 3.30×10^{-3}m internal diameter, and 1.27×10^{-1}m in length insulated from the walls of the tube by an aluminium oxide sleeve. One end of the platinum wire was soldered to a B.N.C. connector the other end protruding beyond the stainless steel tube by 3.0×10^{-3}m. A small boron nitride bead was inserted into the end of the tube, the probe wire passing through it. The tube housing the probe wire was surrounded by a larger stainless steel tube of 9.65×10^{-3}m diameter forming the cooling jacket for the probe. The smaller tube extended 1.27×10^{-2}m beyond the silver solder seal. The boron nitride bead however also conducted at high temperatures and was replaced with a silicon nitride bead producing a similar result. The boron nitride initially used was a general grade containing approximately 10% boric oxide capable of absorbing an appreciable quantity of water, resulting in electrical conduction across the entire cooling jacket. Use of a grade H.P. of boron nitride manufactured by Consolidation Borax Ltd. containing less than 1% boric oxide retained its electrical insultating properties upon insertion into the flame. The beads lost this property with excessive use and required replacement after approximately 12 hour's flame time. The probe was biased 50 volts negative with respect to the burner maintained at earth potential. The probe circuit is also shown in Fig.6.2 . The probe was mounted in a holder such that it could be positioned in various local regions in the flame. Again with excessive use, as with studies using the rotating probe, the probe surface became contaminated. This however was not detrimental to correlation studies since

the frequency content of the signal was not affected, only the magnitude of the signal was reduced. This influenced the turbulent intensity measurements where mean and mean square values are required. As a precaution the probe wire was cleaned before each run in the manner described previously.

6.7 The Flames

Hydrogen flames were used throughout the project since they possess an extremely low level of natural ionisation and therefore provide an ideal medium for the study of ion chemistry at elevated temperatures.

The laminar flames used were premixed hydrogen and oxygen using nitrogen as a diluent. The unburnt gas composition of $H_2:O_2:N_2$ in the ratio 41:14:45. These flames consisted of an inner flame surrounded by a protective outer shield flame from the effects of air entrainment. The shielding was maintained for a distance of 1.0×10^{-1}M above the burner top. The temperature of the laminar flame with the above gas composition was determined to be $2336^0K \pm 10^0K$.

The turbulent diffusion flame had an unburnt gas composition of $H_2:N_2$ in the ratio 3:1 having a nozzle Reynolds Number of 1.0×10^4. The maximum temperature of this flame was $2300^0K \pm 50^0K$ at approximately 2.4×10^{-1}m above the nozzle.

6.8 Atmospheric Pollution

During the course of the preliminary studies using the turbulent flame the observed variation in correlation coefficient values by seeding the flame with different metal additives, obtained earlier in the work, could not be repeated. The

coefficient values were now observed to be equal independent of the metal additive used.

The flame, in the absence of seeding, was observed to have a distinct yellow colour, considered to be due to the presence of sodium impurity following the addition of this element to the flame. The burner assembly and the gas supply tubes to the burner were thoroughly washed with dilute nitric acid followed by distilled water to remove the contaminant. This proved fruitless and it was thereafter considered the impurity lay in the gas supply cylinders. These were replaced together with their reducing valves and the copper tubing which delivered the gases to the Rotameter flow meters. This also produced a negative result.

Upon closer examination of the flame at the upstream regions, near the burner nozzle, a bright luminous streaking effect similar to that produced by solid particles in flames was observed. This was believed to be due to the presence of dust particles in the entrained atmospheric air. These produce carbon particles in the flame, which, when luminous would generate the yellow colouration of the flame. A coil of copper tubing, sealed at one end, with a series of small holes drilled along its length at regular intervals such that it formed a gas ring, was positioned on top of the burner, concentrically with the nozzle. Purified air from a commercial cylinder was fed to the coil such that the flame was surrounded with air from this supply. This was observed to produce a notable reduction in the yellow colouration verifying that the source of contamination to be the laboratory atmosphere.

This problem was overcome by employing two Honeywell electrostatic precipitators capable of removing dust particles down to a size of 0.3 micron. Further, it was found necessary

to conduct the remainder of the project in a smaller laboratory thereby reducing the time required to purify the air between each experiment. In the laboratory used it was found necessary to allow approximately six hours cleaning prior to each run.

6.9 Analog Correlator

The statistical analysis of the fluctuating probe signals was performed using both analog and digital techniques. Most of the correlation analysis was carried out using a Disa type 55Do analog correlator together with an external time delay and sweep drive units. The input impedance of the instrument was 100 K Ω and since the probe current was passed through a 1M Ω load resistor an emitter follower, the circuit of which is given in Fig. 6.5 , was used to correct for the impedance mis-match.

Two signals f_A and f_B to be correlated were each passed through similar emitter followers prior to being fed into the correlator. The signals are amplified and normalised in the correlator and thereafter applied to adder and subtractor circuits followed by two squaring circuits whose instanteous voltage outputs are averaged by means of two time averaging amplifiers. The outputs from these circuits are subsequently applied to the inputs of a ratio computer. This unit performs the following operation on the two time averaged signals I_1 and I_2.

Fig 6.5 Emitter Follower Circuit Diagram

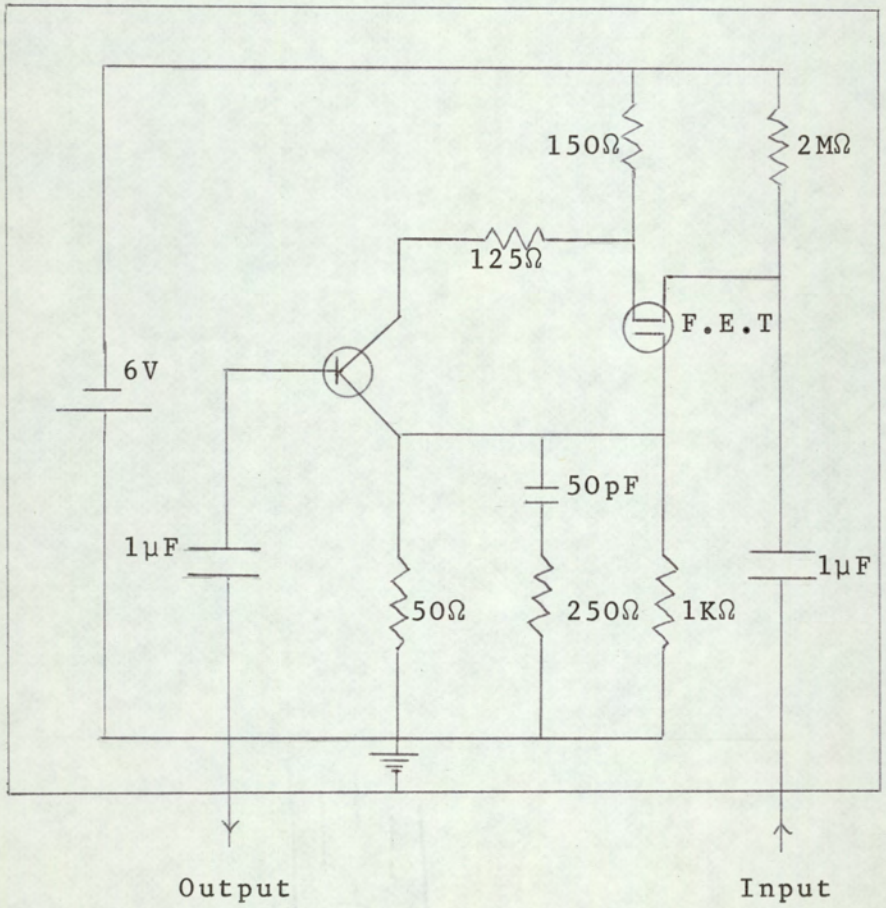

The signals I_1 and I_2 are expressed in terms of f_A and f_B by;

$$I_1 = K\overline{(f_A(t) + f_B(t))^2}$$

$$I_2 = K\overline{(f_A(t) - f_B(t))^2}$$

The overbar denotes the time averaging procedure.

The ratio computer performs the following operation on I_1 and I_2 outputting the signal e_ρ. i.e.

$$e_\rho = \frac{K\,\overline{(f_A(t) + f_B(t))^2} - K\,\overline{(f_A(t) - f_B(t))^2}}{K\,\overline{(f_A(t) + f_B(t))^2} + K\,\overline{(f_A(t) - f_B(t))^2}}$$

$$= K\,\frac{\overline{2f_A(t)f_B(t)}}{\overline{f_A(t)^2}\quad\overline{f_B(t)^2}}$$

This unit also equalises the mean square values of the input signals such that

$$\overline{f_A(t)^2} = \overline{f_B(t)^2} = \overline{f(t)^2}$$

$$\therefore \quad e_\rho = K\,\frac{\overline{f_A(t)\,f_B(t)}}{f(t)^2}$$

The output voltage e_ρ is linearly proportional to the correlation coefficient i.e.

$$\text{Correlation Coefficient } \rho_{AB} = \frac{f_A(t)\, f_B(t)}{\overline{f(t)}}$$

The signal e_ρ is then fed to an output meter linearly calibrated in terms of ρ_{AB}. To obtain correlation coefficient values at different time delays, the time delay unit, driven by the weep drive instruments, was used enabling delays of between zero and 0.1 seconds to be employed. The details of the mode of operation of the time delay unit have not been disclosed by the manufacturer.

6.10 Digital Analysis

Computational analysis to determine autocorrelation power spectra and probability density functions were performed using programs supplied by Mr. H. Williams (joint supervisor). The random positive ion current collected by the electrostatic probe was recorded on magnetic tape using a Data Tape F.M. tape recorder. The recording speed employed throughout was 60 i.p.s. Prior to recording, the probe signals required amplification to a value of 1V R.M.S. Precautions were taken not to saturate the tape by monitoring the recorded signal, during recording, on an oscilloscope.

Prior to analysis the continuous waveform was processed into discrete digits using an analog to digital convertor, an instrument commonly included in computer systems. The process of sampling the continuous record is illustrated below.

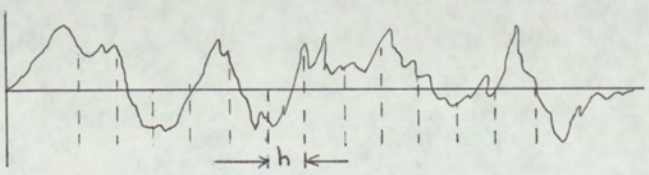

Fig.6

The time interval between the data points is h seconds, hence the sampling rate is $^1/h$ samples per second. It is necessary for h not to be too large otherwise information of the high frequency content of the signal will be lost. This property is called aliasing. All the useful data will be contained in the range 0 - $\frac{1}{2h}$ cycles/second since frequencies present in the data which are higher than $\frac{1}{2}$c.p.s. will become folded into the lower frequency range and become confused with data of this range. The critical frequency above which, aliasing will occur is given by;

$$f_c = \frac{1}{2h}$$

where f_c is known as the Nyquist frequency.

The shortest time interval h available with the computer employed during these studies corresponded to $1X10^{-4}$seconds. The frequency content of the fluctuating signals studies in this work were considered not to contain components in excess of 10 kHz. As mentioned above, since the waveform was recorded at 60 i.p.s. sampling the signal at a playback speed of 30 i.p.s. provided an f_c value of 10kHz as required.

The number of data points necessary to provide reproducible results must also be determined. This must be estimated by trial and error. It was observed that good agreement between autocorrelograms was obtained using 8000 data points. This produced a statistical error of approximately 12% upon sampling at different positions along the recorded waveform.

Autocorrelation Analysis

The autocorrelation function may be determined using the following procedure. For N data points of the sample record x_n where n = 1,2,3 N the auto correlation function is expressed as;

$$R = \frac{1}{N-r} \sum_{n=1}^{N-r} x_n x_{n+r} \qquad r = 0,1,2 \quad m \qquad 6.1$$

where r represents a log number or delay unit and m is the maximum log number. The maximum log number was fixed at 80. Since the sample interval between data points h corresponds to $1X10^{-4}$seconds and by sampling the recorded signal at one half the recorded speed i.e. 30 i.p.s. each unit of r corresponds to;

$$\frac{1.0 \times 10^{-4}}{80 \times 2} = 62.5 \times 10^{-6} \text{ seconds}$$

Following sampling 8000 data points the computer determines the value of t he autocorrelation function by performing the summation in equation 6.1 for each value of n and r. Since when r = 0 the summation is equivalent to the mean square of the data dividing each R value by the mean square value yields the autocorrelation coefficient. The computer print out was given in terms of the coefficient for r values 0,4,8---80. As shown above each r value corresponds to $62.5x10^{-6}$secs. Therefore the maximum time delay m is equivalent to $8.0x10^{-3}$ seconds.

Power Spectral Density Function

The power spectral density function, described in Chapter 2, may be expressed as;

$$G_x(f) = \lim_{\Delta f \to 0} \frac{\Psi^2 (f, f+\Delta f)}{\Delta f}$$

The Fourier analysis program employed to determine the above function was written from an alogorithm due to Singleton.[53] The procedure used to analyse the data points representing the random signal involved determination of the Fourier sine and cosine coefficients for the data contained within a narrow frequency bandwidth Δf set at 125 Hz. The coefficients were computed by performing the following summation operations;

$$a_k = \frac{1}{n} \sum_{j=0}^{2n-1} x_j \cos(\pi jk/n)$$

and $$b_k = \frac{1}{n} \sum_{j=0}^{2n-1} x_j \cos(\pi jK/n)$$

where k = 0,1,2 ---n

and a_k, b_k represent the cosine and sine coefficients respectively. The value n is expressed as the number of degrees of freedom and is given by the following;

$$n = 2B_e T$$

where $B_e = \Delta f = 125$c/s and T represents the length of the sampled waveform. Since h is the sample interval and N the total number per sample points

$$T = Nh$$

Following determination of the respective coefficients within some bandwidths f, f + Δf the value of $\psi^2(f,f + \Delta f)$ may be obtained by summing the squares of the coefficients i.e.

$$a_k(i)^2 + b_k(i)^2 \quad i = 0,1,2---N$$

This procedure is then repeated for the various k values enabling the function $G_x(f)$ to be obtained. The program used, normalised the spectrum function by dividing each mean square value within Δf by the mean square value for the complete signal. This enabled easier comparison of the spectral profiles obtained from data representative of the various flame additives used.

Probability Analysis

Determination of probability density function may be performed digitally by dividing the amplitude range for the function x into a number of class intervals or windows (see Fig. 2.2). The number of class intervals was set at 40, 20 on either side of the zero volts level. Computing the number of occurrences the data is contained within each class interval and enables the probability density function to be plotted. The computer output expressed the probability ρ(x) in terms of counts. It will be recalled that the probability density and cumulative distribution functions are related by

Cumulative Distribution $$P(x) = \int_{-\infty}^{x} \rho(x)\, dx$$

This enables determination of the cumulative distribution function by summing the total number of observations and expressing the number of times the data was contained within any number of consecutive class intervals as a percentage of this total.

CHAPTER 7

THE SELECTION OF ADDITIVES FOR USE IN THE TURBULENT DIFFUSION FLAME

7.1 Prior to the attempt to obtain experimental evidence for the chemistry-turbulence interaction phenomenon by way of studying ion chemical kinetics in a turbulent diffusion flame, it was necessary to select a number of suitable flame additives. The selection procedure was achieved by determination of the Damkohler number D_o, for several ion species. It has been previously discussed in Chapter 4 in order to observe a possible difference in the statistical functions used to characterise the fluctuating ion concentration fields the additives required must include those capable of producing a charged species which undergo either:

(i) A rapid chemical reaction such that the size of the turbulent scales of the ion concentration field become reduced compared with those for a chemically inert constituent

or,

(ii) Little or no chemical reaction.

In the former case the high chemical reaction rate will ensure that chemistry will predominantly control the turbulent characteristics of the fluctuating ion field. In the second case the species will effectively be chemically passive such

that the charged species concentration field will decay at the turbulent mixing rate.

Since the Damkohler number, it may be recalled, is expressed as the ratio of the chemical reaction rate to the appropriate turbulent mixing rate determination of the D_o values for several ion species will provide an indication as to their behaviour in a turbulent flame. Clearly in order to observe the largest difference between the statistical functions those additives that produce ion species having the greatest difference in D_o values should be used.

In order to calculate the D_o values a knowledge of the ion recombination rate constants is required. The constants for most metal ion species are available in the literature. However it was considered to be a useful exercise for their measurement to be conducted in this laboratory. The method to be described was that employed by Soundy and Williams [38] using the rotating electrostatic probe technique in a seeded premixed $H_2:O_2:N_2$ laminar flame.

Mention has been made in Chapter 5 of the success of the Su and Lam continuum theory but of its failure to predict the absolute magnitude of ion currents. This limitation in turn prevents the evaluation of ion concentrations necessary for the determination of ion recombination rate constants. It was therefore necessary to calibrate the probe. The calibration procedure for flames at atmospheric pressure, where known amounts of alkali metal may be added at a constant rate, involves relating experimental measurements to the theoretical Saha equation. This method has an additional advantage in that the atomiser delivery is calibrated simultaneously.

7.2 Calibration of the Probe and Atomiser

Ionisation of Alkali Metals

The equilibrium of an alkali metal atom A to its positive ion and an electron may be expressed by the following

$$A \rightleftharpoons A^+ + E^-$$

having an equilibrium constant:

$$k = \frac{[A^+][E^-]}{[A]} \qquad 7.1$$

This assumes that only A^+ and E^- are the only charged species present

$$k = \frac{[A^+]^2}{[A]} \qquad 7.2$$

Providing the ionisation process is in equilibrium the value of k may be determined theoretically using the same equation for any temperature T. i.e.

$$\log_{10} k = -\frac{5050V}{T} + \frac{5}{2}\log_{10} T - 6.49 + \log_{10} \frac{g_{A^+} g_e}{g_A} \qquad 7.3$$

where V is the ionisation potential of A in electron volts, T the temperature in ^oK, k the equilibrium constant is in atmospheres, and g terms represent the statistical weights for positive ion, electron and neutral atom. For all alkali metals this term is zero.

If $[A_o]$ represents the total alkali metal added i.e.

$$[A_o] = [A] + [A^+] \qquad 7.4$$

by equation 7.2

$$[A^+]^2 + k_1[A^+] - k_1[A_o] = 0 \qquad 7.5$$

This equation does not take into account the influence of side reactions occurring between metal atoms and free radials in the flame gases which can lower the level of ionisation present. For positive ions hydroxide need only be considered, this reduces the number of neutral atoms present and hence the ion concentration. Hydroxide formation has been investigated by Jensen and Padley[39], for alkali metals and their findings show that caesium additions, used in this probe calibration, produces appreciable quantities of CsOH and therefore 6.5 must be modified to account for this.

The alkali metals form hydroxides by the following reaction:

$$A + H_2O \rightleftharpoons AOH + H$$

Thus:

$$[A_o] = [A^+] + [A] + [AOH] \qquad 7.6$$

Let $\phi = \frac{[AOH]}{[A]}$ equation 7.6 may be written as:

$$[A] = \frac{[A_o] - [A^+]}{1 + \phi} \qquad 7.7$$

substituting into equation 7.2

$$k = \frac{[A^+]^2 (1 + \phi)}{[A_o] - [A^+]} \qquad 7.8$$

or

$$[A^+]^2 + \frac{k}{1+\phi}[A^+] - \frac{k}{1+\phi}[A_o] = 0 \qquad 7.9$$

Let $K_1 = k(1+\phi)^{-1}$

$$[A^+]^2 + k_1[A^+] - k_1[A_o] = 0 \qquad 7.10$$

k_1 is the ionisation reaction corrected for hydroxide formation. From equation 7.10 when $A_o >> k_1$

$$A^+ = (k_1 \quad A_o)^{\frac{1}{2}}$$

and when $A_o >> k_1$

$$[A^+] = [A_o]$$

Hence a plot of $\log [A^+]$ against $\log [A_o]$ should be a linear of slope 0.5 for large $[A_o]$ turning over to a slope of unity for small $[A_o]$.

The construction of this curve requires a knowledge of ϕ which for this calibration was determined by Jensen and Padley[39] for caesium hydroxide.

$$K_\phi = \frac{[AOH][H]}{[A][H_2O]} = \phi \frac{[H]}{[H_2O]} \qquad 7.11$$

where $K_\phi = 0.065$, $\frac{[H]}{[H_2O]} = \frac{0.11}{0.365}$ thus $\phi = 2.1$

Substitution of ϕ in equation 7.10 enables a plot of $\log [A^+]$ against $\log [A_o]$ for caesium at 2336°k to be made. The profile obtained is shown in Fig. 7.1.

Calibration Procedure

A rotating electrostatic probe was used to determine absolute ion concentration levels in a laminar premixed flame of $H_2:O_2:N_2$ in the ratio 41:14:45 at a temperature of 2336°k. The flame was seeded, in turn, with aqueous caesium chloride solutions in the concentration range of 2.0×10^{-1} molar to 2.5×10^{-4} molar. The probe was swept through the flame at 2.0×10^{-2} metre above the burner so as to be sufficiently far from the reaction zone where the caesium ionisation is considered to be at equilibrium. The pulse height θ recorded on an oscilloscope was determined as a function of caesium chloride molarity M in the atomiser. By equation 5.6 the ion concentration N_o is proportional to $\theta^{4/3}$ and the caesium concentration in the flame is proportional to the concentration of caesium chloride in the atomiser. A plot of $\log\theta^{4/3}$ against $\log [M]$ exhibits the same characteristics as that obtained with the Saha thermal equilibrium ionisation equation. Thus by plotting the experimental $\log\theta^{4/3}$ against $\log [M]$ on translucent graph paper and superimposing this curve upon the theoretically determined curve the axis may be located. The experimental and theoretical plots are shown in Fig. 7.1. This immediately provides the calibration of $\theta^{4/3}$ in terms of $[C_s^+]$ and $[M]$ in terms of $[C_s]_o$

The calibration factors obtained were:

1 unit of $\theta^{4/3} = 1.38 \times 10^{11}$ C_s^+ cm^{-3}

Fig. 7.1 Calibration Curve for Probe and Atomiser

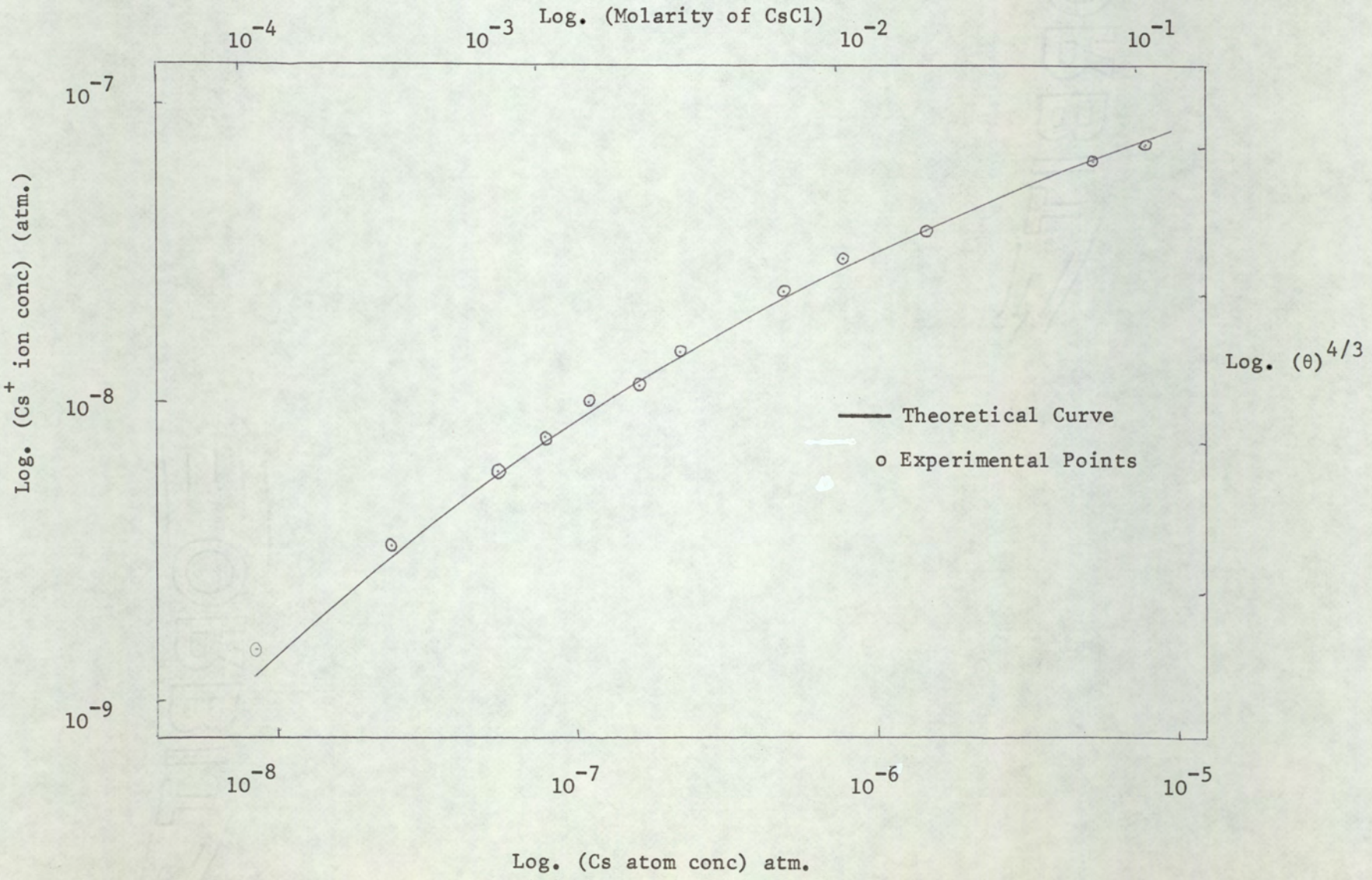

1 unit of M = $3.3 \times 10^{14} Cs_o \ cm^{-3}$

To transfer the caesium calibration curve to ions of different and consequently different mobility in a flame at the same temperature. Soundy and Williams[38] deduced the following equations. For different ions the term controlling mobility in the same gas is $(1 + M_{g/M_i})^{\frac{1}{2}}$ where M_i is the mass of the ion and M_g the mass of a neutral gas molecule. It may be seen that when M_i is large, i.e. for a heavy ion, the mobility is only slightly dependent upon the mass of the ion, however, for a light ion where $M_i < M_g$ the mobility will be strongly dependent upon the mass of the ion and a correction factor must be introduced when the calibration is applied to such ions. The correction factor derived [38] was

$$\left[\frac{1 + {}^{M_g}/_{M_{C_s^+}}}{1 + {}^{M_g}/_{M_i}}\right]^{2/3}$$

where $M_{C_s^+} = 133$, mass of C_s^+ ion and M_i mass of ion under consideration. M_g is the mass of a neutral flame gas molecule taken to be the mean value for the main flame constituents N_2 (28), H_2O(18). This factor may be introduced into the dimensional form of the Su and Lam equation:

$$No = \text{constant} \times \left[\frac{1 + {}^{M_g}/_{M_{C_s^+}}}{1 + {}^{M_g}/_{M_i}}\right]^{2/3} \theta^{4/3} \qquad 7.12$$

Fig. 7.2 Second Order Ion Recombination Plots

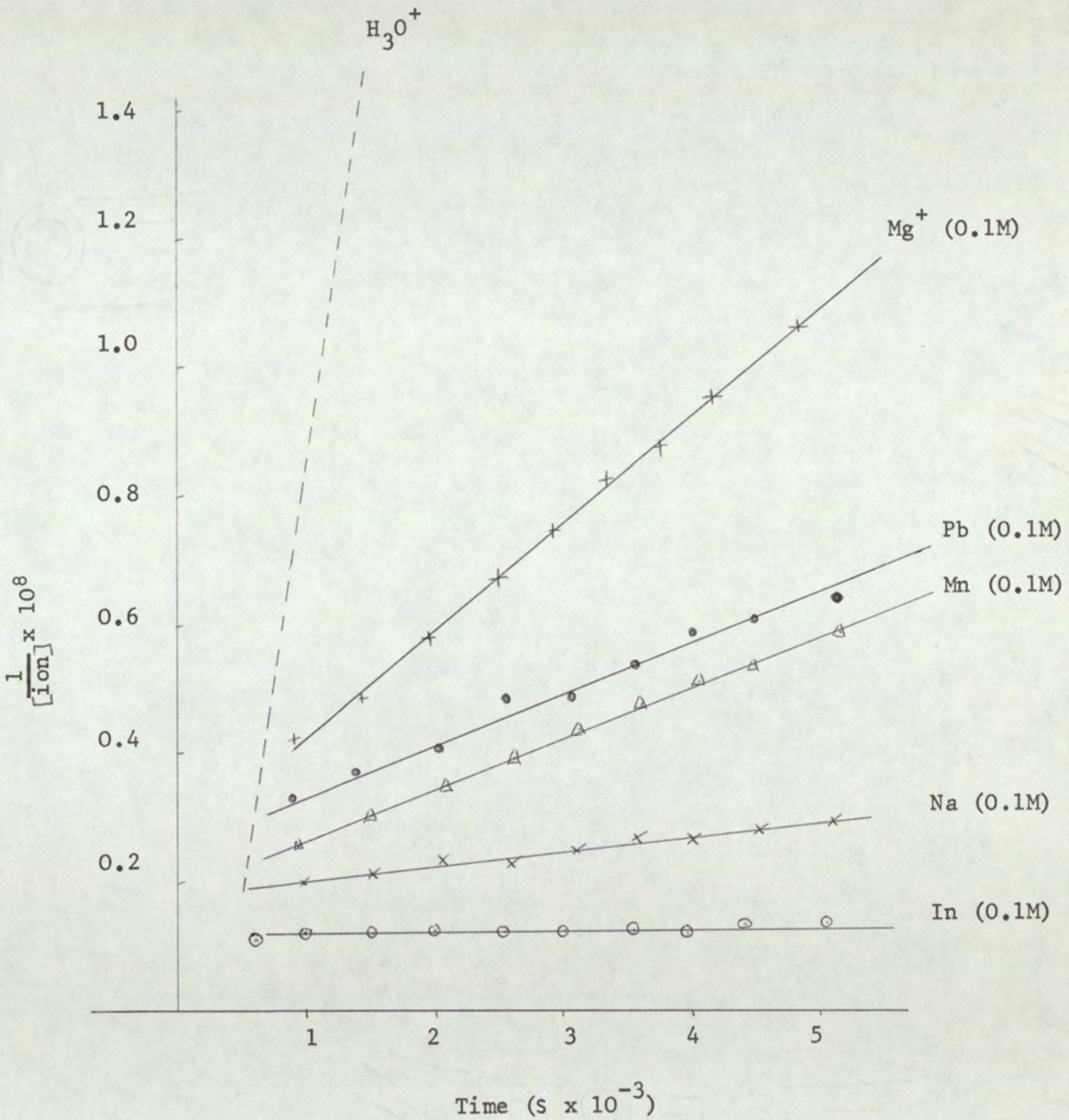

where θ is the deflection seen on an oscilloscope screen, proportionate to probe current. The constant of proportionality is that determined from the caesium calibration procedure. Equation 7.12 enables the absolute ion number density to be determined for other ions produced from metal additives, in the same flame as used for caesuim calibration.

Various metal salt solutions of O.I.M. were added to the $H_2:O_2:N_2$ flame containing a trace of C_2H_2 at temperature 2336^{o}k and the ion number density determined with varying height above the reaction zone. Second order decay curves obtained are shown in Fig. 7.2. Calculation of the second order recombination rate constant were evaluated by taking the recombination rate constant for H_3O^+ decay to be 2.4×10^{-7} cm^3 sec^{-1} determined by Calcote[54] and comparing gradients of the plotted lines. The straight lines provide evidence for the $N_1 \alpha \theta^{4/3}$ proportionality pointed out by Soundy and Williams[38]. The rate constants for the metal additives used are given in Table 7.1.

TABLE 7.1

Ion Recombination Rate Constants and Damkohler Number Values for Various Flame Additives

FLAME ADDITIVE	ION RECOMBINATION RATE CONSTANT cm sec	DAMKOHLER NUMBER D
C_2H_2 (1% total gas)	2.4×10^{-7} (54)	14.2
C_2H_2 + $InCl_3$ 0.1M	3.0×10^{-9}	0.16
" + NaCl 0.1 M	8.9×10^{-9}	0.5
" + CsCl 0.1M	8.9×10^{-9} (55)	0.5
" + $Pb(NO)_2$ 0.1 M	2.0×10^{-8}	1.8
" + $Mg(NO_3)_2$ 0.1M	6.7×10^{-8}	6.0
" + $MnCl_3$ 0.1M	2.0×10^{-8}	1.8

7.3 Determination of Damkohler Number.

It may be recalled the Damkohler number D_o is expressed by the following ratio,

$$D_o = \frac{\text{Chemical reaction rate}}{\text{Turbulent mixing rate}}$$

Since turbulent mixing is a mass transfer operation the mixing rate may be equated to the rate of mass transfer J,

$$J = 1^2 \left| \frac{d\bar{U}}{dx_2} \right| \frac{d\bar{N}}{dx_2}$$

where 1 = mixing length

$\frac{d\bar{U}}{dx_2}$ = mean velocity gradient normal to the direction of mean flow

$\frac{d\bar{N}}{dx_2}$ = mean concentration gradient in ion number density

The eddy diffusivity ε_D is given by,

$$\varepsilon_D = 1^2 \left| \frac{d\bar{U}}{dx_2} \right|$$

Mention was made in Chapter 3 that this term is not a constant but varies throughout the flow field. Therefore, the turbulent mixing rate must also be a varying quantity. A value for the rate has however been determined at the position 42d from the burner nozzle, the shortest distance from the nozzle studied

in this work. Equations relating the rate of turbulent mixing in subsonic free turbulent flames are, as far as the author is aware, not available. It has therefore been necessary to use expressions applicable to the isothermal jet to determine this quantity. It has been discussed in Chapter 4 measurements of mean concentration profiles by Hawthorne[16] showed a larger decay in jets compared to those in flames. This was attributed to a greater turbulent mixing rate in the case of the jet. The calculated rate presented here will therefore be in excess of the true value in the flame. However, since only a measure of the difference in Damkohler numbers for the various metal ion species is required the use of these equations is considered permissable.

The mean velocity at the 42d (≡ 21.0 cms) position is given as ;

$$\bar{U} = \frac{x_{core}}{x} \quad \bar{U}_n$$

where x_{core} = length of the diffusive core ≡ 18.0 cms

x = distance of test point from nozzle

$\bar{U}_n$ = mean gas velocity at the nozzle ≡ 7.6×10^3 cm sec^{-1}

$\therefore \quad \bar{U} = 6.5 \times 10^3$ cm sec^{-1}

The velocity gradient at this position may be determined using the distance "a" given as the radial distance where the mean velocity is one half the axial value, i.e.

$$a = 0.017\ x$$

such that, at the flame height 42d,

$$a = 1.64 \text{ cms}$$

and the mean velocity gradient is therefore;

$$\frac{d\bar{U}}{dx_2} = \frac{6.5 \times 10^3}{2 \times 1.64}$$

The ratio of the mixing length to the "a" value is a constant throughout the flame where

$$1 = 0.22a$$

therefore the mixing length at the 42d position is equal to 0.36 cms.

In the case of the H_3O^+ ion concentration field the mean ion number density for a flame seeded with 1% total gas of acetylene corresponds approximately to 10^{10} ion cm^{-3}. Assuming the concentration gradient to be at a maximum i.e. $\frac{10^{10}}{1.64}$ the rate of turbulent mixing is given as;

$$J = (0.36)^2 \ \frac{6.5 \times 10^3}{2 \times 1.64} \cdot \frac{10^{10}}{1.64}$$

The chemical reaction rate for the H_3O^+ ion recombination process is

$$\frac{dn}{dt} = k_{H_3O^+} |N|^2$$

where $k_{H_3O^+} = 2.4 \times 10^{-7}$ cm^3 sec^{-1} and $N = 10^{10}$

$\therefore$ The Damkohler number for H_3O^+ ion recombination reaction in a turbulent flame of nozzle Reynolds number 1.0×10^4

is equal to 14.2.

The D_o values for the other flame additives would have been determined by a similar procedure using the recombination rate constants given in Table 7.1. The recombination rate constants for these species have all been considered to follow a three body collisional process.

$$M^+ + e^- + X \xrightarrow{k} M + X$$

The rate constant under these conditions is considered to be a function of temperature, i.e.

$$\frac{dn}{dt} = k|N_m+|^2 \, |N_x|$$

$$k = AT^{-1.5}$$

where $A = 2 \times 10^{-22}$ cm^2 mol^{-2} sec^{-1}

and $|N_x| = 10^{18}$ mol cm^{-3}

The ion number densities for 0.1M solution for the various metal additives used may be calculated by way of equation . The Damkohler number values are given in Table 7.1. It may be seen the largest difference is between the values for H_3O^+ and In^+ respectively, expected from the two orders of magnitude difference in their recombination rate constants. The low indium recombination rate constant indicates the ion to be long lived such that it would be expected to behave as a neutral species in the turbulent flame. The H_3O^+ and In^+ species there for fulfil the requirements stated at the beginning of this

Chapter. The other metal ion species provide relatively low D_o values, however since these are for 0.1M solutions it is to be anticipated higher concentration levels would markedly enhance the chemical influence. Of the remaining species present, lead, caesium and sodium were selected to observe the effects of variable solution concentration upon the turbulent ion density pattern.

CHAPTER 8

PRELIMINARY STUDIES OF ION CONCENTRATION FLUCTUATIONS IN A TURBULENT DIFFUSION FLAME

8.1 The aim of the preliminary investigations described in this chapter was to obtain experimental evidence for the chemistry-turbulence interaction phenomenon. The turbulent diffusion flame was seeded, in turn, with the preselected additives, acetylene, caesium, lead, sodium and indium. It has been shown they cover Damkohler number range of 14-0.2 and this was considered sufficient to provide the required difference between the statistical functions used to describe the respective fluctuating ion concentration fields. The functions used for this preliminary study were the auto-correlation and power spectral density functions.

8.2 Experimental Procedure

The turbulent diffusion flame of unburnt gas composition of hydrogen and nitrogen in the ratio of 3:1 was vented through a contoured nozzle of 5.0×10^{-3}M diameter at Reynolds number of 1.0×10^{4} into the filtered laboratory atmosphere. The flame ionisation was generated by the addition of acetylene to the gas flow as approximately 1% of the total gas and/or by seeding the flame with aqueous metal salt solutions using a scent spray atomiser driven by part of the nitrogen supply.

The maximum temperature of the flame was measured to be approximately 2300^{o}K using the sodium "D" line reversal technique. The water-cooled electrostatic probe, described in

detail in Chapter 6, was positioned 4.6 nozzle diameters(d) above the burner such that it sampled the local ion concentration fluctuations on the flame axis. The probe biased at 50V negative with respect to the burner collected the positive ion saturation current which was passed through a 1MΩ resistor to produce the voltage analog. The probe signal was then divided using a "BNC" "T" piece and the two identical signals were fed into the analog correlator for analysis.

8.3 Results and Discussion

The autocorrelograms obtained for the various additives and combinations of additives are shown in Fig. 8.1. The metal salt solutions used for Cs, Na, Pb and In were all of 0.1 molarity. In Table 8.1 is given the turbulent time scales for the various autocorrelograms. The turbulent scale generally defined as the time required for a correlogram to fall to $1/_e$ of its initial value requires correction to allow for the non-linearity in probe response. The corrected time scale, to be discussed in a later section, corresponds to the time required for a correlogram to fall to a value of 0.47.

Addition of Acetylene

It may be observed the smallest time scale occurred for the acetylene seeded flame. As has been stated earlier the most predominant ion above the reaction zone of a hydrogen flame seeded with acetylene is the H_3O^+ ion. Its decay follows the second order recombination reaction

$$H_3O^+ + e^- \xrightarrow{k_1} H_2 + OH$$

where k_1 has the widely accepted value of $2.4 \times 10^{-7} cm^3 sec^{-1}$ (54)

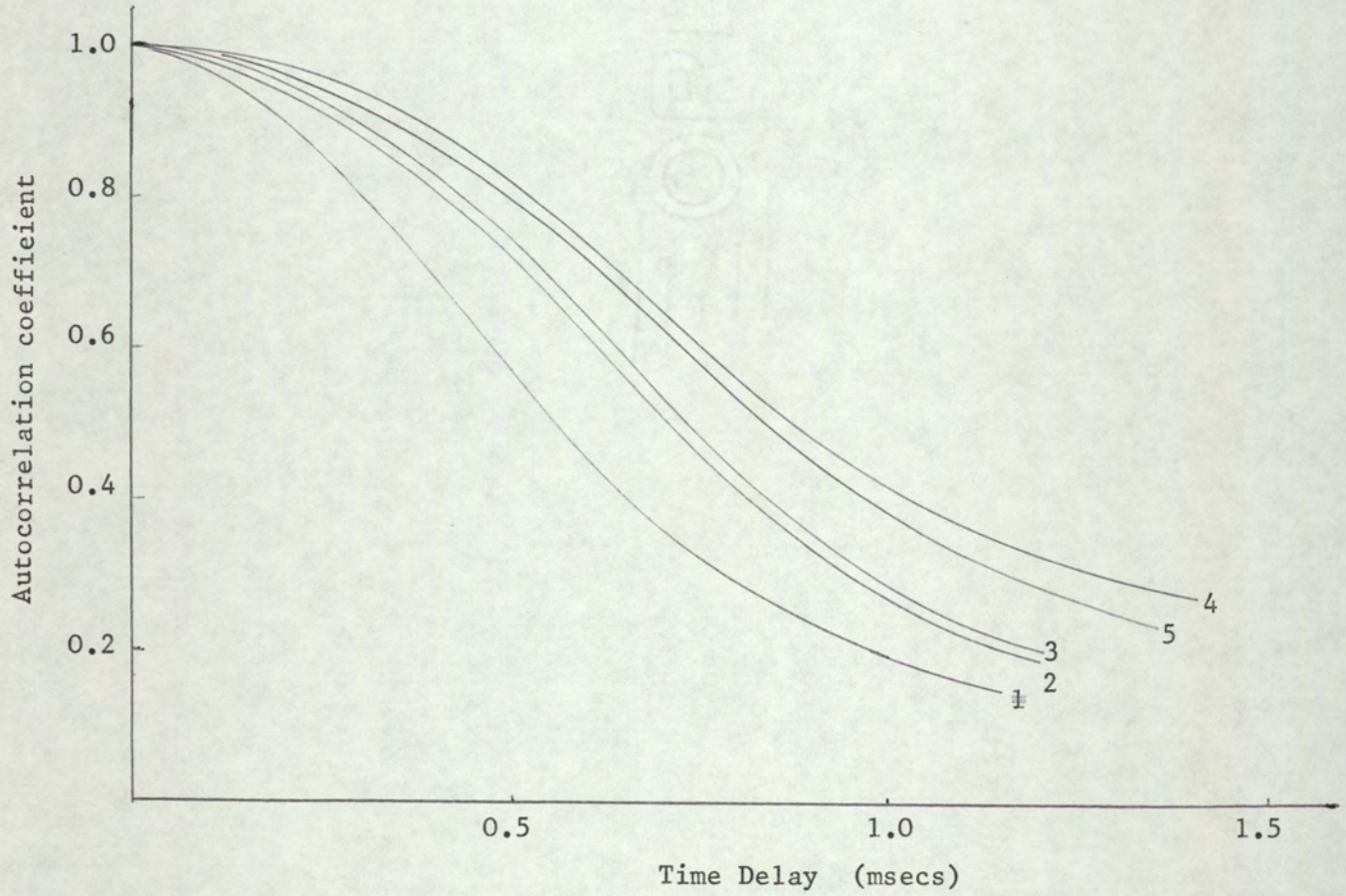

Fig. 8.1 Autocorrelograms for the additives; (1) C_2H_2 only, (2) Cs as CsCl only, (3) C_2H_2 plus Pb as $Pb(NO_3)_2$ (4) C_2H_2 plus In as $InCl_3$ (5) Na as NaCl only.

Table 8.1

The Influence of Rapid Ion Chemical Kinetics upon Turbulent Time Scales

Flame Additive	Turbulent Time Scale (msecs)
C_2H_2 (1% total gas)	0.61
C_2H_2 + $InCl_3$ (0.3M)	1.15
" (0.1M)	1.16
" (0.05M)	1.15
C_2H_2 + $Pb(NO_3)_2$ (0.3M)	1.14
" (0.1M)	0.88
" (0.01M)	0.63
CsCl only	
0.3M	0.63
0.1M	0.89
0.025	1.01
0.0025	1.15
NaCl only	
0.1M	1.01
0.05M	1.10
0.01M	1.15
CsCl (0.1M) + 0.1% C_2H_2	0.82
" + 1.0% C_2H_2	0.76
NaCl (0.1M) + 0.1% C_2H_2	1.14
" + 1.0% C_2H_2	0.90

which is one of the most rapid ion recombination reactions in flames. The small turbulent time scale observed in a Fig. 8.1 is attributed to the speed of this reaction. Variation in the nozzle Reynolds number in the range 1.0×10^4 - 7.0×10^3 produced no effect upon the time scales indicating that decay of the ion concentration field by turbulent mixing to be negligible.

Addition of Indium Trichloride

The addition of indium in the presence of acetylene induces the fast charge exchange reaction

$$In + H_3O^+ \xrightarrow{k_{In}} In^+ + \text{products}$$

The ion formed is long lived having a pseudo bimolecular recombination rate constant of approximately $3.3 \times 10^{-9} cm^3 sec^{-1}$ measured by the technique described in the previous chapter. The largest time scale observed is considered to be representative of decay by turbulent mixing. This is supported by the fact that the indium autocorrelogram exhibited the longest time scale observed in these studies. The time scale was independent upon variation in concentration of indium additive over the range 0.3M to 0.05M. It was further observed that the scale was dependent upon variation in nozzle Reynolds number increasing with decreasing R_e. Over the range of R_e 1.0×10^4 - 7.0×10^3 the time scales changed from 1.15m secs to 1.32 m secs. These observations confirm that due to the long life of the In^+ ion the species behave as a chemically inert constituent such that decay of the In^+ concentration field is controlled by turbulent mixing. This result is of further importance since this time scale is also characteristic of the decay of a stable neutral

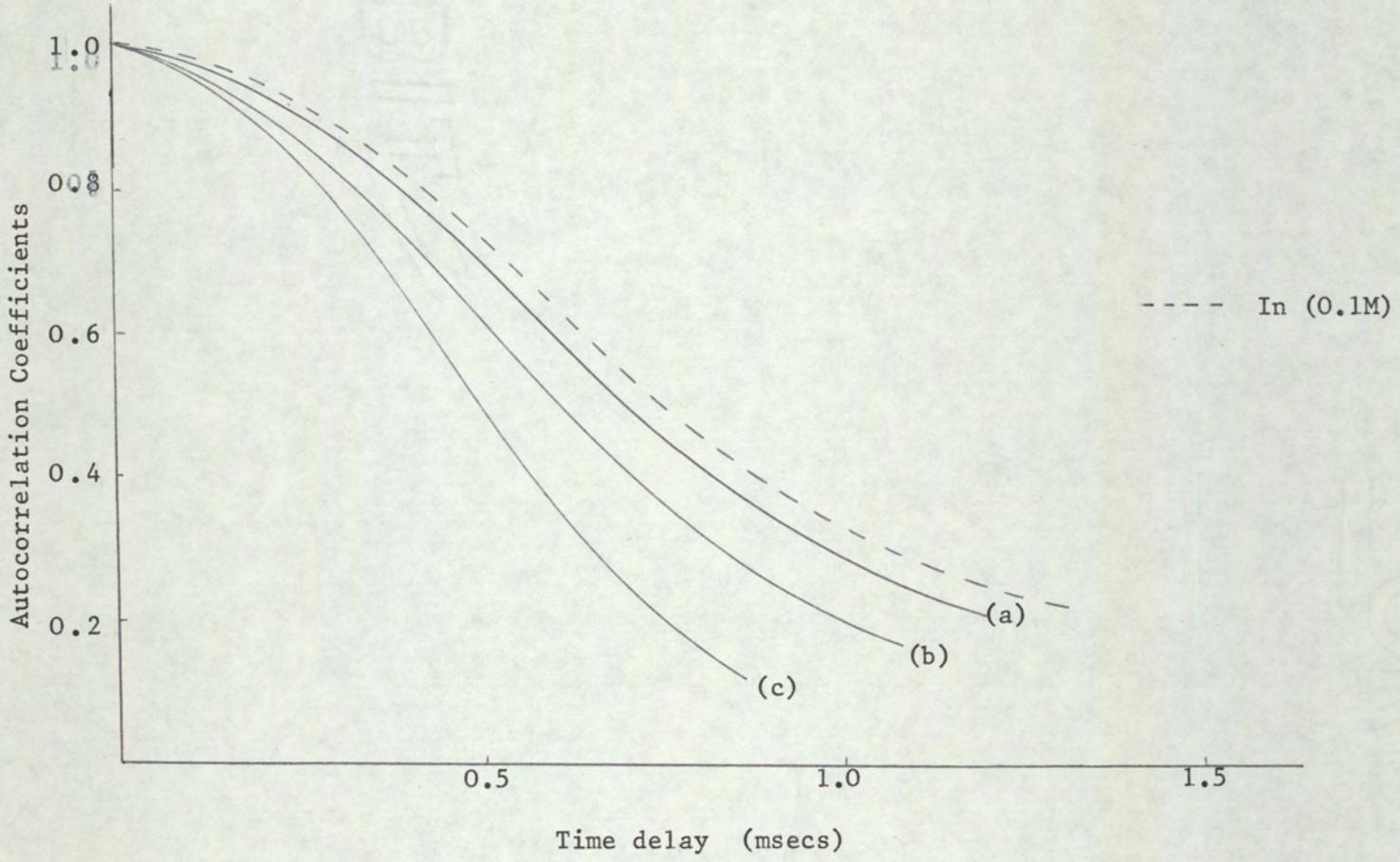

Fig. 8.2 Autocorrelograms for the additives C_2H_2 and the atomiser solutions of $Pb(NO_3)_2$; (a) 0.3M; (b) 0.1M; (c) 0.01M.

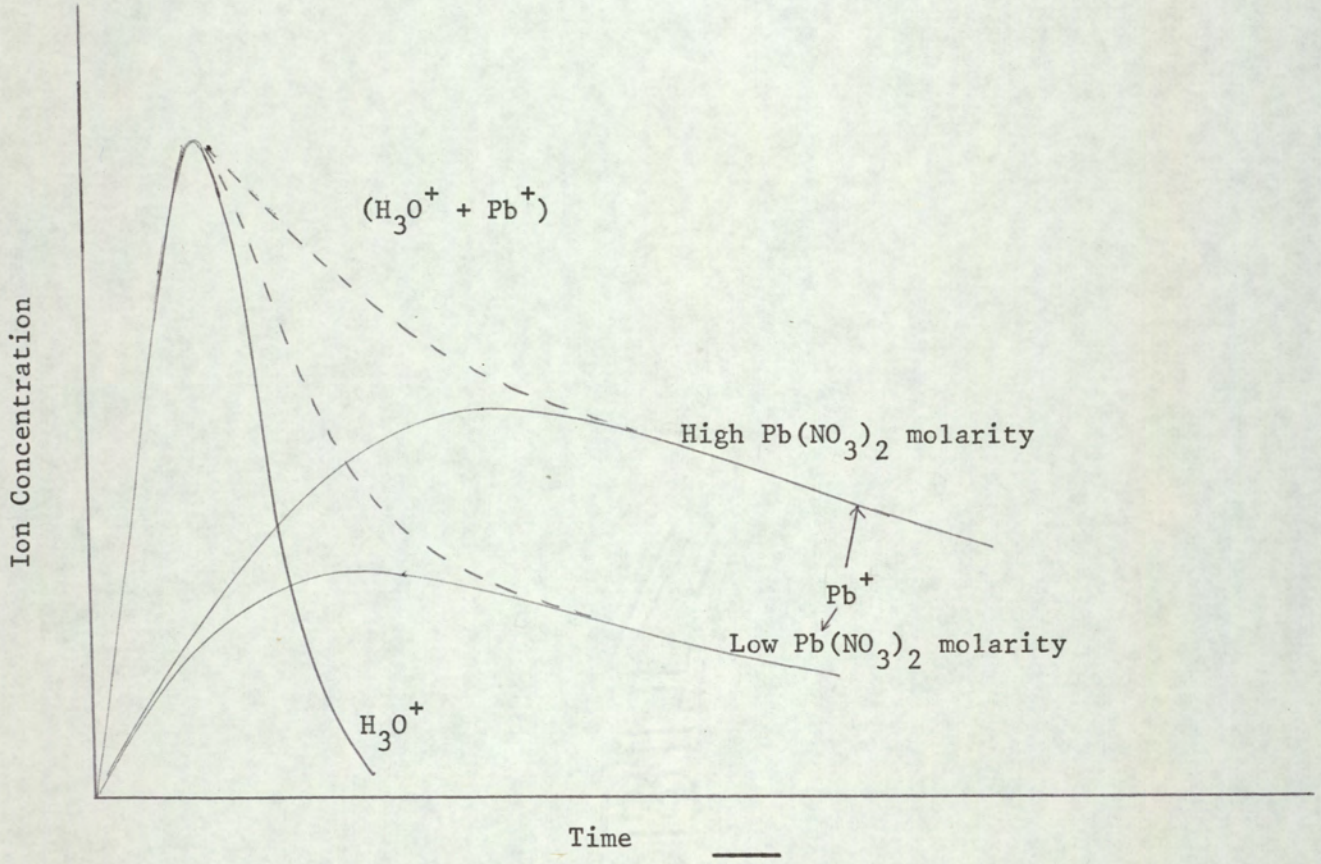

Fig. 8.3 Schematic diagram showing the effect of $Pb(NO_3)_2$ solution concentration on ion decay in a flame containing C_2H_2

species concentration field, e.g. H_2 or H_2O.

Addition of Lead Nitrate

In the case of lead addition, shown as curve 3 in Fig. 8.1 the ion is formed by a charge exchange reaction with H_2O^+ ion and had a measured recombination rate constant of 2.2×10^{-8} $cm^3 sec^{-1}$. Chemical decay controls the turbulent time scale which was observed to be a function of the concentration of lead additive as shown in Fig. 8.2. Upon increasing the molarity of the lead nitrate solution an increase in the turbulent time scale was observed. This effect was not expected since a decrease would occur if the recombination reaction

$$Pb^+ + e^- + M \xrightarrow{K_{Pb}} Pb + M$$

predominated since increased lead concentration would produce a more rapid chemical decay of Pb^+ ions as predicted by the second order rate equation

$$\frac{-d[Pb^+]}{dt} = K_{Pb} [Pb]^2$$

A simple explanation for this result is depicted schematically in Fig. 8.3. The probe cannot differentiate between ions thus the fluctuations are attributed to the decay of the total ion concentration i.e. $(H_3O^+ + Pb^+)$. Increased lead concentration produces an initially slower recombination rate for the total ion concentration resulting in an increased turbulent time scale.

Addition of Caesium nitrate and Sodium Chloride

The addition of both caesium and sodium show time scales that were a function of concentration, the scales decreasing with increased solution molarity. Addition of sodium, in the

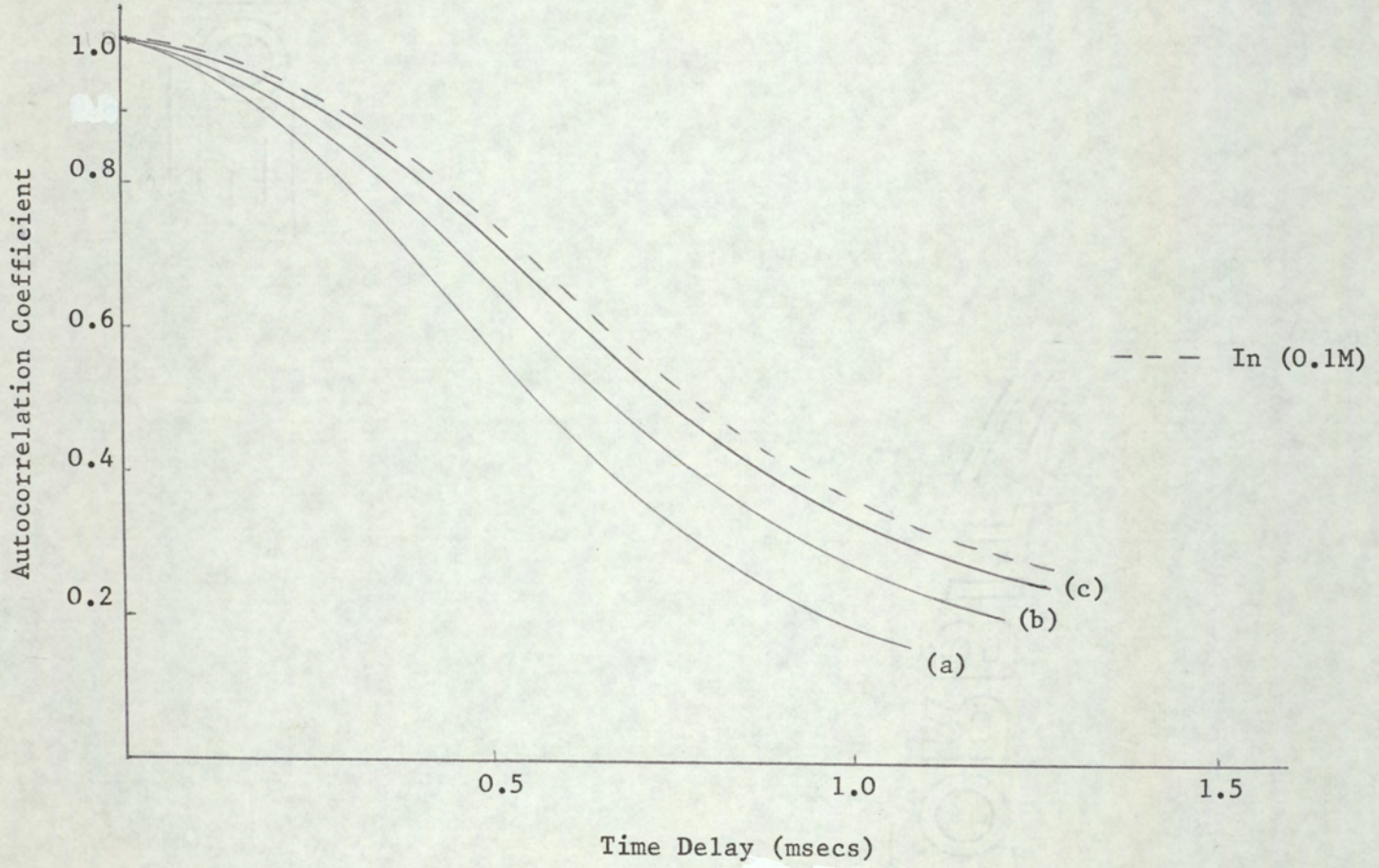

Fig. 8.4 Autocorrelograms for the addition of the atomiser solutions of C_sCl only; (a) 0.1M; (b) 0.025M; (c) 0.0025M.

absence of acetylene, the 0.1M and 0.05M solutions exhibited turbulent scales of 1.01 msecs and 1.10 msecs respectively. The remaining 0.0 1M solution used decayed at a rate characterised by the turbulent mixing time scale. As illustrated in Fig. 8.4 caesium exhibits a complete range of time scales, the 0.3M solution shows a time scale comparable to that for H_3O^+ decay while the time scale for the 2.5×10^{-4}M solution approached that representative of turbulent mixing. It would be expected that equimolar caesium and sodium additives would yield equivalent time scales if their ion density fields were controlled by chemical decay since the ion recombination rate constants for both species is approximately 8.8×10^{-9} cm^3 sec^{-1}. The observed difference (see Table 8.1) suggests the structure of their respective ion density fields is predominantly controlled by ion production where the first order ionisation constant for caesium ion generation is 4000 sec^{-1} while that for the slower sodium ion production is 20 sec^{-1}.[39]

Addition of acetylene, 0.1% total gas, to a flame seeded with 0.1M sodium chloride produced an increase in the time scale to that characterised by turbulent mixing. Upon increased acetylene addition to 1.0% of the total gas resulted in a decrease in scale from 1.15 msecs to 0.90 msecs. The time scale for sodium in the absence of acetylene is considered to

be representative of the thermal ionisation process. The addition of 0.1% acetylene enables the sodium ion concentration to rapidly attain the thermodynamic equilibrium level. At this steady state condition the rate of ion production equals the rate of recombination such that the ion concentration field will decay by turbulent mixing thereby leading to the observed increased time scale. Addition of 1.0% total gas of acetylene, the greater H_3O^+ ion concentration available for charge exchange promotes the sodium ion concentration above the equilibrium level such that the observed decrease in the turbulent scale is attributed to decay of the ion field by the second order recombination mechanism.

The addition 0.1% and 1.0% acetylene to the flame seeded with 0.1M caesium nitrate solution produced a decrease in turbulent scales from 0.89 msecs to 0.82 msecs and 0.89 msecs to 0.76 msecs respectively. This is considered to be due to above equilibrium $[Cs^+]$ level resulting from the charge exchange process with H_3O^+ such that the ion density field is controlled by chemical decay rather than ion production as in the absence of acetylene. The increased acetylene addition promotes a greater $[Cs^+]$ production thus resulting in an increased recombination reaction rate to produce the smaller turbulent scale.

As the level of decay of the reactant species by turbulent mixing may be controlled by variation in Reynolds number it is to be expected that with increased R_e the rate of decay by

Fig. 8.5 The effect of increased nozzle Reynolds number from 1.0×10^4 to 1.5×10^4 causing H_3O^+ and In^+ (0.1M) autocorrelograms to converge

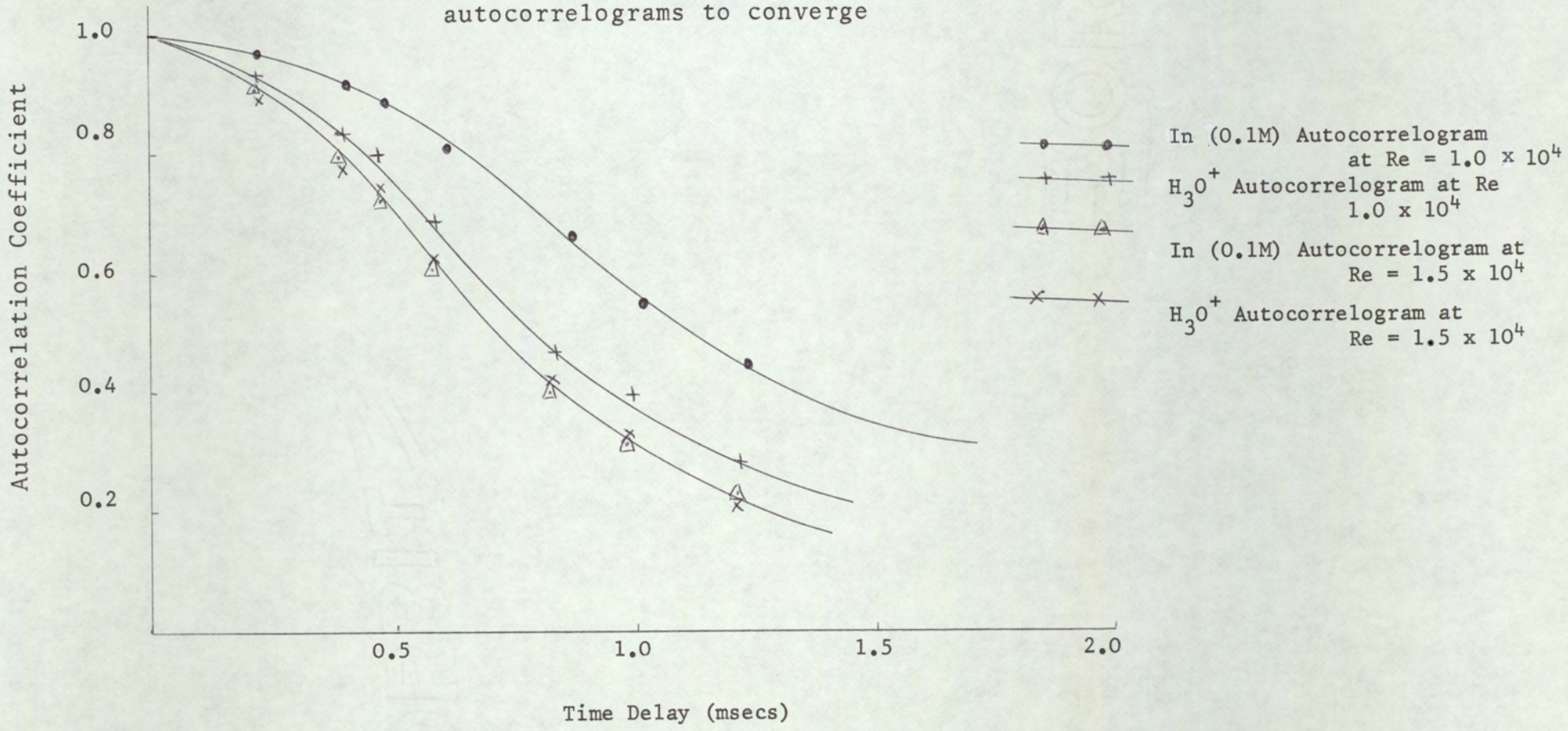

turbulent dissipation will increase and a critical Reynolds number must exist where the mixing process will become dominant over the chemical reaction rate. This has been observed for a Reynolds number of approximately 1.5×10^4 where the auto-correlograms for both H_3O^+ and In^+ ion decay lie superimposed upon each other. This is shown in Fig. 8.5.

The above observations provide experimental evidence that the presence of a rapid chemical reaction where the species are concurrently under the influence of turbulent mixing processes will lead to a reduction in the size of the turbulent scales. In addition evidence has been obtained showing this effect to be independent of the chemical reaction being either an ion production or decay process. This has been predicted theoretically by Lee[3].

8.4 Correction Applied to Turbulent Time Scale Measurements

As mentioned in the preceding section the turbulent time scales given as the time required for an autocorrelogram to fall to $1/e$ of its initial value must be corrected to allow for the non-linearity in probe response. The scales given by the above definition will be characteristic of the random ion current. It is required that the scales be characteristic of fluctuations in ion density.

The Clements and Smy equation relating the probe current I to the plasma density N is given by equation 5.9 This may be expressed as:

$$I = \alpha N^{\frac{3}{4}} \quad \text{where } \alpha = \text{constant} \qquad 8.1$$

If two new variables are introduced as:

$$x_\tau = N(t)\ N(t+\tau) \qquad 8.2$$

and

$$y_\tau = I(t)\ I(t+\tau) \qquad 8.3$$

Then

$$y_\tau = \alpha\ x_\tau^{\frac{3}{4}} \qquad 8.4$$

If N follows a Gaussian distribution x_τ will be similarly distributed with the same variance. However since x_τ and y_τ are related by a power law, y_τ will not be Gaussian distributed This may be illustrated as follows:

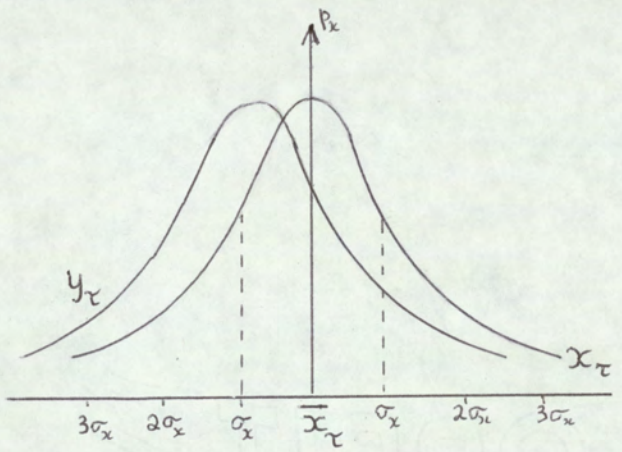

Fig. 8.1

For each value of x_τ the corresponding value for $y_\tau (=\alpha x_\tau^{\frac{3}{4}})$ will have the same probability density function.

Mean values for x_τ and y_τ may be defined as follows:

$$\overline{x_\tau} = \frac{(\overline{x_\tau} + \sigma_x) + (\overline{x}_\tau - \sigma_x)}{2} \qquad 8.5$$

$$\overline{y}_\tau = \frac{\alpha(\overline{x}_\tau + \sigma_x)^{\frac{3}{4}} + \sigma(\overline{x}_\tau - \sigma_x)^{\frac{3}{4}}}{2} \qquad 8.6$$

where σ_x = standard deviation for process x_τ

$$\therefore \quad \bar{y}_\tau = \alpha \bar{x}_\tau^{\frac{3}{4}} + \left(1 + \frac{\sigma_x}{\bar{x}_\tau}\right)^{\frac{3}{4}} + \left(1 - \frac{\sigma_x}{\bar{x}_\tau}\right)^{\frac{3}{4}} \qquad 8.7$$

It may be recalled that turbulent intensity is defined as the ratio of the root mean square of the fluctuating component to the mean value i.e. $\frac{\sigma_x}{\bar{x}_\tau}$

Thus for $\frac{\sigma_x}{\bar{x}_\tau} = 0$ then $\bar{y}_\tau = \alpha \bar{x}^{\frac{3}{4}}$

when $\frac{\sigma_x}{\bar{x}_\tau} \doteq 1$ then $\bar{y}_\tau = 0.88\sigma \bar{x}^{8}$

The term contained in the bracket is only slowly varying i.e. yielding an error of 12% for turbulent intensity value of 100% The turbulent intensity values encountered in these studies were of the order of 10% such that

$\bar{y}_\tau = \alpha \bar{x}_\tau^{\frac{3}{4}}$ is a good approximation for equation 8.7.

Since $\bar{y}_\tau = \overline{I(t)\, I(t+\tau)} = R_\tau(I)$

and $\bar{x}_\tau = \overline{N(t)N(t+\tau)} \doteq R_\tau(N)$

$$R_\tau(I) = \alpha R_\tau(N) \qquad 8.9$$

Therefore the value of $R_\tau(N)$ for $R_\tau(I)$ at $1/e = 0.37$ corresponds to $(0.37)^{\frac{3}{4}} = 0.47$.

Hence the turbulent time scales characteristic of the ion concentration field must be redefined as the time required for the correlogram to fall to 0.47 of the initial value. This correction has been applied to all the turbulent time scales presented in this work.

8.5 Determination of the Power Spectral Density Function

The theoretical studies of Corrsin[2] predict that the influence of a rapid chemical reaction upon the structure of

the reactant concentration field in a turbulent environment would produce an earlier fall off in the power spectral density function. Having observed the effects of chemistry using the autocorrelation coefficient suggest this influence should be repeated in its Fourier transform, the power spectrum.

The fluctuating ion signals collected by the probe were recorded on magnetic tape for each flame additive used for the autocorrelation studies. Each waveform was digitally analysed to obtain the power spectrum using the computer programs given in the Appendix. The resulting spectrum showed a complete absence of an early fall off at the "knee" and within the limits of experimental error they were identical for each flame additive.

This result was initially considered surprising and was examined further. The autocorrelation function was considered to fall exponentially[56] obeying the equation

$$R(\tau) = e^{-a_1 |\tau|} \qquad 8.10$$

where τ is the modulus of the time delay and the constant a is given as the reciprocal of the turbulent time scale i.e.

$$a_1 = \frac{1}{\tau_e}$$

The corresponding power spectral density function is given by

$$G(f) = \frac{4a_1}{a_1^2 + 4\pi^2 f^2} \qquad 8.11$$

Substituting the maximum and minimum turbulent time scales obtained experimentally i.e. 0.61msecs for H_3O^+ decay and 1.15msecs for In^+ decay for "a_1" in equation 8.10 computational analysis enabled power spectra corresponding to the two time scales to be determined. The spectra showed a difference of

approximately 3dB at the high and low frequency portions merging between 500H_z and 3 kH_z as shown in Fig. 8.6. The 3dB difference must be considered to be negligible when a drop of 40-45 dB was encountered between the low and high frequency portions of the spectra. This result therefore illustrates the variation in turbulent time scales is too small to reveal any chemical effect by spectral analysis.

The above result indicates that unless the chemical species can react at a rate considerably higher than the reactions studied in this work thereby producing a greater difference between the turbulent scales for the chemically active and chemically inert species concentration fields, the presence of a chemistry-turbulence interaction will not be revealed by spectral analysis.

It is considered further that since the studied recombination reaction between H_3O^+ ions and electrons is believed to be one of the fastest occurring in flames, the use of acetylene and indium additives possibly presents the largest available difference between turbulent scales. It is therefore reasonable to assume the above condition is unlikely to be fulfilled in a turbulent flame such that a study of the interaction phenomena in such a system using spectral analysis will be of little value. This is of importance to the experimentalist since as mentioned above, it is contrary to the theoretical predictions of Corrsin and Lee who conclude the interaction should be identified by variation in the power spectral density function.

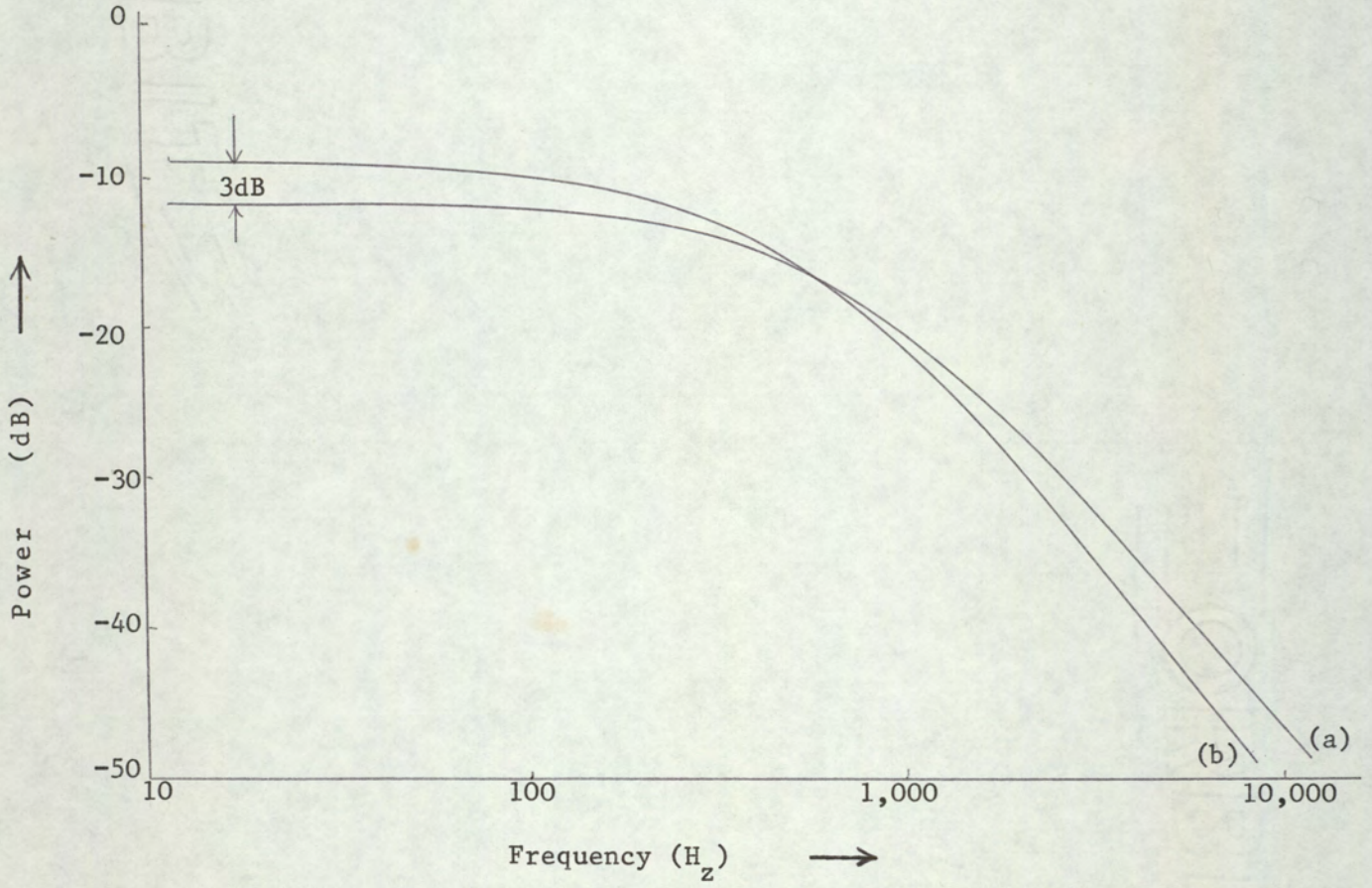

Fig. 8.6 Theoretically determined Power Spectral Density Functions from the autocorrelation functions for (a) C_2H_2 and (b) In.

8.6 The Effect of Chlorine Addition upon the Turbulent Time Scales

The effect of trace amounts of halogens upon the electron concentration in laminar premixed hydrogen flames seeded with alkali metals has been investigated by Padley, Page and Sugden[40]. The addition of halogens, up to 1% of the total gas are effectively distributed between free halogen atoms B and hydrogen halide HB by the reaction,

$$HB + H \rightleftarrows H_2 + B \qquad \text{(i)}$$

The halogen may also react with the alkali metal A to form undisassociated gaseous salt AB and with free electrons to produce negative ions. Both these effects would be expected to lead to a reduction in electron concentration due to the removal of some alkali metal yielding a compound less ionisable and by the direct removal of electrons. The addition of chlorine to a hydrogen flame seeded with sodium and a trace of acetylene was observed, however, to result in an increase in electron concentration reaching a maximum at approximately 0.2% of the total gas. Further chlorine additions produced the expected decrease in electron concentration for the reasons given above.

The phenomenon was considered to be linked with the above equilibrium levels of H and OH radicals present in the burnt gases of hydrogen-rich flames. It was suggested that the presence of chlorine enabled the following reactions to occur:

$$A + B \rightleftarrows A^+ + B^- \qquad \text{(ii)}$$

$$B^- + H \rightleftarrows HB + e^- \qquad \text{(iii)}$$

Algebraic addition of the reactions (i) - (iii) gave the resultant reaction.

$$A + 2H \rightleftarrows A^+ + e^- + H_2 \qquad \text{(iv)}$$

The presence of a high [H] together with the H_2 being approximately at the equilibrium level enables the above reaction to produce a greater steady state electron concentration than the thermal equilibrium level maintained by the reaction.

$$A + X \rightleftarrows A^+ + e^- + X \qquad \text{(v)}$$

where X is a third body. Reaction (iv) is not in direct competition with the collisional ionisation process, being too slow. The presence of chlorine, however, catalyses the mechanism (i) - (iii) such that it becomes the dominant reaction. It was therefore postulated that the electron concentration maximum observed upon the introduction of halogen was due to a transition from the thermal ionisation reaction to that involving H atoms. This process is shown schematically below.

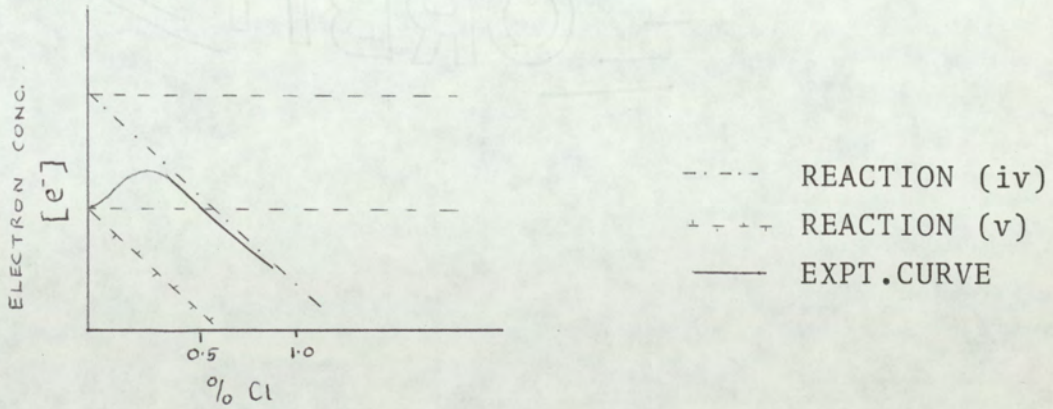

Fig. 8.7

The ability of chlorine to modify electron concentration levels must also be expected to influence the rate of recombination reactions between positive ions and free electrons. With this in mind it was considered to be of value to investigate the effects of chlorine addition upon the turbulent time scales for those reactions studied previously in the turbulent flame.

Chlorine was introduced into the flame by the addition of trace amounts of carbon tetrachloride vapour carried in part of the nitrogen supply.The carbon tetrachloride liquid was held above a glass sinter in a bubble saturator through which nitrogen maintained at a flow rate of 1 litre min^{-1} was passed. The bubbles so formed burst at the surface producing fine droplets of the chloride which were carried in the nitrogen stream into the flame. The saturator was immersed in a constant temperature water bath at 25°C to ensure a constant vapour pressure since fluctuations in this quantity would lead to variation in the chloride content of the flame. Under these conditions it was considered the amount of chlorine present in the flame was of the order of 1% of the total gas flow.

The flame, containing chlorine, was seeded with acetylene and the 0.1M aqueous solutions of lead nitrate, caesium nitrate and indium trichloride used previosly. The electrostatic probe was again biased at 50V negative and located 46d above the burner, on the flame axis. The autocorrelograms were determined for each additive, in the presence of chlorine, using the analog correlator as described earlier. The turbulent time scales are given in Table 8.2 together with those obtained previously in the absence of chlorine for purposes of comparison.

Table 8.2

Effect of Chlorine Addition (1% total gas) upon Turbulent Time Scales

Flame Additive	Turbulent Time Scale (msec)	
	Cl absent	Cl present
C_2H_2	0.61	0.75
C_2H_2 + $Pb(NO_3)$ (0.1M)	0.88	1.0
C_sCl (0.1M)	0.89	0.90
$InCl_3$ (0.1M)	1.15	1.15

The turbulent time scales for acetylene addition (1% of t total gas) was observed to increase in the presence of chlorine. Chlorine ions are produced in the flames by the following reactions

$$H + Cl \rightarrow HCl \qquad \text{(vi)}$$

$$HCl + e^- \rightarrow Cl^- + H \qquad \text{(vii)}$$

The above mechanism thus leads to a reduction in the free electron concentration in the flame. This in turn will cause a decrease in the rate of the H_3O^+ ion recombination reaction.

$$H_3O^+ + e^- \rightarrow H_2 + OH \qquad \text{(viii)}$$

such that the chemical decay of the H_3O^+ ion number density occurs more slowly to produce the observed increased time scale. This may be clearly seen from a consideration of the following kinetic equations:

In the absence of chlorine reaction (viii) only applies:

$$-\frac{d[H_3O^+]}{dt}_{Cl=0} = k_{H_3O^+}\,[H_3O^+][e^-] \quad \text{where } [H_3O^+] = [e^-] \qquad \text{(ix)}$$

In the presence of chlorine

$$[H_3O^+] = [e^-] + [Cl^-]$$

$$\therefore \quad -\frac{d[H_3O^+]}{dt} = k_{H_3O^+}\,[H_3O^+][e^-]$$

$$= k_{H_3O^+}\{[H_3O^+] - [Cl]\}[H_3O^+] \qquad \text{(x)}$$

$$= k_{H_3O^+}[H_3O^+]^2 - k_{H_3O^+}[H_3O^+][Cl^-]$$

$$\text{i.e.} \quad -\frac{d[H_3O^+]}{dt} = \left(\frac{d[H_3O^+]}{dt}\right)_{Cl=0} - k_{H_3O^+}[H_3O^+][Cl^-] \quad \text{xi}$$

Thus equation xi illustrates the presence of chlorine results in a reduction in the H_3O^+ ion decay rate by an amount equal to the final term on the right hand side of equation xi . The H_3O^+ ion concentration may also undergo decay by the reaction.

$$H_3O^+ + Cl^- \xrightarrow{k} H_2O + HCl$$

where $k = 3 \times 10^{-8}$ $cm^3 sec^{-1}$ (41)

It is unlikely that this reaction will be the predominant mechanism for H_3O^+ ion depletion with the chlorine present in trace amounts as e^- > Cl^- is the probable condition. However consideration of a possible contribution to decay by this process would also favour increased time scales since the reaction rate constant is an order of magnitude smaller than the corresponding rate constant for the H_3O^+ ion reaction with a free electron.

Chlorine addition to the flame seeded with 0.1M lead nitrate solution together with a trace of acetylene was observed to increase the time scale to that representative of turbulent mixing. The presence of chlorine thus results in the dissipation of the ion concentration field moving from a chemical to a turbulent process. It has been discussed previously that the probe follows the decay of the total ion concentration, viz $(H_3O^+ + P_b^+)$. The growth in chlorine ion concentration at the expense of a reduced electron concentration will render both the H_3O^+ and P_b^+ ions longer lived, resulting in a persistance of the combined ion concentration level.

Consideration of the above results indicate the turbulent time scales to be controlled by the free electron concentration levels. As the presence of chlorine in the flame gases accompanies a reduction in $[e^-]$ for the amount of chlorine added (i.e. 1%) the chemical decay rate of the ion concentration field occurs more slowly. With these species existing for a greater time the observed increased time scales result.

The addition of chlorine to a caesium seeded flame had no effect upon the time scale. It will be recalled that the caesium time scale is due to an ion production reaction being followed i.e.

$$Cs + M \rightarrow Cs^+ + M + e^-$$

such that a removal of electrons will in no way affect the rate of Cs^+ ion production.

The time scale for indium in chlorine presence was also unaffected. This was expected with the long lived indium ion decaying by turbulent mixing action such that a chemical influence upon the electron concentration would be of no consequence.

CHAPTER 9

Flame Mapping Experiments in the Turbulent Diffusion Flame

The experiments described in this chapter are a continuation of the preliminary studies discussed previously. The aim of this portion of the work was to observe further the effects of rapid ion chemical kinetics upon the fluctuating ion concentration field and to obtain information regarding the overall structure of this field in the turbulent diffusion flame. This was achieved by determination of the autocorrelation, power spectra, probability density and cumulative distribution functions at various locations in the flame. Each individual test point provides information of the local "eddy" structure and collectively they provide an indication as to the behaviour of the fluctuating ion concentration field throughout much of the flame.

9.1 Experimental Procedure

Details of the turbulent diffusion flame and electrostatic probe employed in this study have been described in section 8.2 of the previous chapter. The electrostatic probe was used to map the flame at the axial positions 42, 46, 50 and 54d from the burner. In addition a transverse scan was performed across the flame at 42d up to a distance of 3.6d on either side of the flame axis at intervals of 0.6d giving a total of thirteen radial test points. The flame was seeded with acetylene (1% total gas), caesium, lead and indium using in the case of the latter three, the various solution concentration ranges employed in the preliminary studies. At each

point the random probe signals were recorded on magnetic tape and digitally analysed to determine the above named statistical functions. The autocorrelograms were determined by both digital and analog methods. The digital results will be present here, however it is worthy of note that excellent agreement was obtained between the two techniques. Unfortunately time did not permit a more complete investigation whereby transverse scans could be performed at each axial position studied. However, from the data obtained reasonable predictions regarding the structure of the ion field at other regions in the flame have been possible.

9.2 Autocorrelation Studies

In Table 9.1 is presented the turbulent time scales determined for each flame additive at the relevant axial and radial test positions. The time scales for acetylene addition were again observed to yield the shortest values at each position studied, while those for indium additions were provided the longest time scales. The effects of concentration variation for caesium and lead addition were also repeated, with the caesium time scales decreasing upon increased additive concentration and lead addition exhibiting the opposite effect, the scales increasing with increased concentration. These results were expected from the earlier findings and will not be discussed further having been examined at length in the previous chapter.

Further information given in Table 9.1 shows the turbulent time scales to increase upon moving away from the flame axis at 42d towards the flame/atmosphere boundary. The scales

Table 9.1 Turbulent Time Scales Obtained from Flame Mapping Experiments

FLAME ADDITIVE	RADIAL TURBULENT TIME SCALES (msec) PROBE HEIGHT 42d Radial Probe Positions (Nozzle Diameters from Axis) (Top Row)													AXIAL TURBULENT TIME SCALES (msec) AXIAL DISTANCE FROM BURNER			
	3.6d	3.0d	2.4d	1.8d	1.2d	0.6d	0.0d	0.6d	1.2d	1.8d	2.4d	3.0d	3.6d	42d	46d	50d	54d
C_2H_2	1.48	0.96	0.65	0.85	0.75	0.58	0.61	0.62	0.62	0.54	0.87	1.23	1.36	0.61	0.66	0.81	1.07
C_2H_2 + $InCl_3$ (0.3M)	2.0	-	1.40	-	1.2o	-	1.15	-	1.1	-	1.30	-	1.90	1.15	1.10	1.20	1.50
(0.1M)	2.2	-	1.39	-	1.1	-	1.1	-	1.1	-	1.38	-	1.95	1.10	1.10	1.35	1.58
(0.05M)	-	-	-	-	-	-	1.15	-	-	-	-	-	-	1.15	1.21	1.51	1.61
C_2H_2+$Pb(NO_3)_2$																	
(0.3M)	1.9o	-	1.39	-	1.23	-	1.15	-	1.20	-	1.38	-	1.89	1.15	1.20	1.40	1.50
(0.1M)	1.53	-	1.20	-	0.96	-	0.80	-	1.20	-	1.21	-	1.60	0.80	1.I5	1.25	1.40
(0.01M)	1.33	1.15	0.73	0.87	060	0.76	050	0.64	0.60	0.77	0.82	1.00	1.50	0.50	0.75	1.00	1.13
CsCl only																	
(0.1M)	1.50	-	1.3	-	0.74	-	0.81	-	1.10	-	1.27	-	1.59	0.80	0.75	1.06	1.40
(0.01M)	1.71	-	1.38	-	1.20	-	0.93	-	1.20	-	1.31	-	1.59	0.93	1.40	1.40	1.56
(0.0025M)	-	-	-	-	-	-	1.15	-	-	-	-	-	-	1.15	1.42	1.40	1.56

were also observed to increase with greater distance from the burner. Similar findings have been reported by Lawrence[13] during studies of velocity fluctuations in isothermal air jets. It was discussed in Chapter 3 that the level of correlation is dependent upon the frequency content of a random waveform. The high frequency components, attributed to the presence of small eddies being rapidly convected past the probe wire, will upon the application of a short time delay become uncorrelated causing a decrease in correlation coefficient values. The increased turbulent time scales observed upon moving radially from the flame axis is considered to be due to the gradual disappearance of the small eddies resulting in a reduction in the high frequency content of the probe signal. This will therefore result in greater correlation values to exist over longer delay times.

It has been observed in studies with isothermal air jets that the convective velocity of a turbulence pattern is greatest at the axis and decreases rapidly upon moving out towards the turbulence-atmosphere boundary[42]. It is reasonable to assume this effect also occurs in a turbulent flame. A decrease in velocity upon moving radially from the flame axis will therefore produce a lowering in the local Reynolds number and the smaller fluid elements will remain in the vicinity of the probe for a greater period of time, thereby lowering the high frequency portion of the signal. This effect will clearly become more pronounced at greater distances from the flame axis, thus increased turbulent time scales result. At the outer flame regions where turbulent intermittency is present and the local gas Reynolds numbers are low, it is probable that the fluctuating probe signal is due primarily to the motion of the large air entraining eddies, the smallest eddies having been destroyed

by viscous forces.

By similar reasoning the observed increase in turbulence time scales with greater axial distance from the burner may be explained. The convective velocity decreases gradually with increased downstream distance from the burner such that as discussed above, this will tend to remove high frequency components from the probe signal. Furthermore, it has been seen that the size of the large "permanent" eddies is controlled by the dimensions of the flame. Their size will therefore increase with increased flame height due to the spreading action of the flame. These two effects will therefore result in increasing the low frequency portion of the probe signal thus producing the greater turbulent time scales observed with increased axial distance.

At the highest axial position studied, namely 54d, the turbulent scales for each additive, irrespective of concentration, tended to converge upon the indium time scale at this position. This is a likely result for caesium addition since the caesium ion concentration levels, will at this height have the required time to attain the thermodynamic equilibrium level. Once in this state no chemical effect may be observed and caesium in concentration field will behave as the chemically inert indium field decaying by turbulent mixing only. In the case of acetylene or lead addition this result was not expected and is considered not to be a true effect since no equilibrium condition exists for either charged species, their concentration levels decaying to zero. Therefore at the flame height 54d it would be anticipated that the ion concentration level would be too low for detection by an electrostatic probe, i.e. $<10^8$ ionscm^3. An explanation for this discrepancy is for trace impurity to be present in the entrained atmosphere becoming

evident at the downstream flame regions and accounting for the persistent ionisation level. It is considered the impurity did not influence the upstream flame regions since the turbulent time scales were repeatedly observed to have values suggesting decay of the ion field to be controlled by chemistry rather than by turbulent mixing.

9.3 Power Spectral Density Studies

As in the case for the preliminary investigations, the power spectra for each flame additive were within the limits of experimental error, identical irrespective of the test position in the flame. The conclusions drawn in the previous chapter can only account for this in that the variations in turbulent time scales is not sufficiently large to produce a measurable difference between the spectra.

9.4 Probability Density and Cumulative Distribution Studies

The recorded waveforms have been analysed further for both probability density and cumulative distribution functions. It may be recalled that these functions provide information in the amplitude domain. The purpose for the determination of these functions was to observe if the effects of rapid ion chemical kinetics upon the structure of the ion concentration field were evident in the probability profiles. Due to the time factor only those flames seeded with acetylene and indium respectively have been analysed.

The probability density functions obtained for acetylene and indium addition for the transverse scan across the flame are shown in Fig. 9.1. The close similarity between the profiles

Fig. 9.1 Probability Density Profiles for (a) Acetylene and (b) Indium (0.1M) seeded flames at the given radial positions 42d above the Burner.

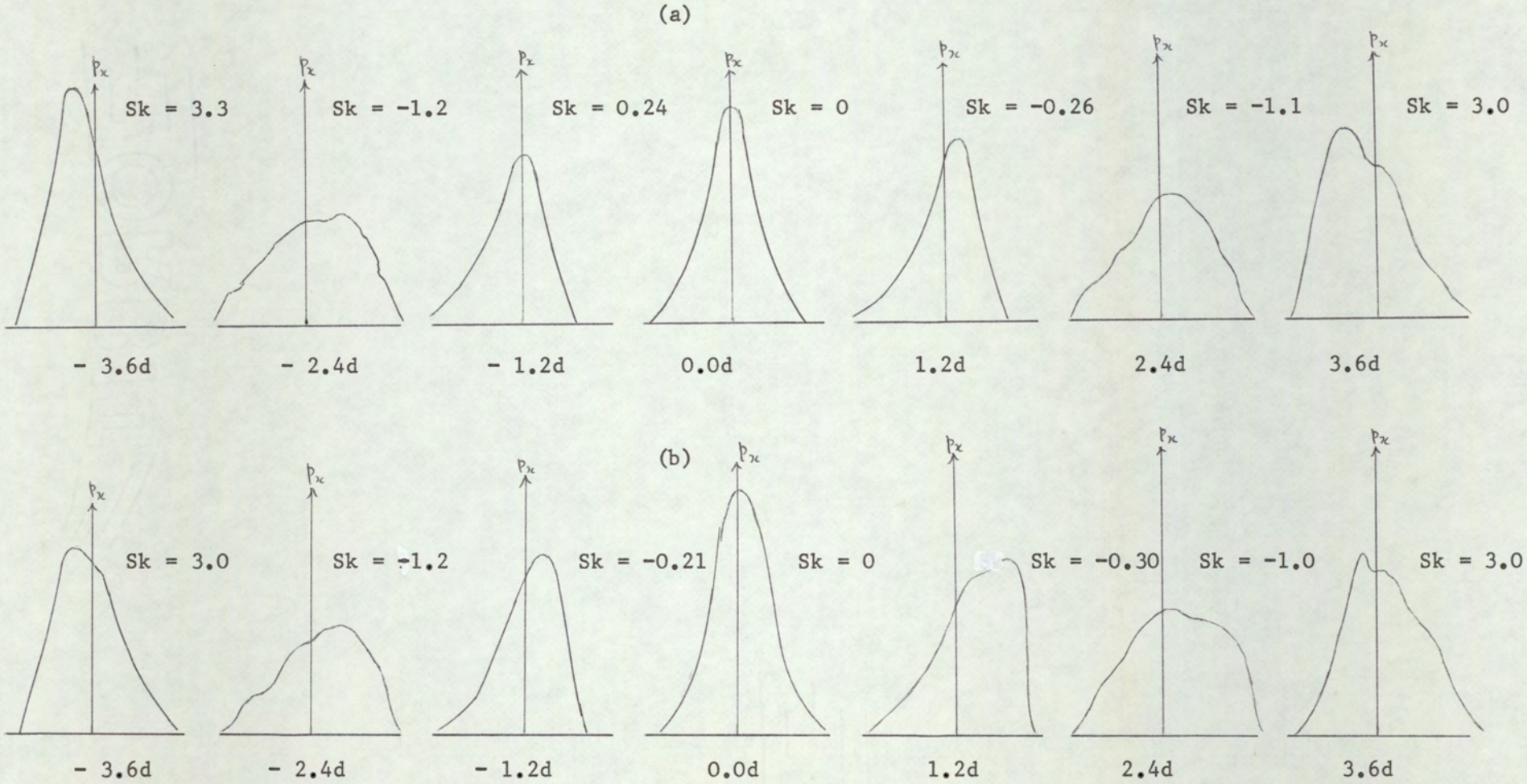

for both seeds may be clearly observed indicative of the absence of a chemical influence. An interesting trend may however be discerned from the shapes of the profiles moving across the flame. It is shown that they have a clear resemblance at the test positions equidistant from the flame axis. Skewness factors are given with each profile which, it may be recalled, provides a measure of the deviation of the random waveforms from the normal or Gaussian probability density function. Normal functions have a skewness factor of zero.

The outermost regions of the flame studied, namely, 3.6d yielded profiles having a positive skewness of 3.3. This is believed to be the result of the little studied phenomenon of turbulent intermittency. The presence of intermittency is illustrated in the oscillogram traces shown in Fig. 9.2 where traces at the axial position 42d and 54d and for comparison those for the positions 3.6d from the axis at the above flame heights are given. The sporadic "spikey" appearance of the waveform due to intermittency where regions of entrained air and combusted gas are convected past the probe. The probe samples the ion concentration in the burnt gas pockets producing the sharp pulses. The air, being void of all ionisation produces the zero signal portions in the trace.

It is of importance to note that unlike velocity fluctuations scalar fluctuations, such as those in ion concentration studied here, the mean level can never tend to zero since this would require the existence of negative concentrations. The positive skewness observed at 3.6d from the flame axis at the height 42d implies the large above mean level pulses must

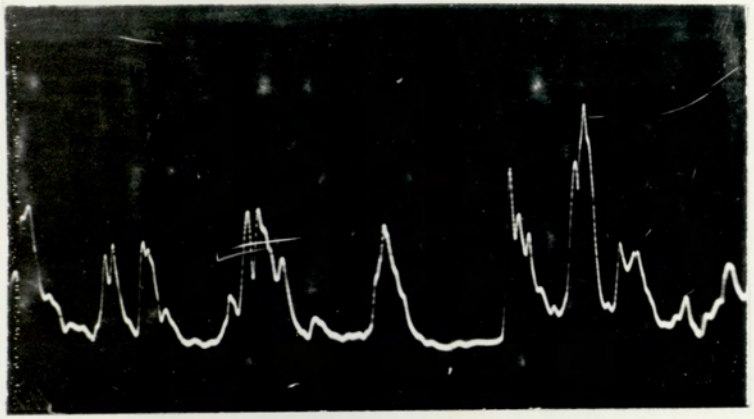

3.6;42

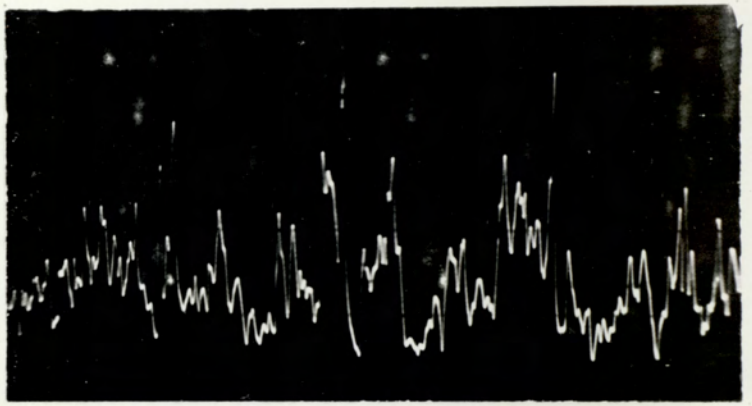

0;42

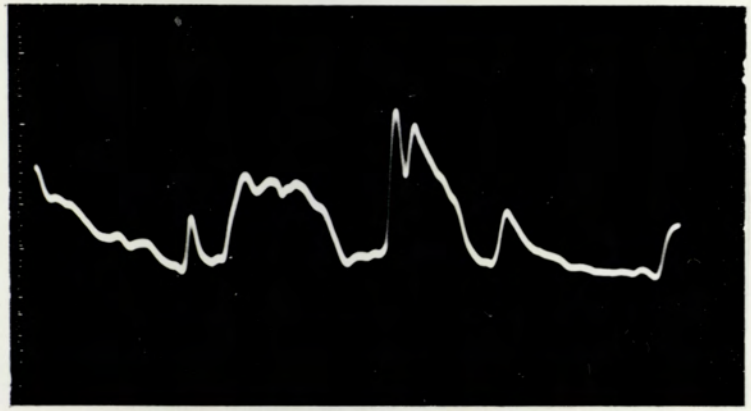

3.6;54

0;54

Fig. 9.2 Oscillograms for acetylene seeded flame illustrating turbulent intermittency at the off axis 3.6d position at flame heights 42d and 54d. Traces at the corresponding axial positions are shown for comparison.

exist for a shorter time than the small below mean level fluctuations since from the probability curve the chance of observing the waveform at some instant in time is greater below the mean level. The sharp spikes in turn are considered to be responsible for the tailing on the right hand side of the profile yielding a positive skewness.

Upon moving in the direction of the flame axis the test point at 2.4d produced a negatively skewed function i.e. Sk = -1.2. In addition the profile has a broad peak indicative of the waveform having a large dispersion about the mean level i.e. a large variance. This is considered to be due to the close proximity of the test point to the reaction zone. Since the flame additives are ionised primarily in the reaction zone higher ion density levels may be expected in this region producing large amplitude fluctuations. Further, since the reaction zone is also the region where lumps of fuel and air meet to enable combustion to occur the probe at the 2.4d radial position will likely be found, at various intervals, in an environment of air with the production of sharp zero signal level pulses. It is considered this effect is responsible for the negative tailing in the profile at this test position.

Since the 3.6d and 2.4d positions yield postively and negatively skewed curves respectively, it is reasonable to assume that the signal at some position located between these points will produce a broad symmetrical probability density profile about the mean. A likely position to produce a symmetrical curve is the centre of the reaction zone. Here the presence of the high ion density levels together with the entrained air pockets would be expected, by the basis of the above findings, to produce a fluctuating signal of even density about the mean.

The probability density function for the signal at 1.2d from the flame axis may also be observed to have a slight negative skewness i.e. Sk = -0.21. In this case however the peak is sharply defined such that the probability of observing the signal at any time instant is greatest at or in the immediate vicinity of the mean level. This indicates that the dispersion or variance of the waveform has decreased upon moving towards the flame axis. At the axis the profile is approximately symmetrical about the mean and again a sharply defined peak is present.

Symmetrical curves about the mean signal level were also observed at the other axial test positions studied, namely, at 46, 50 and 54d. The profiles obtained at the axial position for both the flame additives used are shown in Fig. 9.3. It may be observed that the peak maxima decrease with increased downstream distance from the burner orifice. In addition at the expense of the loss in peak height, the profiles gradually become broader with increased flame height. This is attributed to the reduction in the convective velocity of the fluid elements with increased flame height. This effect results in the pockets of fluid remaining in the vicinity of the probe for a greater length of time such that the fluctuating signal spends a greater portion of time away from the mean level than occurs at the upstream regions where the convective velocity is greater. This will therefore result in an increase in the variance of the waveform with increased flame height leading to a broadening of the probability density profiles and a reduction in peak height.

Fig 9.3 Variation in Probability Density Profiles with Distance from Burner Nozzle for the Addition of (a) Acetylene and (b) Indium (0.1M)

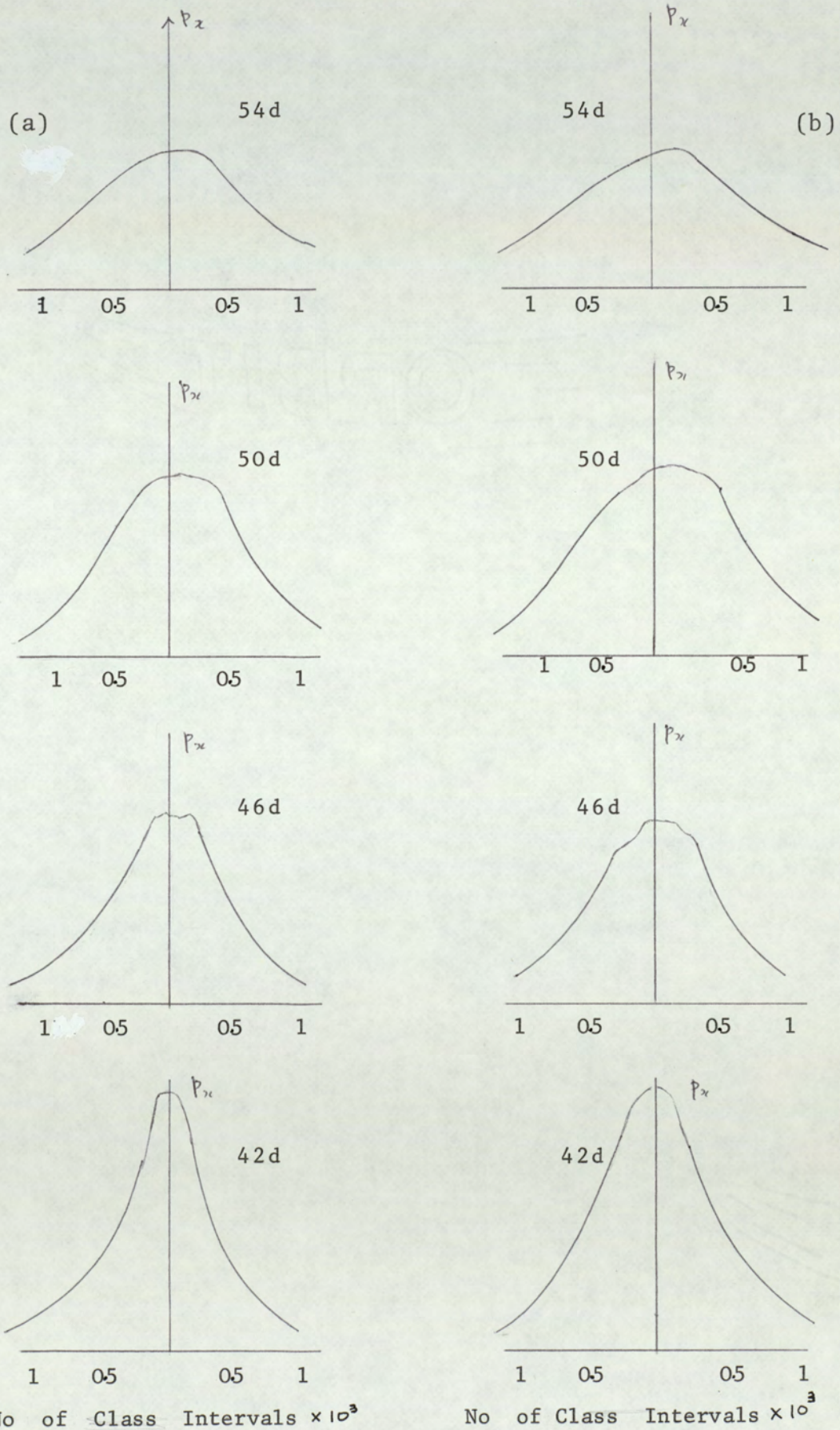

Information not present in the probability density function may sometimes become evident in the cumulative distribution plots. Both linear and logarithmic functions have been determined for the data obtained from the acetylene and indium (0.1M) seeded flames. The distribution values have been plotted on probability graph paper such that straight line graphs indicate either a normal or log-normal distribution.

The linear cumulative plots for acetylene and indium were observed to be similar at coincident test positions. Those corresponding to the radial test points 3.6d and 0.0d at the flame height 42d are shown in Fig. 9.4. The graphs show curved profiles for each additive at the outer flame region studied. This is considered to be due to the presence of turbulent intermittency. The axial positions presented linear plots apart from a slight curvature at the low probability regions. These results are considered to be related to the probability density profiles where, in the first case highly skewed curves were produced and at the axial position an almost Gaussian profile was obtained.

The logarithmic distribution functions determined for the above test positions are given in Fig.9.5. The intermittent signals at the radial 3.6d position are shown to be log-normal. The axial position produced an expected curved profile since, from the above, it was shown to be strongly linear.

The axial position at 54d from the burner provided similar cumulative plots to the 42d axial test point for both additives. This is again considered to be due to the approximate Gaussian probability density function obtained for this flame position.

Fig 9.4 Linear Cumulative Distribution Profiles for (a) Acetylene and (b) Indium (0.1M) Seeded Flame at 0.0d and 3.6d from the axis, 42d above Burner

(a)

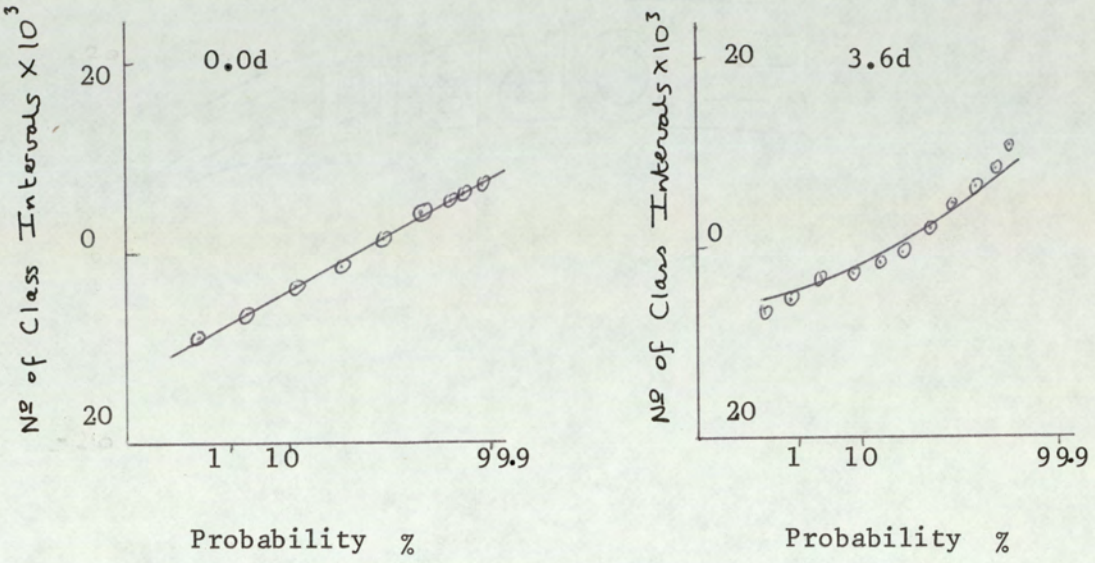

(b)

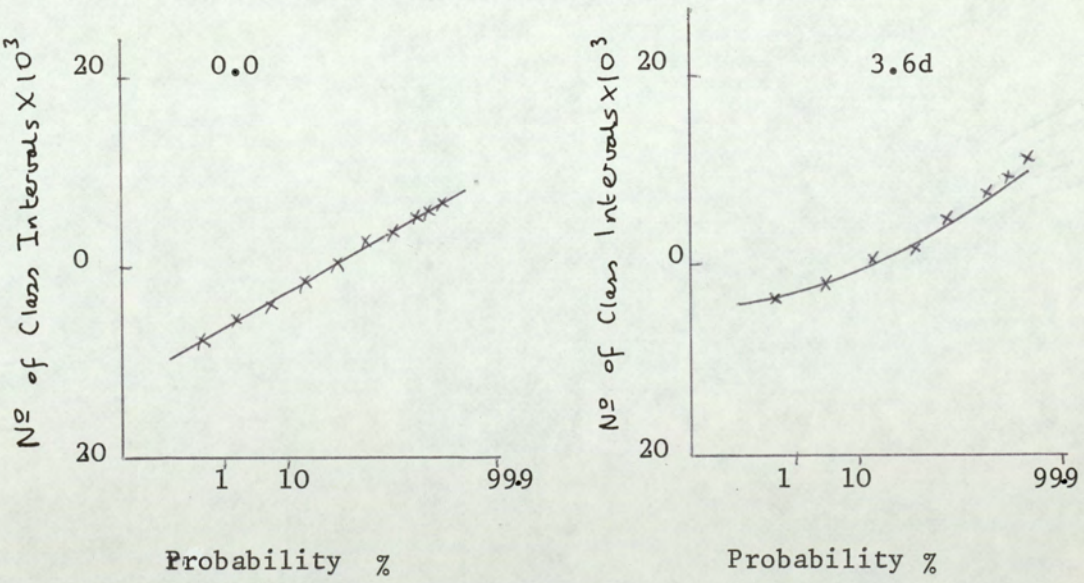

Fig 9.5 Logarithmic Cumulative Distribution Profiles for (a) Acetylene and (b) Indium (0.1M) Seeded Flame at 0.0d and 3.6d from the axis, 42d above the Burner.

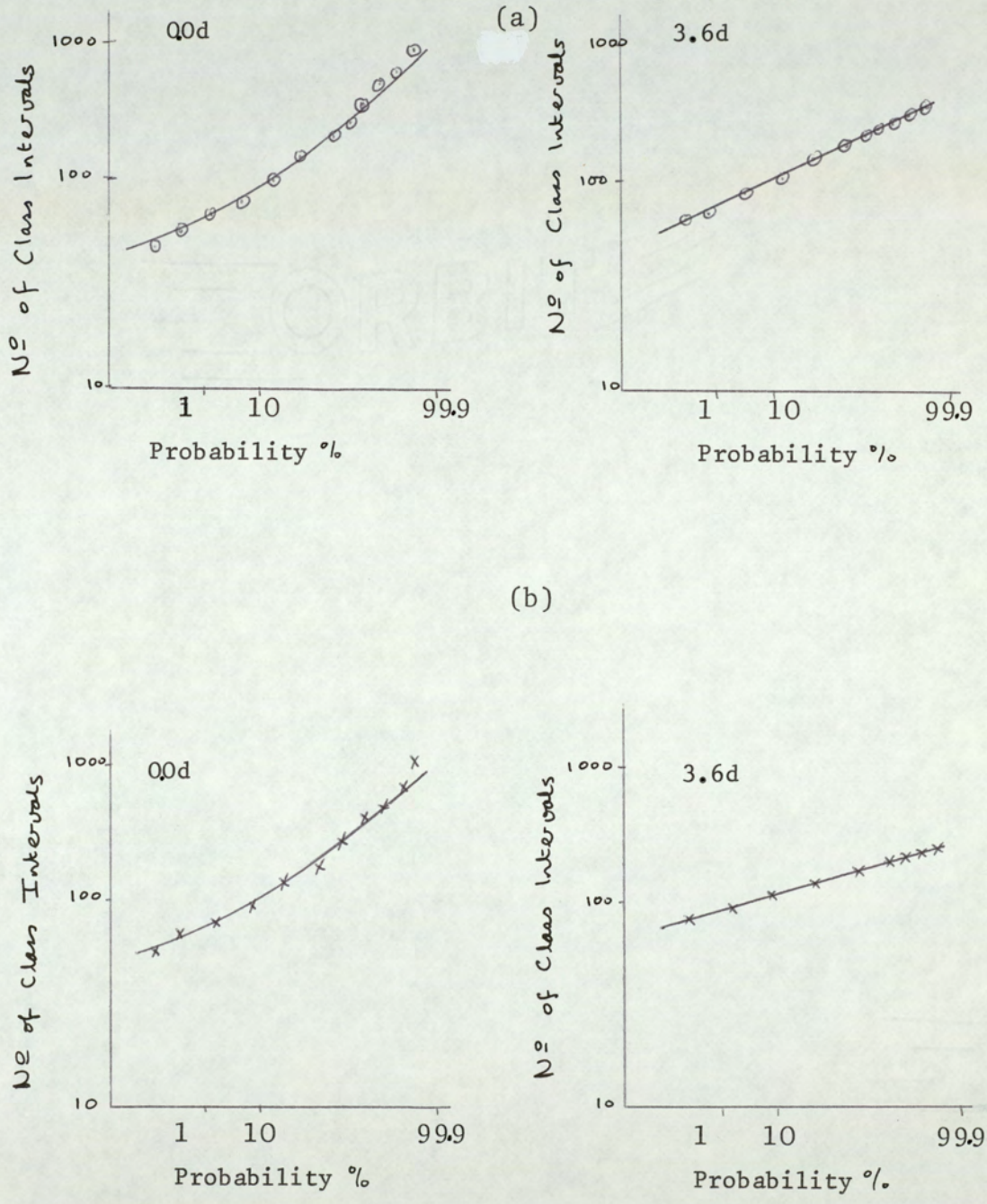

Conclusions drawn from the Flame Mapping Experiments

Of the statistical functions employed in the flame mapping experiments only the autocorrelation function has provided evidence for the chemistry-turbulence interaction phenomenon. The reduced turbulent time scales brought about by the influence of rapid ion chemical kinetics upon the ion density field, observed in the previous chapter has been repeated at each test position studied. The effects of varying the chemical reaction rate by altering the concentration of the flame additives has also been repeated following the tests described in Chapter 8. The transverse scan, normal to the mean gas flow direction at the flame height 42d has shown the turbulent time scales to be smallest at the flame axis, gradually increasing with greater distance from the axis. It has been observed further, that with increased axial distance from the burner an increase in the turbulent scales is produced.

These results indicated the internal physical structure of the turbulent diffusion flame to be similar to that of the isothermal jet as discussed previously in section 9.2.

The probability density and cumulative distribution functions have shown no evidence for the interaction phenomenon. A series of interesting probability density profiles have been obtained for the radial test positions studied. However, it may be concluded that amplitude analysis has shown to be of limited value in deriving information of the structure of ion density field in the turbulent diffusion flame.

CHAPTER 10

CROSS CORRELATION EXPERIMENTS

Further information concerning the local structure of the fluctuating ion concentration field has been obtained from cross correlation studies. This has involved the determination of spacial and space-time cross correlation functions. The former enables a statistical measure of the eddy dimensions to be evaluated, the latter provides a measure of the rate of deformation of a turbulence pattern and allows an estimate of the local convective velocity of such a pattern to be made. The cross correlation functions have been determined using the analog correlator.

10.1 Spacial Cross Correlation Measurements

The longitudinal and transverse cross correlation functions were measured using two electrostatic probes positioned either parallel to or normal to the mean gas flow respectively. The probe separation distance r was gradually increased at regular intervals and the fall in the correlation coefficient ρ_{AB} recorded. No time delay was applied to either signal, the measured function was therefore only dependent upon the distance r. The length required for the correlation coefficient ρ_{AB} to fall to 0.47 of the initial value, is considered to provide a statistical measure of the spacial dimensions of an average eddy, i.e. in longitudinal and radial directions.

Difficulties were encountered during the measurement of the longitudinal correlation function owing to the wake effect created by the upstream probe. This disturbance influenced the

downstream probe signal resulting in spurious correlation values.

Prior to the determination of the spacial cross correlation functions a series of experiments were conducted to observe the extent of the wake effect, and to try and reduce the disturbance to the flow to a minimum if shown to be serious.

10.2 Experiments to observe the Extent of the Wake Effect

A series of autocorrelation functions were determined using a flame seeded with indium with a fixed probe located, 46d from the burner on the flame axis and biased at 50V negative. The autocorrelograms were determined when a movable unbiased probe was swept beneath the fixed probe positioned 2.0d (d = 0.5 cms) upstream and scanning in steps of 0.4d for a distance of 2.0d beyond the vertical plane. With the probes in the vertical plane the wake from the upstream unbiased probe was shown to have the greatest influence upon the autocorrelogram causing the fall to occur more rapidly i.e. $\rho_{AA}(.47) = 0.31$ The effect decreased with increased lateral distance from the vertical plane such that at approximately 2.0d from the plane the autocorrelogram in the absence or presence of the upstream probe were identical with $\rho_{A.A}(.47) = 1.20$ indicating at this lateral position the wake effect as seen by the fixed probe to be negligible.

A similar set of results was obtained when the above procedure was repeated using a biased upstream probe at -10V. Again the maximum disturbance occurred with the probes in the vertical plane $\rho_{AA}(.47) = 0.18$ Determination of the longitudinal

cross correlation coefficient with the upstream probe 2.0d from the vertical plane produced extremely low values i.e. $\rho_{AB}(.47)=0.28$ (Having obtained greater ρ_{AB} values for the spacial transverse cross correlation with probes 2.0d apart the wake influence under these conditions was unacceptable).

The length of the upstream probe wire was increased from 0.3 cms to 1.0 cms. This enabled the probe body to be withdrawn 0.7 cms from the flame with the probe wire effectively remaining in the same position. The above procedure was repeated biasing the upstream probe 10V negative. A marked improvement on the former result was obtained with the wake effect ceasing to influence the autocorrelation function for the upstream probe positioned 0.5 cm from the vertical. The spacial cross correlation coefficient produced a maximum value with the upstream probe at the 0.5 cm lateral position the value was however again low, i.e. $\rho_{AB}(.47)=0.20$.

A possible explanation for this was considered to be the increased noise, that is the uncorrelated portion of the upstream probe signal due to the greater length of probe wire used. The reduction in the upstream probe wire length to 0.5cm produced a similar result to the above.

Following the unsatisfactory results described above, the series of experiments were repeated at the off axis positions of 1d and 2d. At the former position again rather unsatisfactory low cross correlation coefficient values were recorded, probably due either to the wake effect or the lateral position of the movable probe being too great from the vertical.

At the 2d position the autocorrelation experiments indicated a marked improvement with the upstream probe wire length of 0.3cm and position 0.3 cm from the vertical plane, the wake

effect was negligible. The cross correlograms indicated a minor improvement. Greater coefficient values were obtained increasing the upstream probe wire length to 0.5 cm enabling the probe body to be withdrawn by 0.2cm. The coefficient values improved further when the upstream probe was displaced 0.6d out of the vertical plane in the direction of the flame atmosphere boundary. Appreciably smaller readings were attained with displacement towards the flame axis.

The reason for the large difference in correlation coefficient readings with the probe on either side of the vertical plane was considered to be due to the wake, produced by the upstream probe, following a curved trajectory towards the outer regions of the flame. This would result in a minimal disturbance "seen" at the downstream probe. It was observed for closer distances of approach between the probes i.e. $\leq$1.0cm the wake effect became more apparent.

The postulate concerning the wake following a curved path was later confirmed during work carried out by the author at the Thornton Research Centre. The technique used was a helium diffusion method and will be discussed in greater detail in Chapter 14. The experimental procedure involved introducing helium gas into an isothermal air jet via a fine bore tube to simulate the wake. Analysis of the jet gas for helium at 2.0d downstream of the source and in a direction normal to the mean gas flow by mass spectrometer enabled a helium distribution curve to be plotted. Two positions in the jet were examined, (i) the source on the jet axis and (ii) the source at a position 2d from the axis, both at 46d from the burner orifice. The on-axis helium distribution was Gaussian indicating an even probability for observing a helium

Fig 10.1 Helium distribution profiles in an isothermal air jet (a) on the jet axis and (b) 2d off the axis at 46d above the nozzle.

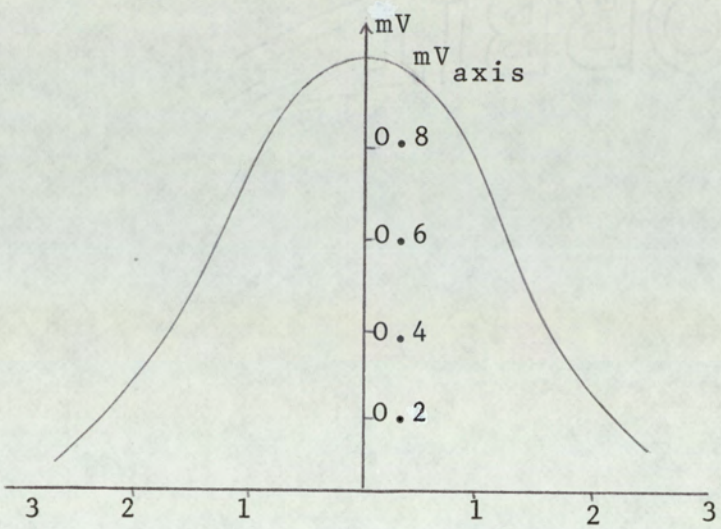

Radial distance from jet axis
(nozzle diameters)

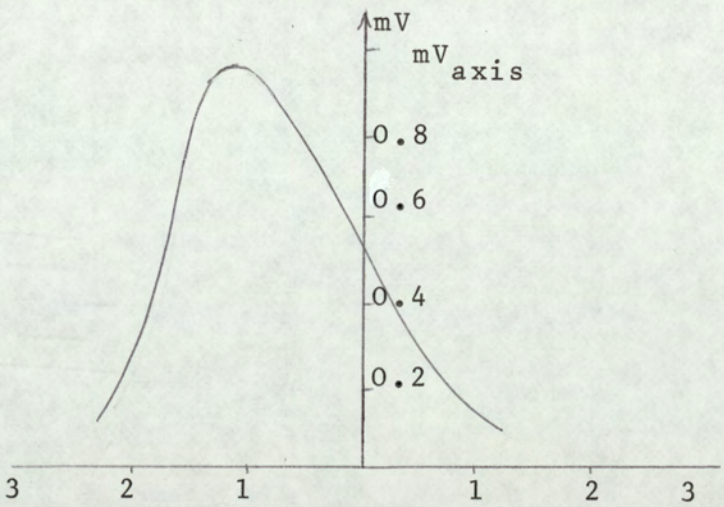

Radial distance from 2d off
axis position
(nozzle diameters)

concentration on either side of the jet axis. For the 2d position a positively skewed distribution was obtained showing the helium wake to have followed a curved path, so producing high concentration levels at the turbulence atmosphere boundary. The profiles are shown in Fig.10.1.

Following these observations both the spacial and space-time cross correlation studies have been performed at the 2d off axis position where the disturbance of the upstream probe wake is considered minimal.

10.3 Experimental Procedure

The spacial cross correlation functions have been determined with the fixed electrostatic probe positioned 2d from the flame axis at the following flame heights, 42, 46, 50 and 54d. During the measurement of the longitudinal cross correlograms the movable probe was maintained upstream of the fixed probe and displaced 0.6d out of the vertical plane towards the flame atmosphere boundary. The radial cross correlation function was determined by varying the position of the movable probe in the direction of the flame axis. For the measurement of both functions the probe separation distance was varied in steps of 0.5d. The fixed probe wire length was set at 3.0×10^{-4}M and biased at 50V negative. The movable probe wire length was 5.0×10^{-4}M biased at 10V negative based upon the findings discussed in the previous section. The flame was seeded with acetylene and indium (0.1Molar) respectively.

10.4 Results and Discussion

The longitudinal and radial spacial correlation functions obtained at the flame heights given above are shown in Fig. 10.2 to Fig. 10.5 and in Fig. 10.6 to Fig. 10.9 for flames seeded with acetylene and indium respectively.

The turbulant length scales for both functions and for the two flame additives are given in Table 10.1. It may be clearly observed that the longitudinal and radial length scales are appreciably smaller for acetylene addition compared to those for indium addition. This result again shows the effects of chemistry upon turbulence where the high ion recombination reaction rate has produced a reduction in the size of the turbulent length scales.

It may be observed in Table 10.1 that the longitudinal and radial turbulent length scales, for both additives, gradually increase in size with increased flame height. This result is clearly analogous to the findings of the flame mapping autocorrelation studies discussed in the previous chapter. The close similarity between the two sets of results was expected since both are due to the same physical processes occurring in the flame. It may be recalled that the size of the large "permanent" eddies is governed by the dimensions of the flame. Further, the size of the smallest dissipating eddies is controlled by the mean flow velocity and the kinematic viscosity of the fluid. If the kinematic viscosity is assumed to remain constant throughout the flame then a decrease in the mean velocity will result in an increase in their size. It will be demonstrated in a later chapter that the mean gas velocity decreases with increased flame height. Therefore upon

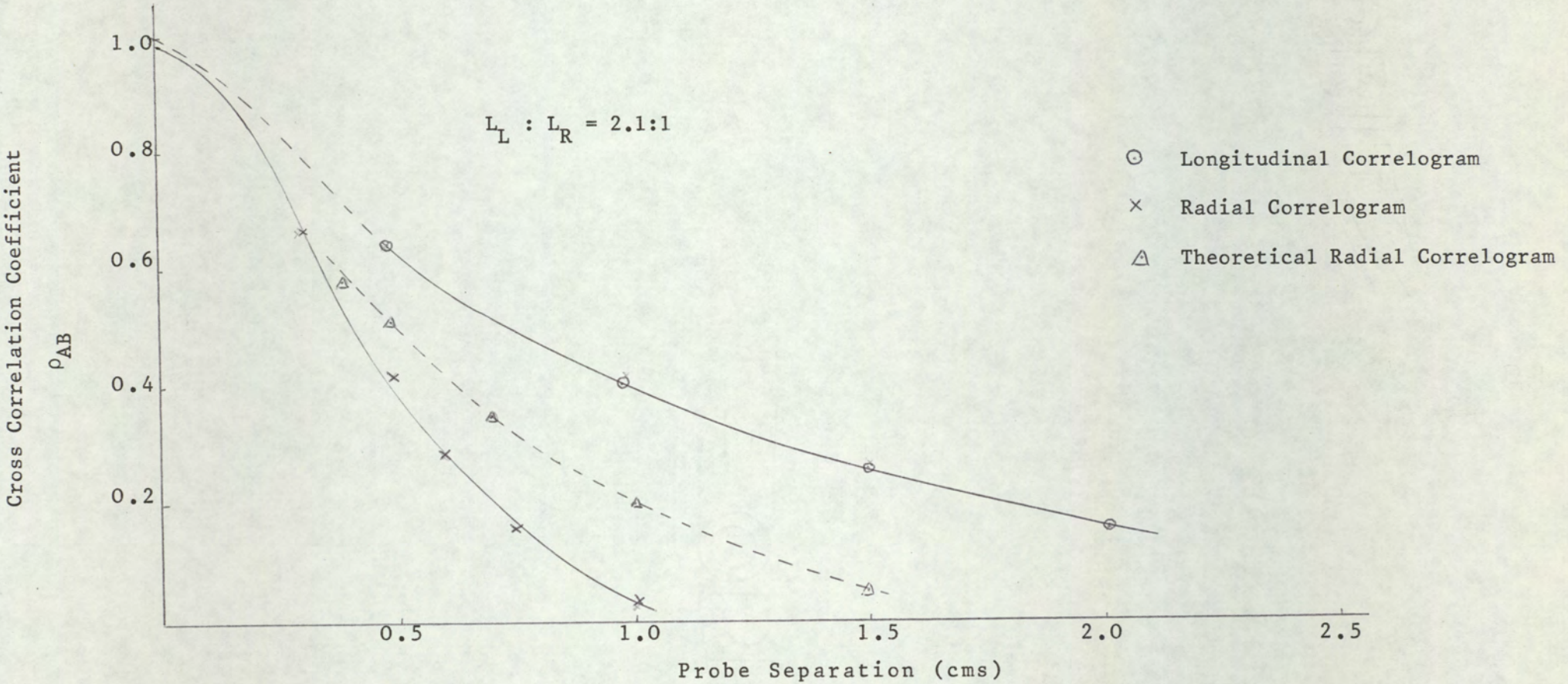

Fig. 10.2 Longitudinal and Radial Spacial Correlograms for Acetylene Seeded Flame at Fixed Probe Position 42d above Burner

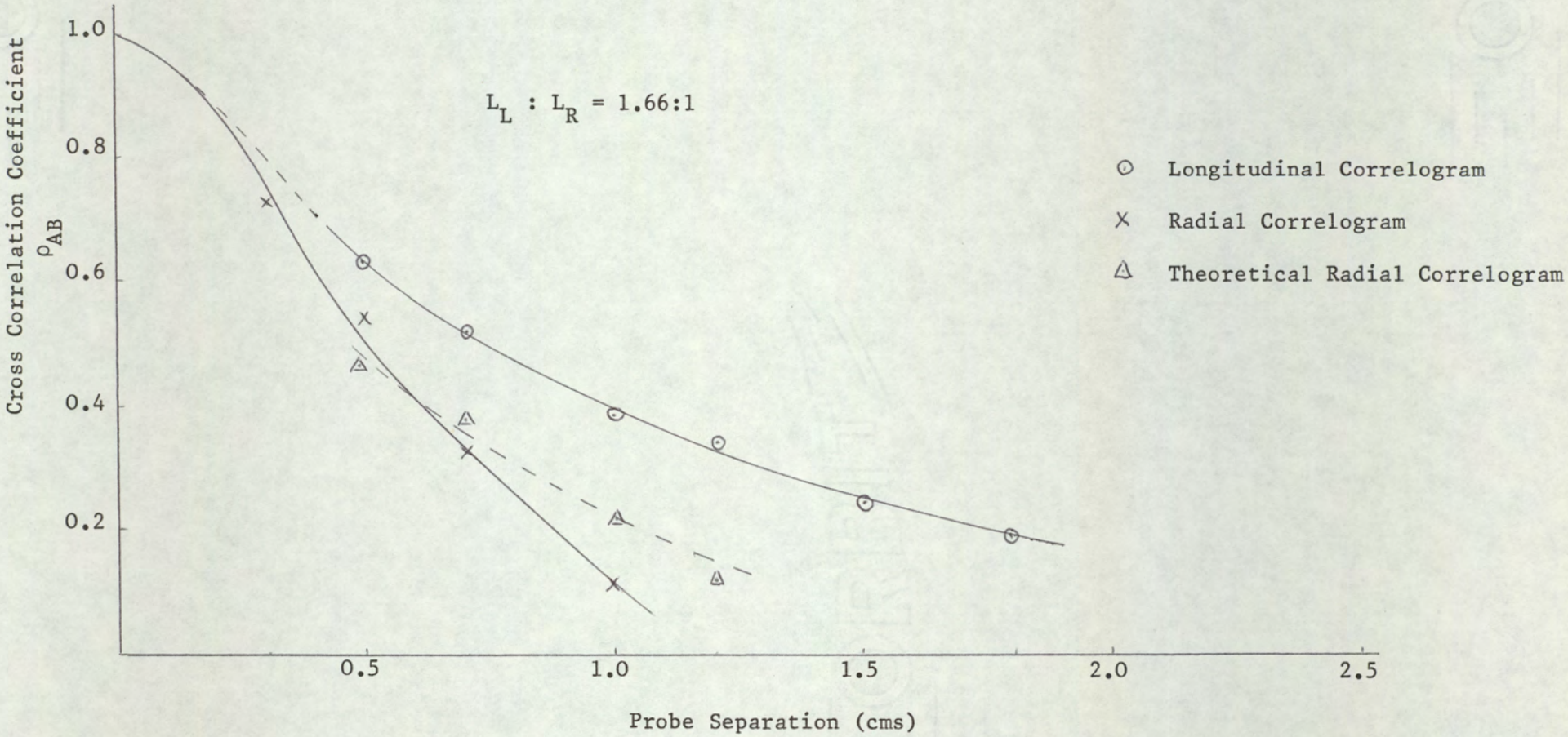

Fig. 10.3 Longitudinal and Radial Spacial Correlograms forAcetylene Seeded Flame at Fixed Probe Position 46d above burner

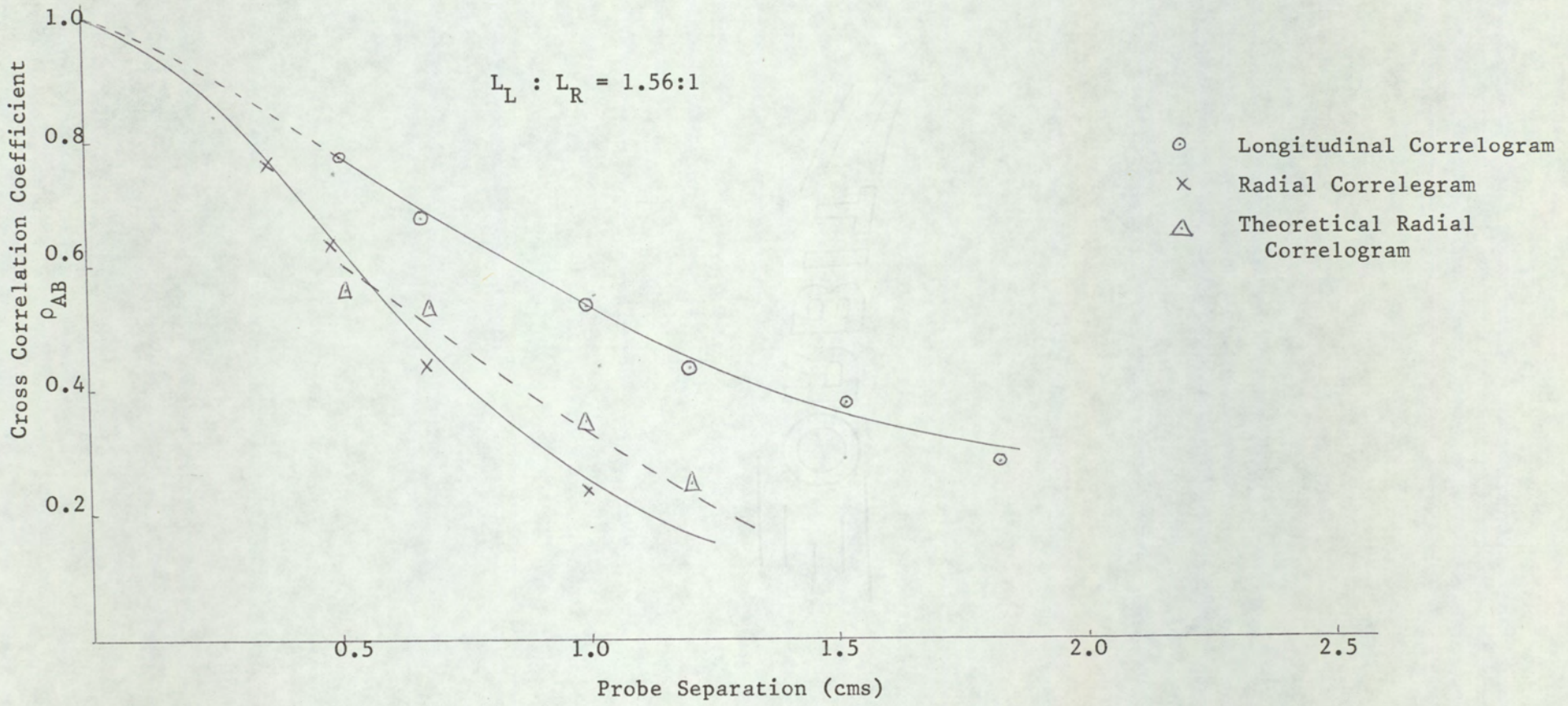

10.4 Longitudinal and Radial Spacial Correlograms for Acetylene Seeded Flame at Fixed Probe Position .50d above Burner

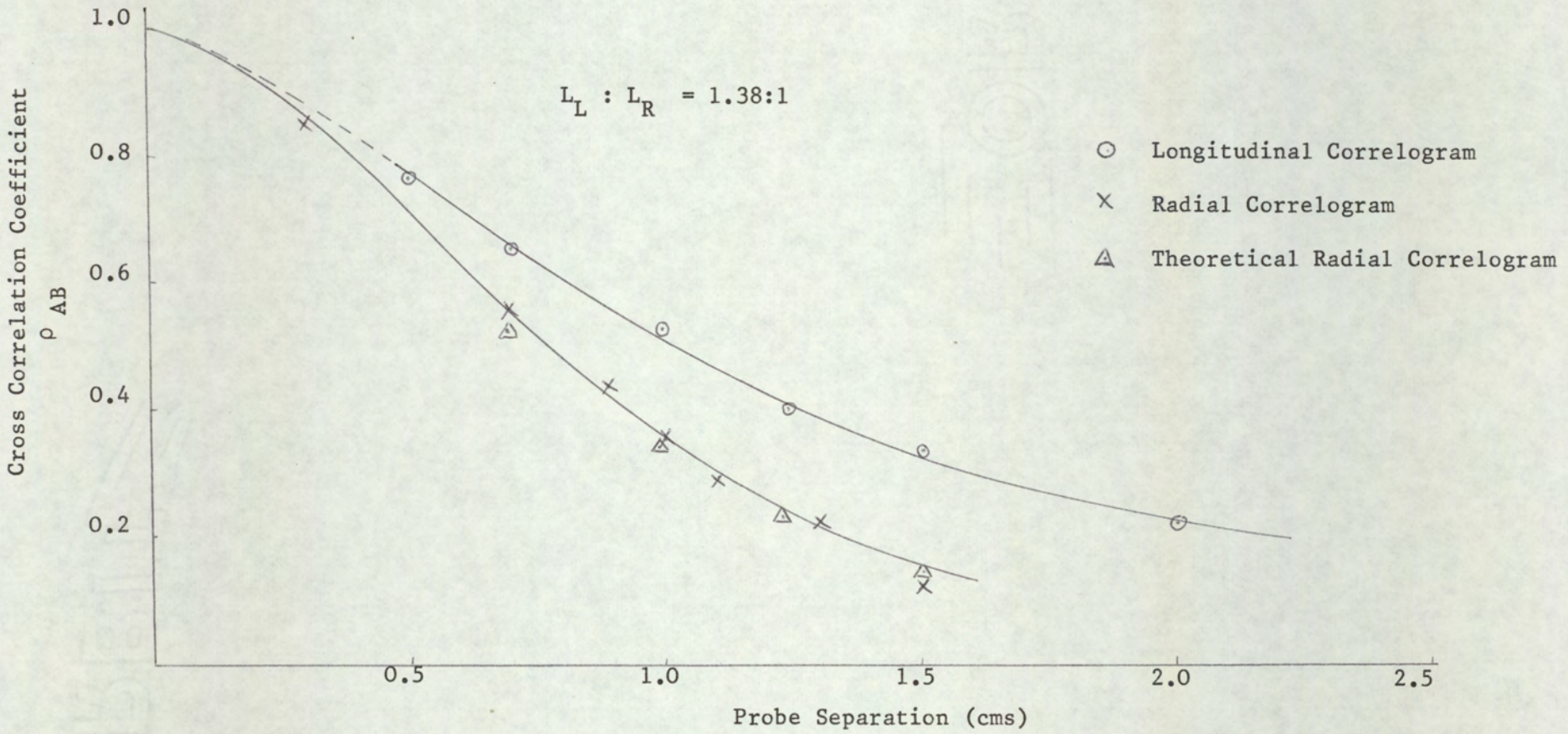

Fig. 10.5 Longitudinal and Radial Spacial Correlograms for Acetylene Seeded Flame at Fixed Probe Position 54d above Burner

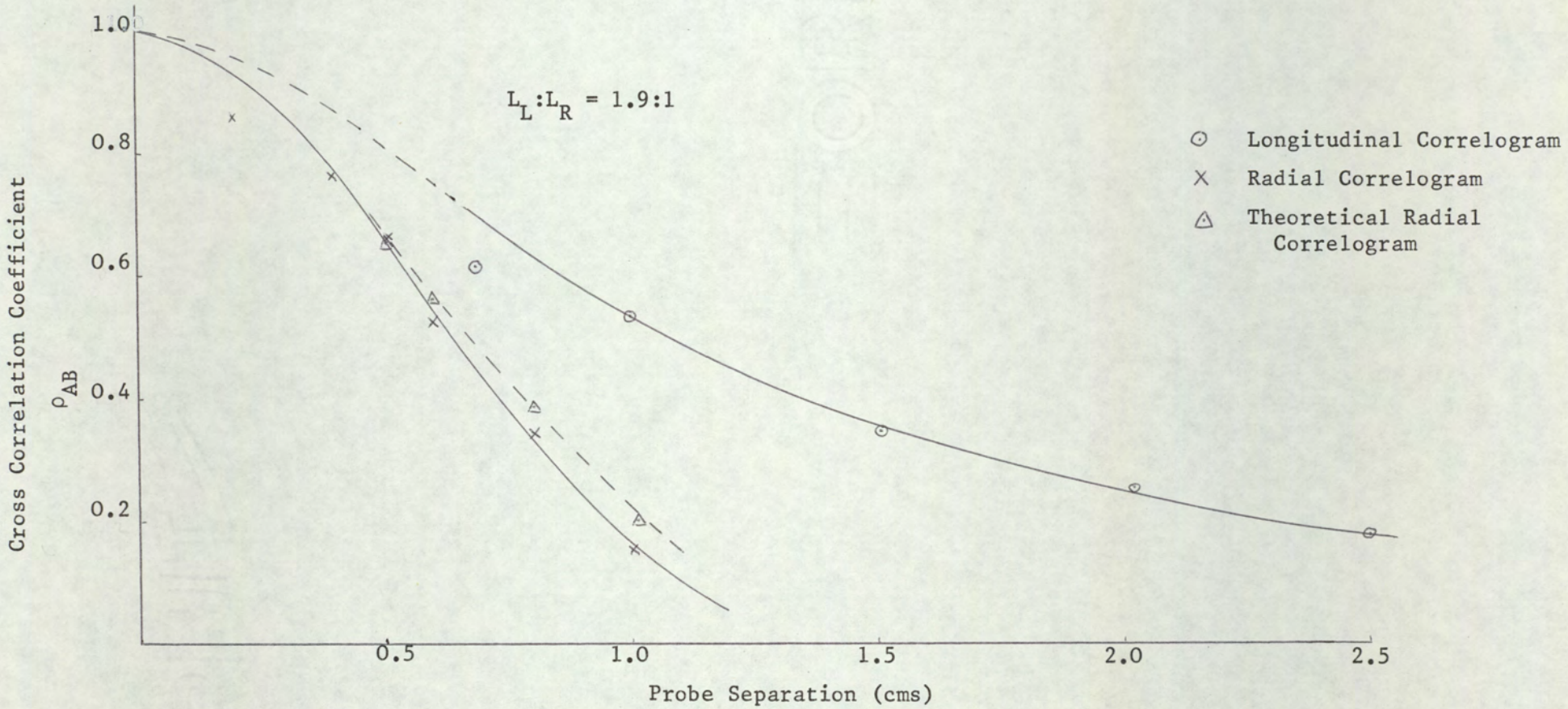

Fig. 10.6 Longitudinal and Radial Spacial Correlograms for Indium (0.1M) Seeded Flame at Fixed Position 42d Above Burner

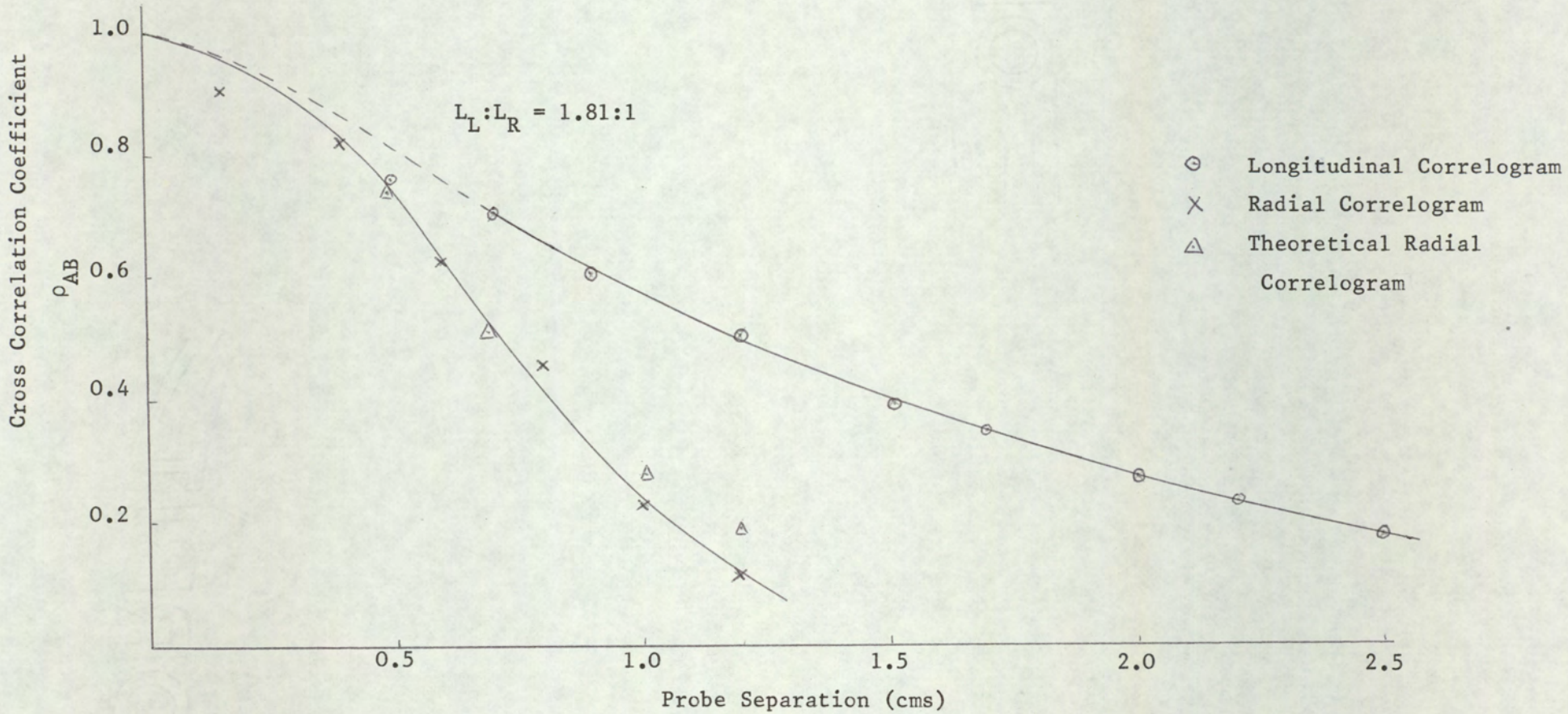

Fig. 10.7 Longitudinal and Radial Spacial Correlograms for Indium (0.1M) Seeded Flame at Fixed Probe Position 46d Above Burner

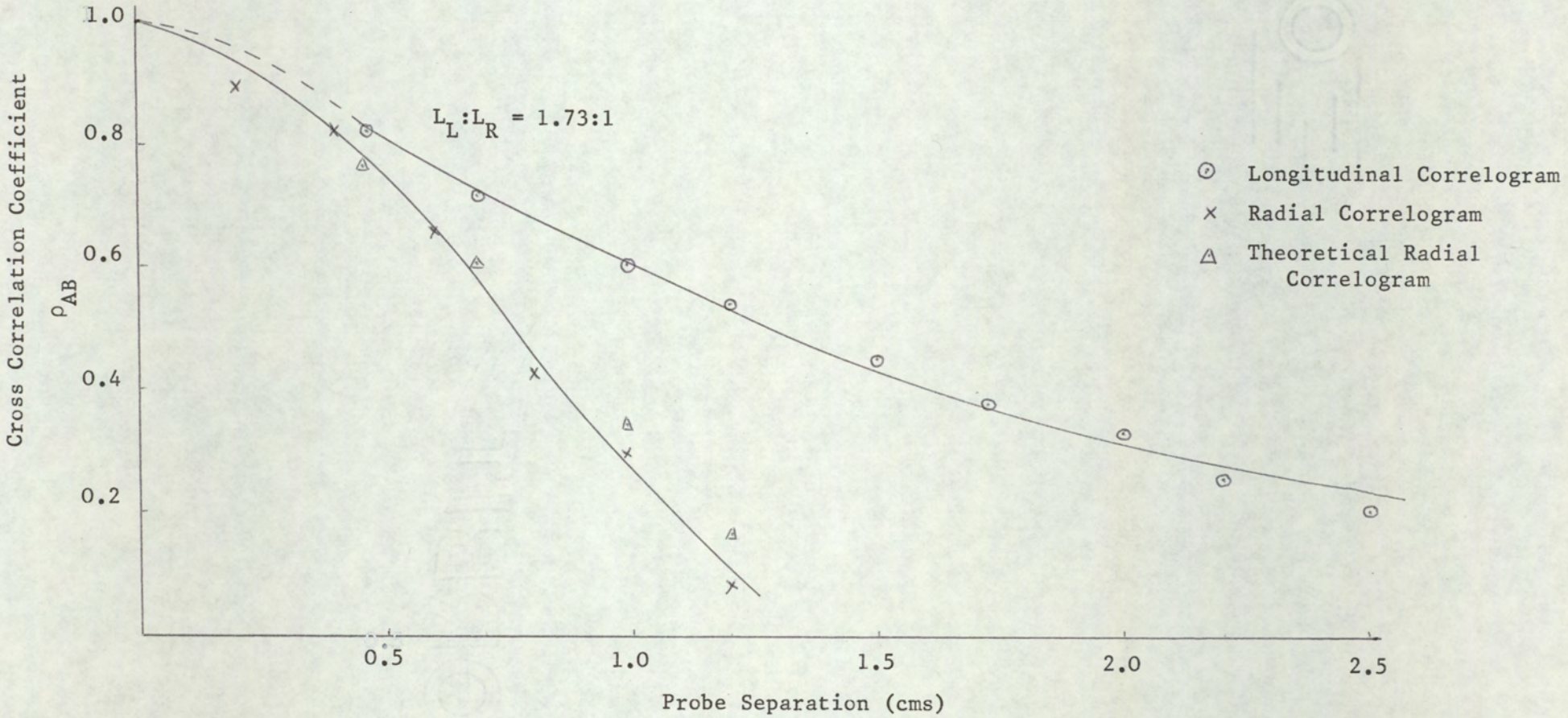

Fig. 10.8 Longitudinal and Radial Spacial Correlograms for Indium (0.1M) Seeded Flame at Fixed Probe Position 50d Above Burner

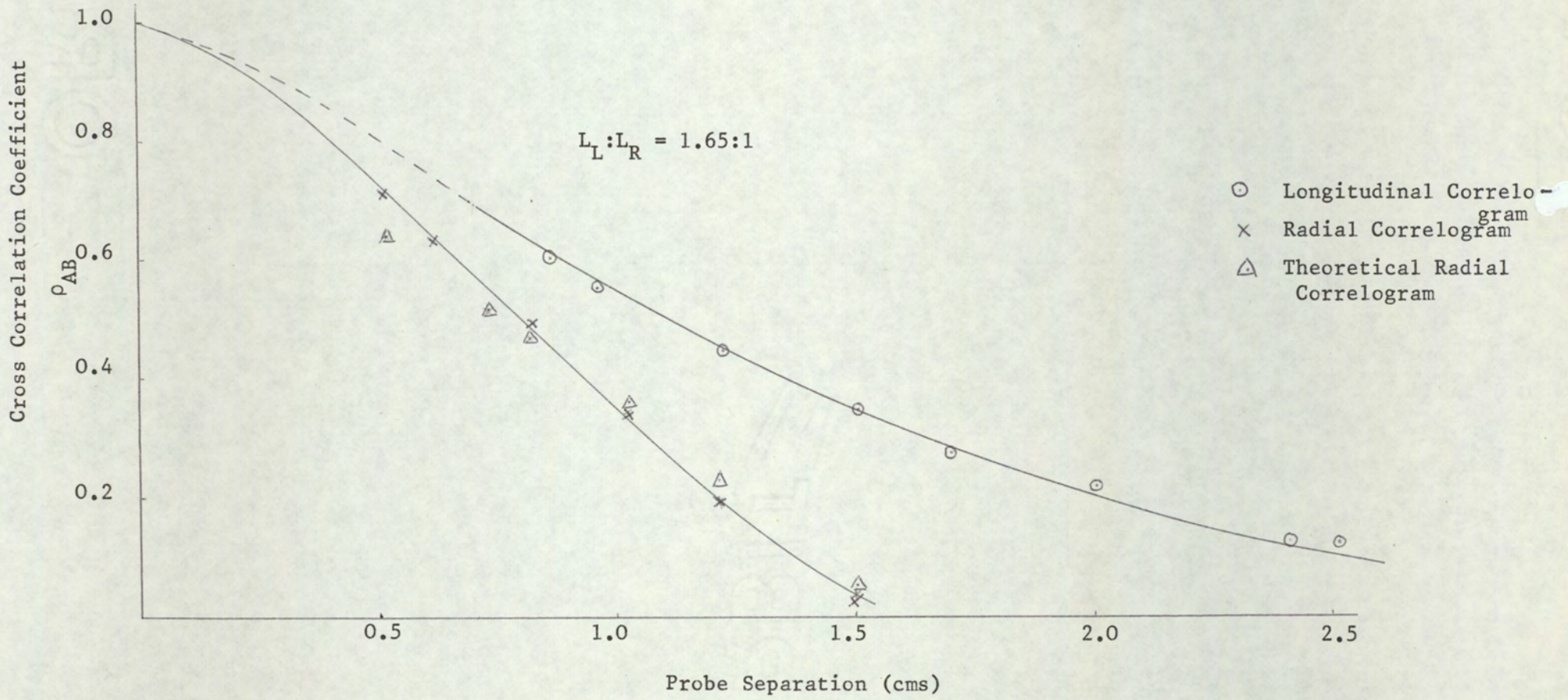

Fig. 10.9 Longitudinal and Radial Spacial Correlograms for Indium (0.1M) Seeded Flame at Fixed Probe Position 54d Above Burner

Fig. 10.1 Longitudinal and Radial Turbulent Length Scales for Acetylene and Indium Seeded Flames.

Fixed Probe Height Above Burner (nozzle diameters)	Turbulent Length Scales (cm)					
	Acetylene (1% total gas)			Indium (0.1M)		
	L_L	L_R	$L_L : L_R$	L_L	L_R	$L_L : L_R$
42	1.10	0.53	2.1 : 1	1.45	0.76	1.9 : 1
46	1.07	0.66	1.7 : 1	1.54	0.84	1.8 : 1
50	1.30	0.83	1.6 : 1	1.75	0.88	2.0 : 1
54	1.35	0.98	1.4 : 1	1.64	0.99	1.7 : 1

L_L Longitudinal Turbulent Scale

L_R Radial Turbulent Scale

moving downstream in the flame the large eddies will grow in size due to the increased dimensions of the flame and the reduction in mean velocity will result in an increase in the dissipating eddy size. Since those eddies passing both probes, at the same instant in time will produce correlated fluctuations, upon moving the probes downstream in the flame the increased eddy dimensions will result in the presence of fluctuations, common to both probes, over greater distances of separation producing the observed increased correlation levels for both longitudinal and radial probe positions.

The values obtained for the turbulent length scales may be considered to provide the dimensions of an "average" eddy in the axial and radial directions. The ratio of the longitudinal to radial length scales have been given on each spacial correlogram. The ratios for the acetylene seeded flame may be observed to vary from 2.1:1 to 1.35:1 while those obtained with the indium seeded flame range from 1:9:1 to 1.69:1 at the respective positions of 42d and 54d from the burner nozzle. The larger longitudinal values compared to the radial measurements at the upstream regions of the flame suggest the eddies may be considered to have an ellipsoidal shape. As the ratios decrease upon moving downstream in the flame the eddy shape must gradually change to one approaching a spherical profile.

This behaviour may be explained by considering the action of the turbulent shear stresses. The mean flow velocity in the flame is in the axial direction. The mean velocity gradients and thus the turbulent shear stresses must therefore occur across the flame in a radial direction. The shear stresses, it may be recalled, are responsible for the distortion of the fluid

elements such that in the upstream regions of the flame their presence will tend to stretch the fluid "lumps" in the axial direction. This, together with the absence of shear stresses in the mean flow direction, accounts for the observed greater longitudinal length scales compared to those in the radial direction.

As the mean velocity decreases with increased flame height the magnitude of the velocity gradients will become reduced producing weaker shear stresses. This will therefore lead to decreased distortion of the eddy structure during travel downstream in the flame thereby causing a reduction in the ratio of longitudinal to radial length scales.

The application of the von Karman-Howarth equation 3.3 has enabled the theoretical determination of the radial cross correlograms from the experimental longitudinal curves. The theoretical curves have been included on each of the spacial correlograms presented in Fig. 10.2 to Fig. 10.9. Comparison between the calculated and measured radial profiles is considered to provide a test of the isotropy of the fluctuating ion concentration fields. In the case of indium the profiles show good agreement whereas an appreciable variation between the radial profiles for acetylene may be observed. This is again considered to be evidence for the effects of chemistry upon the turbulent structure of the ion field where a rapid charged species reaction has tended to enhance the anisotropic nature of the fluctuating reactant concentration field.

Comparison of the turbulent length scales for acetylene and indium at 54d in Table 10.1 indicate similar values. This is

again considered to be due to the introduction of trace amounts of ionisable im purity into the flame from the laboratory atmosphere.

From the above results and those obtained earlier during the preliminary autocorrelation studies it is again possible to make reasonable predictions regarding the addition of varying concentrations of caesium and lead in the flame. Dilute solutions of caesium may be expected to yield turbulent length scales comparable to those of indium. Upon increased concentration the length scales will decrease, tending towards those obtained with acetylene for a high concentration of 0.3M. Addition of lead, the opposite effect would be expected where a 0.01M solution would probably yield scale values comparable to those for acetylene addition with increased concentrations producing greater length scales approaching the limiting indium scale values at approximately a 0.3M concentration.

10.5 Space-time Cross Correlation Measurements.

The space time cross correlation functions have been determined employing two electrostatic probes at the same operating conditions as where used for the measurements of the longitudinal spacial functions. With the fixed probe located 2d from the flame axis and the movable probe positioned 0.6d out of the vertical to minimise the wake effect, the biasing voltage was again maintained at -50V and -10V respectively. Space time correlograms have been determined again using the flame additives, acetylene and indium (0.1M) at the flame heights 46d and54d. These values represent the vertical

distance between the fixed probe and the burner nozzle. The movable probe was maintained in the upstream position, the time delay was therefore applied to this probe signal.

10.6 Results and Discussion

The space-time correlograms obtained for the two additives at 46d and 54d are shown in Fig. 10.10 to Fig. 10.13. The separation distance between the probes is indicated on each correlogram. It may be clearly observed that the amplitude maxima for each profile decreases with greater probe separation. This is attributed to the distortion of the eddy pattern due to the presence of shear stresses. The distortion increases with increased distance of travel such that the lowering in correlation becomes more pronounced with greater probe separation. The correlograms therefore show themselves to be functions of both probe separation distance (space) and time. Comparison of the space-time cross correlograms for acetylene and indium addition at the same flame positions and probe separation distances clearly indicate the peak values for the acetylene profiles to be appreciably smaller. This observation is again considered to be evidence for the effects of chemistry upon the turbulent structure of the fluctuating ion concentration field.

The turbulence pattern of the chemically active H_3O^+ species will undergo greater change during transit between the probes compared to the chemically inert In^+ species due to rapid ion chemical kinetics. Chemistry will therefore lower the similarity between the signals collected at the upstream probe and those collected at the downstream probe, thereby causing a reduction in the correlation peak values. In the

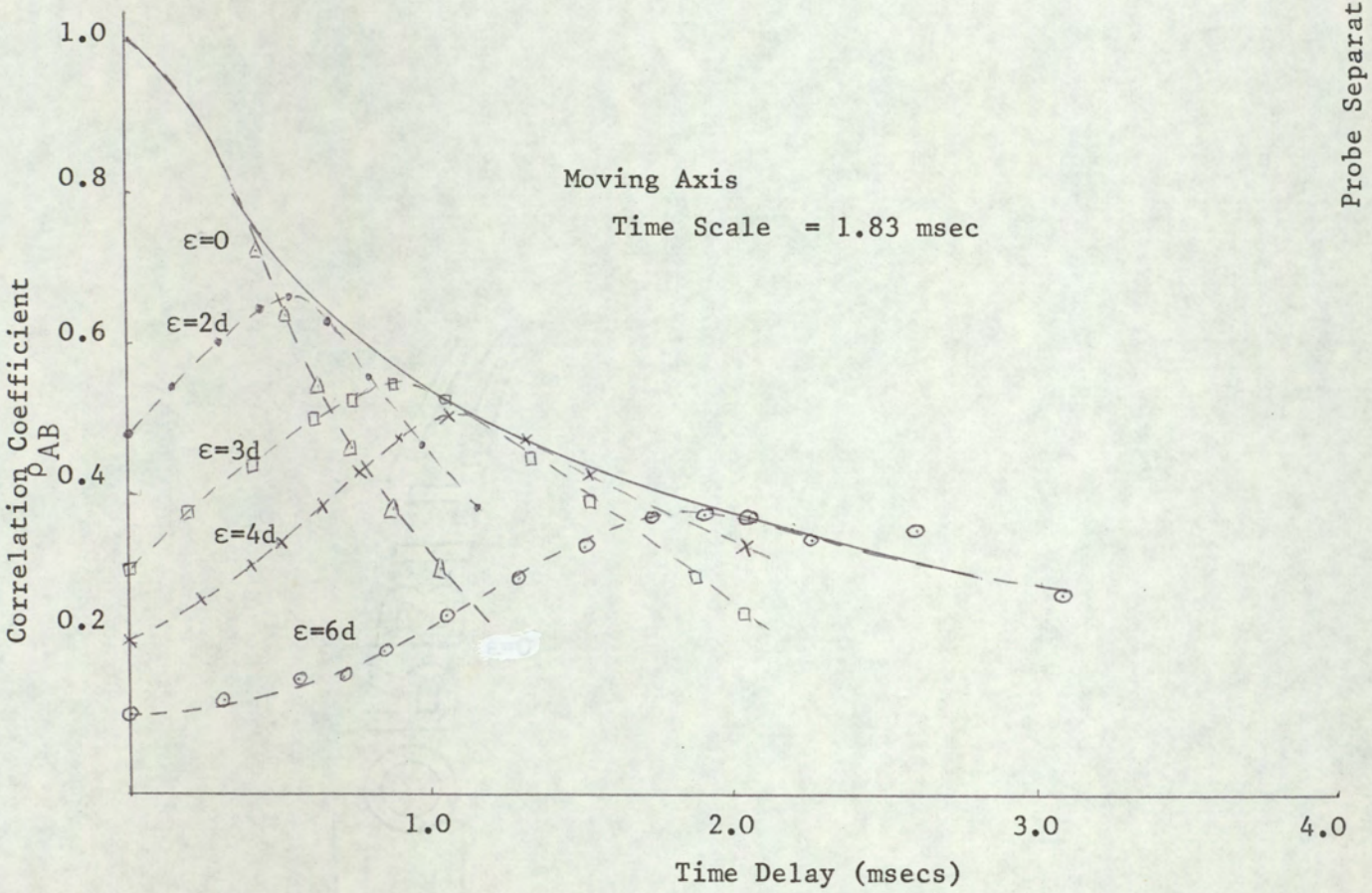

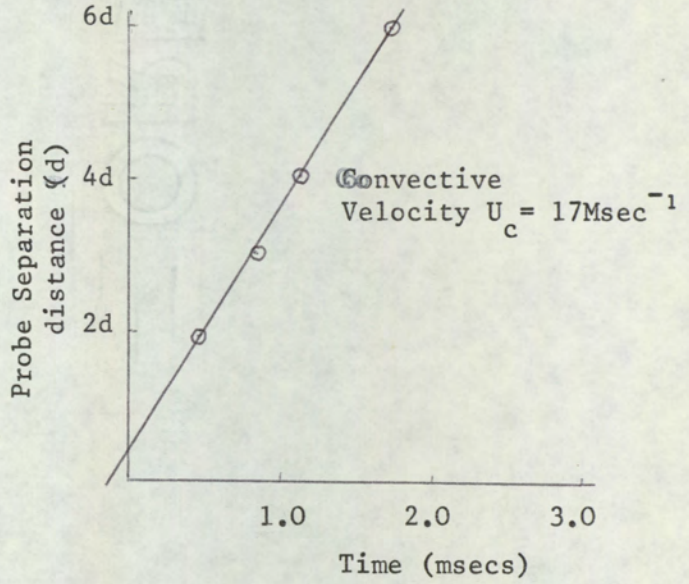

Fig. 10.10 Spare-Time Correlogram for Acetylene Seeded Flame at Fixed Probe Position 46d Above Burner

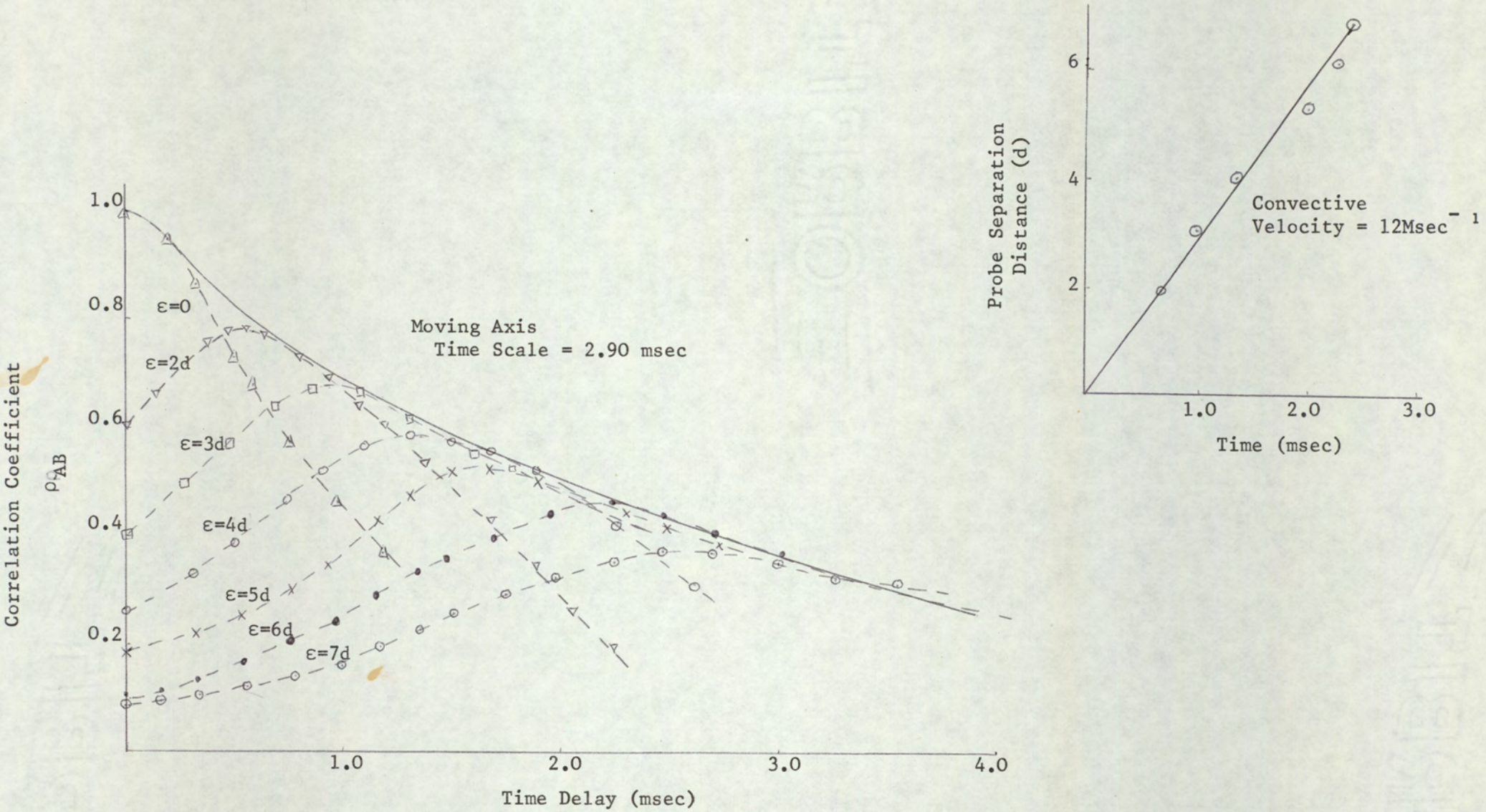

Fig. 10.11 Space-Time Correlogram for Acetylene Seeded Flame at Fixed Probe Position 54d Above Burner

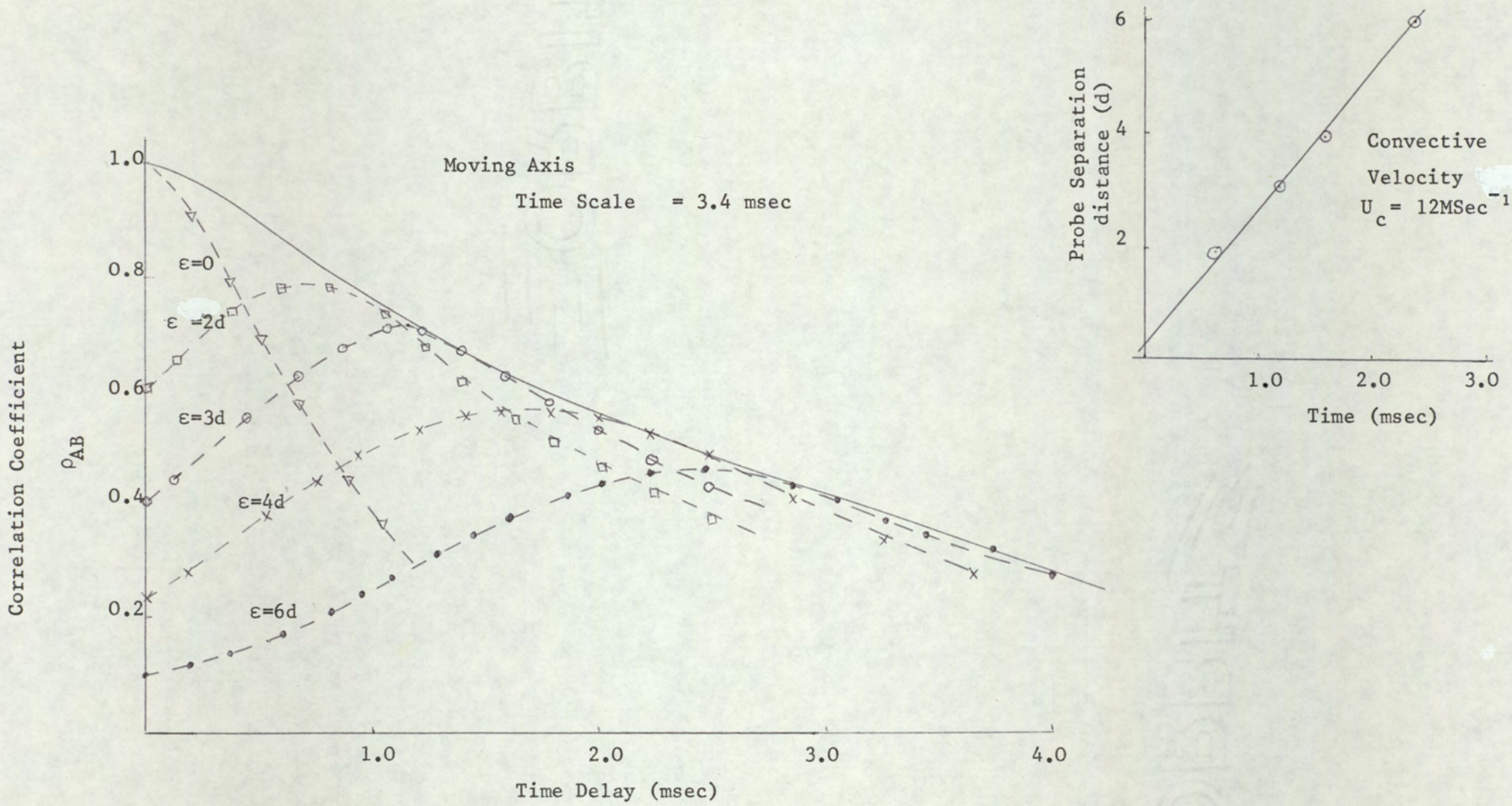

Fig. 10.12 Space-time Correlogram For Indium (0.1M) Seeded Flame at Fixed Probe Position 46d Above Burner

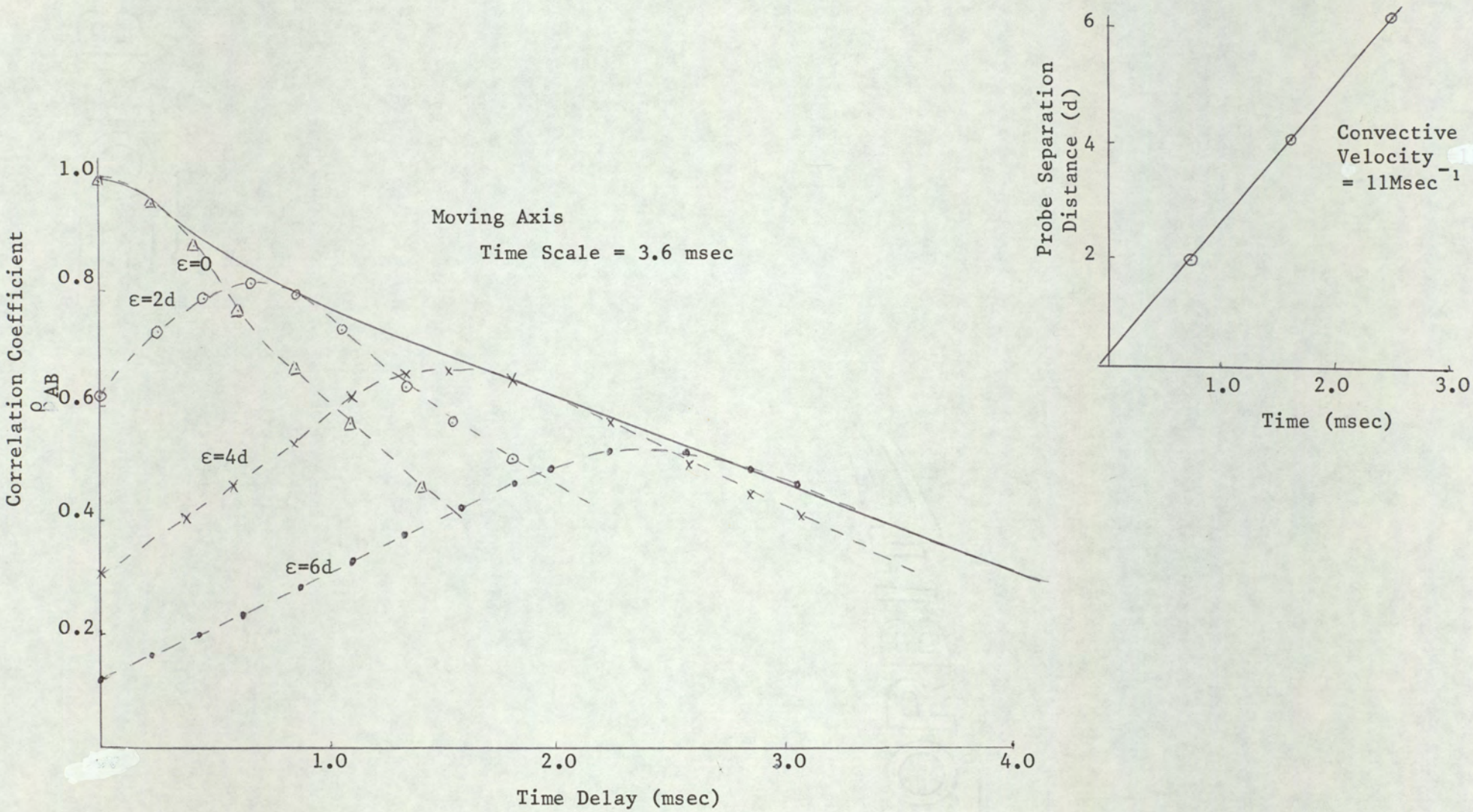

Fig. 10.13 Space-Time Correlogram for Indium (0.1M) Seeded Flame at Fixed Probe Position 54d Above Burner

case of the chemically passive species, distortion of the eddy pattern is due only to the turbulent shear stresses.

A measure of the rate of distortion of the ion density pattern during transit between the probes is given by the time the moving axis autocorrelogram falls to 0.47 ofion initial value. The moving axis time scales for acetylene and indium at 46d were determined to be 1.83 msecs and 3.4 msecs respectively. This appreciable difference between the rates of decay illustrates the effects of a rapid ion recombination reaction upon the H_3O^+ ion concentrations field. A similar observation was made at 54d where the moving axis time scales for H_3O^+ and In^+ ion density fields were 2.90 msecs and 3.4 msecs respectively. At this region of the flame the difference is not as great. A possible reason for this may be the presence of trace impurity in the entrained air. This effect has occurred repeatedly throughout all the correlation studies at this high flame region.

The Determination of Convective Velocity

Further valuable information obtainable from the space-time cross correlation function is the convective velocity of the turbulence pattern. It may be recalled that the convective velocity is a measure of the mean rate of transport of the main energy bearing eddies. Plots of probe separation distance ε against delay time, τ, given as the point where the moving axis auto correlation curve touches the space-time correlogram profiles, yields a straight line graph the gradient of which is equal to the convective velocity. The graphs for both acetylene and indium additives at 46d and 54d are shown in

Figs. 10.10 to 10.13; the convective velocities are indicated on each graph. The local velocity for H_3O^+ and In^+ ion concentration fields at 46d were observed to be $1.7 \times 10^1 msec^{-1}$ and 1.2×10^1 $msec^{-1}$ respectively. This difference was not expected since it was initially considered that the turbulence patterns would have the same transit times between the probes yielding equal convective velocities independent of the presence of any chemical influence.

The studies by Fisher et al[43] of velocity fluctuations in the mixing region of isothermal air jets included the determination of space-time correlation functions of filtered signals. Upon the removal of low frequency components the peak maxima were observed to decrease in magnitude but in addition the peak position also changes, becoming shifted towards shorter time delays. The removal of high frequency components produced the converse effect with increased peak heights occurring at longer delay times. This result provided evidence that the convective velocity was frequency dependent with higher frequency components yielding higher convective velocities compared to those for lower frequencies. This may be expressed alternatively as, the smaller eddies in a turbulent flow field travel at a greater velocity than do the larger eddies.

A similar explanation is believed to account for the discrepancy in the convective velocities observed in this work. It has been established throughout the correlation studies the presence of a rapid chemical reaction leads to a reduction in the size of turbulent time and length scales. Further, since the reduction in scale size will increase the high frequency content of the fluctuating probe signal, upon the evidence cited above, this will therefore result in an increase in the mean convective velocity of the turbulence pattern compared to that

for the chemically inert case. The reason why eddies of varying size travel at different velocities in the flow field remains unknown.

With reference to convective velocities for acetylene and indium at 54d, the values are within experimental error equal. It is again considered that trace ionisable impurity present in the laboratory atmosphere is responsible.

Test for Taylor's Hypothesis

Knowledge of the convective velocity enables the spacial longitudinal cross correlation curve to be constructed theoretically from the autocorrelation function using the Taylor relationship,

$$\rho_{AB}(x) = \rho_{AA}(\tau)\ \overline{U}_c \text{ where } x = \overline{U}_c\ \tau$$

It may be recalled from Chapter 3 that the autocorrelation and spacial cross correlation function are exactly related when a frozen nature of turbulence is considered where the eddies undergo no distortion and travel at the same convective velocity. In practice the presence of turbulent shear stresses will modify this and the deviation between the experimental and theoretical longitudinal correlograms provides an indication as to the degree of distortion the eddy pattern undergoes. Comparison between the experimental and theoretical profiles for H_3O^+ and In^+ decay curves at the flame height 46d are shown in Fig. 10.14 - Fig. 10.15. An appreciable difference between the H_3O^+ curves may be discerned with turbulant length scales of 0.70 cms and 1.00cms for the experimental and constructed correlograms respectively. The corresponding indium correlograms show good agreement with the small difference in

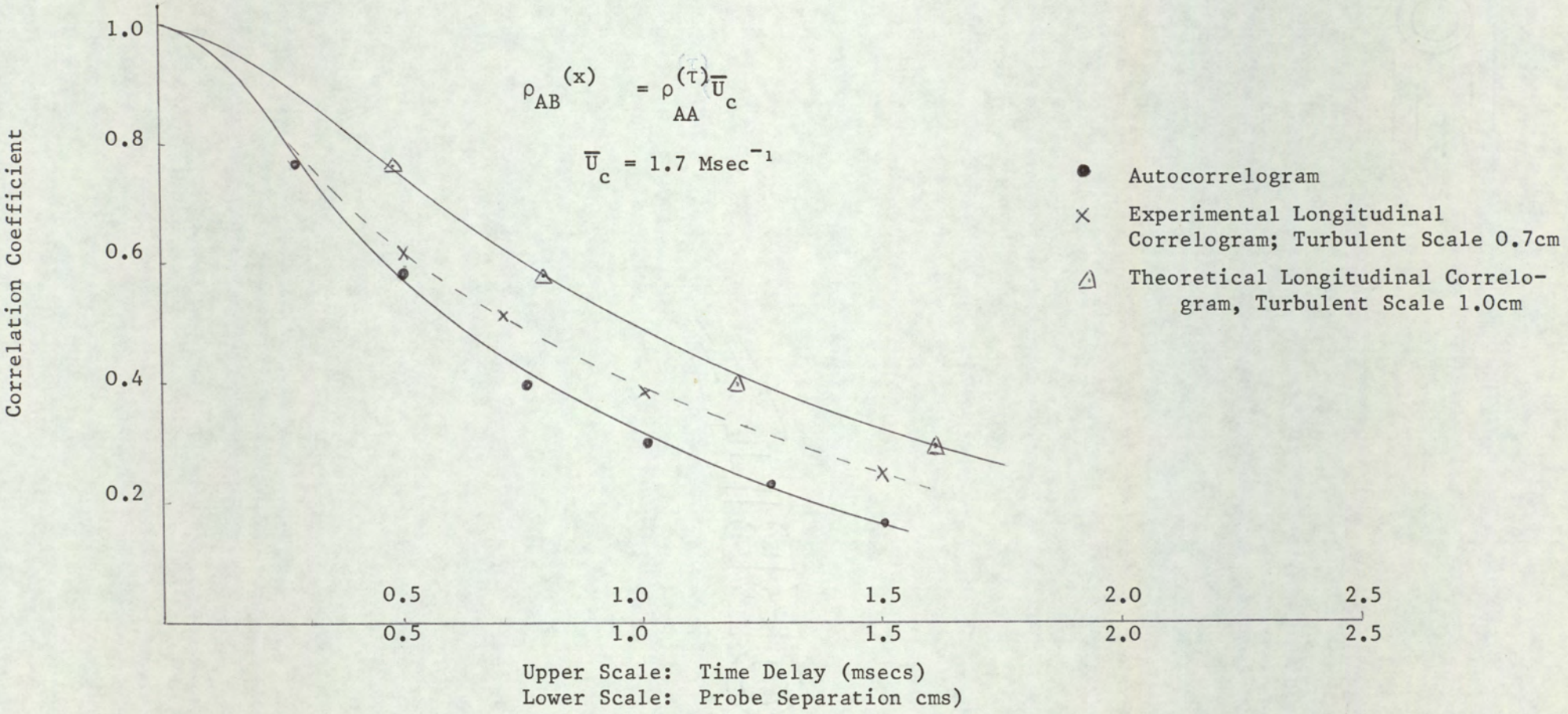

Fig. 10.14 Comparison between Experimental and Theoretical Longitudinal Correlograms Testing Taylor's Hypothesis for Acetylene seeded Flame. Fixed Probe Position 46d above burner, 2d from flame axis

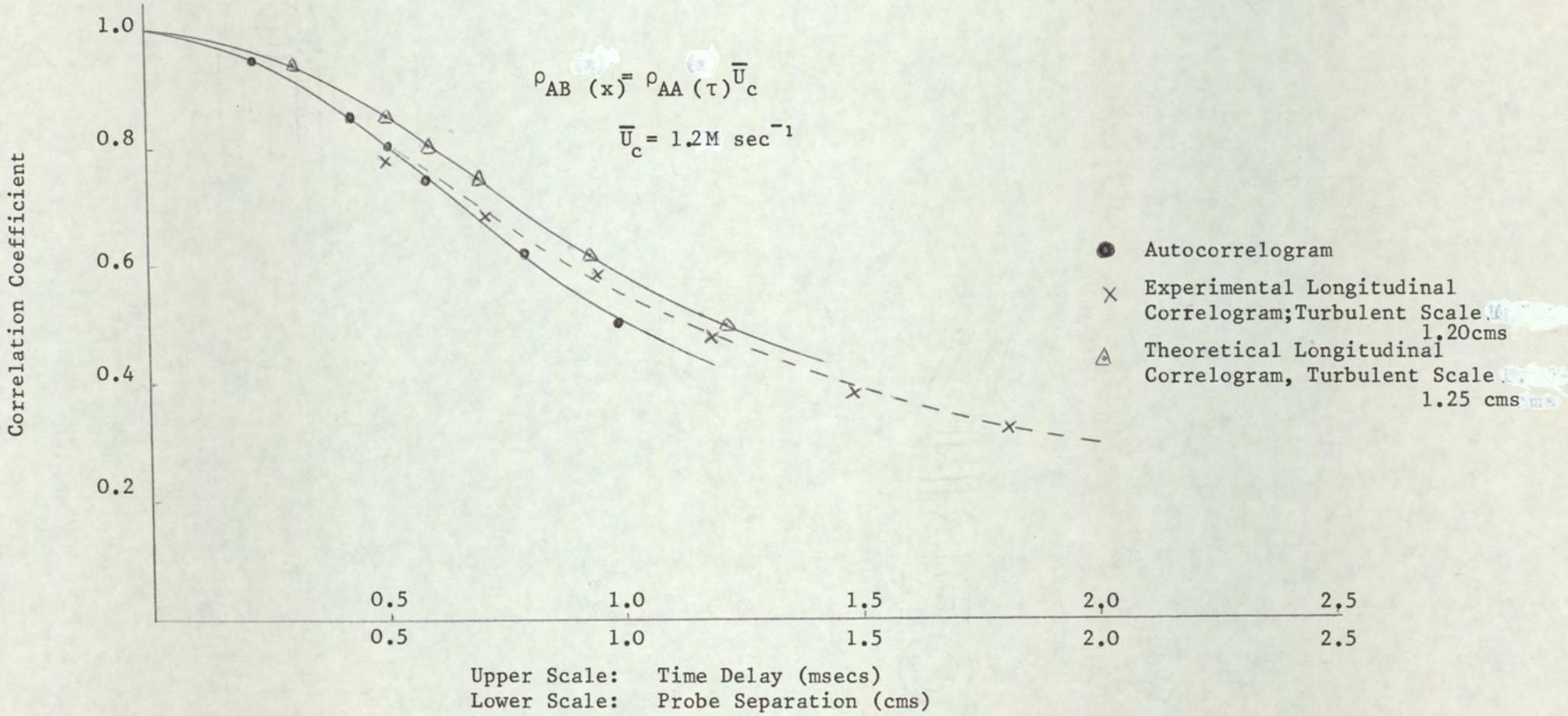

Fig. 10.15 Comparison between Experimental and Theoretical Longitudinal Correlograms Testing Taylor's Hypothesis for Indium(0.1M) seeded Flame. Fixed Probe Position 46d above burner 2d from Flame Axis

length scales of 1.20 cms and 1.25 cms for the experimental and theoretical correlograms.

This result illustrates the effect of a rapid chemical reaction producing a greater change in the turbulence pattern during convection between the two probes in comparison to the much lower rate of decay due to turbulent mixing. A further interesting observation in the case of the indium profiles suggests that due to the close similarity between the experimental and theoretical plots the turbulence pattern undergoes relatively little deformation during its travel downstream. At the 54d location good agreement between the experimental and theoretical spacial correlograms was achieved for both flame additives. This is again considered not to be a true effect but due to the problem of trace impurity present in the atmosphere as discussed previously.

In conclusion, the spacial and space-time cross correlation studies have provided further experimental evidence for the chemistry-turbulence interaction phenomenon. The presence of rapid ion chemical kinetics in a turbulent flow field has been observed to produce a reduction in the size of turbulent length scales.

The cross correlation technique has also provided further information regarding the overall structure of the fluctuating ion concentration field. The spacial longitudinal and radial correlation functions yielded turbulent length scales of what may be considered to be the axial and radial dimensions of an "average" eddy. These values upstream in the flame suggest the eddy to have an elllpsoidal shape. Upon moving downstream in the flow the increased flame dimensions and weaker shew stresses cause the eddy to grow in size and also to assume a more circular

profile. The space-time function have shown by way of moving axis autocorrelation time scales chemistry to contribute to a greater change in turbulence pattern during its motion downstream. This has also been observed to result in an increase in the convective velocity of the pattern of a chemically active reactant compared to that for chemically inert constituents. This effect has been attributed to the reduced turbulent scales brought about by rapid chemical kinetics.

CHAPTER 11

THE MEASUREMENT OF MEAN VELOCITIES IN THE TURBULENT DIFFUSION FLAME

11.1 Introduction:

It may be recalled that mean velocity is defined as the time averaged velocity of the bulk gas flow. A study has been made to determine this quantity throughout a turbulent diffusion flame and an isothermal jet of the same nozzle Reynolds number. The aim of such an investigation was to observe the effects of combustion upon the mean velocity by comparison of values in the flame and jet.

Mean velocity may be determined in a flow using a Pitot static probe. The probe used in these studies was manufactured of quartz such that the instrument could withstand flame temperatures. Advantages offered in the use of Pitot probes are:

(i) Robust and Simple construction

(ii) Rapid Pressure response.

The technique is based upon the relationship between pressure and mean velocity which for incompressible flows such as those studies in this work is given by the Bernoulli equation,

$$P-p = \frac{K}{2} \rho \overline{U}^2 \qquad 11.1$$

where P is the total or stagnation pressure, p the static pressure, ρ the fluid density, $\overline{U}$ the mean velocity and K a calibration factor.

The total or stagnation pressure may be defined as the pressure obtained when the fluid is brought to rest relative to the probe. The static pressure is equivalent to that pressure sensed by a measuring device moving with the fluid. Hence, providing this pressure difference is known, together with the fluid density, the mean gas velocity may be determined.

11.2 Pitot-Static Probe Design

The Pitot probe used was of a type based upon a design given by Prandtl[44] and is drawn in Fig. 11.1. It consists of an outer quartz tube of 1.0×10^{-2}M diameter sealed at one end such that it has a hemispherical nose. Approximately 14 tube diamters from the nose tip the tube was bent at a right angle. At 6 tube diameters from the nose, six 5.0×10^{-4}M diameter holes were located equidistant around the tube. The inner tube 3.0×10^{-3}M diameter also of quartz was positioned concentrically to the outer one with one end embedded in the hemispherical nose. A 1.0×10^{-3}M diamter hole located through the nose tip enabled fluid pressure to be sensed in the inner quartz tube. When the probe is immersed in a moving fluid with the axis parallel to the flow direction a small volume of fluid will be brought to rest near the nose with the pressure sensed in the inner tube equal to the stagnation pressure. The location of this pressure point is displaced a short distance upstream of the nose tip. It has been shown experimentally for the probe design given above in isothermal free jet flows the displacement distance was 0.15 D where D is the outer tube diameter[44]. This displacement of 1.5×10^{-3}M is sufficiently small to warrant the assumption that the

stagnation point

Fig. 11.1 Pitot Probe used for the Measurement of Mean Gas Velocity

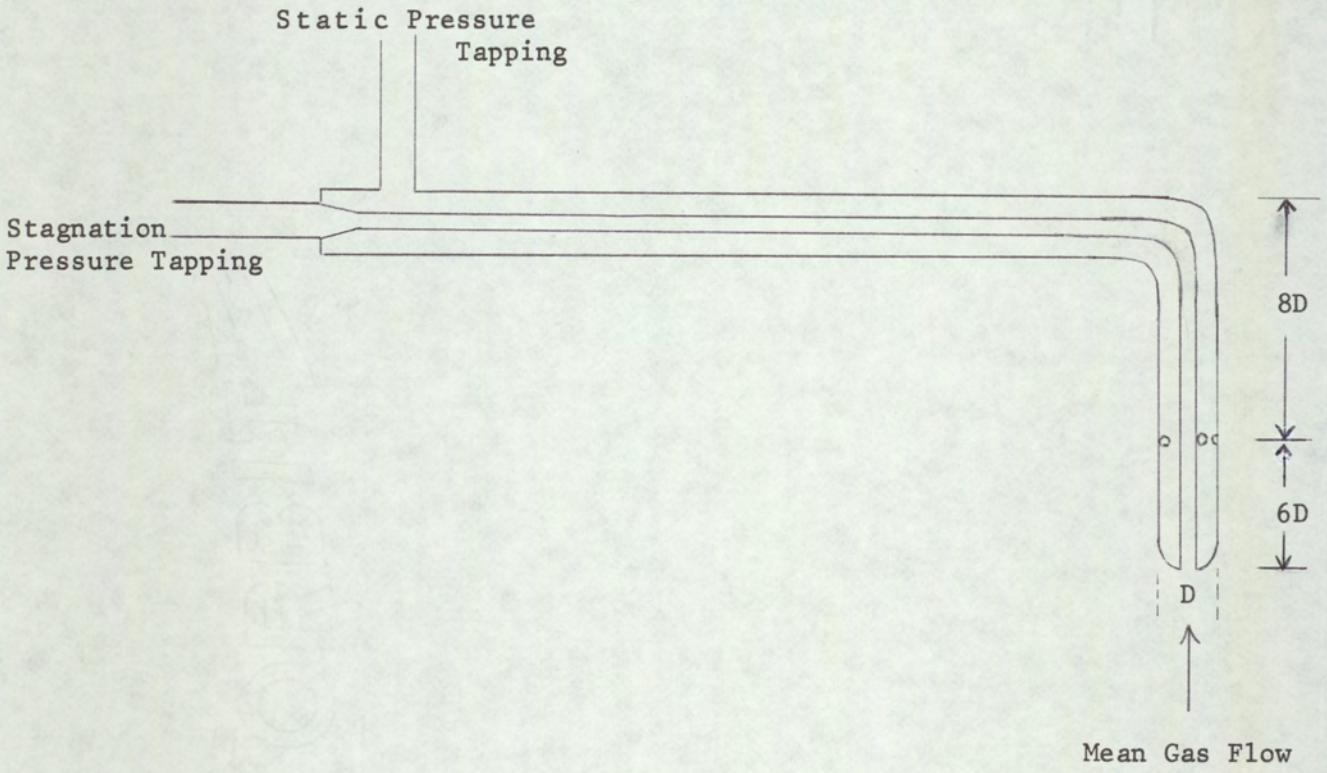

occurred at the nose tip. The stagnation pressure is greater than the pressure in the undisturbed fluid. As the flow accelerates round the hemispherical nose the pressure falls rapidly, followed by a gradual rise until it attains the same pressure as the undisturbed flow. The horizontal portion of the stem of the probe in turn produces an increase in the upstream static pressure above that of the free stream. The location of the six holes for the static pressure measurement is at the position where the pressure reduction created by the nose is balanced by the pressure increase due to the stem, enabling the free stream static pressure to be recorded correctly. The positioning of the six holes is not critical as the calibration factor will allow for small errors due to this in the pressure difference measurement.

The calibration procedure is generally performed in a wind tunnel of known flow rate such the K value may be calculated. Equipment of this nature was not available during these studies. However comparisons between mean velocities were determined using the quartz probe and a commercial Pitot probe having a calibration constant of unity in an isothermal jet produced identical pressure difference readings. On this basis the calibration constant for the quartz instrument was taken as unity.

The monometer used to determine pressure differences consisted of a large reservoir and inclined tube giving greater sensitivity over a simple "U" tube manometer. The stagnation and static pressure tapping points were connected to opposite ends of the manometer system enabling mean pressure differences to be measured directly. The accuracy of the manometer used was 2.0×10^{-4}M of H_2O. The static pressure alone was also monitored on a similar manometer.

Precautions were taken to keep the P.V.C. tubing connecting the probe and manometer as short as possible to improve the pressure response of the overall system by reducing the air volume in the tubing.

11.3 Experimental Procedure

The jet and flame were of unburnt gas composition of H_2: N_2 in the ratio of 3:1 having a nozzle Reynolds number of 1.0×10^4. The Pitot probe was mounted in the same apparatus used to conduct the electrostatic probe studies enabling three-dimensional positioning of the probe in either jet or flame. Mean pressure differences were determined mapping both jet and flame at axial positions between 30d and 60d at intervals of 4d. At each axial position a transverse scan was performed across the jet/flame in steps of 1d intervals up to 5d from the axis.

It has been mentioned in an earlier section that the fluid density is required for the determination of mean velocities. In the case of both jet and flame the air entrainment process leads to a dilution of the vented gases such that the density is a constantly varying quantity increasing with increased distance from the burner orifice. Owing to this complication it has been assumed the jet to be one of air at room temperature and the flame to be of heated air at the flame temperature. The flame temperature was also a varying quantity and this required the flame to be mapped in the manner outlined above using a Pt:Pt 10% Rd thermocouple of 1.3×10^{-4}M diameter wire. The emf thermocouple readings were converted to temperature readings using Tables of Phy sical Constants[45]. These values required correction due to radioactive heat losses by the

Fig. 11.2 Comparison of Mean Velocities in a Turbulent Diffusion Flame and Jet of Nozzle Reynolds Number 1.0×10^4. Height of Pitot Probe above Burner indicated on each Profile.

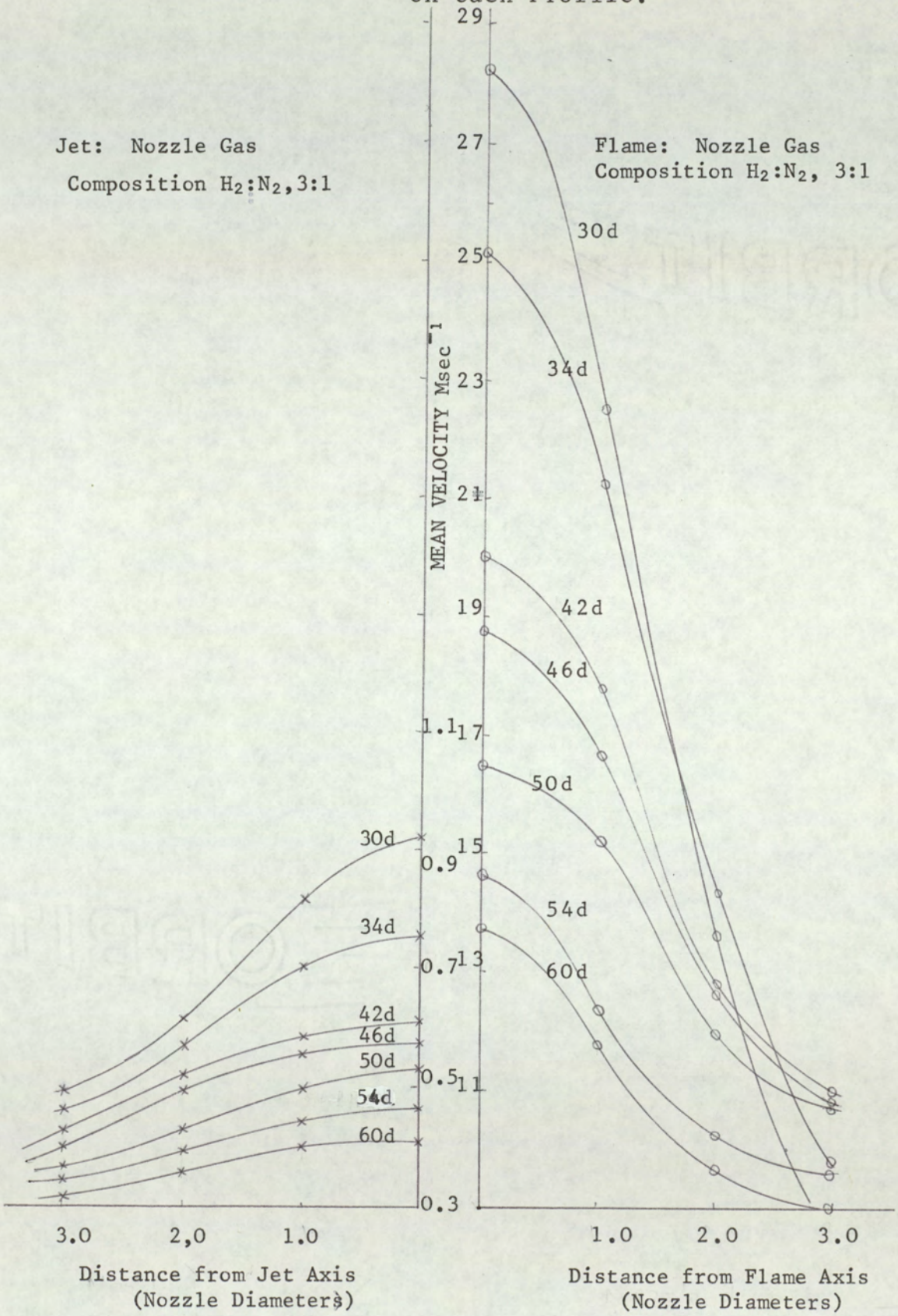

thermocouple. The required true gas temperature T may be expressed as,

$$T = T_W + \Delta T$$

where T_W = thermocouple temp (^oK)

and ΔT = temperature lowering due to radioactive heat loss. The value for ΔT was established using the correction formula given by Bascombe[46], thus enabling the true gas temperature to be established.

i.e. $$\Delta T = \frac{1.12 \times 10^{-7} T^4 M_m d}{270 + T}$$

where d = diameter of thermocouple (cms)

M_m = mean molecular weight of the gas i.e. for air = 28

11.4 Results and Discussion

The mean gas velocities for the mapped jet and flame are both shown in Fig. 11.2. It may be clearly inferred that greater velocities were encountered in the flame in comparison to the corresponding probe positions in the jet. The static pressure manometer readings were observed to be negligible for both flame and jet indicating the free stream pressure in each system to be approximately equal to the atmospheric pressure. Combustion therefore influenced the stagnation pressure only. The increased mean velocities in the flame over those in the jet was not expected. A possible explanation for the observed result may be derived upon consideration of the conservation of momentum in the flame and jet.

The momentum of the unburnt gases at the nozzle is the same for both flame and jet, viz.

$$\rho_c \pi r_N^2 \overline{U}_N^2 \qquad 11.2$$

where ρ_c = density of vented gases at room temp.

r_N = nozzle radius

$\overline{U}_N$ = mean exit velocity

Upon consideration of some point in the flow field the momentum transfer across the jet cross section at the height h must be equal to that at the nozzle i.e. momentum is conserved;

$$\therefore \quad \rho_c \pi r_N^2 \ \overline{U_N}^2 = \rho_c \ \pi r_J^2 \ \overline{U_J}^2 \qquad 11.3$$

where r_J is the radius of the jet cross section at the height h and $\overline{U_J}$ the mean velocity at the point of interest. It is assumed in the case of the isothermal jet the density of the fluid at the nozzle and in the flow field are the same. Consider further the equivalent position in the flame. The momentum of the combusted gases passing through the cross section at height h must be equal to that of the unburnt gases at the nozzle i.e.

$$\rho_c \ \pi r_N^2 = \rho_H \ \pi r_F^2 \ \overline{U_F}^2 \qquad 11.4$$

where ρ_H = density of flame gases

r_F = radius of cross section in the flame

$\overline{U_F}$ = mean flame gas velocity

Then from equation 11.3

$$\rho_C \pi r_J^2 \overline{U_J}^2 = \rho_H \pi r_F^2 \overline{U}^2_F \qquad 11.5$$

Since the radii of the cross sectional areas at h for the flame and jet are assumed to be equal i.e.

$$r_J = r_F$$

Then:

$$\rho_C \overline{U_J}^2 = \rho_H \overline{U}^2_F \qquad 11.6$$

Hence upon the application of the conservation of momentum in the flame and jet at equivalent positions the decrease in flame gas density due to combustion requires an increase in mean flame gas velocity.

Calculation of the local mean flame gas velocities by substituting the measured jet velocities and density values for air at room and for the flame temperature at the position of interest in equation 11.6 yielded values approximately 3 $Msec^{-1}$ below the experimentally determined values. This is considered to be a small error considering the following assumptions have been made during the derivation of equation 11.6.

(i) It is considered that the mean velocity is constant over the cross section of the jet or flame such that the velocities are functions of distance from the nozzle.

(ii) The radii of the cross sections for both jet and flame are equal at the height h. i.e. $r_J = r_F$. In reality the degree of spread of an isothermal jet is slightly greater than that for a flame having the same nozzle Reynolds number[16] i.e. $r_J > r_F$

11.5 Pitot probe in a Fluctuating Media

For a Pitot probe immersed in a turbulent flow it is to be expected that the fluctuations in velocity will influence the mean pressure difference readings. Under these conditions the measured mean pressure difference reading will not be exactly related to the mean gas velocity but will contain a contribution due to the velocity fluctuations. The error in mean velocity measurement upon ignoring the effect of the velocity fluctuations will now be examined.

Assume the instantaneous velocity may be expressed in terms of three components along Cartesian co-ordinate axes, x, y and z.

i.e. $U = U_x + U_y + U_z$

Expressing each instantaneous velocity in terms of the sum of its mean velocity $\overline{U}$ and fluctuating component u :

$$U_x = \overline{U}_x + u_x$$
$$U_y = \overline{U}_y + u_y$$
$$U_z = \overline{U}_z + u_z$$

The measured manometer pressure difference reading is proportional to the square of the instantaneous velocity:

$$P - p \propto U^2$$

Expressing U^2 in terms of its components i.e.

$$U^2 = (\overline{U}_x + u_x)^2 + (\overline{U}_y + u_y)^2 + (\overline{U}_z + u_z)^2$$

Now,

$$(\overline{U}_x + u_x)^2 = \overline{U}_x^2 + \overline{2U_x u_x} + u_x^2$$

$$= \overline{U_x^2} + \overline{u_x^2} \qquad \text{since } \overline{u_x} = 0 \text{ by definition.}$$

Similarly for the other components, thus:

$$U^2 = (\overline{U_x^2} + \overline{u_x^2}) + (\overline{U_y^2} + \overline{u_y^2}) + (\overline{U_z^2} + \overline{u_z^2})$$

In the free jet or flame the mean gas velocity occurs in one direction. Assume this to be $\overline{U}_x$ therefore the other mean velocity components in the y and z directions tend to zero. The fluctuations in velocity are produced by mean velocity gradients in the direction normal to the mean gas flow thus the fluctuations in the mean gas velocity direction u_x may be considered to be negligible.

Following the above assumptions the mean pressure difference reading reduces to:

$$P - p \propto \overline{U_x^2} + \overline{u_y^2} + \overline{u_z^2}$$

$$\propto \overline{U_x^2} \left[1 + \frac{\overline{u_y^2}}{\overline{U_x^2}} + \frac{\overline{u_z^2}}{\overline{U_x^2}} \right]$$

Consider a lateral velocity intensity of the order of 10% for both the y and z components,

$$\frac{(\overline{u_y^2})^{\frac{1}{2}}}{\overline{U}_x} = \frac{(\overline{u_z^2})^{\frac{1}{2}}}{\overline{U}_x} = 10\%$$

$$\text{Mean Pressure Difference, } P - p = \overline{U^2_x}\left(1 + \frac{1}{100} + \frac{1}{100}\right)$$

$$= 1.02\overline{U^2_x}$$

Hence the presence of fluctuations in velocity of 10% intensity will lead to a measured mean gas velocity to be in error by 2%. It is unlikely that a velocity intensity value of 10% will exist in the flame and jet studied here such that the small error due to neglecting the contribution from the velocity fluctuations is acceptable.

CONQUEROR
IMI
LONDON

CHAPTER 12

THE MEASUREMENT OF CONVECTIVE VELOCITIES USING THE INVERTED ELECTROSTATIC PROBE TECHNIQUE

12.1 Introduction

The inverted electrostatic probe is a new technique developed by Ghosh and Richard[47] which has been successfully used for the measurement of convective velocities in low pressure turbulent plasmas. The aim of the work described in this chapter was to observe if the technique could be employed for the determination of local convective velocities in atmospheric pressure turbulent flames. The electrostatic probe is used with the probe wire inverted such that it lies parallel to the direction of the mean gas flow. In this position the higher frequency components of the fluctuating ion density field are averaged out as they travel at their respective convective velocities along the probe wire. The averaging procedure is dependent upon the length of the probe wire which governs the critical frequency at which the filtering effect begins. Under these conditions the probe may be considered to behave as a low pass filter.

The relationship between the probe wire length L and the critical frequency f_c is given by

$$\frac{1}{f_c} = \frac{2}{U_c} L \qquad 12.1$$

where U_c = convective velocity. Since $f\lambda = U_c$ it may be seen from equation 12.1 the critical frequency has a corresponding

wavelenth λ equal to twice the probe wire lengths. The filtering effect has been shown to have a pronounced influence upon the power spectral density function of the random probe signal producing an earlier fall off in the spectrum compared to that obtained with the unfiltered signal. The critical frequency may be determined from the power spectrum for each probe wire length from the intersection point of the asymptote to the filtered frequency portion with the horizontal line drawn through the flat portion of the spectrum. A plot of the reciprocal critical frequency against probe wire length enables the convective velocity to be estimated since the inverse of the critical frequency varies linearly with probe length.

The variation in cut off frequency demonstrates that the length of the inverted probe wire influences the frequency response characteristics of the electrostatic probe. The critical frequency provides a measure of the maximum frequency at which there is no appreciable lack of probe response. As the critical frequency is inversely proportional to the time constant of the probe the length of the probe wire is directly proportional to it. Hence the frequency response is lowered with increased probe length, i.e. increases the time constant of the probe wire, as illustrated by the power spectrum.

12.2 Experimental Procedure

The electrostatic probe wire length was varied between $0 - 3.0 \times 10^{-2}$M at intervals of 5.0×10^{-3}M. The zero length corresponded to the unfiltered signal obtained with the probe wire normal to the mean flow direction. The probe was biased at 50V negative with respect to the burner to collect the positive ion saturation current. The random signals were

Fig. 12.1 Power Spectral Density functions for inverted electrostatic probe signals of probe wire lengths 0.5 to 3.0 cms. Probe positioned 46 d above burner on the flame axis.

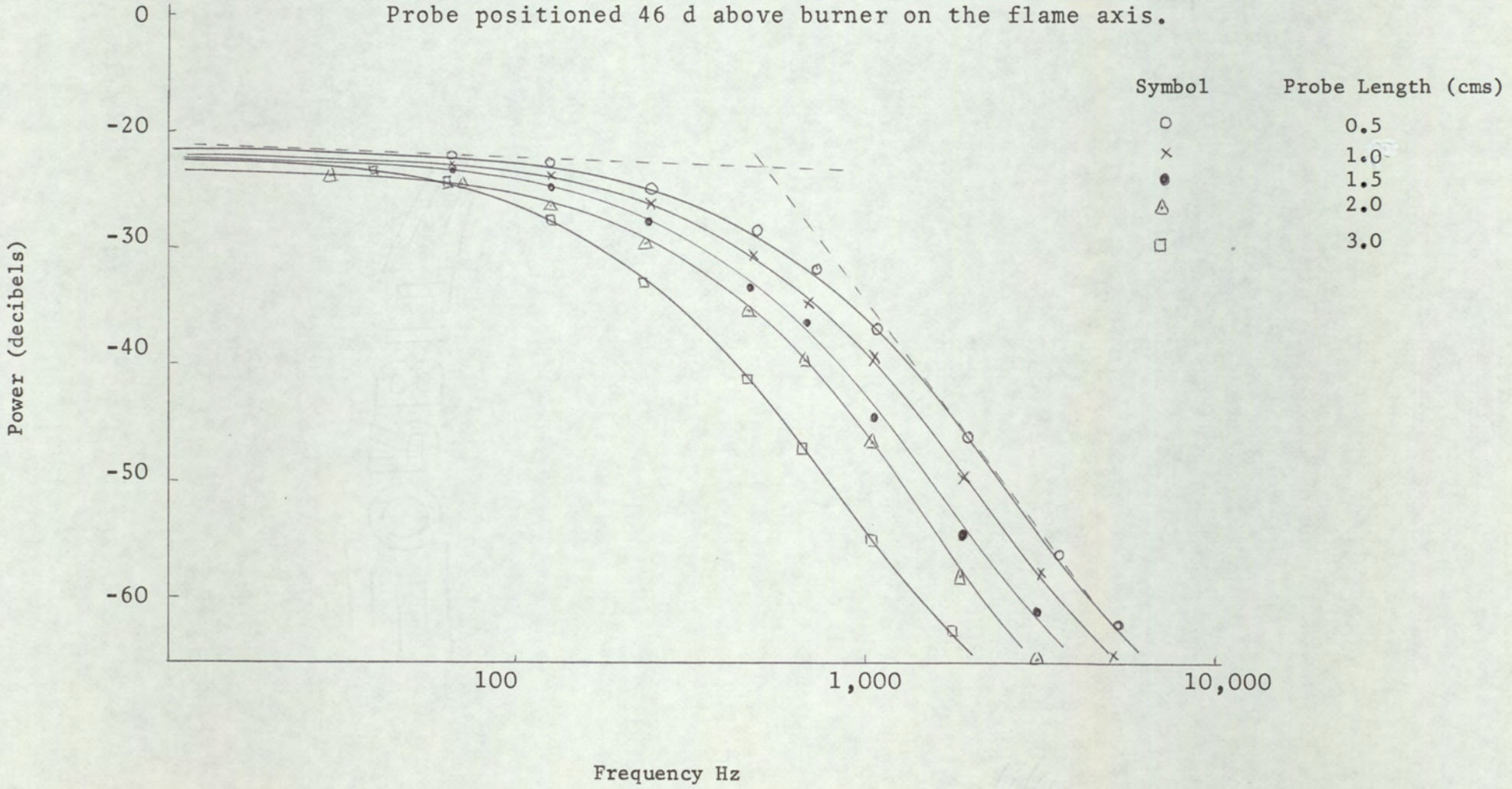

Fig. 12.2 Plot of Inverse Critical Frequency versus Probe Wire Length to determine Convective Velocity. Probe Positioned 46 d above Burner on the flame axis.

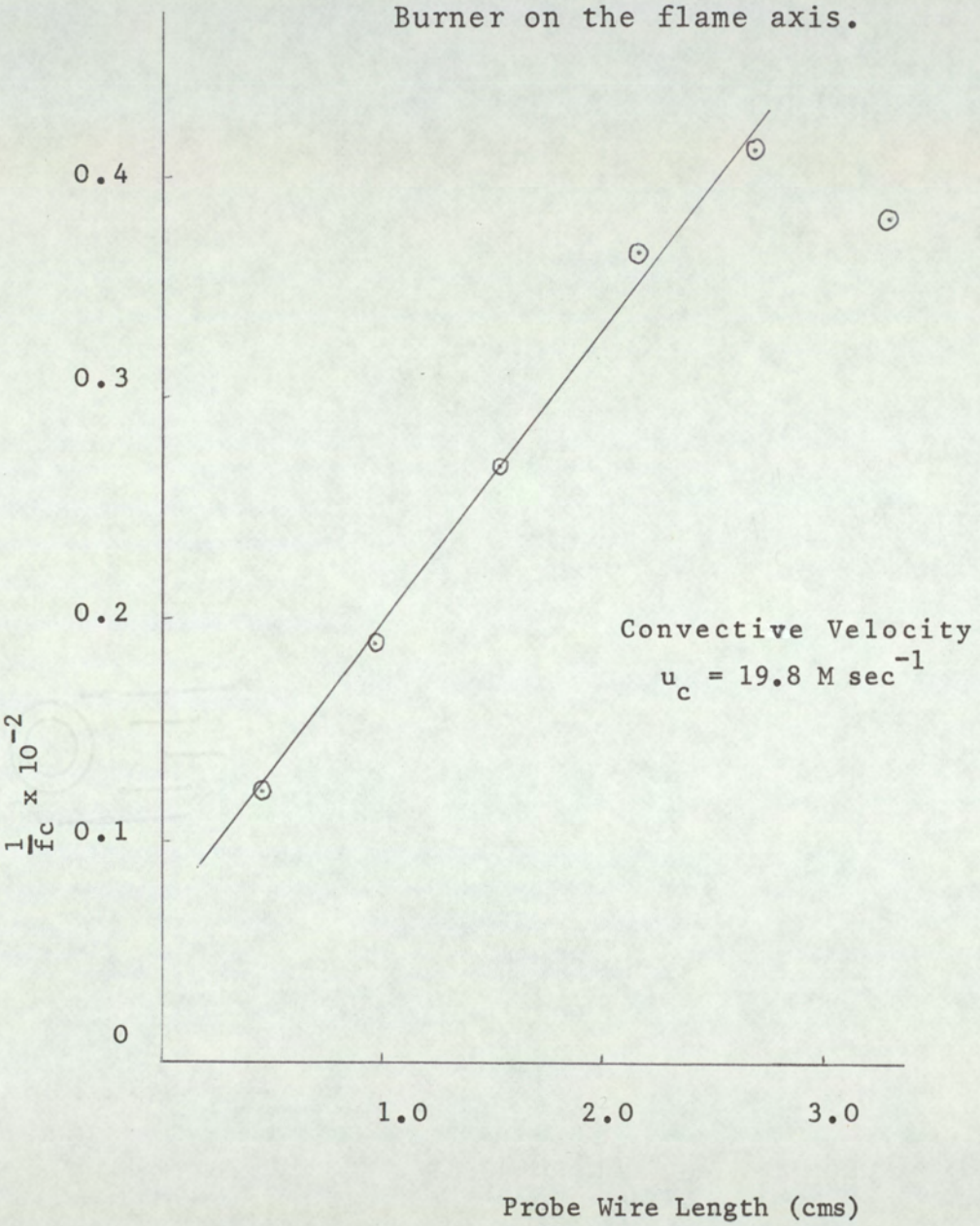

recorded on magnetic tape to enable the spectral analysis to be performed. Recordings were made for each series of probe wire lengths at 42, 46, 50 and 54d above the burner on the flame axis. The flame, having the same flow properties as have been described earlier was seeded with only acetylene Unfortunately time did not permit a more thorough investigation of this technique to be performed, namely, the addition of other metal salt solutions and the determination of convective velocities throughout the flame as had been intended.

A typical series of power spectra obtained for an inverted probe of varying lengths at the 46d position are shown in Fig. 12.1 ..Also illustrated is the method employed for the determination of critical frequencies. A plot of reciprocal critical frequency against the probe wire length together with the convective velocity obtained is shown in Fig. 12.5. Since the power spectral plots obtained at the other flame positions studied were of similar appearance only those determined for the 46d position have been shown to illustrate the technique. It is of interest to note that the $1/f_c$ versus L plots for the longer probe wire lengths i.e. 3.0×10^{-2}M presented a greater spread of points which is considered to be due to slight movement of wire in the flame. Use of a thicker wire i.e. $\geq 5.0 \times 10^{-4}$M would probably overcome this problem.

12.3 Results and Discussion

In Table 12.1 is given the convective velocities obtained using the inverted electrostatic probe technique together for the purposes of comparison are the mean velocities at the corresponding positions determined with the Pitot probe described

TABLE 12.1

Comparison between Convective and Mean Velocity Measurements

FLAME ADDITIVE	Probe Height Above Burner (nozzle diameters)	Inverted probe U_c ($M\ sec^{-1}$)	Pitot Probe $\overline{U}$ (axis) ($M\ sec^{-1}$)	Space Time Correl^n U_c (2d off axis) ($M\ sec^{-1}$)	Pitot probe $\overline{U}$ (2d off axis) ($M\ sec^{-1}$)
C_2H_2 (1% total gas)	42	21.4	20.0	-	13.2
	46	19.8	18.6	17.0	12.7
	50	17.2	16.4	-	11.7
	54	15.0	14.6	12.0	10.6
C_2H_2 + $InCl_3$ (0.1M)	42	-	20.0	-	13.2
	46	-	18.6	12.0	12.7
	50	-	16.4	-	11.7
	54	-	14.6	11.0	10.7

$\overline{U}$ = Mean Velocity (independent of flame additive)

U_c = Convective Velocity

earlier. Also given are the convective velocities determined by the space time correlation technique and the mean velocities at coincident positions.

Although a comparison of convective andmean velocities throughout the flame was not possible some interesting conclusions may be drawn from the data obtained.

Wygnanski and Fiedler [48] have shown that for axial positions in isothermal jets the convective velocities are approximately 90% of the mean velocityvalues, i.e.

$$U_c = 0.9\bar{U}$$

They further observed that moving radially from the jet axis the mean velocity decreases more rapidly than the convective velocity such that a cross over point exists where their values are equal. In Table 12.1 it may be seen that in the case of the indium seeded flame the convective and mean velocities are approximatelyequal which suggests the 2d off axis position is in the vicinity of the cross over point. It is also shown theaxial convective velocities determined in the acetylene seeded flame using the inverted electrostatic probe are in close agreement with the mean velocities at this position whereas at the 2d position a marked difference exists between the convective velocities measured by the correlation method and the mean velocity values.

It may be recalled that convective velocity is frequency dependent since it was observed during the cross correlation measurements the presence of a rapid ion chemical reaction produces a shift in the eddy frequency spectrum towards higher

frequencies due to the generation of smaller scales resulting in higher convective velocities compared to those for a chemically passive species. As the effects of rapid charged species reactions have been observed almost throughout the flame, it is to be expected differences between convective and mean velocities should exist for a flame seeded with a highly reactive species irrespective of position in the flame, as observed at the 2d off axis position for the acetylene additive.

From the close agreement between the convective and mean velocities on the flame axis, in agreement with the work cited above, it may be inferred that the inverted electrostatic probe provides a valuable method for the measurement of convective velocities in high pressure turbulent flames. This technique, however, appears not to offer the sensitivity of the space time correlation method since for the reasons given above, greater convective velocity values would have been anticipated. It is therefore unlikely this instrument would detect differences in convective velocities due to the presence of a chemically active species in the flow field as observed using the correlation method such that the presence of the chemistry turbulence interaction would not be revealed. It may be recalled a similar result was obtained in Chapter 8 where the power spectral density function yielded no evidence for the interaction phenomenon.

A major advantage the inverted electrostatic probe offers over the correlation technique would be in the measurement of local convective velocities throughout the flame since no problems due to the disturbing wake effects would arise as were observed to present continual difficulties using the cross correlation method apart from a limited region off the flame axis.

CHAPTER 13

TURBULENT INTENSITY MEASUREMENTS

13.1 Introduction

It may be recalled that turbulent intensity provides a measure of the violence of the fluctuating turbulent motion. The generally accepted definition is given as the ratio of the root mean square value of the fluctuating component to the mean signal level. Intensity may also be termed the degree or level of turbulence.

Sutton[49] studied the fluctuation intensities of a scalar quantity in isothermal free jet flows. He deduced the following semi-empirical formula for the conservation of fluctuation intensity for a dynamically passive species present in the flow.

$$u\frac{\partial\overline{n^2}}{\partial x} + v\frac{\partial\overline{n^2}}{\partial r} = \frac{e_D}{r}\frac{\partial}{\partial r}\left(r\frac{\partial\overline{n^2}}{\partial r}\right) + 2e_D\frac{\overline{n^2}}{\overline{u^2}} + 2e_D\frac{\partial\bar{n}}{\partial r} \qquad 13.1$$

where $\overline{n^2}$ is the mean square of the scalar fluctuations, e_D the diffusion coefficient for scalar species. This expression assumes

$$\frac{\partial\bar{n}}{\partial x} << \frac{\partial\bar{n}}{\partial r} \qquad 13.2$$

which is valid for incompressible axisymmetric jets.
The terms on the left hand side represent convective transport terms. The first term on the right hand side represents the diffusion of the mean square fluctuations by the large scale eddies. The second term describes the destruction of the fluctuations due to small high frequency eddies by viscous effects. The third term represents a source term by which

the fluctuations are produced by radial mean concentration gradients.

From this equation a balance may be considered to exist between the generation of fluctuations and their destruction by dissipative smearing. Sutton has shown the above equation to be obeyed for experimental observations of temperature and smoke particle fluctuations in isothermal air jets.

It was considered that the above processes occur in a turbulent flame but, in addition, the presence of a chemical reaction may be expected to influence the balance of the fluctuations in the reactant concentration field. Therefore, the measurement of turbulent intensity in the turbulent hydrogen flame seeded with the chemically active additives used previously would be expected to exhibit differing intensity values compared to those for a chemically inert constituent. Observation of this effect would thus provide further experimental evidence for the chemistry-turbulence interaction phenomenon. The method by which this information was determined will now be described.

13.2 Experimental Procedure

Details of the turbulent flame employed in this study are given in Chapter 8. Turbulent intensity measurements of the fluctuating ion concentration field were conducted using an electrostatic probe. The flame was mapped at the heights 42, 46, 50 and 54d above the burner orifice performing a transverse scan at each height at intervals of 0.5d across the flame up to a distance of 2.5d from the flame axis. Mean square values for the fluctuating component of the probe

signal at each test point were determined using an additional facility of the analog correlator thereby enabling the root mean square values to be calculated. The mean signal levels were measured using a D.C. micro voltmeter. Precautions were taken to ensure the probe wire was cleaned prior to each flame scan. This was necessary since the magnitude of the probe signal was measured and any contamination of the wire would produce adverse effects upon the intensity readings. Owing to the shortage of time, experiments using all the additives used previously, together with the various solution concentrations was not possible. The additives used included acetylene(1.0% total gas), indium (0.1M), caesium (0.1M) and lead (0.1M).

13.3 Results and Discussion

The plots of turbulent intensity against distance of the test point from the flame axis for acetylene and indium additives are shown in Fig. 13.1. The curves are, within the limits of experimental error, identical such that the expected difference between the intensity values for chemically active and chemically passive species concentration fields is not present. It may be further observed that the profiles are parabolic in shape indicating turbulent intensity increases rapidly upon moving radially from the flame axis. In some cases increases in intensity of greater than 100% were recorded at the flame-atmosphere boundary compared to axial values. This was considered not to be a true phenomenon however and is believed to be a misrepresentation due to the effects of turbulent intermittency having been observed to be present at the outer flame regions earlier in the work. Parabolic shaped intensity profiles have been obtained by other workers studying free

Fig 13.1 Plots of Turbulent Intensity against Radial Distance from Flame Axis

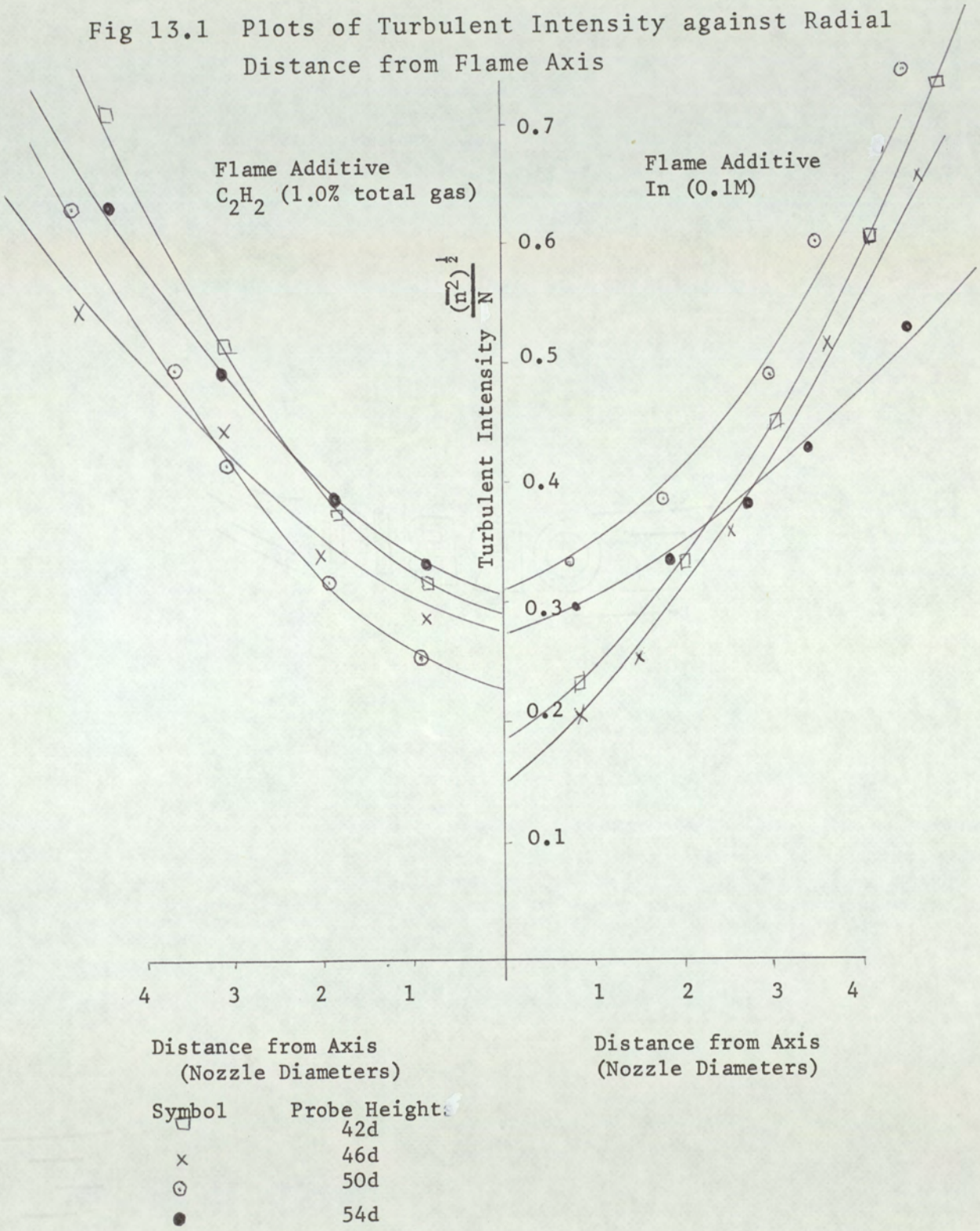

turbulence but the reasons for this are at present not clear.

An attempt to extract more useful information from the intensity readings, graphs of the ratio of root mean square to axial mean values against the location of test points yielded profiles of two off axis peaks decreasing in magnitude with increased flame height, a result expected on the findings of other work in isothermal air jets[50]. The curves however proved difficult to interpret with some curves merging into others such that no distinct trend could be discerned.

A more satisfactory means of analysis was achieved by replacing turbulent intensity values for normalised root mean square values. The normalising procedure involved the determination of the ratio of the root mean square values at each test point to the root mean square level on the flame axis at the relevant height.

The profiles so obtained for the flame additives used are shown in Fig. 13.2.(Half flame shown). The ratio RMS/RMS_{axis} may be considered to represent a measure of the relative turbulent intensity across the flame. It does not provide a measure of absolute intensity. Hereon this ratio will be termed relative turbulent intensity.

The profiles clearly indicate two off axis intensity peaks for each additive at the upstream regions of the flame studied. The maxima decrease in magnitude with increased flame height and gradually move towards the flame axis culminating with a single on axis peak at the highest region studied, namely 54d. The application of Sutton's equation to a turbulent flame attributes the generation of fluctuations in the charged species number density to the presence of radial mean ion concentration

Fig. 13.2 Effect of Ion Chemistry upon Relative Turbulent Intensity, RMS/RMS_{axis}

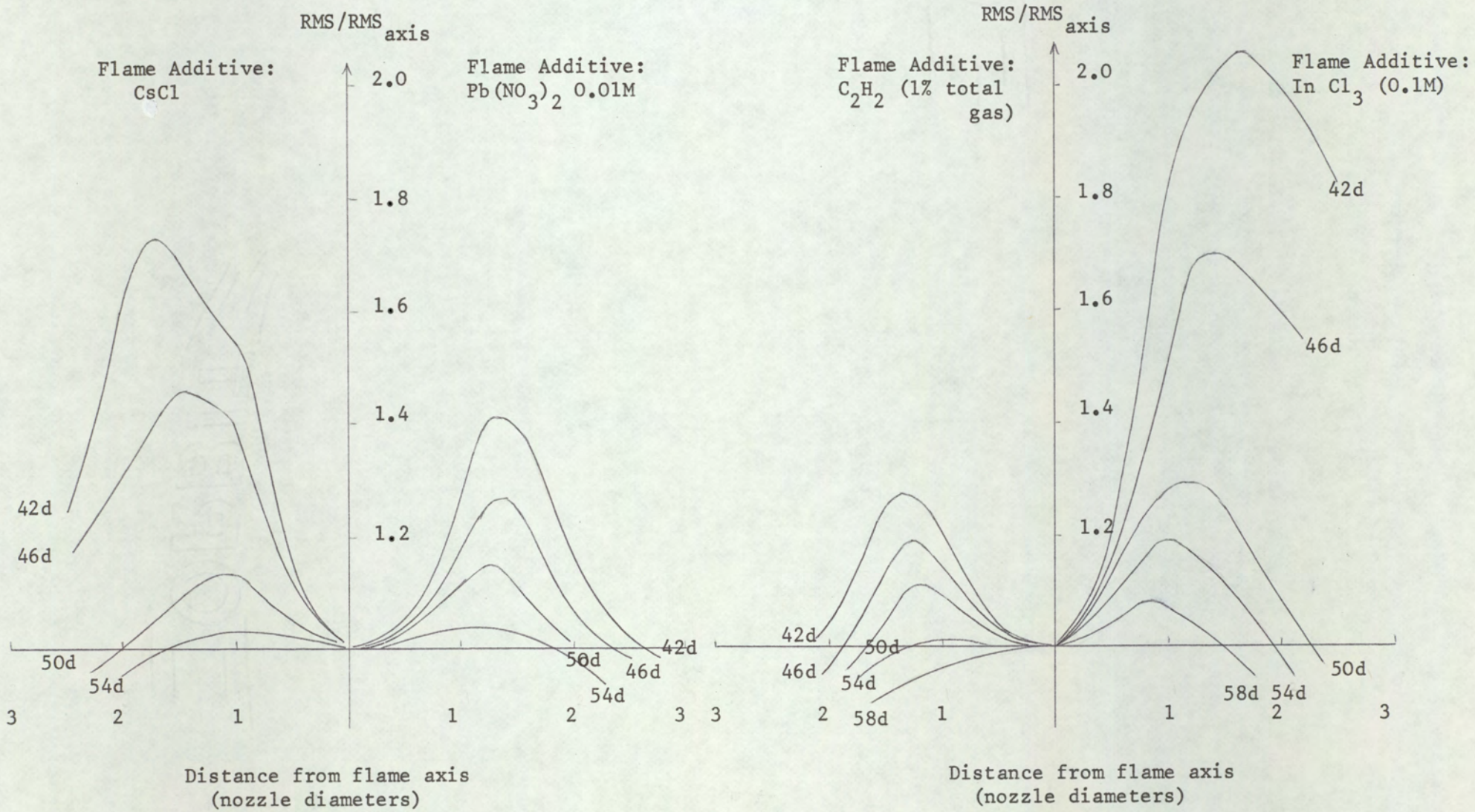

gradients across the flame. It may be recalled that the reaction zone of diffusion flames occurs where the "lumps" of fuel and air become adjacent so that combustion occurs at their common surface. Since the ionisation of the flame additives occurs primarily in the reaction zone the mean ion density levels attain a maximum in this region. Further, the close proximity of pockets of gas containing such high ion concentration levels to those of air, being void of charged species, will result in this region having a mean ion concentration gradient also at a maximum. Hence the fluctuations in ion concentration will be most intense in the vicinity of the reaction zone of a turbulent diffusion flame thereby producing the observed two off axis intensity peaks.

Increased flame height leads to a decrease in the quantity of unburnt fuel together with increased air entrainment such that the stoichiometric combustion mixture tends to move towards the flame axis. The formation of the single on axis peak obtained at the highest point studied is due to the stoichiometric mixture arriving at the axis. The reduction in peak maxima with increased distance from the burner is due to the chemical and turbulent dissipative processes lowering the ion density levels and thus the ion density gradients.

A further interesting property of the profiles illustrated in Fig. 13.2 is the variation in the peak intensity values for the additives used. The indium peak maxima exhibit the largest intensity values for all the heights studied with the acetylene additive providing the lowest values. As considered previously the indium seeded flame presents a chemically frozen system where the balance of the Sutton equation applies with the generation of fluctuations by the radial ion concentration

gradients equated to their destruction by dissipative smearing. When the charged species undergo a rapid recombination reaction as has been observed previously for H_3O^+ ions the ion density will become reduced producing a simultaneous lowering in the ion density gradients. Chemistry therefore in the case of ion recombination reaction provides an additional mechanism for the destruction of the ion density fluctuations leading to the observed decrease in intensity peak values for the acetylene seeded flame.

The addition of Pb(0.01M) to the flame yielded relative intensity values slightly greater than those obtained for acetylene addition. It was observed during the autocorrelation studies the decay of the total ion concentration ($Pb^+ + H_3O^+$) occurs at a slower rate than does the H_3O^+ concentration field. The chemical influence upon the mean ion concentration gradients is therefore lower for Pb addition resulting in the increased intensity values.

The caesium additive (0.1M) provided normalised root mean square values lower in comparison to those for indium. It has been observed previously that caesium addition leads predominantly to caesium ion production. The above experimental observations therefore indicate the presence of a rapid charged species reaction in a turbulent environment produces a lowering in the relative turbulent intensity compared to that for the chemically passive species irrespective of whether ion production or ion recombination dominates. These findings are analagous to those observed during the preliminary autocorrelation studies described in Chapter 8 and they provide further evidence for the chemistry-turbulence interaction phenomenon.

Using the two sets of results enables the effect of variation in seed concentration upon relative turbulent intensity to be predicted. The low Pb solution concentration of 0.01M has been shown above to produce relative intensity profiles slightly larger than those for acetylene addition. It has also been observed earlier in the work that increased lead concentration produces a lowering in the chemical decay rate of the total ion concentration field i.e. $(H_3O^+ + Pb^+)$. This in turn would lower the chemical contribution to the ion fluctuation dissipation such that the mean ion concentration gradients will be greater, therefore larger intensity values would be anticipated. On the basis of the autocorrelation results a high Pb solution concentration e.g. 0.3M would be expected to yield normalised root mean square profiles comparable to those for indium. Conversely, since the rate for caesium ion production decreases upon lowering the solution concentration the relative turbulent intensity profiles for a dilute caesium solution e.g. 0.0025M would be expected to converge on those values for the chemically passive (indium) case.

To conclude, further experimental evidence for the chemistry turbulence interaction has been obtained by use of a parameter referred to in the text as relative turbulent intensity. This has been defined as the ratio of the root mean square level of the probe signal to that at the flame axis at the relevant height i.e. RMS/RMS_{axial}. The presence of rapid ion chemical kinetics in a turbulent flame has been shown to produce a lowering in the relative intensity values compared to those for a chemically inert species. These results are closely analogous to those obtained during the

autocorrelation studies. Both sets of data have been employed to predict the effect of variation in additive concentration upon the relative intensity values. It has been further established during this investigation that turbulent intensity defined as $RMS/_{Mean}$ has in no way revealed the presence of the interaction phenomenon.

CHAPTER 14

A STUDY OF TURBULENT INTENSITY IN JETS AND TURBULENT DIFFUSION FLAMES

14.1 Introduction

The work discussed in this chapter was conducted at the Thornton Research Laboratories of the Royal-Dutch Shell Group. An investigation was made to determine whether the helium diffusion technique provided a suitable method for the measurement of turbulent intensity of velocity fluctuations in turbulent methane diffusion flames. At present disagreement exists between values of intensity measurements determined by different methods. Owing to this unsatisfactory situation it was considered to be of value to compare the helium diffusion method utilised by Westenburg [12] with the well established hot wire anemometer in isothermal air jets.

14.2 The Statistical theory of turbulent diffusions

The mechanism of turbulent diffusion is commonly compared to that of molecular diffusion where a molecule moves and collides with other molecules such that it migrates from some initial point. In the case of turbulent diffusion lumps of fluid migrate by a similar process, however the distances transversed are much greater. To consider turbulent diffusion in detail, assume the process occurs in a turbulent flow having a steady mean velocity $\overline{U}$ along the x axis of a Cartesian co-ordinate system. At the origin of the coordinate system a point source emits a continuous mass of fluid Q per unit time

at the velocity $\overline{U}$ into the turbulent flow. After a time t the fluid elements will become displaced normal to the x axis and turbulent diffusion theory gives the time averaged concentration. distribution of the diffusing fluid downstream of the point source as

$$\overline{S} = \frac{Q}{2\pi U \overline{y^2}_{av}} \exp -\frac{(y^2 + z^2)}{2 \overline{y^2}_{av}} \qquad 14.1$$

where $\overline{y^2}_{av}$ is the mean square displacement of the fluid elements in the direction normal to the x axis after a diffusion time $t = x/\overline{U}$. The concentration distribution thus obeys a Gaussian Law. The above equation does not take into account diffusion in the x direction. This has been shown to be valid for the conditions where the turbulent intensity $(\overline{u^2})^{\frac{1}{2}} / U \ll 1$

Since equation 14.1 represents a Gaussian distribution $\overline{y^2}_{av}$ may be identified as the variance or $(\overline{y^2}_{av})^{\frac{1}{2}}$ as the standard deviation. Providing the above inequality is obeyed the following applies:

$$(y)^2_{av} = (u)^2_{av} t^2 = \overline{(u)^2}_{av} x^2/U^2 \qquad 14.2$$

Thus the intensity of turbulence may be determined from a measure of the standard deviation of a distribution when the diffusion time is small i.e.

$$\left(\overline{(y)^2}_{av} \right)^{\frac{1}{2}} / x = \left((u)^2_{av} \right)^{\frac{1}{2}} / U \qquad 14.3$$

Hence by the use of a suitable tracer issued continuously from a point source and determining the spread of the tracer

after a short time interval enables the turbulent intensity to be evaluated. In this work helium was used since it is chemically and dynamically inert and its high thermal conductivity enables detection of its presence in very low concentrations using a katharometer detector.

14.3 Apparatus

The helium tracer was detected by a katharometer and a Topatron time of flight mass spectrometer.

The katharometer consists basically of a Wheatstone's bridge circuit. Two oppositing arms of the bridge consist of two heated metal filaments which behave as resistance elements. Reference and sample gases pass over the filaments. If the sample gas contains a tracer such as helium the rate of heat loss from the wire filament changes due to the high thermal conductivity for the gas. The temperature of the wire will change and thus its resistance causing imbalance in the bridge circuit. The out of balance signal may be recorded on a digital voltmeter and its value is a function of instantaneous concentration of tracer.

The time of flight mass spectrometer provides greater accuracy to be achieved in tracer detection since it yielded a measure of the absolute concentration. In this case no reference sample is required. The sample is introduced into the ionisation chamber where the ions formed by electron bombardment are accelerated by an electrostatic field of potential U. The velocity of the ions is related to their mass and the applied potential by the equation

$$v = \frac{2eU}{m}$$

where v = ion velocity, U = applied potential, m = mass of ion and e = electronic charge. Hence from the above expression the velocity is dependent upon the ion mass. The accelerated ions are then projected through a field free drift tube where ions of different mass become separated since the velocity is mass dependent. Thus the lighter, faster moving ions arrive at the end of the drift tube before the heavier slower moving species. The ions strike an electron multiplier and a scanning device enables the current collected/of ions of a specific mass to be measured.

Hot Wire Anemometer

The hot wire anemometer is the most widely used instrument for studying velocity fluctuations in isothermal turbulent flows. The device used in these studies was of the constant temperature type. The detecting element of the instrument used consisted of a 1.0×10^{-3} M length. The wire is maintained at a constant temperature and therefore at constant resistance. When the probe wire is inserted in a flow field fluctuations in current are produced. The probe is built into a Wheatstone's bridge circuit and an electronic feedback system compensates for any temperature and thus resistance variation resulting from the thermal loss produced by the turbulent flow. The feedback system changes the current through the wire when such changes in resistance occur almost instantaneously. The thermal loss from the wire is dependent upon the nature, temperature and velocity of the fluid being studied and also upon the type of probe used. If only the velocity is varied the fluctuations in current, recorded in terms of anemometer output voltage,

will be representative of the fluctuations in velocity. The relationship between the output voltage and flow velocity is highly non linear such that prior to use the hot wire probe requires calibration.

Calibration Procedure

The hot wire probe was positioned at the burner nozzle in the centre of the flow with the axis of the wire normal to the mean flow direction. One of the gas inlet tubes to the burner assembly was connected to a simple "U" tube water manometer. Air was fed through the other inlet tube such that the pressure drop across the nozzle was recorded on the manometer. By means of the Bernoulli equation the mean velocity of the air flow at the nozzle may be determined from the pressure difference reading:

$$\text{Pressure difference } \Delta P = \tfrac{1}{2} \rho \overline{U}^2$$

The D.C. component of anemometer output voltage V_B was recorded using a digital voltmeter such that for a series of air flow velocities the corresponding V_B readings enable a calibration curve to be plotted. The relationship between the output voltage and flow velocity was formulated by King and is given by:

$$V_B^2 = V_o^2 + K\overline{U}^n \qquad 14.4$$

where K is a constant. The exponent n has over a wide range of Reynolds numbers i.e.

$$0.1 < Re < 10^5$$

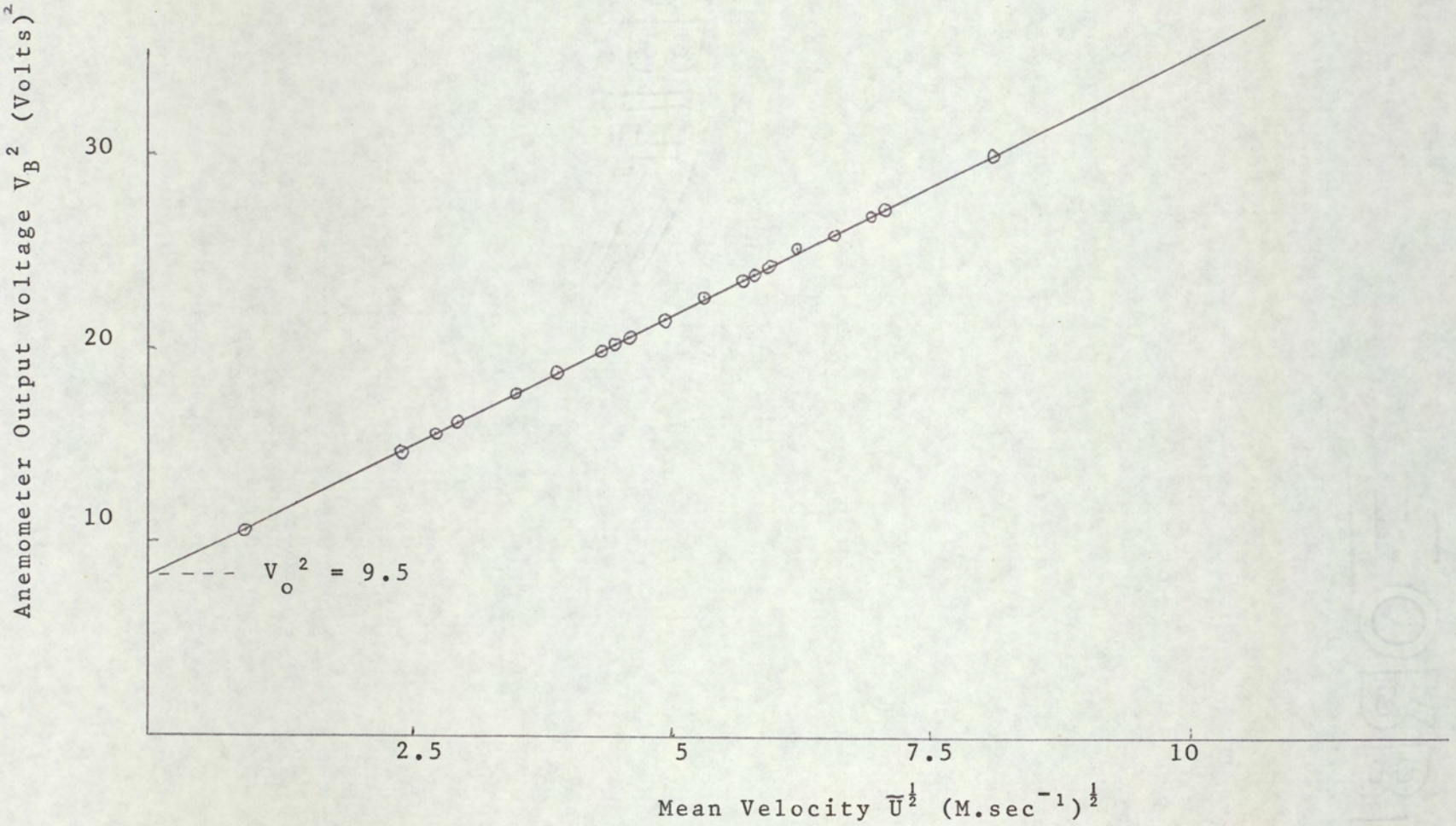

Fig. 14.1 Calibration Curve for Constant Temperature Hot Wire Anemometer using King's Law

$$V_B^2 = V_o^2 + BU^{\frac{1}{2}}$$

almost a constant value of between 0.4 - 0.5.

It was observed that under the conditions employed in this study a plot of V_B^2 versus $U^{\frac{1}{2}}$ produced a straight line graph indicating n = 0.5.

The calibration curve is shown in Fig. 14.1. The value of V_o^2 is also included, given as the value where the curve crosses the V_B^2 axis.

Measurement of Turbulent Intensity

The measurement of turbulent intensity is performed using the slope of the calibration plot. The graph has been shown to be a function of the type

$$V_B^2 = V_o^2 + KU^n \qquad 14.4$$

The slope of the plot is $\frac{dV_B}{dU}$ but

turbulent intensity $\frac{dU}{U}$ is required. Its derivation is as follows:

Differentiate equation 14.44 with respect to U

$$\text{i.e.} \qquad 2V_B \frac{dV_B}{dU} = nKU^{n-1} \qquad 14.5$$

$$\text{Since } K = \frac{V_B^2 - V_o^2}{U^n} \qquad 14.6$$

Substituting for K in equation 14.5

$$2 V_B \frac{dV_B}{dU} = n \frac{V_B^2 - V_o^2}{U^n} U^{n-1} = n \frac{V_B^2 - V_B^2}{U}$$

Rearranging:

$$\frac{dU}{U} = \frac{dV_B}{n} \frac{2}{V_B^2 - V_o^2} \qquad 14.7$$

The calibration plot has shown n = 0.5
Therefore using the V_o^2 value determined from the calibration graph and measurement of the root mean square value of the fluctuating component of the anemometer output voltage dV_B and that of the mean signal level V_B using a digital voltmeter enabled the turbulent intensity of velocity fluctuations to be evaluated.

14.4 Experimental Procedure

The turbulent diffusion flames and isothermal jets were generated using a burner comprising a mixing chamber and contoured nozzle of 6.25×10^{-3} M diameter to produce a flat mean velocity profile at the orifice. The jets, supplied with air from commercial cylinders, were operated at a nozzle Reynolds number of 2.4×10^4. The methane diffusion flame was observed to be susceptible to blow off at high flow rates; however a stable flame could be maintained at a nozzle Reynolds number of 6.0×10^3 and all measurements in the flame were determined at this value.

The helium tracer was introduced into both jet and flame from a quartz tube of 9.0×10^{-3}M internal diameter drawn out to approximately 5.0×10^{-4}M internal diameter. A right angled bend located at 1.0×10^{-2}M from the tube end enabled helium to be introduced into the turbulent flow in a direction parallel

Fig 14.2 Block Diagram of the Apparatus used for Helium Diffusion Experiments

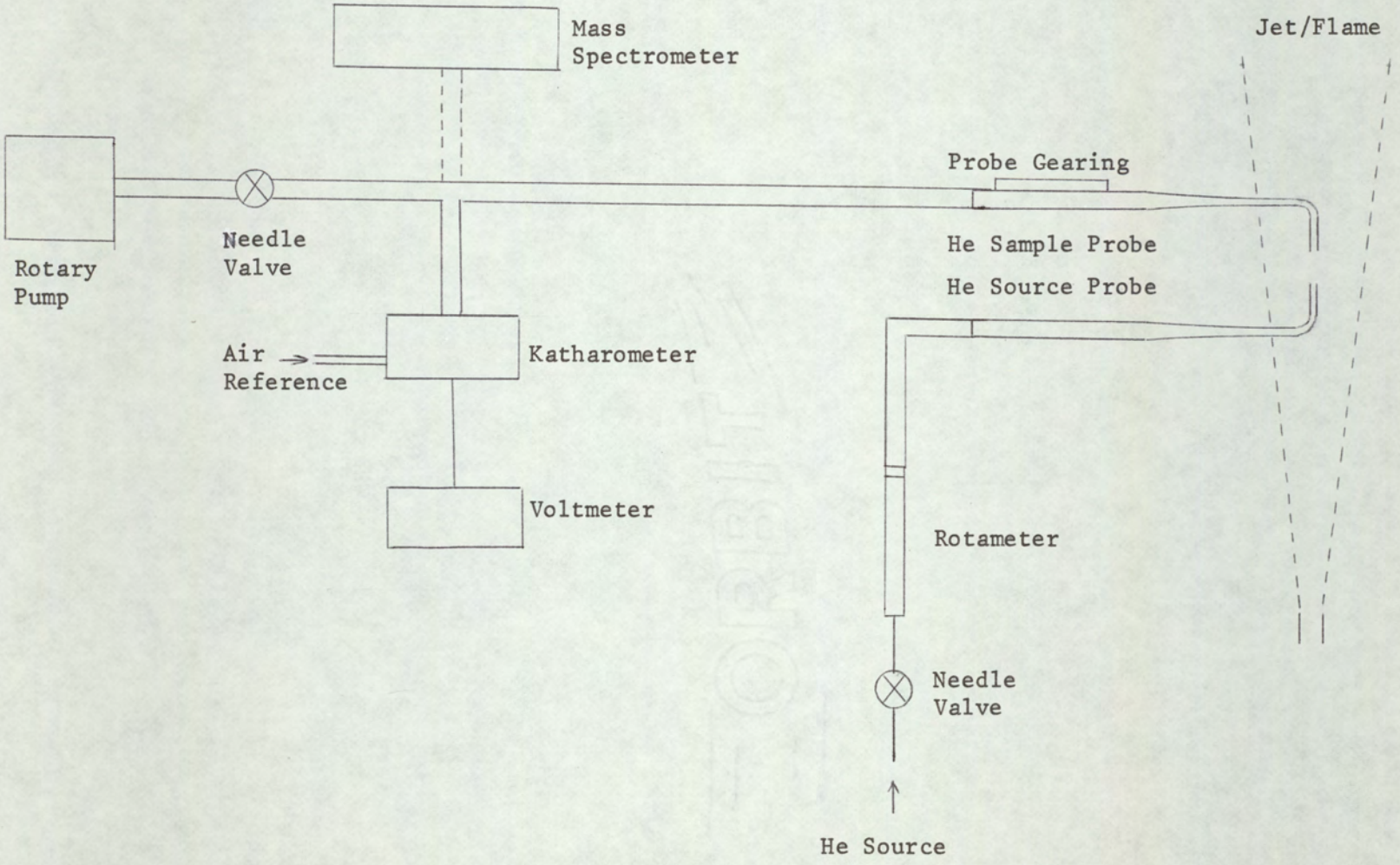

to the mean gas flow. The helium detector probe of similar construction, was positioned downstream of the source tube in the same vertical plane. The probe was mounted on an assembly driven by a fine screw thread such that a transverse scan across the source could be performed. This apparatus was also used to hold the hot wire probe. The helium flow into the source tube was monitored on a calibrated rotameter. The gas samples from the probe were drawn with the aid of a rotary pump, controlled using a Clockhouse needle valve at the inlet to the pump. Finer adjustment was obtained using Negretti diaphram valves which regulated the flow rates for the sample and reference gases into the katharometer. The flow rates were also monitored on calibrated rotameters. The reference gas was drawn from the atmosphere. The apparatus was modified when the mass spectrometer detector was used. The probe tube was connected directly to the rotary pump via a "T" junction, the remaining opening of the junction was attached to the inlet system of the mass spectrometer. The partial pressure within the instrument was maintained at 5.0×10^{-5} atm . A block diagram of the apparatus is shown in Fig. 14.2.

The turbulent intensity measurements were determined on the axis of the jets between one and twenty nozzle diameters above the burner at intervals of two nozzle diameters. The helium tracer concentrations were determined by scanning the probe across the source for a distance of 2.0×10^{-2}M on either side of the vertical at intervals of 2.0×10^{-3}M. The standard deviation of the distribution profiles were determined using the "61 per cent method". This is a simple procedure where the standard deviation $y = (\overline{y^2})^{\frac{1}{2}}$ occurs at 61% of the maximum ordinate i.e.

$$y = \exp(-\tfrac{1}{2}) = 0.607$$

The profiles were normalised such that the maximum ordinate was unity in each case.

14.5 Results and Discussion

A series of preliminary experiments were initially conducted in the air jet to determine the effects of:

(1) Variation in the flow rate of helium through the source tube upon intensity
(2) Variation in the sample flow rate through the probe.
(3) Variation in the separation distance between the source and probe tubes.

The helium diffusion method was observed to yield good Gaussian concentration distribution profiles independent of the mode of detection at all the positions studied. The helium flow velocity through the source tube was varied between $6 M sec^{-1}$ - $16 M sec^{-1}$ at a position where the mean gas velocity, determined using the hot wire anemometer, was $10 M sec^{-1}$. The intensity measurements showed, within the limits of experimental error, no effect within this velocity range. This suggested that irrespective of the exit velocity the helium tracer rapidly attained the mean stream velocity. This enabled the velocity to be fixed at all positions studied without requiring correction to account for changes in the mean gas velocity with distance from the burner. The flow velocity of the sampled gases from the jet at the probe nozzle was also varied between $6 M sec^{-1}$ and $16 M sec^{-1}$ at the same location. The intensity measurements were again observed

to be independent of the sample velocity over this range.

The variation in separation distance between the source and probe in the range 6.0×10^{-3}M - 1.85×10^{-2}M produced negligible change in the intensity measurements. This was expected on the basis of the turbulent diffusion theory via equation 14.3. These experiments were conducted using the katharometer detector only. Similar observations were made by Westenburg[12] in a premixed pentane air flame.

The turbulent intensity profiles determined on the axis of the isothermal air jet determined by:

(i) Hot wire anemometer
(ii) Helium diffusion using katharometer detector
(iii) Helium diffusion using mass spectrometer detector

are shown in Fig. 14.3.

Excellent agreement was observed for the values determined using the hot wire and the helium diffusion technique using the mass spectrometer detector. Slight deviation occurs at intensity values greater than 20%. The hot wire is considered not to yield reliable readings at and above 20% intensity. The profile obtained using the katharometer detector may be observed to yield low intensity values in comparison. The shape of this curve also does not have any resemblance to the other curves. These results imply the katharometer detector does not provide satisfactory intensity measurements suggesting greater accuracy is required for the determination of the tracer concentration, as achieved using a mass spectrometer.

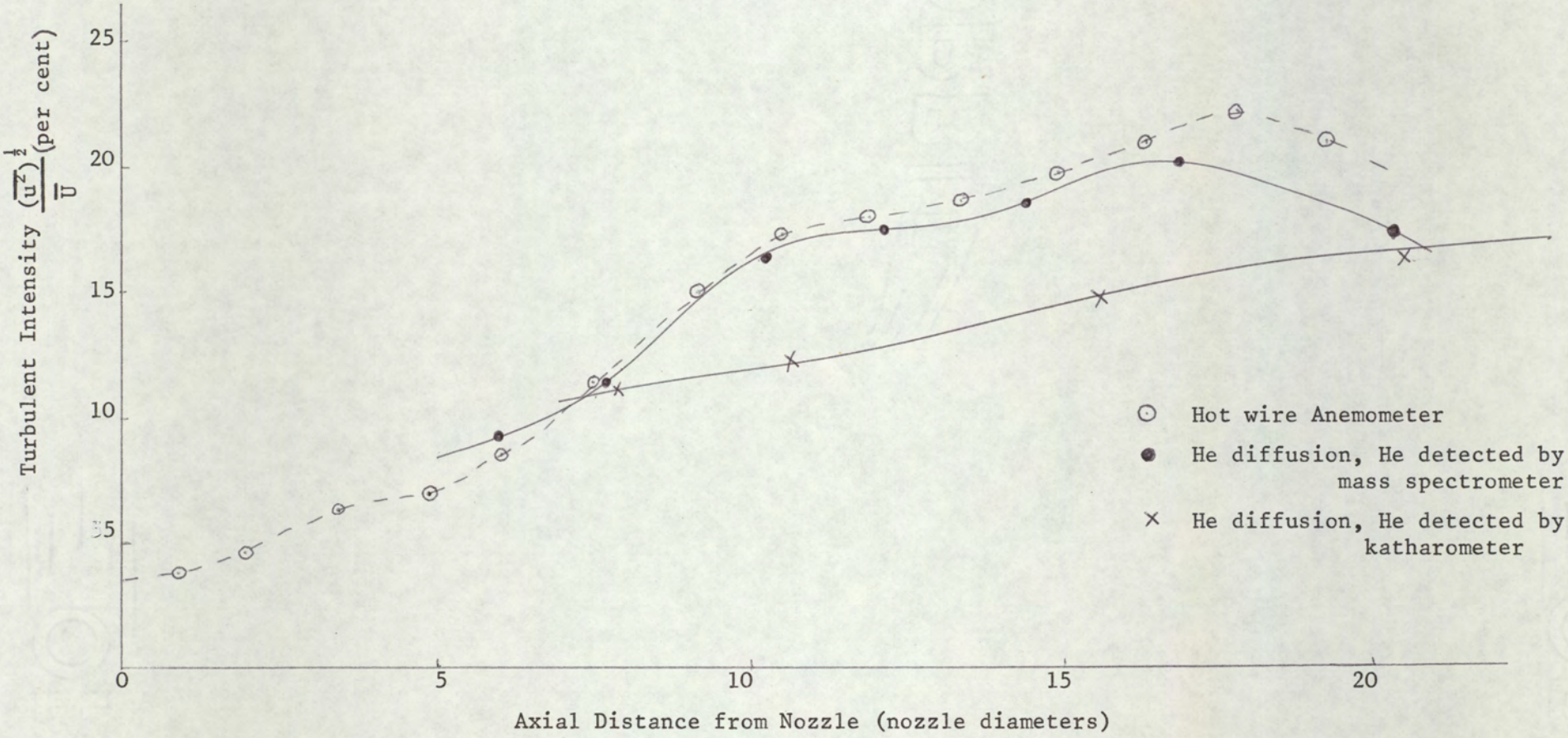

Fig. 14.3 Comparison between Axial Turbulent Intensity Profiles in Isothermal Air Jet of Nozzle Reynolds Number 2.4×10^4 using (a) Hot Wire Anemometer and (b) Helium Diffusion Technique

An interesting feature of the intensity curves is their shape (not observed using the katharometer). A high rate of increased intensity occurred between 2d - 3.5d followed by an almost horizontal portion to 5d. Between 5d - 10d the sharp rate of increase re-occurred terminating in a gradual decrease in values at greater axial distances. Similar profiles have been observed by other experimentalists[51] using hot wire anemometers in isothermal air jets however no explanation for the almost flat portion of the intensity curve has been given.

Owing to limited time few intensity measurements were performed in the turbulent methane flame. A comparison was however made of the intensities in the unignited methane gas jet and the flame at the axial positions 45d and 48d respectively. It was considered this experiment would provide insight into the effects of combustion upon turbulent intensity. The intensity values were determined using the helium diffusion technique employing the mass spectrometer to determine the tracer concentration distribution. Gaussian curves were again obtained for both jet and flame as shown in Fig. 14.4 and Fig. 14.5. The flame intensity values require correction to account for the contribution from molecular diffusion appreciable in the case of helium at elevated flame temperatures.

The diffusion due to turbulence and molecular motion are considered additive on the basis they both obey a Gaussian law[12].

$$\overline{y^2} = \overline{y^2}_{turb} + \overline{y^2}_{mol}$$

Fig. 14.4 Helium Distribution Profiles in (a) Methane Diffusion Flame and (b) Methane Jet each of nozzle Reynolds Number 6.0×10^3. Probe positioned 45d above burner on the flame axis.

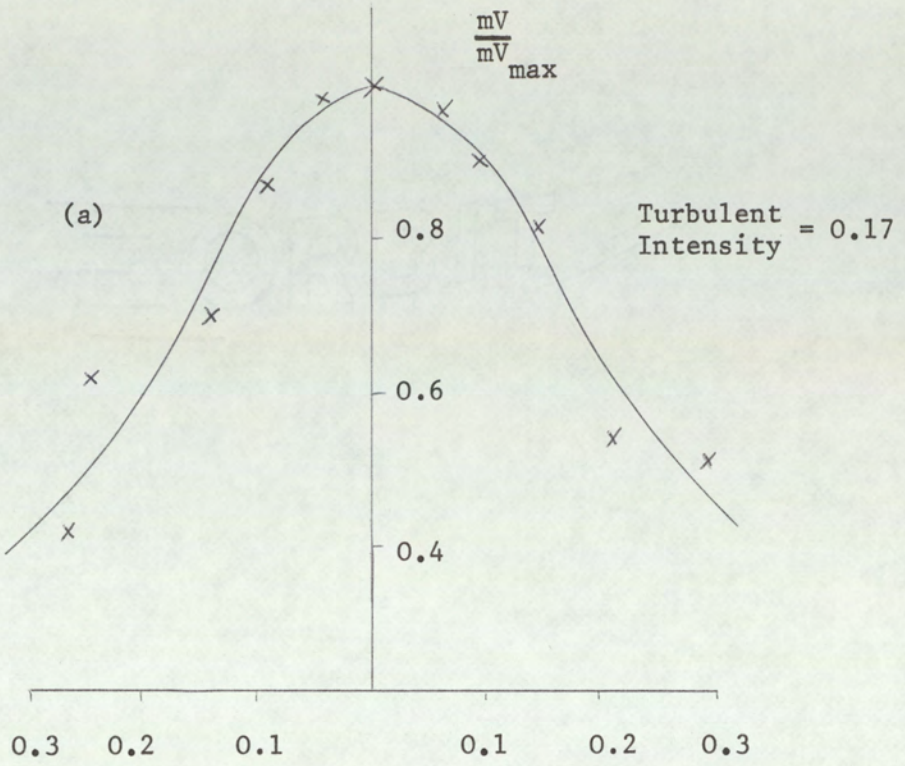

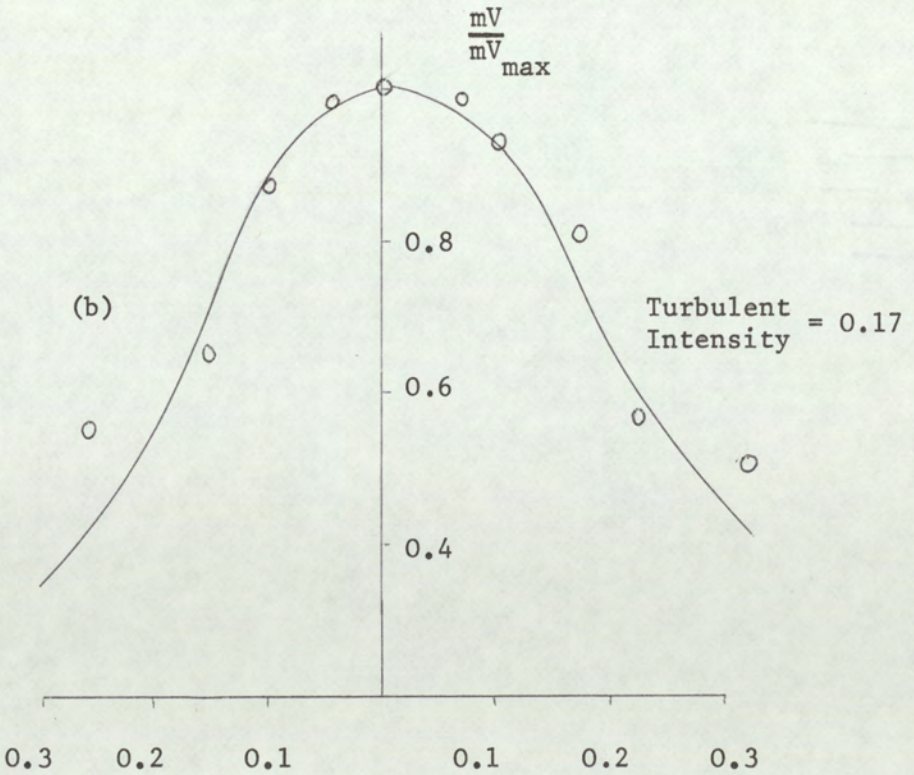

Fig. 14.5 Helium Distribution Profiles in (a) Methane Diffusion Flame and (b) Methane Jet each of nozzle Reynolds Number 6.0×10^3. Probe positioned 48d above burner on the flame axis.

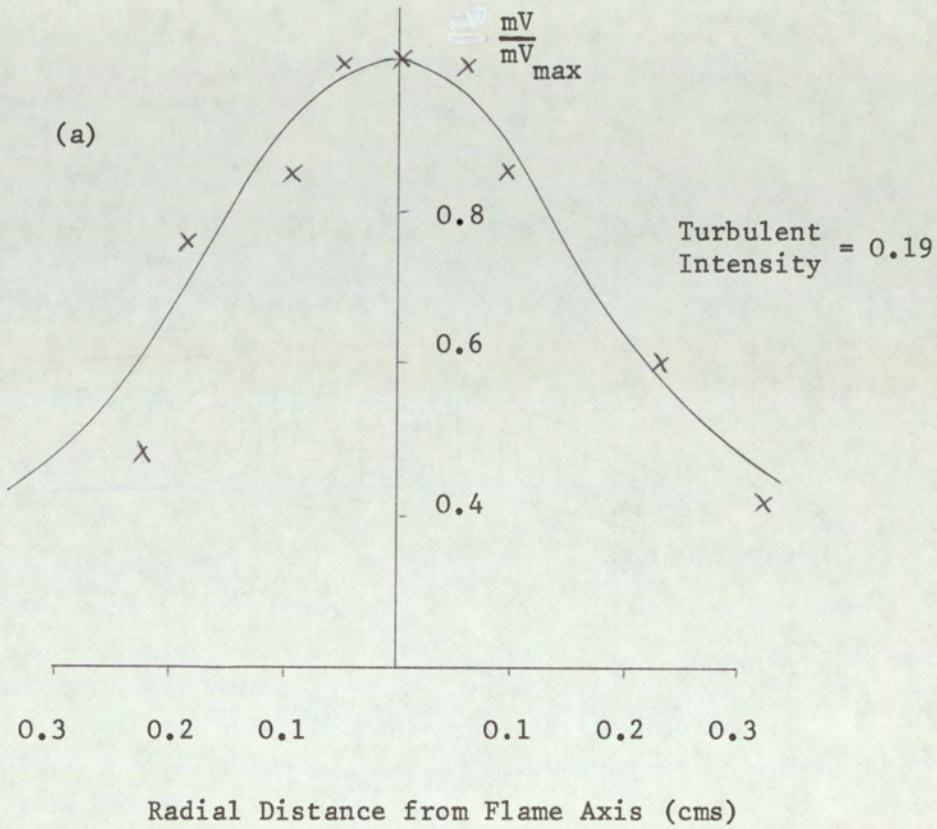

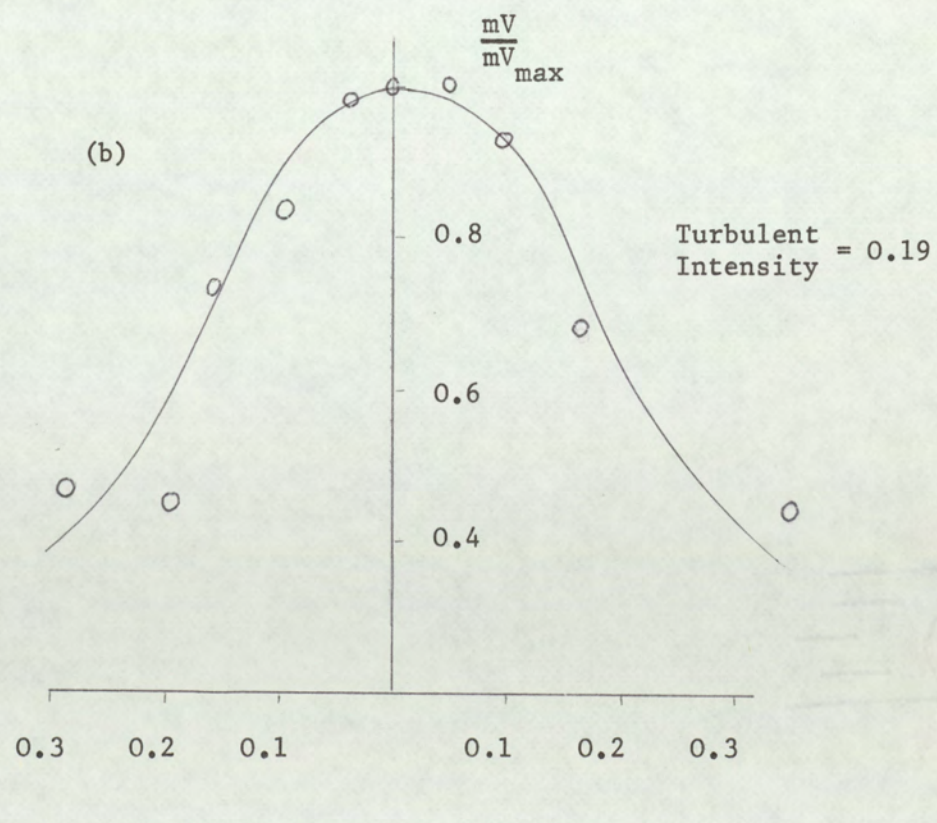

where $\overline{y^2_{mol}} = 2Dt$

D = coefficient of molecular diffusion for helium

t = observation time for diffusion process.

The term $\overline{y^2_{mol}}$ was not evaluated owing to the shortage of time. Its determination required a knowledge of the diffusion time t determined from the source probe separation distance and the mean gas velocity $\overline{U}$ at the position of interest i.e. $t = x/\overline{U}$. The mean gas velocity $\overline{U}$ may be determined using a Pitot probe as has been seen in earlier studies. The flame temperature is also required to enable determination of the diffusion coefficient for helium at this temperature. Despite this an important conclusion may be derived from the observed results. The uncorrected flame intensity values were observed to be equal to those at equivalent positions in the isothermal methane jet. Turbulent intensity measurements of 0.17 and 0.19 were recorded at the 45d and 48d positions respectively. Westenburg has estimated at 50% contribution due to molecular diffusion. It is reasonable to assume a similar influence in the turbulent methane flames studied here which suggests the combustion process leads to a considerable reduction in the turbulent intensity compared to values at corresponding positions in the unignited methane jet.

This observation therefore provides little evidence for flame generated turbulence in free turbulent methane diffusion flames. Similar conclusions regarding the influence of combustion upon turbulent intensity has been observed by Eichoff[17] and Becker and Brown[18]. A possible explanation for the above phenomenon was suggested by Eichoff to be due to a density

effect. He observed reduced intensities for jets spreading into surroundings of higher density and considered the reduced density upon ignition to behave similarly.

To conclude, the measurement of turbulent intensities have been satisfactorily determined using the helium diffusion technique providing the tracer concentration is measured using a mass spectrometer. The variation in intensity along the axis of isothermal air jets compare well with values measured using the well established hot wire anemometer. Poor agreement was observed when the helium tracer was detected by thermal conductivity methods. The comparison between intensity values in methane jets and flames suggest a decrease in values upon the onset of combustion.

CHAPTER 15

CONCLUSIONS

The main conclusions to be drawn from the project may be summarised as follows:

(i) Experimental evidence for the chemistry-turbulence interaction has been obtained by studying non-equilibrium ion chemical kinetics in a turbulent hydrogen diffusion flame. The presence of charged species capable of undergoing a rapid chemical reaction concurrently with turbulent mixing has been shown to have a pronounced effect upon the reactant species concentration field resulting in a reduction in the size of turbulent time and length scales compared to those for a chemically inert constituent. Evidence for this phenomenon was revealed using correlation analysis; power spectral density and probability functions provided no such information.

(ii) The autocorrelation and spacial cross correlation studies have, in addition, provided a simple picture of the structure of the ion concentration field throughout the flame, indicating it to be analogous to that of a scaler field in an isothermal jet.

(iii) The space-time cross correlation studies have shown the reduced turbulent scales produced by rapid chemical kinetics leads to an increase in the convective velocity of the turbulence pattern compared to that of a chemically passive species.

(iv) Comparison of mean velocity measurements in an isothermal hydrogen jet and turbulent hydrogen diffusion flame indicates combustion leads to an increase in mean gas flow rates. From conservation of momentum arguments this has been attributed to the reduced gas density as a result of the combustion process.

(v) The inverted electrostatic probe has proved to be a valuable instrument for the measurement of convective velocities in turbulent flames. This technique offers positive advantages over the space-time correlation method since no disturbing wake effects are created. It is considered the method does not provide the accuracy of the correlation function such that it should be regarded as a complementary rather than a replacement for the correlation method.

(vi) Further evidence for the interaction phenomenon was obtained from normalised root mean square measurements where similar trends to the autocorrelation studies have been discerned. The turbulent intensity measurements defined as the ratio of root mean square to mean signal level provided no such information.

(vii) The measurement of turbulent intensities of velocity fluctuations in an isothermal air jet using a helium diffusion technique, employing a mass spectrometer to detect the helium tracer, have shown good agreement with values determined using a hot wire anemometer. No such agreement was achieved using a katharometer to detect helium. Brief studies in a methane

isothermal jet and diffusion flame suggest a marked reduction in turbulent intensity upon combustion providing little evidence for the flame generated turbulence concept.

Having obtained experimental evidence for the chemistry-turbulence interaction, the author considers further work in the field might be directed towards the construction of a mathematical model of a turbulent flame relating the interaction process in terms of a correlation function. Attempts to derive such a relationship were made by the author, however following advice concerning the complexity of the mathematics this was not continued.

The electrostatic probe technique has shown itself to be a versatile and valuable diagnostic tool for the study of charged species reactions in a turbulent environment. Its combined properties of high spacial and temporal resolution make the instrument suitable for the measurement of local turbulent parameters. A disadvantage of the technique in the time varying situation is the disturbance created to the dynamic gas flow. This problem, it may be recalled became particularly apparent during the longitudinal and space-time correlation studies. It is considered the probes employed in these studies could be reduced in size to alleviate the problem, however whenever a body is immersed in a turbulent flow a disturbance to the flow will always be created.

The use of newly developed optical techniques for the study of other flow properties are beginning to overcome some of the instrumental difficulties in combustion systems. Of these, the crossed beam correlation technique[50] has been successfully

used for the measurement of cross correlation functions for velocity fluctuations. A major difficulty in the use of such equipment for determination of local turbulent parameters is the low signal to noise ratio such that the correlation coefficient levels are extremely small. Under such conditions the use of the present analog devices as employed in this work are not sufficiently sensitive making the requirement of expensive recording and data sampling equipment essential. The study of other flow properties such as velocity, temperature and highly reactive radical species is however necessary to provide further information of the chemical and physical processes occurring in turbulent combustion and to elucidate the mechanism for turbulent propagation.

APPENDIX

COMPUTER PROGRAMS

```
FAST FOURIER TRANSFORM
;

begin
      real AV,PTW,ptw,scanrate,SUM,mn,rm;
      integer CY,I,J,m,N,NOCY,cyl,head,sector,cylstoreloft,firstcyl,lastcyl,
              wks, p, storem,storen,dev,dev2,cm,comd,data,id,MAINCT,SUBCNT,
      boolean SHORT RUN,first;
      integer array CNTRL[1:14];


  begin
            comment CBS:;
            real array B,A[0:4096], PRESGR[0:150];
            comment CBS : ;
            integer array C[0:50] ,MAINTT,SUBTT[0:24];

            switch SSS :=dispatch;

            first:=true;

            code  30  <+4> : 72 5120
                  75  5122 : 20 i
                  70  0    : 03 <+2097152>
                  20  j    :                ;
            if j=0 then begin
             code 30 <9ALP>  : 20 nR;
             ne:=2;
             end else begin
             code 30 <9CHAR> : 20 nR;
             ne:=11;
             end;
            if i=0 or j=0  then SHORT RUN:=true else SHORT RUN :=false;
            if SHORT RUN then begin  code 30 <9ERRINT> :20 1;
                                     entercp(1,1,0);
                              end;
dispatch:
begin comment segment :; integer qwe;
                        switch sqp:= found,getcomn,error;
            if first then begin
                        print punch(3),ß£1? Disc ready ßu? ?;
                        if SHORT RUN then wait;
                        CNTRL[1]:=4136;  CNTRL[2]:=4852;   CNTRL[3]:=4638;
                        storem:=m:=12;storen:= N:=8192;    scanrate:=16000;
                        CNTRL[4]:=5038;  CNTRL[5]:=4753;   CNTRL[6]:=3353;
                        CNTRL[7]:=4836;  CNTRL[8]:=3838;   CNTRL[9]:=4841;
                        CNTRL[10]:=5152; CNTRL[11]:=3536;  data:=id:=0;
                        CNTRL[12]:=5240; CNTRL[13]:=4540;  CNTRL[14]:=5140;
                        cm:=TOTCT:=MAINCT:=SUBCNT:=MHP:=SHP:=TH:=0;
```

```
        MAINCT:=MAINCT+1; SUBCNT:=SUBCNT+1; TOTCT:=TOTCT+1;
        print ££14? MEAN ?, samoline,mn,£  MEAN SQUARE ?,rm;
        goto dispatch;
    end;
    end;



    begin comment segment : ; real XYZ ;
    procedure data onto disc (firstcyl, lastcyl);
    value firstcyl, lastcyl ;
    integer firstcyl,lastcyl ;
       begin integer   A1,A2  ;
            integer   holdimask, i, j, a1, a2, wks, N , head,sector,
            switch ss := again, exit, start, notav, finish, st ag,

       boolean procedure  key(n) ;
            value n ;
            integer  n ;
            begin     code  70  0 : 23  n ;
                      key := n ≠ 0 ;
            end;
       library  ins  1;
```

comment This program transfers data at a maximum input rate of just over 10 KHz to disc store. The starting and finishing cylinders are specified by the user,and the data is stored continuously between them (inclusively).

```
    cyl := firstcyl - 1 ;
    A1:=a1;
    A2:=a2;
    head := sector := 0 ;



        discdata(firstcyl,head,sector, 64, A1, cylstoreleft, true );

    st ag: print punch(3), ££1?startrans key1?;
        i := if key(1) then 1 else 0 ;

    keydelay:  if i = 1 then
        begin
           if key(1)  then  goto keydelay  else  goto start ;
        end  else
        begin
           if not  key(1)  then  goto keydelay  else  goto  start ;
        end;
    start:      code   36 7886      : 20 holdimask;
                code   76 7680      : 03 <+1>
                       42 3,        : 40 notav
                       30 <00 1275 : 00 0> : 27 8191
```

```
                    30 <+5242880> : 67  a2
                    77 0          : 30 2,
                    73 7932       : 44 8147 ;
      goto  again ;
notav:print punch(3),£€1?poriphoral devico not availablo?;
      wait ;
      goto st ag;

comment   OMITTED;

again: head := sector := 0 ;
      cyl := cyl + 1 ;
      code  02 lastcyl: 05 cyl
            42 exit   :;

      code  76 7680 : 03  <+1>
            42  3,  : 40  finish
            30 <00 1403 : 00 0> : 27 8191
            30 <+5242880>: 67 a1
            77  0 : 30  2,
            73 7932 : 44 8147 ;
      discdata(cyl, head,sector, 1280, A2, cylstoreleft,true);
      code  76 7680 : 03  <+1>
            42  3,  : 40  finish
            30 <00 1147 : 00 0> : 27  8191
            30 <+5242880> : 67 a2
            77 0 : 30  2,
            73  7932 : 44 8147 ;
      discdata(cyl, head,sector, 1408, A1, cylstoreleft, true);
      code  76 7680 : 03  <+1>
            42  3,  :  40  finish
            30 <00 1275 : 00 0> : 27 8191
            30 <+5242880> : 67  a1
            77  0 : 30  2,
            73 7932 : 44 8147 ;
      discdata(cyl,head,sector,1152,A2,cylstoreleft,true);
      code  76 7680 : 03  <+1>
            42  3,  :  40  finish
            30 <00 1275 : 00 0> : 27 8191
            30 <+5242880> : 67  a2
            77  0 : 30  2,
            73 7932 : 44 8147 ;
      discdata(cyl,head,sector,1280,A1, cylstoreleft,true);
      code  76 7680 : 03  <+1>
            42  3,  : 40  finish
            30 <00 1275 : 00 0> : 27 8191
            30 <+5242880> : 67  a1
            77  0  : 30  2,
            73 7932 : 44 8147 ;
      discdata(cyl,head,sector, 1280, A2,cylstoreleft,true);

      code 30 a1 : 10 a2
           20 a1 :30  A1
           10 A2 : 20 A1;

      code  40 again :;
```

```
finish:print punch(3), ¢£1?end of transfer.Last cyl complotely filled =?,
                        samoline, cyl - 1 ;


exit:  code  76 7680     : 03 <+8>
             42 2,       : 40 0,
             30 holdimask: 20 7886
             ;
end;
if cm=3 then begin read reader(dev),firstcyl,lastcyl;

      if SHORT RUN then data onto disc(firstcyl,lastcyl)else stop;
      goto dispatch;
      end;
      end;
begin comment segment : ; real A3D ; integer  Z ;
            library  ins 2;
            if cm=4 then begin switch sad:=exit; read reader(dev),cyl;
            print sameline,cyl;
            head := sector := 0 ;
            p := 2↑m ;
            for k := 0 step 1 until 2 do
            begin
            for j := 0 step 1 until 3 do
            begin
                  discdata(cyl,head,sector,1600,Z,cylstoreloft,false);
                  for i := 1 step 1 until 1600 do
            begin

                  code      .   30 Z : 04 i
                                20 wks/30 0
                                41 4,: 03 <+4095>
                                20  wks :40  5,
                                03 <+4095>:21  wks  ;
                  l := i + j*1600 + k*6400 ;
                  if l < p then A[l-1] :=wks else B[l-p-1] := wks ;
                  if l = 2*p then goto exit ;
                  end;
            end;
            cyl := cyl + 1 ;
            head := sector := 0 ;
            end;
exit:       j:=address(A);k:=address(B);mn:=rm:=0;
for i:=0 step 1 until N/2-1 do
      code 30 i : 04 j
           72 5120 : 75 5122
           20 SUM : 60 mn
           20 mn :30 SUM
           63 SUM : 60 rm
           20 rm : 30 i
           04 k : 72 5120
           75 5122 : 20 SUM
           60 mn : 20 mn
           30 SUM: 63 SUM
```

```
            60 rm : 20 rm;
        mn:=mn/N; rm:=rm/N;
print lineprinter,ff14??,samoline,f Moan of data ?,mn,£   Moan square?,rm;
data:=1; goto dispatch; end;


        if cm = 5 then
        begin
        read reader(dev),i;
        print samoline,i,ff12??;


            if i = 1 then
            begin
                real  a2 ;
                integer  a1, i;
                punch(1) ;
                print ff60??;
                for  i := address(A),address(B) do
                begin
                      for j := i  step 1 until i + p - 1 do
                      begin
                            code  30  j :
                                  72  5120 : 75 5122
                                  20  a2 : ;
                            a1 := entier(a2 + 0.5) ;
                            print digits(4), a1 ;
                            if entier((j-i)/100)*100=j-i then print ff10??;
                      end;
                      print  ff30??;
                end;
            end;

            if i = 2 then
            begin
                integer  char, a1, i ;
                real a2 ;
                library output ASTON;

                punch(1) ;
                print ff60??;
                for j := address(A), address(B) do
                begin
                      for i := j  step 1 until j   p - 1 do
                      begin
                            code  30  i :
                                  72 5120 : 75 5122
                                  20  a2 : ;
                            a1 := entier(a2 + 0.5) ;
if a1 < 0 then begin   outpu(29) ;  a1 := - a1 ; end  else outpu(30) ;
char := a1 div 1000 ;
if char ≠ 0 then outpu(char) ;
wks := char ;
a1 := a1 - char*1000 ;
char := a1div 100 ;
```

```
        if char = 0 and wks = 0  then a1 := a1 else outpu(char) ;
        wks := char ;
        a1 := a1 - char*100 ;
        char := a1div 10 ;
        if char = 0 and wks = 0 then a1 := a1 else outpu(char) ;
        a1 := a1 - char*10 ;
        char := a1;
        outpu(char);
        outpu(10) ;
    end;
print ££r30??;
end;
end;


        if i = 3 then
        begin
              integer i ;
               j := 9 ;
              for i := 0 step 1 until p-1  do
              begin
                    print sameline, A[i] ;
                    if i = j then
                    begin
                       print ££1??;
                       j := j + 10 ;
                    end;
              end;
              print ££14??;
              j := 9 ;
              for i := 0 step 1 until p-1 do
              begin
                    print sameline, B[i] ;
                    if i = j then
                    begin
                       print ££1??;
                       j := j + 10 ;
                    end;
              end;

end;
goto dispatch;
end;
comment Autocorrelation;
begin
      real SUM,RZERO;
      integer I,Int,M,R;integer s,N;

      if cm=6 then
      begin
      read reader(dev),N,M,Int;
      print sameline,N,M,Int;
      s:=storen/2-1;
      begin
            comment CBS:; real array MEAN[0:M];
            i:=address(A);j:=address(B);
```

```
                RZERO:=0;
                for I:=0 step 1 until N-1 do
                codo  30 s: 05 I
                      41 6,: 30 i
                      04 I : 72 5120
                      75 5122 : 20 AV
                      63 AV : 60 RZERO
                      20 RZERO : 40 8,
                      30 I : 05 s
                      04 j :44 2,;
                RZERO:=RZERO/N;
                for R:=0 step Int until M do
                begin
                      SUM:=0;
                      for I:=0 step 1 until N-R-1 do
                      codo  30 s :05 I
                            45 4, :30 i
                            04 I : 72 5120
                            75 5122 : 20 AV
                            44 6, : 30 I
                            05 s : 04 j
                            44 2, : 30 I
                            04 R : 20 1
                            30 s : 05 1
                            45 13, : 30 i
                            04 1 : 72 5120
                            75 5122 : 63 AV
                            60 SUM : 20 SUM

                            40 16, :30 1
                            05 s : 04 j
                            44 10, :;
                      MEAN[R]:=SUM/(N-R);
                end;
                      print ¢£12s8?R¢s0?T SECS£s9?MEAN?;
                for I:=0 step Int until M do
                print  £1??,I,££s6??,sameline,I/scanrate,¢£s6??,scaled(4),
                print ¢£1?Mean Square =?,sameline,RZERO,¢£1??;
        end;
        goto dispatch;
end;
end;


comment  pdf;
begin real  min,max,wka,wkb; integer under,over,ilog;

if cm=7 then begin read reader(dev),ilog,min,max,j;
print sameline,ilog,min,max,j;

begin
comment CBS:;
real array ara[0:j];
comment CBS:;
integer array con[1:j];
ptw:=(max-min)/j; ara[0]:=min;
```

```
for i :=1step 1 until j do
begin
con[i]:=0;
 ara[i]:=ara[i-1]+p'w;
end;
under:=over:=0;
for i := 0 step 1 until N/2-1 do
begin
wka:=if ilog#1 then A[i] else  4342944819*ln(A[i]+3162.27766);
wkb:=if ilog#1 then B[i] else .4342944819*ln(B[i]+3162.27766);
begin switch pgr:=WERE,WERE2;
if wka<min then begin under:=under+1; goto WERE; end;
if wka>max then begin over:=over+1; goto WERE; end;
m:=entier((wka-min)/ptw)+1;
con[m]:=con[m]+1;
WERE:
if wkb<min then begin under:=under+1; goto WERE2; end;
if wkb max then begin over:=over+1; goto WERE2 ; end;
m:=entier((wkb-min)/ptw)+1;
con[m]:=con[m]+1;
WERE2:end;
end;
print £1?
lowlim      highlim          mid            counts
------      -------          ---            ------

?;

print ££1??,samelino,ara[0],£s2??,ara[0],£s2??,ara[0],£s2??,under;
for i:=1 step 1 until j do begin
print £1??,samelino,ara[i-1], £s2??,ara[i],£s2??,(ara[i-1]+ara[i])/2,
end;

print £1??,samelin ,ara[j], £s2??,ara[j],£s2??,ara[j], £s2??,over;
print  £14??;
   SUM:=0;
for i:=1 step 1 until j do
SUM:=SUM con[i];
SUM:=SUM over under;
print £1s20?SUM =?,samelin , £s10??,SUM;
if ilog=1 then  print    £1?          distr bution of log(x+3162.27766)
                  N.B. log 3162.27766= ,5 ?;

end;end;end;
end;



begin comment segmen :; real POR ;
library  fourier pack;
if cm=8 then begin
            REALTRANSFORM(A,B,m,false);
            for I:=0 step 1 until 2^m do
            A[I]:=A[I]*A[I]+B[I]*B[I];
            if id#1 then begin print punch(3),£1?ERROR ID  ?;
if not SHORT RUN then stop; data:=0
wait; goto dispatch; end;
```

```
                data:=2;

                print ££1s10?          POWER SPECTRAL DENSITY?;
                print ??12??s5?FREQUENCY       (Hz)                    POWER (db/Hz)?;
                begin
                      PTW:=scanrate/N;
                      C[0]:=-1;
                      B[0]:=0.0;
                      for CY:=1 step 1 until NOCY do
                      begin
                            B[CY] := PRESCR[CY] ;
                            if PTW≤B[CY] then
                            begin
                                  C[CY]:=entier(B[CY]/PTW);
                                  if C[CY]≠C[CY-1] then
                                  begin
                                        SUM:=0;
                                        for J:=C[CY-1] + 1 step 1 until C[CY] do
                                        begin
                                              if J>N/2 then begin print ££1?
                                        goto dispatch;
                                              end;
                                              SUM:=SUM+A[J];
                                        end;
                                        AV:=SUM/(B[CY]-B[CY-1]);
                                        print ££1??,sameline,B[CY-1],??s3??,

                                  end;
                            end else
                            begin
                                  C[CY]:=C[CY-1];
                                  B[CY]:=B[CY-1];
                            end;
                      end;
                      if C[NOCY]≠entier(2↑m) then
                      begin
                            SUM:=0;
                            for J:=C[NOCY]+1 step 1 until entier(2↑m) do
                            SUM:=SUM+A[J];
                            AV:=SUM/(scanrate/2-B[NOCY]);
                            print ??12?? ABOVE ?,sameline,B[NOCY],??s12??
                            print ??1??;
                      end;print ??1??;
          gotodispatch ;

and;  end;  begin  comment CBS: ;
  integer array c[0:140];
if cm≠9or not SHORT RUN  then goto dispatch;
library loggplot pack;
begin switch sdf:=label1;
            axes(1,1,2,10.0,3,true,1000.0,10.0,3,0,0,10,1.0,0.0);
                  c[0]:=-1;
                  B[0]:=0.0;

                  for CY:=1 step 1 until 140 do
                        begin
                        B[CY]:=10+(CY↑1.8-1);
```

```
if PTW<B[CY]then
      begin
            c[CY]:=entier(B[CY]/PTW);
            if c[CY]≠c[CY-1]then
                  begin
                        SUM:=0;
                        for J:=c[CY-1]+1 step 1 until c[CY]do
                        if J>N/2 then goto labelt else
                        SUM:=SUM+A[J];
                        AV:=4.3429*ln((SUM/(B[CY]-B[CY-1]))/rm);
                        movepen(B[CY],AV,1);
                  end;
      end else
      begin
            c[CY]:=c[CY-1];
            B[CY]:=B[CY-1];
                        end;
                  labelt: i:=0;
            end;
          movepen(400,-4,0);
          print plotter(2,1),£ FREQUENCY ?;
          movepen(400,-7,0);
          print plotter(2,1),£     HZ?;
          movepen(5,0,0);
          print plotter(2,7),£ dB/HZ?;
          movepen(100,10,0);
          print plotter(4,1),£ POWER SPECTRAL DENSITY.?;
          movepen(100,-10,0); print plotter(2,1),TOTCT,MAINCT,SUBCNT;
          movepen(10,0,0);
          stoplot;
          end;
          goto dispatch;
    end;
end;
end;

end;
```

ACKNOWLEDGMENTS

I wish to express my gratitude to Mr. H. Williams and Professor F.M. Page for their continued guidance and encouragement throughout the course of this work.

I also wish to thank Dr. Z.M. Ranic, formerly of the Physics Department for many useful and informative discussions on the use of statistical methods for the analysis of random data, Mr. J. Ludlow and Mr. L. Parker for constructing much of the apparatus used during the project, and to Mrs. M. Bellamy for typing this thesis. Finally, my thanks to the Science Research Council and the Royal Dutch Shell Company for a C.A.P.S. award.

References

1. Glassman, I and Eberstein, I.J, A.I.A.A., Vol. 1, No. 6 (1963)
2. Corrsin, S, J. Fluid. Mech., 11, 406 (1963)
3. Lee, J., J. Phys. Fluids, 9, 9, 1753 (1966)
4. O'Brien, E.E., J. Phys. Fluids, 14, 7, 1326 (1971)
5. Su, C.H. and Lam, S.H., J. Phys. Fluids 6, 10, (1963)
6. Clements R.M. and Smy, P.R., Proc. I.E.E., 117, 8, (1970)
7. Hinze, J.O., Turbulence, 1, McGraw-Hill Book Company (1959)
8. Hinze, J.O., Turbulence, 148, McGraw-Hill Book Company (1959)
9. Knewstubb, P.F and Sugden, T.M., Nature 181, 474, (1958)
10. Padley, P.J. and Sugden, T.M. Eighth Symposium (Int.) on Combustion. Williams and Wilkins, Baltimore, 164, (1962)
11. Karlovitz, B, Denniston, D.W., Wells, F.E., J. Chem. Phys., 19, 541, (1951)
12. Westenburg, A.A., J. Chem. Phys., 22, 5, 814, (1954)
13. Lawrence J.C., N.A.C.A. Rept. 1292.1 (1956)
14. Corrsin, S and Uberoi, M.S., N.A.C.A, T.N. 1865 (1949)
15. Hawthorne W.R., Weddell, D.S and Hottel, H.C., Third Symposium (International) on Combustion 266, Williams and Wilkins, Baltimore (1949)
16. Hawthorne, W.R. and Hottel, H.C. Third Symposium (Int.) on Combustion 254, Williams and Wilkins (1951)
17. Eickhoff, H, Chem. Ing. Techn., 40 (22), 995, (1968)
18. Becker, M.A., and Brown, A.P.G., Twelfth Symposium (International) on Combustion 1059 Williams and Wilkins (1969)
19. Gunther, R and Simon, H, Twelfth Symposium (International) on Combustion, 1069, Williams and Wilkins (1969)
20. Damkohler, G, Z. Elektrochem, 46, 601, (1940)
21. Shchelkin, I, J. Tech. Phys. (U.S.S.R), 13, 520 (1943)
22. Williams, D.T and Bollinger, L.M., Third Symposium (International) on Combustion, 176, Williams and Wilkins, 1949

23. Richmond, J.K., Donaldson, W.F., Burgess, D.S., Jet Propulsion, 28, 393 (1959)

24. Summerfield, M., Reiter, H.S., Kebely, V., Mascodo, R.W., Jet Propulsion, 25, 577, (1955)

25. Basu, P. and Bhaduri, D., Combustion and Flame, 18, 303, (1972)

26. Langmuir, L and Mott-Smith, H.M., Phys. REv., 28, 727, (1926)

27. Johnson, E.O., Malter, L., Phys. Rev., 80, 58, (1950)

28. Travers, B.E.L. and Williams, H, Tenth Symposium (International) on Combustion 657, Williams and Wilkins (1965)

29. Shultz, G.J. and Brown, S.C., Phys. Rev. 98, 1642 (1955)

30. Cohen, I.M., J. Phys. Fluids, 6, 10, 1492, (1963)

31. Padley, P.J. and Sugden, T.M., Eighth Symposium (International) on Combustion, 164, Williams and Wilkins (1962)

32. Thomas, D.L., J. Phys. Fluids, 12, 356, (1969)

33. Lam, S.H., J. A.I.A.A., 2, 356, (1964)

34. Miller, E.R., Ph.D Thesis, University of Aston, 1969

35. Griffiths E. and Awbrey, J.H., Proc. Roy. Soc., A, 123, 401 (1929)

36. Gaydon, A.G. and Wolfhard, H.G., Flames 239, Chapman and Hall Ltd. (1970)

37. Mavrodineanu, R., Ubiteux, H., Flame Spectroscopy, 30, John Wiley and Son, Inc., (1965)

38. Soundy, R.C. and Williams, H, 26th Meeting of Propulsion and Energetics Panel, Agard, Pisa, Italy, September (1969)

39. Jensen, D.E. and Padley, P.J. Trans Farad Soc., 62, 2132 (1966)

40. Padley, P.J., Page, F.M. and Sugden, T.M., Trans Farad Soc. 57, 1552, (1961)

41. Jensen, D.E. and Kurzius, S.C., Rate Constants for Calcs. on Rocket exhaust flow fields, p. 8, Aerochem. Research Laboratories, Inc., (1967)

42. Wygnanski, I. and Fieldler, H.E., Boeing Scientific Research Laboratories, D1 - 82 - 0951, p. 41, 1970.

43. Fisher, M.J. and P.O.A.L. Davies, J. Fluid Mech., 18, 97 1963

44. Bryer, D.W. and Pankhurst, R.C., Pressure probe methods for determining wind speed and flow direction, H.M.S.O. London (1971)

45. Kaye, G.T. and Laby, T.H., Tables of Physical and Chemical Constants, 13th edition, Longmans (1966)

46. Bascombe, K.N., Ministry of Aviation, TM 11/M/66 (1966)

47. Ghosh, A.K. and Richard, C., J.A.I.A.A., 9, 10, 2104 (1971)

48. Wygnanski, I. and Fiedler, H., J. Fluid Mech. 38, 3, 577 (1969)

49. Sutton, G.W., J.A.I.A.A., 7, 1, 90 (1965)

50. Fisher, M.J. and Johnson, K.D., A.I.A.A., NASA IN D-5206 (1971)

51. Crow, S.C. and Champagne, F.H., J. Fluid Mech. 48, 547, (1971)

52. Williams, H. Private Communication.

53. Singleton, R. C. Collected Algorithms C.A.C.M. No. 338. 339. and 345.

54. Calcote, H. F. Tenth Symposium (International) on Combustion p605 (1965)

55. Jensen, D.E. and Padley, P.J. Eleventh Symposium (International) on Combustion. 351 (1966)

56. Bendat, J. S. and Piersol A. G. Measurement and Analysis of Random Data. p86 - 87. John. Wiley and Sons. (1966)